U.PORTO
FEUP FACULDADE DE ENGENHARIA
UNIVERSIDADE DO PORTO

Adsorption System for the Removal of Arsenic and Antimony from Water and Wastewater by Iron-coated Cork Granulates

PhD Dissertation in Environmental Engineering by

Mariko de Almeida Carneiro

Supervisors:

Doutora Ariana A. M. Pintor

Profª. Cidália M. S. Botelho

SRE
CM

Laboratory of Separation and Reaction Engineering – Laboratory of Catalysis and Materials

Associate Laboratory LSRE – LCM

Faculdade de Engenharia

Universidade do Porto

May 2025

To my grandmothers (in memoriam), Célia Rocha Carneiro and Maria Alves de Carvalho.

"I can promise you that women working together – linked, informed and educated – can bring peace and prosperity to this forsaken planet."

Isabel Allende

This work was financially supported by LA/P/0045/2020 (ALiCE), UIDB/50020/2020 and UIDP/50020/2020 (LSRE-LCM), funded by national funds through FCT/MCTES (PIDDAC). Mariko Carneiro acknowledges her Ph.D. scholarship by FCT [2020.07233.BD].







Acknowledgments

I would like to start by thanking my supervisors, Drª Ariana Pintor and Profª Cidália Botelho, for their immense support through this five-years journey. Thank you for believing in me and giving me this opportunity even before getting to know me. Thank you for holding my back in this rollercoaster period of my life, not only with academic supervision but also with caring and respect. Thank you also for all the knowledge shared on adsorption, arsenic, antimony, cork, water treatment, statistics, publishing, writing, and also on ethics and integrity. Thank you for the support in many ways, I will be always thankful for you two.

Thank you to Profº Rui Boaventura, for the helpful insights, proof-reading of the papers that compose this thesis, and finance support to equipment and conferences. Thank you to Silvia Santos, who was always helpful in the lab, especially with the AAS equipment. Thank you to Eng. Liliana Pereira for carrying out all the ICP analysis, even with a very busy schedule. Thank you to the students Joana, Tânia and Pedro for the contribution during the internships.

Thank you to the Chemical Engineering Department (DEQ) of FEUP and the Associate Laboratory LSRE-LCM, where I could carry out the theoretical and practical parts of this thesis. Thank you FCT, for the financial support with my PhD scholarship, that allowed me to achieve such important goals in my life, professionally and personally, including the financial support for the international mobility to the Netherlands. Thank you also to UPTEC, namely Susana Pinheiro, for the FilterCork incubation and contribution to our business idea. Thank you to NHL Stenden University of Applied Sciences for receiving me during the mobility studies, namely Prof. Luewton Agostinho, Dr. Cláudia Sousa, and Dr. Kelly Moreira. Thank you to the Water Application Center (WAC) at Van Hall Larestein, where I could conduct my assays during Erasmus.

Thank you for the friends and colleagues from the E404A lab, Isabella, Ariana, Ricardo; from the Café FEUP group; from our office E416; and the girls from Tricot FEUP. I couldn't imagine how it would be without you all.

Thank you to my wife, Juliana, who accepted the challenge to change the whole life to be part of this unique time of my life. Thank you for the love, incentive and understanding shared with me every day. Thank you to my mother, Albanita, who has always incentivized me to pursue my dreams and supported me in my decisions. For helping me since the beginning of this journey, with all the bureaucracy on the visa and the citizenship processes; for taking some time to visit me and trying to be part of my life here. Thank you to my families in Caruaru and Ponte Nova, who has always been very happy for me and my achievements. Thank you to Lena, my second mother, who always had a good laugh to cheer my day up. Thank you to my sister and mother-in-law, Stephanie and Toca, for picking up the phone whenever we needed and for the good laughs shared by distance as well.

Thank you to my friends in Portugal: Amanda, Monica, Gabi, Lucas, Papi, Rafa, Fred, Matheus, Nuno, Consuelo, Rafael, who made the winters warmer and the summers happier. Thank you to my friends from Leeuwarden for the great welcome during Erasmus. Thank you to my psychologist, Lara Melo, who even far away, in Joao Pessoa, could take some time weekly to help me with my mental health. Thank you to my CBTU friends and work colleagues, especially Diogo Soares, who helped me with my study leaving and gave me a safe background to do my PhD. Thank you to my best girlfriends in Brazil, from Recife and Viçosa (but not only), who have always believed in me and sent me love and strength throughout this time of my life.

Abstract

Arsenic (As) and antimony (Sb) are both metalloids from the pnictogen group of the periodic table. They share a lot of characteristics including being very toxic for humans, carcinogenic and classified as high-priority pollutants by the European Union and the United States. They can exist naturally in the environment, and are often combined; nevertheless, anthropogenic activities are also responsible for their occurrence in waters at hazardous levels. The World Health Organization (WHO) recommends limit concentrations in drinking water as 10 µg L^{-1} and 20 µg L^{-1} for As and Sb, respectively. Since As and Sb pose a threat to human health, and are subject to legal limits, the removal of As and Sb from water and wastewater is mandatory.

Adsorption is considered one of the most attractive water treatment technologies due to its simple design requirements, high removal efficiency, low cost, and easy operation. The use of non-conventional adsorbents, such as natural biomass-based materials and novel functional composites, can increase the cost-effectiveness and the environmental friendliness of the adsorption process. Coating a common and cheap material to turn it into an adsorbent is a common practice among researchers to improve adsorption capacity and increase adsorption rate. Beyond the increase in adsorbent capacity, iron-impregnated adsorbents are non-toxic, low cost and accessible in large quantities. Most of the adsorbents presented in literature are developed based only on tests conducted in batch mode. For industrial and commercial purposes, the adsorption treatment in continuous mode, more specifically in a fixed-bed column, is preferable. Hence, this thesis aimed at scaling-up iron-coated cork granulates for the adsorption of arsenic or antimony in continuous mode.

Results for arsenic removal from aqueous solution showed that most experimental parameters of breakthrough curves (BTC) depend on flow rate, bed height, pH, and initial arsenic concentration. The temperature did not significantly affect arsenate removal in continuous mode; however, it affected the adsorption capacity in batch mode. The thermodynamic parameters suggest that the adsorption process is spontaneous and endothermic. The maximum adsorption capacity in fixed-bed column of ICG for As(V) removal at pH 3 was 4.2 ± 0.3 mg $g^{-1}$and for As(III) at pH 9 was 1.6 ± 0.2 mg g^{-1}. ICG were able to treat As(V) from 100 µg L^{-1} to under 10 µg L^{-1} and 50 µg L^{-1} for 895 and 1633 bed volumes, and As(III) for 569 and 861 bed volumes, respectively, both at pH 7. The application of ICG in arsenic oxyanions remediation was found to be effective under various conditions.

The chemical desorption of arsenic from saturated iron-coated cork granulates (ICG) and the regeneration capacity of this adsorbent for further reuse was investigated in batch and continuous modes. The Elovich model fitted best ($r^2 > 0.98$) the desorption kinetics when using NaOH as eluent. The basic solution of NaOH 0.01 M proved to be less aggressive to ICG compared to NaOH 0.1M and allowed media regeneration for at least four adsorption-desorption cycles, while remaining an arsenic adsorption capacity of 1 mg g^{-1} in both batch and continuous modes. The adsorbent was also successfully applied in continuous mode to remove arsenic from real groundwater and was able to maintain arsenic concentration under 10 and 50 µg L^{-1} for 140 and 341 bed volumes, respectively.

The adsorption-desorption of Sb assays using iron-coated cork granulates (ICG) were carried out in both batch and continuous modes to evaluate the material´s adsorption and regeneration performance, as well as the possibility of antimony recovery. Maximum adsorption capacities of 13 ± 2 mg g^{-1} and 10 ± 1 mg g^{-1} for Sb(III) and Sb(V), respectively, were achieved in continuous mode at pH 3. Moreover, ICG was able to remove Sb within the WHO guideline of 20 µg L^{-1} at pH 6. Among the different classes of eluents tested for Sb(V) desorption, the acids achieved the highest desorption rates - $81 \pm 9\%$ and $66 \pm 8\%$ for HCl 1M and ascorbic acid 0.1M,

respectively. The desorption kinetics showed that HCl 1 M reached equilibrium in 4 h, but ascorbic acid 0.1 M took 16 h.
The impact of different groundwater (GW) matrices, from wells in Portugal (pH 6.95 ± 0.01, NO_3^- = 30 mg L^{-1}, Cl^- = 20.4 mg L^{-1}, PO_4^{3-} = 0.12 mg L^{-1}) and The Netherlands (pH = 7.4 ± 0.1, NO_3^- < 0.27 mg L^{-1}, Cl^- = 1,097 mg L^{-1}, $PO4_3^-$ = 0.502 mg L^{-1}), on arsenic adsorption onto iron-coated cork granulates were investigated. Groundwater (As-spiked or not) was treated in lab-scale fixed-bed columns from initial concentrations (11 - 300 µg L^{-1}) until the arsenic WHO guideline and European Union Directive 2020/2184 of 10 µg L^{-1}. The effect of an oxidation-filtration pretreatment was also investigated. The ICG demonstrated the capacity to treat real groundwater across a wide range of arsenic concentrations under the WHO guidelines and the European Commission's legal limit. The ICG performed better in the GW matrix from The Netherlands than that from Portugal. That could be attributed to the elevated concentrations of nitrate in the Portuguese matrix, which might have a stronger competitiveness with the arsenic oxyanions for the ferric sites in the adsorbent, compared to the more abundant chloride in the Dutch matrix. Moreover, the pretreatment using the aeration/sand filter reactor improved the arsenic removal in the Dutch matrix, and it reached values of breakthrough time, treated volume at breakthrough and bed volumes at breakthrough of 39 ± 5 h, 12 ± 2 L, 202 ± 27 and, respectively, for an initial concentration of 300 ± 10 µg L^{-1}.
The environmental impacts associated with the production of 1kg of iron-coated cork granulates (ICG) on a lab scale were evaluated using life-cycle analysis (LCA). Also, a comparison of the environmental performance between the treatment of arsenic-contaminated water using either ICG or commercial iron oxide adsorbent, Bayoxide E33, was carried out. Finally, the LCA of the adsorption using regenerated ICG was investigated. The treatment of arsenic-contaminated water using ICG (Global warming 3.71 Kg CO_2 eq.) demonstrated a lower impact in 16 out of 18 categories compared to the use of the commercial adsorbent Bayoxide E33 (Global warming 5.13 Kg CO_2 eq.). The results showed that the electricity spent in the ICG laboratory scale production was the input with the biggest contribution to the environmental impacts. Expanding the lifespan of the adsorbent by carrying out adsorption-desorption cycles (using NaOH 0.1M) had a higher environmental impact than using the adsorbent only once, because of the need to add a hazardous waste treatment (incineration) for the desorbed solution containing high concentrations of arsenic.
This work developed here allowed to increase the technology readiness level (TRL) of iron-coated cork granulates as efficient adsorbents for arsenic and antimony removal from water.

Keywords: Adsorption-Desorption, Arsenic, Antimony, Kinetics, Scale-up, Groundwater, Cork granulates, LCA

Resumo

O arsénio (As) e o antimónio (Sb) são ambos metaloides do grupo dos pnictogênicos da tabela periódica. Eles compartilham muitas características, inclusive a de serem muito tóxicos para os seres humanos, carcinogênicos e classificados como poluentes de alta prioridade pela União Europeia e pelos Estados Unidos. Eles podem existir naturalmente no meio ambiente e são frequentemente combinados; no entanto, as atividades antropogênicas também são responsáveis por sua ocorrência em águas em níveis perigosos. A Organização Mundial da Saúde (OMS) recomenda que as concentrações-limite na água potável sejam de 10 µg L^{-1} e 20 µg L^{-1} para As e Sb, respectivamente. Como o As e o Sb representam uma ameaça à saúde humana e estão sujeitos a limites legais, a remoção do As e do Sb da água e das águas residuais é obrigatória.

A adsorção é considerada uma das tecnologias de tratamento de água mais atraentes devido ao seu simplificado requisito de projeto, alta eficiência de remoção, baixo custo e fácil operação. O uso de adsorventes não convencionais, como materiais naturais à base de biomassa e novos compostos funcionais, pode aumentar a relação custo-benefício e a compatibilidade ambiental do processo de adsorção. O revestimento de um material comum e barato para transformá-lo em um adsorvente é uma prática comum entre os pesquisadores para melhorar a capacidade de adsorção e aumentar a taxa de adsorção. Além do aumento da capacidade de adsorção, os adsorventes impregnados com ferro não são tóxicos, são de baixo custo e acessíveis em grandes quantidades. A maioria dos adsorventes apresentados na literatura é desenvolvida com base apenas em testes realizados em modo de batelada. Para fins industriais e comerciais, o tratamento de adsorção em modo contínuo, mais especificamente em uma coluna de leito fixo, é preferível. Portanto, esta tese teve como objetivo aumentar a escala dos granulados de cortiça revestidos com ferro para a adsorção de arsénio ou antimónio em modo contínuo.

Os resultados da remoção de arsénio em solução aquosa mostraram que a maioria dos parâmetros experimentais das curvas de ruptura (BTC) depende do caudal, da altura do leito, do pH e da concentração inicial de arsénio. A temperatura não afetou significativamente a remoção de arsénio no modo contínuo; no entanto, afetou a capacidade de adsorção no modo de batelada. Os parâmetros termodinâmicos sugerem que o processo de adsorção é espontâneo e endotérmico. A capacidade máxima de adsorção em coluna de leito fixo de ICG para remoção de As(V) em pH 3 foi de 4,2 $\pm$ 0,3 mg g^{-1} e para As(III) em pH 9 foi de 1,6 $\pm$ 0,2 mg g^{-1}. O ICG foi capaz de tratar o As(V) de 100 µg L^{-1} para menos de 10 µg L^{-1} e 50 µg L^{-1} após 895 e 1633 volumes de leito, e o As(III) após 569 e 861 volumes de leito, respectivamente, ambos em pH 7. A aplicação do ICG na remediação de oxiânions de arsénio foi considerada eficaz em várias condições.

A dessorção química de arsénio de granulados de cortiça revestidos com ferro (ICG) saturados e a capacidade de regeneração desse adsorvente para reutilização posterior foram investigadas nos modos contínuo e em batelada. O modelo de Elovich se ajustou melhor ($r^2 >$ 0,98) à cinética de dessorção ao usar NaOH como eluente. A solução básica de NaOH 0,01 M demonstrou ser menos agressiva para o ICG em comparação com NaOH 0,1 M e permitiu a regeneração do meio por pelo menos quatro ciclos de adsorção-dessorção, mantendo uma capacidade de adsorção de arsénio de 1 mg g^{-1} nos modos contínuo e em batelada. O adsorvente também foi aplicado com sucesso no modo contínuo para remover o arsénio de águas subterrâneas reais e conseguiu manter a concentração de arsénio abaixo de 10 e 50 µg L^{-1} para 140 e 341 volumes de leito, respectivamente.

Os ensaios de adsorção-dessorção de Sb usando granulados de cortiça revestidos com ferro (ICG) foram realizados nos modos contínuo e em batelada para avaliar o desempenho de

adsorção e regeneração do material, bem como a possibilidade de recuperação de antimónio. As capacidades máximas de adsorção de 13 ± 2 mg g^{-1} e 10 ± 1 mg g^{-1} para Sb(III) e Sb(V), respectivamente, foram alcançadas no modo contínuo em pH 3. Além disso, o ICG foi capaz de remover Sb dentro da diretriz da OMS de 20 µg L^{-1} em pH 6. Entre as diferentes classes de eluentes testados para a dessorção de Sb(V), os ácidos alcançaram as maiores taxas de dessorção - 81 ± 9% e 66 ± 8% para HCl 1M e ácido ascórbico 0,1M, respectivamente. A cinética de dessorção mostrou que o HCl 1 M atingiu o equilíbrio em 4 h, mas o ácido ascórbico 0,1 M levou 16 h.

Foi investigado o impacto de diferentes matrizes de água subterrânea (GW) de poços em Portugal (pH 6,95 ± 0,01, NO_3^- = 30 mg L^{-1}, Cl- = 20,4 mg L^{-1}, PO_4^{3-} = 0,12 mg L^{-1}) e nos Países Baixos (pH = 7,4 ± 0,1, NO_3^- < 0,27 mg L^{-1}, Cl^- = 1.097 mg L^{-1}, PO_4^{3-} = 0,502 mg L^{-1}) na adsorção de arsênico em granulados de cortiça revestidos de ferro. A água subterrânea (com ou sem adição de As) foi tratada em colunas de leito fixo em escala de laboratório a partir de concentrações iniciais (11 - 300 µg L^{-1}) até a diretriz de arsénio da OMS e a Diretiva 2020/2184 da União Europeia de 10 µg L^{-1}. O efeito de um pré-tratamento de oxidação-filtração também foi investigado. O ICG demonstrou a capacidade de tratar águas subterrâneas reais em uma ampla gama de concentrações de arsénio de acordo com as diretrizes da OMS e o limite legal da Comissão Europeia. O ICG teve um desempenho melhor na matriz GW da Holanda do que na de Portugal. Isso pode ser atribuído às concentrações elevadas de nitrato na matriz portuguesa, que pode ter uma competitividade mais forte com os oxiânions de arsénio para os locais férricos no adsorvente, em comparação com o cloreto mais abundante na matriz holandesa. Além disso, o pré-tratamento usando o reator de aeração/filtro de areia melhorou a remoção de arsénio na matriz holandesa, atingindo valores de tempo de ruptura, volume tratado na ruptura e volumes de leito na ruptura de 39 ± 5 h, 12 ± 2 L, 202 ± 27, respectivamente, para uma concentração inicial de 300 ± 10 µg L^{-1}.

Os impactos ambientais associados à produção de 1 kg de granulados de cortiça revestidos com ferro (ICG) em escala laboratorial foram avaliados por meio da análise do ciclo de vida (ACV). Além disso, foi realizada uma comparação do desempenho ambiental entre o tratamento de água contaminada com arsénio usando ICG ou o adsorvente comercial de óxido de ferro, Bayoxide E33. Por fim, a ACV da adsorção usando ICG regenerado foi investigada. O tratamento de água contaminada com arsénio usando ICG (aquecimento global de 3,71 kg de CO_2 eq.) demonstrou um impacto menor em 13 das 18 categorias em comparação com o uso do adsorvente comercial Bayoxide E33 (aquecimento global de 5,36 kg de CO_2 eq.). Os resultados mostraram que a eletricidade gasta na produção em escala laboratorial do ICG foi o insumo com a maior contribuição para os impactos ambientais. A expansão da vida útil do adsorvente por meio da realização de ciclos de adsorção-dessorção (usando NaOH 0,1M) teve um impacto ambiental maior do que o uso do adsorvente apenas uma vez, devido à necessidade de adicionar um tratamento de resíduos perigosos para a solução dessorvida contendo altas concentrações de arsênio.

O trabalho desenvolvido aqui permitiu aumentar o Nível de Prontidão de Tecnologia (TRL) dos granulados de cortiça revestidos com ferro como adsorventes eficientes para a remoção de arsénio e antimónio da água.

Palavras-chave: Adsorção-Dessorção; Arsénio; Antimónio; Cinética; Aumento de escala; Água subterrânea; Granulados de cortiça; ACV

Table of Contents

1 INTRODUCTION 1

1.1 Motivation and Relevance 1

1.1.1 The adsorbates: arsenic and antimony 1

1.1.2 The process: adsorption 4

1.1.3 The adsorbent: iron-coated cork granulates 5

1.2 Thesis objectives and Layout 9

1.3 References 10

2 LITERATURE REVIEW 16

2.1 Arsenic adsorption in continuous mode: adsorbents type 17

2.1.1 Introduction 17

2.1.2 Metal (hydr)oxides 17

2.1.3 Zero-Valent Iron (ZVI) 18

2.1.4 Minerals 19

2.1.5 Soil and Rock 22

2.1.6 Carbon-Based Adsorbents 25

2.1.7 Biosorbents 27

2.1.8 Industrial Waste and By-products 37

2.1.9 Nanocomposites 39

2.1.10 Granular ferric hydroxide (GFH) and Commercial adsorbents 42

2.1.11 Layered Double Hydroxides (LDH) 43

2.1.12 Antimony adsorption in continuous mode 44

2.1.12 Conclusions 44

2.2 Desorption of arsenic and antimony in continuous mode 46

2.2.1 Introduction 46

2.2.2 Short bibliometrics 46

2.2.3 Adsorption of pnictogens 50

2.2.4 Desorption parameters 51

2.2.5 Desorption mechanism 53

2.2.6 Desorption of arsenic 55
2.2.7 Desorption of antimony 63
2.2.8 Batch *vs* continuous mode desorption 71
2.2.9 Regeneration and fate of spent adsorbent 72
2.2.10 Recovery and fate of desorbed solution 74
2.2.11 Challenges 75
2.2.12 Final remarks 76
2.3 References 77

3 REMOVAL OF ARSENIC FROM AQUEOUS SOLUTION BY CONTINUOUS ADSORPTION ONTO IRON-COATED CORK GRANULATES 101

3.1 Introduction 103
3.2 Materials and methods 103
3.2.1 Materials 103
3.2.2 Analytical Methods 104
3.2.3 Evaluation of temperature effect in batch operation mode and thermodynamic studies 104
3.2.4 Fixed-bed column experiments 106
3.3 Results and discussion 111
3.3.1 Evaluation of temperature effect on batch mode operation and thermodynamic studies 111
3.3.2 Fixed-bed column adsorption experiments 116
3.4 Conclusions 137
3.5 References 138

4 REGENERATION OF ARSENIC-LOADED IRON-COATED CORK GRANULATES 143

4.1 Introduction 145
4.2 Materials and methods 145
4.2.1 Materials 145
4.2.2 Analysis 146
4.2.3 Batch adsorption-desorption experiments 147
4.2.4 Continuous adsorption-desorption experiments 148
4.2.5 Analysis breakthrough curves 149

4.3 Results and discussion 150
4.3.1 Desorption in batch operation mode 150
4.3.2 Adsorption-desorption cycles in a fixed-bed column 157
4.4 Conclusions 176
4.5 References 177
5 ANTIMONY ADSORPTION AND DESORPTION: BATCH AND CONTINUOUS MODE STUDIES 181
5.1 Introduction 183
5.2 Materials and methods 183
5.2.1 Materials 183
5.2.2 Analytical Methods 184
5.2.3 Adsorption in continuous mode 184
5.2.4 Adsorption on a batch operation mode 185
5.2.5 Desorption in batch mode 185
5.2.6 Desorption in continuous mode 186
5.2.7 Adsorption in continuous mode using recycled iron-coated cork granulates 187
5.2.8 Material characterization 187
5.3 Results and discussion 188
5.3.1 Adsorption in continuous mode 188
5.3.2 Adsorption in batch mode 191
5.3.3 Desorption in batch mode 197
5.3.4 Desorption in continuous mode 204
5.3.5 Analysis of fresh, regenerated and recycled adsorbent 205
5.4 Conclusions 208
5.5 References 209
6 ARSENIC REMOVAL FROM DIFFERENT GROUNDWATER MATRICES 213
6.1 Introduction 215
6.2 Materials and methods 215
6.2.1 Adsorbent preparation 215
6.2.2 Fixed-bed adsorption column studies in Portugal 217
6.2.3 Fixed-bed adsorption column studies in The Netherlands 218
6.2.4 Analysis of breakthrough curves 227

6.2.5 Adsorbent digestion....228
6.3 Results and discussion....228
6.3.1 Effect of coating time and solution reuse in the adsorbent performance....228
6.3.2 Fixed-bed adsorption column studies in Portugal....230
6.3.3 Fixed-bed adsorption column studies in The Netherlands....231
6.3.4 Comparison of arsenic removal efficiency from the groundwater sources....241
6.4 Conclusions....242
6.5 References....242

7 ENVIRONMENTAL IMPACTS OF ARSENIC REMOVAL FROM WATER USING IRON-COATED CORK GRANULATES 247

7.1 Introduction....249
7.2 Materials and methods....249
7.2.1 Goal and scope definition....249
7.2.2 Life cycle inventory....251
7.2.3 Software and LCA methodology....254
7.2.4 Cost analysis....255
7.3 Results and discussion....255
7.3.1 Life cycle inventory (LCI)....255
7.3.2 Impact assessment of iron-coated cork granulates production....258
7.3.3 Environmental impact of arsenic removal from water....263
7.3.4 Impact assessment of desorption cycles....272
7.3.5 Cost analysis....276
7.4 Conclusions....277
7.5 References....278

8 CONCLUSIONS AND FUTURE WORK....285

8.1 General Conclusions....285
8.2 Future Work....286

List of Figures

Figure 1.1: Illustration of batch and continuous treatment. 5

Figure 1.2. Comparison between a) specific compressive strength and specific modulus, and b) thermal conductivity and compressive strength, for cork and other foamed materials (Silva, Sabino et al. 2005, Duarte and Bordado 2015) 6

Figure 1.3: SEM micrographs of a) raw and b) iron-coated cork granulates (500x magnification), c) raw and d) iron-coated cork granulates (2.000x magnification), e) detailed iron coating (50,000x magnification) (Pintor, Vieira et al. 2018). 8

Figure 2.1: Published documents for each term on arsenic and antimony adsorption and desorption from water. 47

Figure 2.2: Global distribution of academic publications about a) "desorption AND arsenic AND water", and b) "desorption AND antimony AND water". 49

Figure 2.3: Schematic illustration of the adsorption-desorption process of As/Sb in water. 52

Figure 2.4: Examples of curves of antimony/arsenic a) adsorption and b) desorption in batch mode; and c) adsorption and d) desorption in continuous mode. 54

Figure 2.5: Percentage of eluents used for arsenic desorption studies presented in Table 2.10. 61

Figure 2.6: Desorption efficiencies of arsenic-loaded adsorbents by NaOH at different concentrations reported in the literature. 62

Figure 2.7: Percentage of eluents used for antimony desorption studies presented in Table 2.11. 68

Figure 2.8: Desorption efficiency of antimony-loaded adsorbents by HCl at different concentrations reported in the literature. 70

Figure 3.1: Schematic diagram of the lab-scale adsorption system of fixed-bed column 106

Figure 3.2: Linearized form of a) Langmuir and b) Freundlich (bottom) isotherms, for temperatures of 10, 20 and 30 °C. 113

Figure 3.3: Langmuir adsorption isotherms of As(V) on ICG (pH 3.0; S/L ratio = 2.5 g L^{-1}; contact time = 48 h) for temperatures of 10, 20 and 30 °C (Error bars: maximum absolute deviation). 114

Figure 3.4: Correlation curves between Langmuir maximum adsorption capacity, Qmax (mg g^{-1}) (left) or Freundlich constant, K_F ($mg^{(1-1/n)} L^{1/n} g^{-1}$) (right) and temperature (°C) (Error bars: standard error of the mean). 114

Figure 3.5: Ln Ko versus 1/TK graph for the determination of thermodynamic parameters for ICG adsorption (pH 3; S/L ratio = 2.5 g L^{-1}; contact time = 48 h) for temperatures of 10, 20 and 30 °C. 115

Figure 3.6: Main effect plots for: a) breakthrough time (tb), b) saturation time (ts), c) treated volume at breakthrough (Vb), and d) MTZ/Bed height ratio. 123

Figure 3.7: Temperature effect in iron leached from ICG in the effluent in fixed-bed column (pH 3; flow rate of 5 mL min^{-1}; Ci (As(V)) = 1 mg L^{-1}) 124

Figure 3.8: Iron leaching behavior through column experiments conducted at 30oC (pH: 3; Co As(V): 1 mg L^{-1}). 124

Figure 3.9: Experimental and predicted breakthrough curves obtained for each 2^3 factorial design run, pH = 3 and C_0 = 1 mg L^{-1}: a) run 1, b) run 2, c) run 3, d) run 4, e) run 5, f) run 6, g) run 7, and h) run 8 127

Figure 3.10: Theoretical (Yan model) and experimental breakthrough curves of arsenic adsorption onto ICG at different temperatures: 10, 20 and 30°C (bed height: 12 cm, flow rate: 5 mL min^{-1}, pH 3.0, $C_{0As(V)}$ 1 mg L^{-1}). 128

Figure 3.11: Experimental and theoretical (Yan model) breakthrough curves of arsenic adsorption onto ICG for different pH values: a) As(III), pH of 7 and 9; b) As(V) pH of 3, 7 and 9 130

Figure 3.12: pH effect in BTC parameters for As(V) column experiments and trend lines (C_0 = 1 mg L^{-1}; flow rate of 5 mL min^{-1}; bed height of 12 cm; T = 20°C): a) adsorption capacity (mg g^{-1}), b) adsorption time (h), c) bed volumes, d) treated volume (L),), and e) arsenic removal (%). 134

Figure 3.13: Experimental and theoretical (Yan model) breakthrough curves of arsenic adsorption onto ICG with initial concentration values of 0.1 and 1 mg L^{-1} (pH 7 and *T* = 20°C): a) As(III); b) As(V). 137

Figure 4.1: Arsenate desorption efficiency and iron leaching from ICG for different eluents and concentrations (S/L ratio of 2.5 g L^{-1}; T = 20°C). 152

Figure 4.2: Arsenate desorption efficiency using NaOH and Na_2CO_3 solutions at different concentration (S/L ratio - 2.5 g L^{-1}; T = 20°C). 153

Figure 4.3: Desorption kinetics for arsenate from iron-coated cork granulates using different concentrations of NaOH (20ºC; S/L = 2.5 g L^{-1}) (Error bars: standard errors). 155

Figure 4.4: Coloration of desorption batch assays samples: a) kinetics of desorption using NaOH 0.1 M (left), b) 24h contact time desorption using NaOH 0.1 M and 0.01 M (right). 156

Figure 4.5: Total organic carbon in solution after contacting As-loaded ICG with NaOH. 156

Figure 4.6: Experimental (points) and predicted (lines) breakthrough curves for fresh (1st cycle) and regenerated ICG after NaOH treatment (flow rate 5 mL min^{-1} and 6 g of ICG, C_i = 1 mg As(V) L^{-1}, pH 3.0). 158

Figure 4.7: Adsorption capacities of regenerated ICG, using NaOH 0.1 M and 0.01 M, in successive adsorption-desorption cycles in continuous mode (flow rate 5 mL min^{-1} and 6 g of ICG): a) at saturation (left), b) at breakthrough (right).....161

Figure 4.8: Desorption profile using: 0.1 M NaOH (left), 0.01 M NaOH (right). 163

Figure 4.9: Continuous desorption samples for NaOH 0.1 M (left) and 0.01 M (right). 164

Figure 4.10: Boxplot graph of total organic carbon for desorption cycles in continuous mode, using 0.1 M NaOH (top) and 0.01 M NaOH (bottom). 165

Figure 4.11: Iron leaching from desorption cycles in continuous mode, using 0.1 M NaOH (top) and 0.01 M NaOH (bottom). 167

Figure 4.12: SEM micrographs of: a) iron-coated cork granulates, 500x magnification, b) iron-coated cork granulates treated with NaOH 0.01 M, 500x magnification; c) iron-coated cork granulates treated with NaOH 0.1 M, 500x magnification 169

Figure 4.13: EDS analysis of a) iron-coated cork granulates, b) iron-coated cork granulates treated with NaOH 0.01 M, c) iron-coated cork granulates treated with NaOH 0.1 M. 170

Figure 4.14: Adsorption-desorption cycles: a) Experimental (points) and predicted (lines) breakthrough curves for new (1st cycle) and regenerated (2nd and 3rd cycles) ICG using real-spiked groundwater (flow rate 5 mL min^{-1} and 6 g of ICG), b) desorption profiles for three cycles using 0.1 M NaOH. 172

Figure 4.15: Adsorbed and desorbed amount of As in three adsorption-desorption cycles by ICG using As-spiked groundwater (flow rate of 5 mL min^{-1}; 6 g of ICG; 20ºC; C_i = 0.1 mg L^{-1}). 172

Figure 4.16: Arsenic and iron concentrations from desorption of saturated ICG after real water treatment. 176

Figure 5.1: Representation of lab-scale batch operating mode of antimony adsorption and desorption onto iron-coated cork granules. 186

Figure 5.2: pH effect on the Sb(III) and Sb(V) removal in the fixed-bed column (dots = experimental data, lines = Yan model predicted curves) (Inlet Sb(III)/Sb(V) concentration 1 mg L^{-1}; Bed height: 12 cm; Flow rate: 5 mL min^{-1}; Temperature: 20ºC).....188

Figure 5.3: Adsorption equilibrium of Sb(III) on iron-coated cork granulates: experimental and model-fitting data (pH 3.0; 2.5 g L^{-1}; 24 h; 20ºC) (Error bars: maximum absolute deviation). 192

Figure 5.4: Adsorption kinetics (S/L = 2.5 g L^{-1}, 20ºC, pH 3) with experimental and fitted pseudo-second-order model of Sb(III) for initial concentration of: a) 1 mg L^{-1} and b) 15 mg L^{-1}. 196

Figure 5.5: Desorption efficiency of Sb(V) from ICG in batch mode and iron leaching for each eluent (S/L = 2.5 g L-1; 20ºC; 10 ± 1 mg Sb(V)/g ICG; Initial iron loading = 29 ± 3 mg Fe/g ICG).....198

Figure 5.6: Desorption efficiency of Sb(V) versus eluent´s concentration (S/L = 2.5 g L^{-1}; 20ºC; 10 ± 1 mg Sb(V)/g ICG). 200

Figure 5.7: Desorption kinetics of Sb(V) by a) ascorbic acid 0.1 M and b) HCl 1 M (S/L = 2.5 g L^{-1}; 20ºC, 10 ± 1 mg Sb(V)/g ICG): experimental data and fits to pseudo-first-order, pseudo-second-order and Elovich models.....202

Figure 5.8: Experimental and predicted (Yan model) breakthrough curves for Sb(V) adsorption from fresh ICG, regenerated ICG (after Sb desorption) and recycled ICG (after Fe reloading) (Ci = 5 mg L^{-1}; pH = 3.0, FR = 5 mL min^{-1}, 6 g of ICG, T = 20º C).....204

Figure 5.9: SEM micrographs of: ICG after Sb(V) adsorption, a) 500x magnification, and b) 2500x magnification; recycled ICG after Sb(V) adsorption, c) 500x magnification, and d) 2500x magnification; ICG after Sb(V) desorption e) with acid ascorbic 0.1 M, 500x magnification and f) with HCl 1 M, 500x magnification. 207

Figure 5.10: EDS analysis of a) Sb(V)-loaded ICG before desorption, b) ICG after desorption with ascorbic acid 0.1 M, c) ICG after desorption with HCl 1 M.....208

Figure 6.1: Rotator mixers with 16L (left) and 1.2 L capacity (right).....216

Figure 6.2: Oxidation-filtration system to remove iron from the groundwater in the Water Application Center: front view(left) and top view (right). 222

Figure 6.3: Lab installation at the Water Application Center for arsenic adsorption from groundwater in a fixed-bed column.....223

Figure 6.4: Scheme of continuous adsorption system for arsenic removal from groundwater onto iron-coated cork granulates at the Water Application Center (The Netherlands): a) assay 1, b) assay 2. 224

Figure 6.5: Simplified pE-pH diagram for iron in water (Manahan 2017). 225

Figure 6.6: DO (red circle) and flow meters (yellow circle) to monitoring the treated groundwater. 227

Figure 6.7: Iron impregnation in the iron-coated cork granulates at different coating times using fresh ( )and recycled FeCl3 solution: 2nd recycling ( ), 3rd ( ) and 4th ( ) recycling cycles. 229

Figure 6.8: Arsenic concentration in the fixed-bed column effluent (adsorbent mass = 6g, flow rate = 5 $mL.min^{-1}$, temperature = 20°C). 230

Figure 6.9: Influent and effluent concentrations of a) manganese, b) lead, c) iron, and d) zinc in the fixed-bed column (adsorbent mass = 6g, flow rate = 5 $mL.min^{-1}$, temperature = 20°C). 231

Figure 6.10: Boxplot of pH (left) and conductivity (right) from the assays using untread groundwater (red) and treated groundwater (blue). 232

Figure 6.11: Inlet and outlet total iron concentration versus time for a) Filter A, b) Filter B, c) Filter C1, and d) Filter C2. 233

Figure 6.12: Iron deposits in the outlet tubes from Filter A. 234

Figure 6.13: Implementation of experimental data in a pE-pH iron diagram. 235

Figure 6.14: Inlet and outlet manganese concentration versus time for a) Filter A, b) Filter B, c) Filter C1, and d) Filter C2. 236

Figure 6.15: Arsenic concentration versus time on Filter A effluent. 237

Figure 6.16: Boxplot of influent (orange/left) and effluent (green/right) arsenic concentration from the experiments with different groundwater and operation mode (A-Untreated GW under semi-continuous operation, B-Pretreated GW under semi-continuous operation, C1 and C2 – Pretreated GW under continuous operation). 237

Figure 6.17: Experimental – dots - and predicted (Yan model) – lines - breakthrough curves of arsenic adsorption onto ICG in the pretreated Dutch groundwater matrix (FR = 5 $mL.min^{-1}$, adsorbent mass = 6 g, EBCT = 12 min, BV = 59 mL). 238

Figure 6.18: Variation of a) flow rate, b) dissolved oxygen and temperature of treated groundwater. ..... **Error! Bookmark not defined.**

Figure 6.19: ANOVA results for temperature and dissolved oxygen of pretreated groundwater. ..... **Error! Bookmark not defined.**

Figure 7.1: System boundaries for the production of a) iron-coated cork granulates, and 1000 L of arsenic-free water using b) iron-coated cork granulates and c) crystalline α-ferric oxide hydroxide (Bayoxide E33). 251

Figure 7.2: Process contribution to environmental impacts associated with the production of 1 kg iron-coated cork granulates on lab-scale production..... 259

Figure 7.3: Life cycle analysis tree for iron-coated cork granulates (ICG) production: material, energy and waste treatment and their corresponding impact on global warming for the treatment of 1000L of arsenic-contaminated water (C_0 = 1 mg L^{-1})..... 264

Figure 7.4: Life cycle analysis tree for Bayoxide E33 production: material, energy and waste treatment and their corresponding impact on global warming for the treatment of 1000L of arsenic-contaminated water (C_0 = 1 mg L^{-1}). 265

Figure 7.5: Relative comparison between the environmental impacts of the treatment of arsenic-contaminated water (C_0 = 1 As(V) mg L^{-1}) by adsorption onto iron-cork granulates and Bayoxide E33, using the ReCiPe 2016 Midpoint (H) method. 266

Figure 7.6: Material contribution for marine eutrophication in the treatment of 1000 L of arsenic-contaminated (C_0 = 1 mg L^{-1}) water using iron-coated cork granulates. 267

Figure 7.7: Material contribution for a) marine toxicity, b) freshwater toxicity and c) non-carcinogenic toxicity in the treatment of 1000 L of arsenic-contaminated (C_0 = 1 mg L^{-1}) water using iron-coated cork granulates. 268

Figure 7.8: Contributions of materials/energy emission for the environmental impacts of iron-coated cork granulates (%). 269

Figure 7.9: Contributions of materials/energy emission for the environmental impacts of Bayoxide E33 (%). 270

Figure 7.10: Life cycle analysis tree for the treatment of 1000 L of arsenic-spiked groundwater (C_0 = 100 μL^{-1}) using ICG without desorption cycles: material, energy and waste treatment and their corresponding impact on global warming..... 274

Figure 7.11: Life cycle analysis tree for the treatment of 1000 L of arsenic-spiked groundwater (C_0 = 100 µg L-1) using regenerated ICG with desorption cycles: material, energy and waste treatment and their corresponding impact on global warming. 275

Figure 7.12: Environmental impacts of scenarios 1 and 2 for arsenic removal from water using iron-coated cork granulates. 276

List of Tables

Table 2.1: Comparison between dynamic tests using metal (hydr)oxides and zero valent iron (ZVI) as adsorbents for arsenic removal. 18

Table 2.2: Comparison of dynamic tests using minerals as adsorbents for arsenic removal. 21

Table 2.3: Comparison of dynamic tests using soil and rock as adsorbents for arsenic removal. 24

Table 2.4: Comparison of dynamic tests using carbon-based adsorbents for arsenic removal.26

Table 2.5: Comparison of dynamic tests using biosorbents for arsenic removal. 34

Table 2.6: Comparison of dynamic tests using industrial waste and by-products as adsorbents for arsenic removal. 38

Table 2.7: Comparison of dynamic tests using nanocomposites, GFH and commercial adsorbents for arsenic removal. 40

Table 2.8: Comparison of dynamic tests using LDH as adsorbents for arsenic removal..... 43

Table 2.9: Batch desorption kinetics for different adsorbents. *55*

Table 2.10: Desorption of arsenic and regeneration performance of adsorbents in batch mode. *55*

Table 2.11: Desorption of antimony and regeneration performance of adsorbents in batch operation mode. 64

Table 2.12: Desorption of As and Sb and regeneration performance of adsorbents in continuous mode. *71*

Table 2.13. TCLP results from arsenic contaminated bed. *74*

Table 3.1: Levels of each factor for each fixed-bed column run of the 2^3 factorial design. ..107

Table 3.2: Equilibrium model parameters ($\pm$ standard error of mean). 112

Table 3.3: Thermodynamic parameters at various temperatures for As(V) adsorption onto iron-coated cork granulates (S/L = 2.5 g L^{-1}, pH = 3, time = 48 h) 115

able 3.4. Experimental BTC parameters values observed in each column adsorption experiment from 23 factorial design. 116

Table 3.5: ANOVA tables with significant ($p < 0.05$) results for the 2^3 factorial design using BTC parameters as response variables: a) breakthrough time (t_b), b) saturation time (t_s); c) treated volume at breakthrough (V_b); and, d) MTZ/Bed height ratio. 118

Table 3.6: ANOVA tables design without significant ($p < 0.05$) results, using BTC parameters from the 2^3 factorial design as response variables: a) adsorption capacity at breakthrough (q_b), b) adsorption capacity at saturation (q_s), c) bed volumes at breakthrough (BV_b), d) bed volumes at saturation (BV_s), e) treated volume at saturation (Vs), f) arsenic removal at breakthrough (y_b), and g) arsenic removal at saturation (y_s).....121

Table 3.7: Parameters of Thomas, Yoon-Nelson and Yan models.....125

Table 3.8: Experimental and predicted breakthrough parameters of pH effect in As(V) and As(III) adsorption (C_0 = 1 mg L^{-1}, T = 20ºC) (± standard error of mean). 131

Table 3.9: Fixed-bed column performances reported in other works for As(III) and As(V) removal with an initial concentration of 1 mg L^{-1}.....133

Table 3.10: Fixed-bed column performances reported in other works for As(III) and As(V) removal with an initial concentration of 1 mg L^{-1}.....135

Table 4.1: Desorption capacity, desorption efficiency, and iron leached for various eluents (± standard error of the mean) 151

Table 4.2: Parameters obtained in the fitting of kinetic models to experimental data of desorption kinetics of As(V) from ICG using NaOH (20ºC; S/L = 2.5 g L^{-1}) (± standard error of the mean). 155

Table 4.3: Performance of ICG on adsorption-desorption cycles using NaOH in batch mode (± standard error of the mean). 157

Table 4.4: Experimental and theoretical parameters (Yan model) of arsenate continuous adsorption from arsenic aqueous solution onto fresh (first cycle) and regenerated (other cycles) ICG with NaOH (flow rate 5 mL min^{-1} and 6 g of ICG, C_i = 1 mg As(V) L^{-1}; pH 3.0).....160

Table 4.5: Parameters from desorption cycles of ICG regeneration after continuous adsorption with arsenic aqueous solution. 162

Table 4.6: Iron leaching from each adsorption-desorption cycle in continuous mode using NaOH 0.1 M and NaOH 0.01M.....164

Table 4.7: Iron content of ICG before and after adsorption-desorption cycles in continuous mode using NaOH, measured by FAAS after acid digestion. 167

Table 4.8: Comparison between new and regenerated adsorbents for As(V) removal in continuous mode.....168

Table 4.9: Characteristics of the groundwater sample collected in Northeastern Portugal. ...171

Table 4.10: Experimental and predicted breakthrough parameters of arsenic adsorption from real groundwater onto fresh (first cycle) and regenerated (second and third cycle) ICG (± standard error of mean). 173

Table 4.11: Performance of alternative adsorbents on the removal of arsenic from real (spiked) groundwater in a fixed-bed column. 175

Table 5.1: Experimental and predicted breakthrough parameters on pH effect in Sb(III) and Sb(V) adsorption (Ci = 1 mg L^{-1}, T = 20°C, FR = 5 mL min^{-1}; Bed height = 12 cm) (±standard error of the mean). 189

Table 5.2: Comparison between adsorption of antimony in fixed-bed columns. 191

Table 5.3: Equilibrium model parameters for Sb(III) at pH 3.0 (C_i = 10 mg L^{-1}) (± standard error of the mean). 192

Table 5.4: Parameters from pseudo-first-order, pseudo-second-order and Elovich fitting to experimental data of adsorption kinetics of Sb(III) onto iron-coated cork granulates (pH 3; 20°C; S/L = 2.5 g L^{-1}) (± standard error of the mean). 197

Table 5.5: Experimental data of desorption of Sb(V) in batch mode from iron-coated cork granulates using different eluents (S/L = 2.5 g L^{-1}; 20°C; 10 ± 1 mg Sb(V)/g ICG). 199

Table 5.6: Parameters obtained in the fitting of kinetic models to experimental data of desorption kinetics of Sb(V) from ICG. 201

Table 5.7: Experimental and predicted parameters (Yan model) of antimonate continuous adsorption using fresh ICG (1st cycle), regenerated ICG (2nd cycle), and recycled ICG (3rd cycle) (± standard error of the mean). 204

Table 6.1: Parameters of iron-coated cork granulates production in lab scale. 216

Table 6.2: Groundwater composition from Portuguese well. 217

Table 6.3: Groundwater composition from the Dutch well, before (untreated) and after (treated) the pretreatment for iron removal in April 2023. 219

Table 6.4: Parameters and methods for the experiments in The Netherlands. 221

Table 6.5: pH, conductivity and pE values. 226

Table 6.6: Comparison of different coating times for ICG preparation. 228

Table 6.7: Reuse of coating solution to produce ICG. 229

Table 6.8: pH, conductivity and pE values. 234

Table 6.9: Experimental and predicted parameters (Yan model) of arsenic continuous adsorption from arsenic-spiked groundwater onto ICG (flow rate 5 mL.min^{-1} and 6 g of ICG, bed height 25.5 cm) 238

Table 6.10: Pearson correlation between filter effluent parameters a) Filter A (raw groundwater), b) Filter B - treated groundwater with overnight interruption, c) Filter C1 – treated groundwater with manual sampling, d) Filter C2 – treated groundwater with automatic sampling. Legend for the colors: green = r > 0.900, red = 0.900 > r > 0.500, black = r < 0.500. ... 239

Table 6.11: Descriptive statistics of dissolved oxygen and temperature of treated groundwater from a 2-day monitoring campaign in August 2023. ..... **Error! Bookmark not defined.**

Table 6.12: Experimental parameters of arsenic continuous adsorption from different groundwater matrices onto ICG (flow rate 5 mL.min^{-1} and 6 g of ICG, EBCT of 12 min, breakthrough point of 10 µg L^{-1}). 241

Table 7.1: Operating conditions of lab-scale fixed-bed column treatment with ICG and Bayoxide E33. 253

Table 7.2: Inventory of 1kg iron-coated cork granulates as an adsorbent for treating arsenic-contaminated water. 256

Table 7.3: Inventory for producing 1 ton of cork granulates (0.25 – 8 mm). 257

Table 7.4: Energy necessary to produce 1 kg of iron-coated cork granulates in medium lab scale. 257

Table 7.5: Inventory for using 1 kg of Bayoxide E33 (crystalline α-ferric oxide hydroxide) as adsorbent for treating arsenic-contaminated water. The inventory data were obtained from Hu, Rana et al. (2020), who extracted data from Bonton, Bouchard et al. (2012), Encina, Distaso et al. (2015), Gurung, Tang et al. (2018) and Villacís-García, Ugalde-Arzate et al. (2015). .. 258

Table 7.6 : Environmental impacts of each lab scale production phase for 1 kg of iron-coated cork granulates, including cork granulates impacts. 260

Table 7.7: Comparison between the environmental impact of producing 1 kg of each adsorbent. 262

Table 7.8: Estimates of the life cycle impacts of the amount of each adsorbent needed for the treatment of 1000 L of arsenic-contaminated water by ReCIPe 2016 method. 271

Table 7.9: Cost analysis for arsenic removal from water (C_0 = 1 mg As(V) L^{-1}) by adsorption onto iron-coated cork granulates or Bayoxide E33 (1 m^3). 277

List of symbols

Nomenclature

a	Initial rate of adsorption/desorption (mg g^{-1} h^{-1})
a_{ya}	Yan model empirical parameter
BV_b	Bed volume at breakthrough
b	Coverage scale factor that corresponds to the reciprocal of the coverage at which the adsorption/desorption rate has fallen to 1/e of its initial value (g mg^{-1})
BV_b	Bed volume at breakthrough
BV_s	Bed volume at saturation
C	Concentration of adsorbate at time t (mg L^{-1})
C_d	Concentration of adsorbate left in the solution (mg L^{-1})
C_f	Final concentration of the adsorbate (mg L^{-1})
C_i	Initial concentration of the adsorbate (mg L^{-1})
C_0	Initial concentration (mg L^{-1})
d_e	Desorption efficiency (%)
Eh	Electrical potential (V)
F	Faraday constant (23061 cal/V)
k_1	Pseudo-first-order kinetic constant (h^{-1})
k_2	Pseudo-second-order kinetic constant (g mg^{-1} h^{-1})
K_o	Standard equilibrium constant
K_F	Freundlich constant ($mg^{(1-1/n)}$ $L^{1/n}$ g^{-1})
K_L	Langmuir constant (L mg^{-1})
K_{YN}	kinetic constant of Yoon-Nelson model (min^{-1})
m	Mass of adsorbent (g)
M	Mass of adsorbent in the column (g)

n	Dimensionless parameter related to adsorbent-adsorbate affinity
p	Probability of observing variation in results due to random factors
q	Adsorption capacity (mg g^{-1})
q_{ad}	Adsorption capacity (mg g^{-1})
q_b	Adsorption capacity at breakthrough (mg g^{-1})
q_d	Desorption capacity (mg g^{-1})
q_e	Adsorption capacity at equilibrium (mg g^{-1})
q_{loss}	Reduction in the adsorption capacity (%)
q_{max}	Maximum adsorption capacity (mg g^{-1})
q_o	Initial adsorption capacity of the fresh adsorbent (mg g^{-1})
q_t	Adsorbed/desorbed amount at time t (mg g^{-1})
q_{TH}	Thomas model predicted adsorption capacity (mg g^{-1})
q_s	Adsorption capacity at saturation point (mg g^{-1})
Q	Flow rate (L min^{-1})
Q_{ya}	Yan model predicted adsorption capacity (mg g^{-1})
r^2	Coeficient of determination
R	Gas constant of 8.314×10^{-3}kJ/(mol K)
t	Time (h)
t_b	Time of breakthrough (h)
t_{exp} 50%	Time required to achieve 50% saturation (min)
t_s	Saturation time
t_{YN} 50%	Yoon-Nelson predicted time required to achieve 50% saturation (min)
T	Temperature (°C)
T_K	Temperature (K)
V	Solution volume (L)
V_b	Breakthrough volume (L)

V_s	Saturation volume (L)
y_b	Arsenic removal efficiency at breakthrough (%)
y_s	Arsenic removal efficiency at saturation (%)
α	Significance level
ΔG^0	Standard Gibbs free energy change
ΔH^0	Enthalpy change
ΔS^0	Entropy change

Indices

As	Arsenic
As(III)	Arsenite
As(V)	Arsenate
As_2O_3	Arsenic trioxide
Cl^-	Chloride
EDTA	Di-sodium ethylenediaminetetra-acetate
Fe	Iron
$FeCl_3$	Iron(III) chloride
Fe^{2+}	Ferrous cation
Fe^{3+}	Ferric cation
$Fe(OH)_3$	Iron hydroxide
$HAsNa_2O_4{\cdot}7H_2O$	Sodium Arsenate Dibasic Heptahydrate
$HAsO_4^{2-}$	Hydrogen arsenate
$H_2AsO_3^-$	Dihydrogen arsenite
$H_2AsO_4^-$	Dihydrogen arsernate
H_3AsO_3	Arsenous acid
HCl	Hydrochloric acid
HNO_3	Nitric acid

KNO_3	Potassium nitrate
KOH	Potassium hydroxide
$KSb(OH)_6$	Potassium Hexahydroxoantimonate
NaCl	Sodium chloride
Na_2CO_3	Sodium carbonate anhydrous
Na_2HPO_4	Di-sodium hydrogen phosphate dihydrate
NaOH	Sodium hydroxide
Ni	Nickel
NO_3^-	Nitrate
PO_4^{3-}	Phosphate
Sb	Antimony
Sb(III)	Antimonite
Sb(V)	Antimonate
$SbCl_3$	Antimony trichloride
SO_4^{2-}	Sulfate

Acronyms and Abbreviations

AD	Adsorption
ANOVA	Analysis of variance
ATP	Adenosine triphosphate
BDP	Bengal Delta Plain
BTC	Breakthrough curve
BV	Bed volume
DE	Desorption
DO	Dissolved oxygen
DoE	Design of experiments

EBCT	Empty Bed Contact Time
EDS	Electron dispersive X-ray spectroscopy
EDTA	Ethylenediaminetetraacetic acid
EIA	Environmental Impact Assessment
FAAS	Flame Atomic Absorption Spectrometry
FHS	Ferric Hydroxide-based Sorbent
FR	Flow Rate
FU	Functional Unit
GAC	Granular Activated Carbon
GFAAS	Graphite Furnace Atomic Absorption Spectrometry
GLO	Global
GFH	Granular Ferric Hydroxide
GW	Groundwater
HRT	Hydraulic Retention Time
ICG	Iron-coated Cork Granulates
ICP-OES	Inductively Coupled Plasma – Optical Emission Spectrometry
LCA	Life Cycle Assessment
LCI	Life Cycle Inventory
MTZ	Mass transfer zone
MOFs	Metal-Organic Frameworks
NGOs	Non-governmental Organizations
OECD	Organization for Economic Co-operation and Development
PET	Polyethylene Terephthalate
PFAS	Poly- and Perfluoroalkyl Substances
pH_{PZC}	Point of Zero Charge
PT	Portugal
RER	Region of Europe

SE	Standard Error
SEM	Scanning Electron Microscopy
SDGs	Sustainable Development Goals
STLC	Soluble Threshold Limit Concentration
S/L	Solid/Liquid ratio
TCLP	Toxicity Characteristic Leaching Procedure
TTLP	Total Threshold Limit Concentration
TDS	Total Dissolved Solids
TOC	Total Organic Carbon
TRL	Technology Readiness Level
USPHS	U.S. Public Health Service
WHO	World Health Organization
WTRs	Water Treatment Residues

1 INTRODUCTION

1.1 Motivation and Relevance

1.1.1 The adsorbates: arsenic and antimony

1.1.1.1 Arsenic

Arsenic (As) is a pnictogen, chemically classified as a metalloid, which shares the same periodic table group with antimony (Sb) and phosphorus (P). Arsenic is environmentally present in both organic and inorganic species, being the inorganic forms more toxic and found in water bodies (Asere, Stevens et al. 2019). The most common inorganic species contain either pentavalent or trivalent As, being the trivalent form much more toxic to human health (Pintor, Vieira et al. 2018). "Arsenates" are by definition compounds of As(V) and oxygen, and "arsenite" compounds of As(III) and oxygen. Arsenate can act as a potential oxidative phosphorylation inhibitor, and arsenite can bind with reactive sulfur atoms present in many enzymes (Lim, Shukor et al. 2014). The consumption of these forms of As is a serious concern due to their ability to interfere in vital

processes in the human body, such as ATP production and respiration (Lim, Shukor et al. 2014). Arsenic belongs to group 1 from carcinogen agents, and its major human exposure routes are through direct drinking of contaminated water and ingestion of food grown or cooked by polluted water (Sharma, Tjell et al. 2014, Natasha, Shahid et al. 2021).

Arsenic can be released into water bodies from both natural and anthropogenic sources. Arsenic appears in water mainly from a combination of natural processes, such as: weathering reactions, biological activity, volcanic emissions, and fluvial transport of As-containing mineral deposits (Smedley and Kinniburgh 2002, Villaescusa and Bollinger 2008). In addition to natural causes, anthropogenic activities such as the use of arsenic compounds in agriculture and livestock, as well as mining and industry, are strong causes of groundwater and surface water arsenic contamination (Ungureanu, Santos et al. 2015). The prevention of arsenic water pollution from anthropological activities requires a proper water management plan and actions from local authorities, however, controlling natural sources of As is more complex and relies upon mitigation technologies and strict management of prevention measures (Li, Yang et al. 2020).

Arsenic's first guideline for drinking water was established 80 years ago (at least in the U.S) (USPHS 1943, Pontius 1994). In 1958, the World Health Organization (WHO) published the first International Standards for Drinking Water which fixed an admissible level of arsenic at 0.2 mg L^{-1} (World Health 1958). Nevertheless, the concern about its consumption has been known for millennia, and for some time, its name was used as a synonym for poison. Much time has passed, but water contamination with arsenic is still an obstacle in many parts of the globe. And not surprisingly, the publications of academic papers about arsenic in drinking water have raised, in two decades (1992-2011), from the least to the most researched contaminant among the most frequently studied pollutants: arsenic, nitrate, fluoride, lead, and cadmium (Fu, Wang et al. 2013). Moreover, in the last decade there was an increase of nearly 50% in the number of Scopus-Indexes documents related to arsenic and drinking water.

Arsenic poisoning can lead to serious human health effects even at low concentrations. Approximately 230 million people worldwide are affected by arsenic contamination in 108 countries, spread in all six continents, but mainly in Southeast Asia (Shaji, Santosh et al. 2021), where water infrastructure is deficient in attaining safe limits, and the solution primarily depends on affordable treatment technologies. In addition, 92% of OECD nations are affected by arsenic contamination in groundwater (Shaji, Santosh et al. 2021). So, exposure to arsenic is still a major global health issue, and further deep investigation should be conducted on its effects on human health (Quansah, Armah et al. 2015). The last WHO and the European Directive 98/83/EC

guideline value for As in drinking water was established as 10 µg L^{-1}, however, some developing countries still use less safe guidelines such as 30 and 50 µg L^{-1}.

Various researchers are developing more sustainable and cost-effective technologies to limit the impacts of arsenic-polluted water, from biosensors for As detection (Dieudonné, Prévéral et al. 2020) to biosorbents for As removal from water (Baig, Sheng et al. 2015, Asere, Stevens et al. 2019). Adhering to WHO guideline for arsenic in drinking water of 10 µL^{-1} is one of the best ways to control poisoning and morbidity (Duker, Carranza et al. 2005, WHO 2017).

1.1.1.2 Antimony

Antimony is a hazardous pollutant and toxic for humans which can enter the body through oral, skin, and inhalation forms (Nishad and Bhaskarapillai 2021). In surface and groundwaters, antimony (Sb) usually exists in two oxidative states, as the inorganic oxyanions, Sb(III) and Sb(V) (Zhang, O'Loughlin et al. 2022). The less oxidized form is ten times more harmful than the more oxidized one (Qi, Wang et al. 2021). Antimony (Sb) is also a metalloid from the pnictogen group of the periodic table and shares many characteristics with arsenic, including its toxicity to humans and its adsorption behavior. The more oxidized species of both metalloids are usually found under oxic conditions, just as the more reduced species are found under anoxic conditions (Gebel 1997, Smichowski, Madrid et al. 1998, Müller, Chavez-Capilla et al. 2022).

There are various sources of contamination of water bodies by antimony, from natural erosion of antimony ores or minerals to anthropogenic sources, such as industrial and mining activities. A recent concern is related to the leaching of antimony from PET plastics (Nishad and Bhaskarapillai 2021). The industrial application of antimony is wide, for example, in the production of semiconductors, infrared detectors, acid batteries, ceramics, glasses, plastics, and flame retardants (Zhang, Ding et al. 2021, Dembele, Akcil et al. 2022). Due to its limited availability it will be in risk of supply in the future (Cole-Hamilton 2020).

Sb levels in drinking water may not exceed 20 µg L^{-1} per liter, as guidelines from the World Health Organization suggest (WHO 2022). More restricted limits were established by the European Union (EU) of 10 µg L^{-1} (European Union 2020), the United States (USA) and Canada of 6 µg L^{-1} (Canada 1999, EPA 2002), and China of 5 µg L^{-1} ((MOH) 2006). Currently, the presence of antimony in the aquatic systems of countries like China, the USA, Mexico, Australia, Spain, Slovakia and New Zealand is a serious problem (Herath, Vithanage et al. 2017). High levels of antimony were also reported in other countries in the water close to abandoned mining areas: 15,000 µg L^{-1} in Italy (Cidu, Biddau et al. 2013), 2,500 µg L^{-1} in Poland (Lewińska,

Karczewska et al. 2018), 2,138 µg L^{-1} in Portugal (Carvalho, Neiva et al. 2014), 750 µg L^{-1} in Ghana (Serfor-Armah, Nyarko et al. 2006), and 271.6 µg L^{-1} in Turkey (Kurt, Yıldırım et al. 2021).

1.1.2 The process: adsorption

In terms of advanced water treatment technologies, adsorption is considered the most efficient and inexpensive solution (Patel 2019, Dudek and Kołodyńska 2022), and it holds better prospects than other treatment techniques for arsenic removal (Alka, Shahir et al. 2021), e.g., ion-exchange, phytoremediation, phytobial remediation, chemical precipitation, electrokinetic techniques, electrocoagulation, and membrane separation. Conventional processes such as precipitation, coagulation and membrane separation for advanced water treatment are disadvantageous either due to high operational cost (Brion-Roby, Gagnon et al. 2018) or formation of toxic sludge (Ungureanu, Santos et al. 2017). Adsorption is particularly suited for places requiring systems with simple operation, little toxic sludge formation, and regeneration possibility (Asere, Stevens et al. 2019).

The high selectivity of adsorption makes it an important technique for wastewater treatment, particularly for highly toxic species given its efficacy in low concentrations. Moreover, adsorption can be used to recover valuable substances, thereby contributing to the sustainability of several industries that depend on these essential materials.

The adsorbents can be divided into three groups: synthetic, natural, and semi-synthetic, being the last one also known as “modified biosorbents” and considered the group with the most cost-effective results (Patel 2019). Among different modification methods, iron incorporation is the most common transformation of biosorbents to increase arsenic removal rates.

Commercially available adsorbents, such as activated carbon, present some disadvantages, such as high production price and difficulty in regeneration, leading to an increase in treatment costs (Zeng, Yu et al. 2020). Worldwide studies are being conducted to develop more efficient, economic, and sustainable adsorbents to remove arsenic from water, biosorbents being one of the most promising alternatives to remove toxic metals and metalloids from contaminated waters.

Coating a common and cheap material to turn it into an adsorbent is a common practice among researchers to improve adsorption capacity and increase adsorption rate. The most common coating materials are iron and alumina and other metals, such as zirconium and manganese.

Beyond the increase in adsorbent capacity, iron-impregnated adsorbents are non-toxic, low cost and accessible in large quantities (Hao, Liu et al. 2018).

Most of the adsorbents presented in literature are developed based only on tests conducted in batch mode, where the influent is treated sequentially (in cycles) in the reactor, for a pre-determined time (Bullen, Lapinee et al. 2020). In continuous mode the influent and effluent are continuously pumped into and out of the reactor. Figure 1.1 illustrates batch and continuous operation modes.

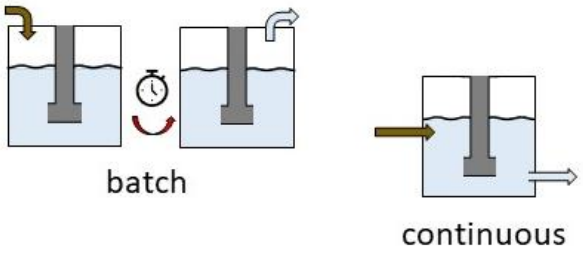


Figure 1.1: Illustration of batch and continuous treatment.

For industrial and commercial purposes, the adsorption treatment in continuous mode, more specifically in a fixed-bed column, is preferable (Patel 2019). The performance of fixed-bed columns for arsenic treatment could be affected by temperature, pH, flow rate, adsorbent quantity (bed height), hydraulic retention time, initial concentration of adsorbate, and the presence of other chemical components, such as competitive ions (sulphate, phosphate, bicarbonate, nitrate, chloride), and natural organic matter (Sosa, Armienta et al. 2020).

1.1.3 The adsorbent: iron-coated cork granulates

Raw lignocellulosic biomasses have been gaining attention in recent years to produce more sustainable adsorbents (Maia, Soares et al. 2021). Cork is a lignocellulosic natural material extracted from the bark of the cork oak tree, and it is known for its traditional usage as stopper for wine bottling (Pintor, Ferreira et al. 2012). Cork is extracted from the trunk and major branches of the *Quercus suber* L. tree in semi-tubular shapes, with sufficient care not to damage the tree, which is supposed to recover and regenerate the cork (Oliveira and Costa 2012). Cork granulates of varying densities and qualities are produced from the several waste materials that result either from cork oak forest extraction process or from the processing operations (Jesus, Nunes da Silva et al. 2023). Cork granulates ranges from 0.25 to 8 mm and below that size, the material is usually designated as cork powder (Pintor, Ferreira et al. 2012, Rives, Fernandez-Rodriguez et al. 2013). Cork oak forests are mostly located in Portugal (34%),

Spain (27%), Morocco (18%), Algeria (11%), Tunisia (4%), France (3%) and Italy (3%), being Portugal also the largest producer (46%) and cork exporter (APCOR 2020).

The general properties of cork have been previously reported in the literature (Gibson, Easterling et al. 1981, Rosa, Pereira et al. 1990, Vaz and Fortes 1998, Gandini, Pascoal Neto et al. 2006, Şen, Van den Bulcke et al. 2014). Cork has mechanical and thermal properties compared to natural and synthetic foams (Figure 1.2), making it elastic, durable, antimicrobial, and shock-adsorbent.

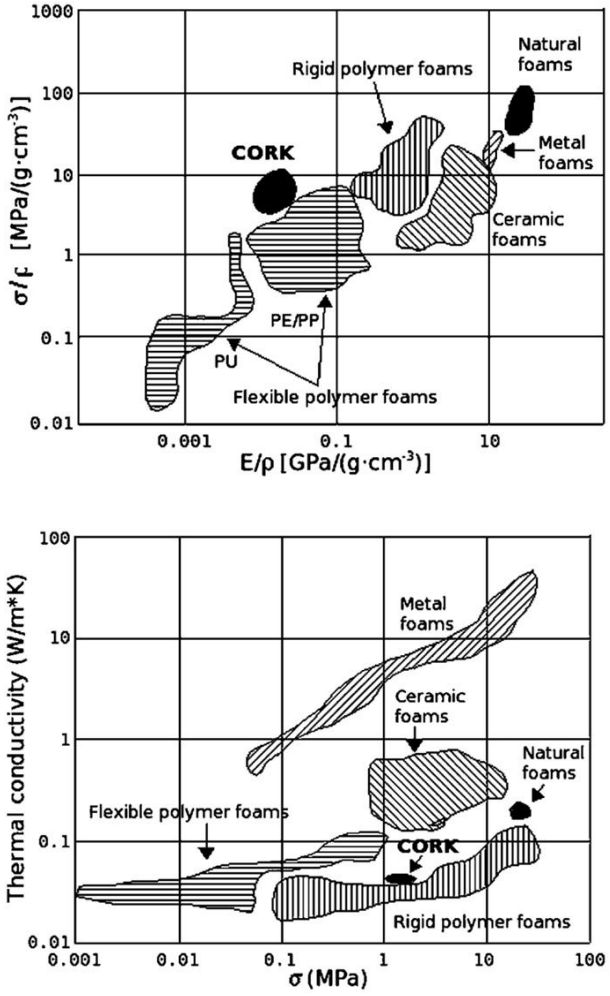


Figure 1.2. Comparison between a) specific compressive strength and specific modulus, and b) thermal conductivity and compressive strength, for cork and other foamed materials (Silva, Sabino et al. 2005, Duarte and Bordado 2015)

Cork is chemically composed of suberin (33-62%), lignin (13-29%), polysaccharides (6-26%), and extractives (8.5-24%) with a low density of 120-240 kg m^{-3} (Pintor, Ferreira et al. 2012). Due to its high porosity, chemical and physical stability, and original renewable characteristic, cork-based materials has been widely studied as a biosorbent for water pollutants, including heavy metals, oils, and contaminants of emerging concern, such as pesticides, hormones,

pharmaceuticals, among others (López-Mesas, Navarrete et al. 2011, Crespo-Alonso, Nurchi et al. 2013, Krika, Azzouz et al. 2016, Mallek, Chtourou et al. 2018, de Aguiar, Guimarães Neto et al. 2019, Manzo, Goya-Pacheco et al. 2019, Silva, Martins et al. 2020, Wang, Luo et al. 2022). The first commercial application of cork for environmental problems were for sorption of oil spill (Pintor, Ferreira et al. 2012).

Raw cork has good adsorption capacities towards a wide variety of heavy metals and organic pollutants as reported by (Pintor, Ferreira et al. 2012, Jesus, Nunes da Silva et al. 2023). Nevertheless, novel adaptations on cork materials, such as metal impregnation, chemical activation and carbonatization seek to improve performance to levels comparable to commercial adsorbents.

Due to their low density and high chemical and physical resiliency, cork granulates were shown to be particularly effective as supports. They are generated as byproducts of the cork industry, by grinding cork to millimetre-sized particles. The surface area of cork granulates with size of 1-2 mm was reported as 16.3 $m^2\ g^{-1}$, with a pore diameter of 1-1.34 μm and a pore volume of 2.83 $cm^3 g^{-1}$ which indicates the presence of macropores (Pintor, Ferreira et al. 2012).

Research by the group has resulted in the development of iron-coated natural adsorbents for removing arsenic with good results (Vieira, Pintor et al. 2017, Pintor, Vieira et al. 2018). The adsorption capacity of ICG in bath mode was found to be 4.9±0.3 mg As(V) g^{-1} and 4.3±0.1 mg As(III) g^{-1} (Pintor, Vieira et al. 2018). The iron-coated cork granulates were also tested in batch mode for the adsorption of antimony, achieving an adsorption capacity of 12±2 mg Sb(V) g^{-1} and 5.8±0.5 mg Sb(III) g^{-1} (Pintor, Vieira et al. 2020); phosphorus (Pintor, Vieira et al. 2020) and multicomponent solutions (Pintor, Brandão et al. 2020).

Iron-coated cork granulates (ICG) are then modified biosorbents that were developed and optimised by this research group developed by the optimization of cork type (low density cork granulates and regranulated cork granulates), coating pH (5 and 7), coating temperature (10 and 30°C), iron concentration (0.05 and 0.1) and solid liquid ratio (10 and 20 g L^{-1}) (Pintor, Vieira et al. 2018). Characterization of the optimized material has previously been carried out through Scanning Electron Microscopy (SEM) and Energy-Dispersive X-ray Spectroscopy (EDS) analysis (Pintor, Vieira et al. 2018). SEM micrographs of cork granulates before and after coating revealed that the iron was deposited inside the macropores in uneven distribution, rather than as a homogeneous thin layer on the surface of the cork granulates (Figure 1.3). EDS analysis revealed iron peaks after the ferric loading. The pH_{PZC} of iron-coated cork granulates was found to be approximately 6, lying between cork and ferrihydrite (Pintor, Vieira et al. 2018).

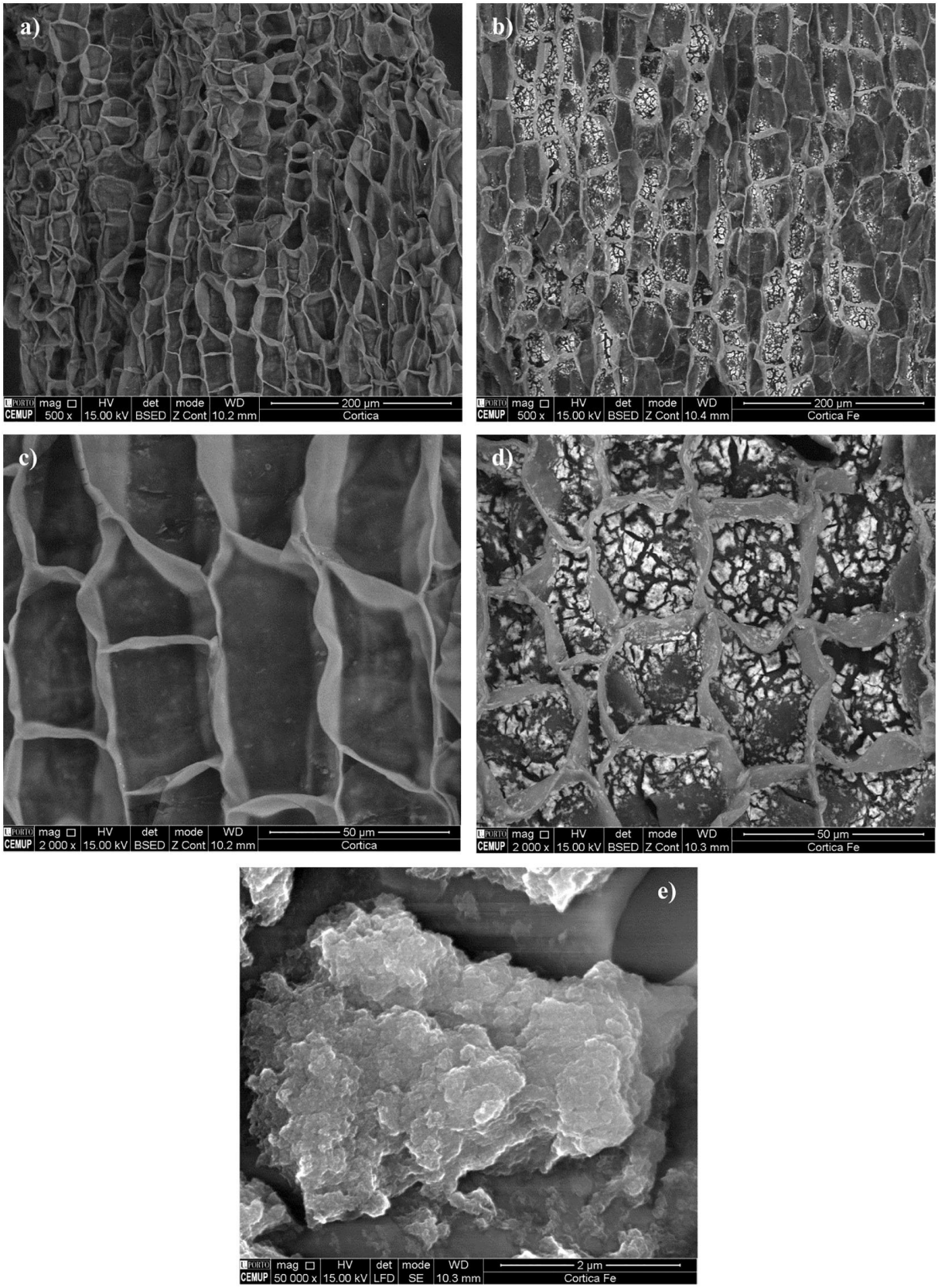


Figure 1.3: SEM micrographs of a) raw and b) iron-coated cork granulates (500x magnification), c) raw and d) iron-coated cork granulates (2.000x magnification), e) detailed iron coating (50,000x magnification) (Pintor, Vieira et al. 2018).

1.2 Thesis objectives and Layout

The main goal of this these is to develop a novel adsorption column to remove arsenic and antimony in continuous mode from water using iron-coated cork granulates as adsorbents. First, a literature review on both adsorption and desorption of arsenic and antimony in continuous mode was carried out to establish the context for the development of the study. Afterwards, experimental work using iron-coated cork granulates as adsorbents and synthetic and real water as contaminated water samples were executed, with the following objectives in mind:

i. To select optimal design parameters of a lab-scale fixed-bed column based on flow rate, bed high (adsorbent mass) and temperature according to their effect on breakthrough parameters;
ii. To investigate the removal efficiency of As(V), As(III), Sb(V) and Sb(III) in a optimized fixed-bed adsorption column, and the influence of pH and adsorbate initial concentration;
iii. To evaluate both As and Sb recovery and adsorbent regeneration and its influencing factors, such as flow rate, eluent type, eluent concentration, pH and desorption time in continuous mode;
iv. To investigate the effect of different water matrices in the arsenic removal performance and breakthrough parameters;
v. To analyse the sustainability performance with life cycle assessment (LCA) of the novel adsorption column and to compare it to a commercial adsorbent.

The execution of this work also aims to achieve the following environmental and social goals: providing more cost effective and environmentally friendly technologies for As and Sb remediation; designing easy-to-operate treatment solutions that can be applied in rural areas or remote mining field. Furthermore, this thesis aims to add value to the cork sector by providing a new application for cork byproducts.

Following this line of thought, the present thesis is organized into eight chapters that address general and specific concepts, experimental results and discussion, and the main conclusions. To highlight that, the thesis is presented based on publication outputs (accepted or under submission), namely two review articles and five experimental-based articles.

The eight chapters are organised as follows:

- This chapter, **Chapter 1 (Introduction),**
- **Chapter 2** consists of a **Literature Review** on the adsorption of arsenic and antimony in continuous mode using different adsorbents. It also presents a review on the desorption of arsenic and antimony, by exploring the differences between eluent and adsorbent types.
- **Chapter 3 (Removal of arsenic from aqueous solution by continuous adsorption onto iron-coated cork granulates)** presents the first results of adsorption of arsenic in continuous mode onto iron-coated cork granulates (ICG). It includes an optimization of the fixed-bed adsorption column using the design of experiment, a thermodynamic study and the investigation of the effect of pH, temperature and initial concentration on the breakthrough curves.
- **Chapter 4 (Regeneration of arsenic-loaded iron-coated cork granulates)** reports the results of the desorption of arsenic-saturated ICG using different eluents. The study includes the desorption kinetics of arsenic by the best eluents and the effect of different water matrices on the ICG regeneration after many adsorption-desorption cycles.
- **Chapter 5 (Antimony adsorption and desorption: batch and continuous mode studies)** presents the results of both adsorption and desorption of antimony from ICG in continuous mode. The adsorption tests were carried out in similar conditions from Chapter 3 and different eluents were investigated from the antimony desorption. The effect of the Sb desorption on the ICG integrity was also studied.
- **Chapter 6 (Adsorption of arsenic from arsenic-contaminated groundwaters)** focuses on the adsorption of arsenic from natural groundwaters onto ICG.
- **Chapter 7 (Environmental impacts of arsenic removal from water using iron-coated cork granulates)** presents a life-cycle assessment of ICG production and use to treat arsenic-contaminated water. The environmental performance was compared to those of a commercial adsorbent.
- **Chapter 8 (Conclusion and Future work)** summarizes the main conclusions of this thesis. Some suggestions for future research are also provided in this last chapter.

1.3 References

(1943). "Public Health Service Drinking Water Standards." Public Health Reports (1896-1970) **58**(3): 69-82.

(MOH), M. o. H. o. t. P. s. R. o. C. (2006). Chinese National Standards GB 3838-2002: Sanitary Standards for Drinking Water Quality;. S. A. o. C. (SAC). Hongkong, China., China Water Risk:.

Alka, S., S. Shahir, N. Ibrahim, M. J. Ndejiko, D.-V. N. Vo and F. A. Manan (2021). "Arsenic removal technologies and future trends: A mini review." Journal of Cleaner Production **278**: 123805.

APCOR. (2020). "Boletim estatístico - Cork 2020." from https://www.apcor.pt/portfolio-posts/boletim-estatistico-2020/#dearflip-df_22474/17/.

Asere, T. G., C. V. Stevens and G. Du Laing (2019). "Use of (modified) natural adsorbents for arsenic remediation: A review." Science of The Total Environment **676**: 706-720.

Baig, S. A., T. Sheng, Y. Hu, J. Xu and X. Xu (2015). "Arsenic Removal from Natural Water Using Low Cost Granulated Adsorbents: A Review." CLEAN – Soil, Air, Water **43**(1): 13-26.

Brion-Roby, R., J. Gagnon, J.-S. Deschênes and B. Chabot (2018). "Investigation of fixed bed adsorption column operation parameters using a chitosan material for treatment of arsenate contaminated water." Journal of Environmental Chemical Engineering **6**(1): 505-511.

Canada, H. (1999). Guidelines for Canadian Drinking Water Quality: Guideline Technical Document – Antimony. Otawwa, Ontario.

Carvalho, P. C. S., A. M. R. Neiva, M. M. V. G. Silva and E. A. F. da Silva (2014). "Geochemical comparison of waters and stream sediments close to abandoned Sb-Au and As-Au mining areas, northern Portugal." Geochemistry **74**(2): 267-283.

Cidu, R., R. Biddau, E. Dore and A. Vacca (2013). "Antimony Dispersion at Abandoned Mines in Sardinia, Italy." Procedia Earth and Planetary Science **7**: 171-174.

Cole-Hamilton, D. (2020). "The Role of Chemists and Chemical Engineers in a Sustainable World." Chemistry **26**(9): 1894-1899.

Crespo-Alonso, M., V. M. Nurchi, R. Biesuz, G. Alberti, N. Spano, M. I. Pilo and G. Sanna (2013). "Biomass against emerging pollution in wastewater: ability of cork for the removal of ofloxacin from aqueous solutions at different pH." Journal of Environmental Chemical Engineering **1**(4): 1199-1204.

de Aguiar, T. R., J. O. A. Guimarães Neto, U. Şen and H. Pereira (2019). "Study of two cork species as natural biosorbents for five selected pesticides in water." Heliyon **5**(1): e01189.

Dembele, S., A. Akcil and S. Panda (2022). "Technological trends, emerging applications and metallurgical strategies in antimony recovery from stibnite." Minerals Engineering **175**: 107304.

Dieudonné, A., S. Prévéral, D. Pignol and A. J. M. Stams (2020). "A Sensitive Magnetic Arsenite-Specific Biosensor Hosted in Magnetotactic Bacteria." Applied and Environmental Microbiology **86**(14): e00803-00820.

Duarte, A. P. and J. C. Bordado (2015). "Cork – A Renewable Raw Material: Forecast of Industrial Potential and Development Priorities." Frontiers in Materials **2**.

Dudek, S. and D. Kołodyńska (2022). "Arsenic(V) removal on the lanthanum-modified ion exchanger with quaternary ammonium groups based on iron oxide." Journal of Molecular Liquids **347**: 117985.

Duker, A. A., E. J. M. Carranza and M. Hale (2005). "Arsenic geochemistry and health." Environment International **31**(5): 631-641.

EPA, E. P. A. (2002). "National primary drinking water regulations: long term 1 enhanced surface water treatment rule. Final rule." Federal register **67**(9): 1811-1844.

European Union, C. (2008). Council Directive 98/83/EC of 3 November 1998 on the quality of water intended for human consumption, Off. J. Eur. Commun. L. **330:** 32.

Fu, H.-Z., M.-H. Wang and Y.-S. Ho (2013). "Mapping of drinking water research: A bibliometric analysis of research output during 1992–2011." Science of The Total Environment **443**: 757-765.

Gandini, A., C. Pascoal Neto and A. J. D. Silvestre (2006). "Suberin: A promising renewable resource for novel macromolecular materials." Progress in Polymer Science **31**(10): 878-892.

Gebel, T. (1997). "Arsenic and antimony: comparative approach on mechanistic toxicology." Chemico-Biological Interactions **107**(3): 131-144.

Gibson, L. J., K. E. Easterling and M. F. Ashby (1981). "The structure and mechanics of cork." Proceedings of the Royal Society of London. A. Mathematical and Physical Sciences **377**(1769): 99-117.

Hao, L., M. Liu, N. Wang and G. Li (2018). "A critical review on arsenic removal from water using iron-based adsorbents." RSC advances **8**(69): 39545-39560.

Herath, I., M. Vithanage and J. Bundschuh (2017). "Antimony as a global dilemma: Geochemistry, mobility, fate and transport." Environmental Pollution **223**: 545-559.

Jesus, J., R. Nunes da Silva and A. Pintor (2023). "Advances in Cork Use in Adsorption Applications: An Overview of the Last Decade of Research." Separations **10**(7): 390.

Krika, F., N. Azzouz and M. C. Ncibi (2016). "Adsorptive removal of cadmium from aqueous solution by cork biomass: Equilibrium, dynamic and thermodynamic studies." Arabian Journal of Chemistry **9**: S1077-S1083.

Kurt, M. A., Ü. Yıldırım, C. Güler and O. Güven (2021). "Antimony and arsenic contamination in water from antimonite mineralization: a case study from Turhal (Tokat, Northern Turkey)." Environmental Forensics: 1-13.

Lewińska, K., A. Karczewska, M. Siepak and B. Gałka (2018). "The Release of Antimony from Mine Dump Soils in the Presence and Absence of Forest Litter." International journal of environmental research and public health **15**(12): 2631.

Li, Z., Q. Yang, Y. Yang, C. Xie and H. Ma (2020). "Hydrogeochemical controls on arsenic contamination potential and health threat in an intensive agricultural area, northern China." Environmental Pollution **256**: 113455.

Lim, K. T., M. Y. Shukor and H. Wasoh (2014). "Physical, chemical, and biological methods for the removal of arsenic compounds." BioMed research international **2014**: 503784-503784.

López-Mesas, M., E. R. Navarrete, F. Carrillo and C. Palet (2011). "Bioseparation of Pb(II) and Cd(II) from aqueous solution using cork waste biomass. Modeling and optimization of the parameters of the biosorption step." Chemical Engineering Journal **174**(1): 9-17.

Maia, L. C., L. C. Soares and L. V. Alves Gurgel (2021). "A review on the use of lignocellulosic materials for arsenic adsorption." Journal of Environmental Management **288**: 112397.

Mallek, M., M. Chtourou, M. Portillo, H. Monclús, K. Walha, A. b. Salah and V. Salvadó (2018). "Granulated cork as biosorbent for the removal of phenol derivatives and emerging contaminants." Journal of Environmental Management **223**: 576-585.

Manzo, V., J. Goya-Pacheco, D. Arismendi, M. Becerra-Herrera, A. Castillo-Aguirre, R. Castillo-Felices, M. Rosero-Moreano, E. Carasek and P. Richter (2019). "Cork sheet as a sorptive phase to extract hormones from water by rotating-disk sorptive extraction (RDSE)." Analytica Chimica Acta **1087**: 1-10.

Müller, V., T. Chavez-Capilla, J. Feldmann and A. Mestrot (2022). "Increasing temperature and flooding enhance arsenic release and biotransformations in Swiss soils." Science of The Total Environment **838**: 156049.

Natasha, M. Shahid, S. Khalid, N. K. Niazi, B. Murtaza, N. Ahmad, A. Farooq, A. Zakir, M. Imran and G. Abbas (2021). "Health risks of arsenic buildup in soil and food crops after wastewater irrigation." Science of The Total Environment **772**: 145266.

Nishad, P. A. and A. Bhaskarapillai (2021). "Antimony, a pollutant of emerging concern: A review on industrial sources and remediation technologies." Chemosphere **277**: 130252.

Oliveira, G. and A. Costa (2012). "How resilient is Quercus suber L. to cork harvesting? A review and identification of knowledge gaps." Forest Ecology and Management **270**: 257-272.

Patel, H. (2019). "Fixed-bed column adsorption study: a comprehensive review." Applied Water Science **9**(3): 1-17.

Pintor, A. M. A., C. C. Brandão, R. A. R. Boaventura and C. M. S. Botelho (2020). "Multicomponent adsorption of pentavalent As, Sb and P onto iron-coated cork granulates." Journal of Hazardous Materials: 124339.

Pintor, A. M. A., C. I. A. Ferreira, J. C. Pereira, P. Correia, S. P. Silva, V. J. P. Vilar, C. M. S. Botelho and R. A. R. Boaventura (2012). "Use of cork powder and granules for the adsorption of pollutants: A review." Water Research **46**(10): 3152-3166.

Pintor, A. M. A., B. R. C. Vieira, R. A. R. Boaventura and C. M. S. Botelho (2020). "Removal of antimony from water by iron-coated cork granulates." Separation and Purification Technology **233**: 116020.

Pintor, A. M. A., B. R. C. Vieira, C. C. Brandão, R. A. R. Boaventura and C. M. S. Botelho (2020). "Complexation mechanisms in arsenic and phosphorus adsorption onto iron-coated cork granulates." Journal of Environmental Chemical Engineering **8**(5): 104184.

Pintor, A. M. A., B. R. C. Vieira, S. C. R. Santos, R. A. R. Boaventura and C. M. S. Botelho (2018). "Arsenate and arsenite adsorption onto iron-coated cork granulates." Science of The Total Environment **642**: 1075-1089.

Pintor, A. M. A., B. R. C. Vieira, S. C. R. Santos, R. A. R. Boaventura and C. M. S. Botelho (2018). "Arsenate and arsenite adsorption onto iron-coated cork granulates." Sci Total Environ **642**: 1075-1089.

Pontius, F. W. (1994). "Crafting a New Arsenic Rule." Journal AWWA **86**(9): 6-104.

Qi, P., Y. Wang, J. Zeng, K. Sui and J. Zhao (2021). "Progress in antimony capturing by superior materials: Mechanisms, properties and perspectives." Chemical Engineering Journal **419**: 130013.

Quansah, R., F. A. Armah, D. K. Essumang, I. Luginaah, E. Clarke, K. Marfoh, S. J. Cobbina, E. Nketiah-Amponsah, P. B. Namujju, S. Obiri and M. Dzodzomenyo (2015). "Association of Arsenic with Adverse Pregnancy Outcomes/Infant Mortality: A Systematic Review and Meta-Analysis." Environmental Health Perspectives **123**(5): 412-421.

Rives, J., I. Fernandez-Rodriguez, J. Rieradevall and X. Gabarrell (2013). "Integrated environmental analysis of the main cork products in southern Europe (Catalonia – Spain)." Journal of Cleaner Production **51**: 289-298.

Rosa, M. E., H. Pereira and M. Fortes (1990). "Effects of hot water treatment on the structure and properties of cork." Wood and Fiber Science: 149-164.

Şen, A., J. Van den Bulcke, N. Defoirdt, J. Van Acker and H. Pereira (2014). "Thermal behaviour of cork and cork components." Thermochimica Acta **582**: 94-100.

Serfor-Armah, Y., B. J. B. Nyarko, S. B. Dampare and D. Adomako (2006). "Levels of Arsenic and Antimony in Water and Sediment from Prestea, A Gold Mining Town in Ghana and its Environs." Water, Air, and Soil Pollution **175**(1): 181.

Shaji, E., M. Santosh, K. V. Sarath, P. Prakash, V. Deepchand and B. V. Divya (2021). "Arsenic contamination of groundwater: A global synopsis with focus on the Indian Peninsula." Geoscience Frontiers **12**(3): 101079.

Sharma, A. K., J. C. Tjell, J. J. Sloth and P. E. Holm (2014). "Review of arsenic contamination, exposure through water and food and low cost mitigation options for rural areas." Applied Geochemistry **41**: 11-33.

Silva, B., M. Martins, M. Rosca, V. Rocha, A. Lago, I. C. Neves and T. Tavares (2020). "Waste-based biosorbents as cost-effective alternatives to commercial adsorbents for the retention of fluoxetine from water." Separation and Purification Technology **235**: 116139.

Silva, S. P., M. A. Sabino, E. M. Fernandes, V. M. Correlo, L. F. Boesel and R. L. Reis (2005). "Cork: properties, capabilities and applications." International Materials Reviews **50**(6): 345-365.

Smedley, P. L. and D. G. Kinniburgh (2002). "A review of the source, behaviour and distribution of arsenic in natural waters." Applied Geochemistry **17**(5): 517-568.

Smichowski, P., Y. Madrid and C. Cámara (1998). "Analytical methods for antimony speciation in waters at trace and ultratrace levels. A review." Fresenius' Journal of Analytical Chemistry **360**(6): 623-629.

Sosa, A., M. A. Armienta, A. Aguayo and O. Cruz (2020). "Evaluation of the influence of main groundwater ions on arsenic removal by limestones through column experiments." Science of The Total Environment ***727***: 138459.

Ungureanu, G., S. Santos, R. Boaventura and C. Botelho (2015). "Arsenic and antimony in water and wastewater: Overview of removal techniques with special reference to latest advances in adsorption." Journal of Environmental Management **151**: 326-342.

Ungureanu, G., S. C. R. Santos, I. Volf, R. A. R. Boaventura and C. M. S. Botelho (2017). "Biosorption of antimony oxyanions by brown seaweeds: Batch and column studies." Journal of Environmental Chemical Engineering **5**(4): 3463-3471.

Vaz, M. F. and M. Fortes (1998). "Friction properties of cork." Journal of materials science **33**: 2087-2093.

Vieira, B. R. C., A. M. A. Pintor, R. A. R. Boaventura, C. M. S. Botelho and S. C. R. Santos (2017). "Arsenic removal from water using iron-coated seaweeds." Journal of Environmental Management **192**: 224-233.

Villaescusa, I. and J.-C. Bollinger (2008). "Arsenic in drinking water: sources, occurrence and health effects (a review)." Reviews in Environmental Science and Bio/Technology **7**(4): 307-323.

Wang, Q., C. Luo, Z. Lai, S. Chen, D. He and J. Mu (2022). "Honeycomb-like cork activated carbon with ultra-high adsorption capacity for anionic, cationic and mixed dye: Preparation, performance and mechanism." Bioresource Technology **357**: 127363.

WHO (2022). Guidelines for drinking-water quality: incorporating the first and second addenda. Geneva, World Health Organization.

World Health, O. (1958). International standards for drinking-water. Geneva, World Health Organization.

World Health, O. (2017). Guidelines for drinking-water quality: fourth edition incorporating first addendum. Geneva, World Health Organization.

Zeng, H., Y. Yu, F. Wang, J. Zhang and D. Li (2020). "Arsenic(V) removal by granular adsorbents made from water treatment residuals materials and chitosan." Colloids and Surfaces A: Physicochemical and Engineering Aspects **585**: 124036.

Zhang, Y., C. Ding, D. Gong, Y. Deng, Y. Huang, J. Zheng, S. Xiong, R. Tang, Y. Wang and L. Su (2021). "A review of the environmental chemical behavior, detection and treatment of antimony." Environmental Technology & Innovation **24**: 102026.

Zhang, Y., E. J. O'Loughlin and M. J. Kwon (2022). "Antimony Redox Processes in the Environment: A Critical Review of Associated Oxidants and Reductants." Journal of Hazardous Materials: 128607.

2 LITERATURE REVIEW

This section is based on:

M. A. Carneiro, A. M. A. Pintor, R. A. R. Boaventura and C. M. S. Botelho, *Current Trends of Arsenic Adsorption in Continuous Mode: Literature Review and Future Perspectives*. Sustainability, 2021. 13(3): p. 1186.

Carneiro, M. A., Pintor, A. M. A., Boaventura, R. A. R., & Botelho, C. M. S. (2024). Arsenic and antimony desorption in water treatment processes: Scaling up challenges with emerging adsorbents. Science of The Total Environment, 929, 172602. doi:https://doi.org/10.1016/j.scitotenv.2024.172602.

2.1 Arsenic adsorption in continuous mode: adsorbents type

2.1.1 Introduction

This first section of the literature review chapter aims to summarize the tendency of research on arsenic removal in continuous mode, based on an analysis of published articles in the last 25 years. The results reported in the literature will be compared in terms of initial concentration (C_o), maximum adsorption capacity (Q_{max}), time of breakthrough (t_b) at 10 µg L^{-1}, bed volumes treated before breakthrough (BV_b) at 10 µg L^{-1}. Part of this research focuses on (modified) biosorbents, which are important materials the aiming circularity of the water treatment processes. Antimony will be discussed in the end of this section since there are significantly fewer studies published about adsorption in continuous mode of this element.

2.1.2 Metal (hydr)oxides

Iron oxides are created by the precipitation of Fe^{3+} and the resulting substance characteristics such as chemical structure, composition and physical aspects can vary with different preparative techniques (Streat, Hellgardt et al. 2008). Iron oxides and hydroxides are the most common coating substances in sand columns for arsenic removal (Khan, Rasul et al. 2000, Thirunavukkarasu, Viraraghavan et al. 2002, Manna, Dey et al. 2003, Guo, Stüben et al. 2007, Chang, Song et al. 2008, Wang, Sun et al. 2016, Chaudhry, Zaidi et al. 2017) due to their affinity with arsenic and relatively higher abundance in nature.

The combination of iron with another metal oxide is commonly investigated in column operation mode to increase arsenic removal (Gupta and Ghosh 2009, Bullen, Lapinee et al. 2020). Iron-zirconium binary oxide-coated sand (IZBOCS) achieved a maximum adsorption capacity of 28.95 mg g^{-1} by the Thomas model (Chaudhry, Zaidi et al. 2017), while zirconium oxide-coated sand only achieved an adsorption capacity of 0.042 mg g^{-1} using the same adsorption model (Chaudhry, Khan et al. 2017).

Dynamic tests with other metal-based adsorbents also show good results. Zirconium metal-organic framework column experiments were able to reduce arsenic initial concentration from 100 µg L^{-1} to 10 µg L^{-1} for 2270 and 1775 bed volumes (BV), for As(III) and As(V), respectively (He, Deng et al. 2019). Manganese performance was also investigated in column experiments conducted with natural manganese oxides (Ouvrard, Simonnot et al. 2002) and manganese-coated sand (MCS) (Chang, Song et al. 2008) for arsenic removal. Table 2.1shows characteristics of dynamic adsorption studies conducted with metal (hydr)oxides.

The crystalline hydrous ferric oxide (CHFO) was able to treat a great amount of arsenic-contaminated solution (14,000 BV) with an outlet concentration below WHO recommended value. The longer time of breakthrough of 18 days was achieved by manganese-coated sand (MCS) in a pilot-scale plant. Metal (hydr)oxides are usually impregnated in other materials to increase arsenic removal efficiency or/and reduce the treatment costs, as it will be discussed in the following sections.

2.1.3 Zero-Valent Iron (ZVI)

The mechanism and behavior of arsenic adsorption by zero valent iron (ZVI) in dynamic systems were investigated in some studies (Melitas, Wang et al. 2002, Su and Puls 2004, Leupin and Hug 2005, Biterna, Arditsoglou et al. 2007, Ludwig, Smyth et al. 2009, Biterna, Antonoglou et al. 2010). Earlier investigations in column mode with zero valent iron filings, which were carried out with an inlet arsenic solution of 100 μg L^{-1} (pH 7.0), led to an outlet concentration below 1 μg L^{-1} for 500 and 12,600 pore volumes (PV), with a time residence of 20 s and 25 min, respectively (Melitas, Wang et al. 2002).

Results of dynamic adsorption studies conducted with zero valent iron presented a performance similar to metal (hydr)oxides, however the column studies with ZVI showed a substantial iron leaching of 8 to 17 mg L^{-1} in the final effluent (Leupin and Hug 2005, Biterna, Antonoglou et al. 2010), which can be a hindrance in the application of ZVI to remediate contaminated waters. The corrosion of iron by acid waters increases the iron release, which can result in an effluent with an iron concentration of 90-130 mg L^{-1} (Biterna, Antonoglou et al. 2010).

Table 2.1: Comparison between dynamic tests using metal (hydr)oxides and zero valent iron (ZVI) as adsorbents for arsenic removal.

Adsorbent	Arsenic species	C_o (μg L^{-1})	Q_{max} (mg g^{-1})	BV_b	t_b (h)	Ref.
Manganese-coated sand (MCS)	As	1,000	0.079	250 pore volumes	18 days[1]	(Chang, Song et al. 2008)
Iron-Zirconium Binary Oxide-Coated Sand (IZBOCS)	As(V)	125	25.09-28.95		0.5-0.75	(Chaudhry, Zaidi et al. 2017)
Natural iron mineral-quartz sand columns	As(V)	500		7,000 pore volumes		(Guo, Stüben et al. 2007)

Adsorbent	Arsenic species	C_o (µg L^{-1})	Q_{max} (mg g^{-1})	BV_b	t_b (h)	Ref.
Crystalline hydrous ferric oxide (CHFO)	As	320-400		14,000		(Manna, Dey et al. 2003)
Zirconium oxide-coated sand	As(III)	500	0.03310-0.04223		5.33-8.33	(Chaudhry, Khan et al. 2017)
Zirconium metal organic frameworks (UiO-66)	As(III)	100		2,270		(He, Deng et al. 2019)
	As(V)	100		1,775		(He, Deng et al. 2019)
Hydrated stannic oxide (HSO)	As(III)	1000		2,400		(Manna and Ghosh 2007)
	As(V)	1000		450		(Manna and Ghosh 2007)
Zero valent iron (ZVI)	As(V)	100		1900		(Biterna, Arditsoglou et al. 2007)
				500-12,600 PV[2]		(Melitas, Wang et al. 2002)
					20	(Biterna, Antonoglou et al. 2010)

[1]Pilot-scale [2]For a breakthrough point of 1 µg L^{-1}

2.1.4 Minerals

Column experiments to investigate arsenic removal were carried out using a variety of minerals as adsorbents: akaganeite (Deliyanni, Bakoyannakis et al. 2003), attapulgite (Yin, Kong et al. 2017), bauxite (Bhakat, Gupta et al. 2006, Ayoob, Gupta et al. 2007, Ayoob, Gupta et al. 2007, Bhakat, Gupta et al. 2007), goethite (Ramirez-Muñiz, Perez-Rodriguez et al. 2018), hematite (Guo, Stüben et al. 2007, Guo, Stüben et al. 2008), mackinawite (Zhou, Chen et al. 2018), magnetite (Navarathna, Karunanayake et al. 2019, Shahid, Phearom et al. 2019, Shahid, Phearom et al. 2019, Shahid, Phearom et al. 2020), siderite (Guo, Stüben et al. 2007, Guo, Stüben et al. 2007, Guo, Stüben et al. 2008), schwertmannite (Dou, Mohan et al. 2013) and zeolite (Jeon, Baek et al. 2009, Baskan and Pala 2013). Iron and aluminum-based minerals are considered good adsorbents due to their known affinity for heavy metals and metalloids and to their abundance in nature.

Iron modified calcined bauxite (MCB) was investigated in column experiments for arsenic removal from aqueous solution (Bhakat, Gupta et al. 2006, Ayoob, Gupta et al. 2007, Ayoob, Gupta et al. 2007, Bhakat, Gupta et al. 2007). The breakthrough point of 10 μg L^{-1} for a 10 cm bed depth (2 cm diameter) was reached after 31 h (~270 BV) at 5 mL min^{-1} with an As(V) solution of 2 mg L^{-1} (Ayoob, Gupta et al. 2007). The breakthrough point (10 μg L^{-1}) for an As(III) solution of 1 mg L^{-1}, in similar conditions of flow rate and bed depth, was reached after 50 h (~470 BV) (Bhakat, Gupta et al. 2007). The MCB maximum adsorption capacities reported in column mode were 0.606 mg g^{-1} and 0.490 mg g^{-1}, for As(V) and As(III), respectively (Ayoob, Gupta et al. 2007, Bhakat, Gupta et al. 2007).

A novel adsorbent consisting of magnetite-rich particles (MEP) was developed with a low magnetic intensity separation from mill scale, which is constituted of wustite (FeO), hematite (α-Fe_2O_3), magnetite (Fe_3O_4), elemental iron and residual oil and grease (Shahid, Phearom et al. 2019). Column adsorption tests were carried out in four sets of packed-bed columns, each with 3.5 cm diameter and 20 cm bed height and 550 g of MEP. A synthetic wastewater containing 500 μg L^{-1} of As(V) was fed into the column at different flow rates. Breakthrough point (~10 μg L^{-1}) was reached after about 17 d and 30 d, at a feed flow rate of 6.4 mL min^{-1} and 3.2 mL min^{-1}, respectively. After saturation, at the 48th day of operation, MEP columns were regenerated with 0.2 N NaOH for 24 h at a flow rate of 1 mL min^{-1} and the sorption capacity was reinstated to the initial condition.

Column tests with natural occurring siderite, an iron carbonated mineral, led to a final effluent below 1.0 μg L^{-1} (26,000 pore volumes), using a solution containing 250 μg L^{-1} As(III) and 250 μg L^{-1} As(V) (Guo, Stüben et al. 2007). A similar study with a column packed with half siderite and half hematite content had achieved As concentration of 1.0 μg L^{-1} after 7,200 pore volumes (PV) (Guo, Stüben et al. 2007). The addition of hematite in siderite filters reduces the arsenic removal efficiency because siderite is usually more efficient to uptake As from water than hematite (Guo, Stüben et al. 2007). Siderite-hematite filters were activated with H_2O_2 which increased arsenic adsorption efficiency up to a throughput of 500 PV (Guo, Stüben et al. 2008).

Three types of granular schwertmannite, a Fe(III)-oxyhydroxy sulfate mineral, were investigated in column tests for arsenate removal (Dou, Mohan et al. 2013). The experiments were conducted in a lab-scale column with 2 cm diameter and 20 cm bed height, fed with simulated groundwater containing 210 μg L^{-1} of As(V). The irregular shape (IS) type achieved best performance and breakthrough of 10 μg L^{-1} occurred after 8,100 BV, followed by the cylindrical shape (CS) type

with 4,200 BV and the spherical shape (SS) type with 120 BV. The adsorption capacities of IS, CS and SS were 0.93, 0.66 and 0.33 mg g^{-1}, respectively.

Table 2.2 shows the results of dynamic adsorption studies conducted with minerals. It is possible to highlight the performance of magnetite derived from mill scale compared to other column studies using minerals as arsenic adsorbent. Natural siderite also achieved good results, even better than the siderite-hematite media. The other minerals, most of them modified iron, presented relatively similar results for arsenic removal.

Table 2.2: Comparison of dynamic tests using minerals as adsorbents for arsenic removal.

Adsorbent	**Arsenic species**	**C_o (µg L^{-1})**	**Q_{max} (mg g^{-1})**	**BV_b**	**t_b (h)**	**Ref.**
Iron modified calcined bauxite (MCB)	As(V)	2,000-8,000	0.470-0.606	269.2-300.64	2.15-59	(Ayoob, Gupta et al. 2007)
Iron modified calcined bauxite (MCB)	As(III)	1,000		428.02-489.17	28-96	(Ayoob, Gupta et al. 2007)
Iron modified calcined bauxite (MCB)	As(III)	1,000	0.392-0.459	427.85-489.17	28-96	(Bhakat, Gupta et al. 2007)
Iron-modified clinoptilolite	As(V)	100		300		(Baskan and Pala 2013)
Mill-scale derived magnetite particles	As(V)	100	3.60-5.00		>100	(Shahid, Phearom et al. 2019)
Magnetite-enriched particles (MEP)	As(V)	500			17-30 days	(Shahid, Phearom et al. 2019)
Mixed-valent iron oxide/magnetite	As(V)	100-1,000	10		888-1032	(Shahid, Phearom et al. 2020)

Adsorbent	Arsenic species	C_o (µg L^{-1})	Q_{max} (mg g^{-1})	BV_b	t_b (h)	Ref.
Natural siderite	As(III) + As(V)	250 + 250	1.090-2.000	11,600-26,000 PV		(Guo, Stüben et al. 2007)
Siderite-hematite	As(III) + As(V)	250 + 250		7,200 PV		(Guo, Stüben et al. 2007)
Activated Siderite-hematite	Total As	500	0.177-0.185	8,160 PV		(Guo, Stüben et al. 2008)
Goethite-polyacrylamide composite (goethite-P(AAm)	As	300		400[1]		(Ramirez-Muñiz, Perez-Rodriguez et al. 2018)
Granular schwertmannite	As(V)	200	0.33-0.93	120-8,100		(Dou, Mohan et al. 2013)
Iron-coated zeolite (ICZ)	As(V)	2,000	0.69	300		(Jeon, Baek et al. 2009)
Iron impregnated charred granulated attapulgite	As(V) As(III)	200		397 175		(Yin, Kong et al. 2017)

[1]For breakthrough point of 25 µg L^{-1}

2.1.5 Soil and Rock

Soils and rocks are also natural abundant materials, often containing minerals that enhance their arsenic uptake capacity. They stand out from other adsorbents due to the advantages of being low-cost and locally available.

The arsenic uptake capacity of natural occurring laterite soil was studied in column operation mode using arsenic solutions and real samples (Maji, Pal et al. 2007, Maji, Pal et al. 2007, Maiti, DasGupta et al. 2008, Maji, Pal et al. 2008). Fixed bed column studies conducted in a 2 cm diameter column and a bed depth of 30 cm, fed with arsenic solution of 500 µg L^{-1} at 7.75

mL min^{-1} flow rate, reached the breakthrough point at 10 µg L^{-1} after 32 h for As (V) (Maji, Pal et al. 2007), and 18.5 h for As (III) (Maji, Pal et al. 2007). The total arsenic removal by laterite soil, in similar column experiments (10 cm bed depth), with a groundwater (tube-well) sample of 0.33 ppm of arsenic was 98% (Maji, Pal et al. 2008).

Moreover, recent research has developed a novel laterite soil filter for arsenic that provides potable water to a population higher than 5,000 people (Mondal, Mondal et al. 2019). A model to predict the lifetime of the filter was validated by lab-scale and field-scale experiments. It was predicted that the novel laterite filter could last from 10 to 100 months, depending upon flow rate, size, and the arsenic concentration of the feed water.

The arsenic adsorption behavior of another soil, originated from limestone and heavily iron-coated, was investigated (Williams, Barnett et al. 2003) in a glass column with 1 cm diameter, packed with 2 g of adsorbent (1.7 cm depth). The system was fed with an arsenate solution of 1 mg L^{-1}, in order to investigate the effect of pH, pore water velocity and presence of phosphate (PO_4^{3-}). The phosphate ions produced a major effect on As(V) mobility and recovery, followed by the pore water velocity effect, with the least effect being observed due to pH variation.

A few studies reported rocks as adsorbents for arsenic removal from water. Pisolite, a mining waste composed of iron and manganese aggregate, was applied for this purpose (Pereira, Dutra et al. 2007). After 180 min of column operation, 1.0 g of pisolite removed 1.41 mg of As and 1.0 g of activated (400 °C heating) pisolite removed 3.51 mg of As. Native limestones were investigated in column experiments fed by solutions with similar characteristics to As-rich well water from Mexico (Sosa, Armienta et al. 2020). The authors observed the interference of bicarbonate and sulfate in As removal and indicated native limestones for the treatment of arsenic-contaminated water. Diatomite coated with hydrous ferric oxide (HFO) was able to treat about 1100 BV of As(III) solution (500 µg L^{-1}) until a breakthrough point of 10 µg L^{-1} (Jang, Min et al. 2006).

The arsenic removal efficiency by an iron-oxide-coated natural rock (IOCNR) was studied in a fixed-bed column with 2 cm diameter, fed at 8 mL min^{-1} flow rate at a pH of 5.7 (Maji, Kao et al. 2012). The rock used in the study was Fe(III)-loaded granite . The breakthrough point of 10 µg L^{-1} for an initial As(III) concentration of 600 µg L^{-1} was reached after 31 h, 49 h and 63 h for bed depths of 10 cm (~48 g), 15 cm (~73g) and 20 cm (~97g), respectively. A similar dynamic study was conducted with IOCNR and the adsorption exhausted sludge of As(III) and As(V) was mixed with Portland cement to reduce the impact and the cost of the water treatment process (Maji, Kao et al. 2015). The study evaluated the As mobility

in the material and the leaching test allowed to conclude that the adsorption column sludge mixed with Portland cement is an environmental friendly material that could be applied in building construction.

Table 2.3 shows characteristics of dynamic adsorption studies conducted with soil and rock. Rock-based adsorbents presented better results for arsenic removal than soil-based ones. The longest breakthrough time was achieved by limestones, which maintained arsenic effluent solution under 10 µg L^{-1} for weeks, followed by IOCNR, that kept effluent concentration under the WHO standard for more than 60 h.

Table 2.3: Comparison of dynamic tests using soil and rock as adsorbents for arsenic removal.

Adsorbent	**Treatment**	**Arsenic species**	**C_o (µg L^{-1})**	**t_b (h)**	**Q_{max} (mg g^{-1})**	**BV_b**	**Ref.**
Laterite soil	None	As	330	6.75			(Maji, Pal et al. 2008)
Laterite soil	None	As(III)	500-1,000	2.8-32			(Maji, Pal et al. 2007)
Laterite soil	None	As(V)	500-1,000	1.65-18.5	0.047		(Maji, Pal et al. 2007)
Laterite soil	None	As(V)	500-1,002	4.95-8.12	0.112-0.147		(Maiti, DasGupta et al. 2008)
Laterite soil	None	As	80-100				(Mondal, Mondal et al. 2019)
Laterite soil	HCl	As	200	0.76 (at 60 µg L^{-1})			(Karki, Timalsina et al. 2022)
Iron-impregnated tablet ceramic (ITCA)	$FeCl_3$	As(V)	1,000	16			(Chen, Zhang et al. 2012)

Adsorbent	Treatment	Arsenic species	C_o (µg L^{-1})	t_b (h)	Q_{max} (mg g^{-1})	BV_b	Ref.
Iron-oxide containing soil	None	As(V)	1,000			15-875	(Williams, Barnett et al. 2003)
Pisolite	Thermic (400°C)	As(V)	50,000		1.41-3.51		(Pereira, Dutra et al. 2007)
Limestones	None	As(V)	1,190-1,340	3-15 weeks			(Sosa, Armienta et al. 2020)
Iron-incorporated diatomite [Fe(25%)-diatomite)]	$Fe(NO_3)_3 \cdot 9H_2O$	As(V) As(III)	500 500			1,100 1,100	(Jang, Min et al. 2006)
Iron-oxide-coated natural rock (IOCNR)	$Fe(NO_3)_3 \cdot 9H_2O$	As(III)	600	31-63			(Maji, Kao et al. 2012)
		As(III) As(V)	300-1,000 1,000-3,000	20-65 5-18			(Maji, Kao et al. 2015)

2.1.6 Carbon-Based Adsorbents

Most of the carbon-based adsorbent investigations in column operation mode for arsenic adsorption were conducted with activated carbon (AC) or granular activated carbon (GAC) loaded with iron, to benefit from the properties of both materials (Gu, Fang et al. 2005, Chen, Parette et al. 2007, Zhang, Lin et al. 2007, Zhuang, Hobenshield et al. 2008, Sigrist, Brusa et al. 2014, Kalaruban, Loganathan et al. 2019). The use of AC, especially GAC, as a support for metal oxides/hydroxides, provides a more stable structure for As removal in comparison with the application of the metal oxide/hydroxide alone, mainly in fixed-bed column processes (Kalaruban, Loganathan et al. 2019).

A continuous mode study using iron-impregnated GAC (GAC-Fe) and pristine GAC was conducted for As(V) removal (Kalaruban, Loganathan et al. 2019). The maximum As adsorption

capacity observed was 0.470 mg g^{-1} for the GAC-Fe column, which performed approximately four times better than the GAC column of 0.133 mg g^{-1} (Kalaruban, Loganathan et al. 2019).

Hydrous ferric oxide was immobilized onto GAC using phenol formaldehyde (PF) to provide an economically feasible solution for As removal from water (Zhuang, Hobenshield et al. 2008).

Another methodology to prepare ferric AC was by precipitating amorphous HFO onto AC (FeO/AC) (Zhang, Lin et al. 2007). Laboratory column experiments with FeO/AC were performed at 8.33 ml min^{-1} with an As(V) initial concentration of 500 µg L^{-1}. FeO/AC was able to remove at least 99.8% of arsenic from the influent and the breakthrough point of 50 µg L^{-1} was achieved after approximately four times more throughput volume compared to AC without iron loading. Table 2.4 presents the results of dynamic adsorption studies using carbon-based adsorbents. The iron impregnation of GAC and AC was able to increase As uptake from water in about four times, considering column experiments results (Zhang, Lin et al. 2007, Kalaruban, Loganathan et al. 2019). However, GAC/AC are usually more expensive adsorbents and their adsorption capacities obtained in dynamic experiments were found to be similar or inferior to other from low-cost adsorbents such as minerals, soil and rock, biosorbents and industrial waste and by-products.

Table 2.4: Comparison of dynamic tests using carbon-based adsorbents for arsenic removal.

Adsorbent	**Treatment**	**Arsenic species**	**C_o (µg L^{-1})**	**Q_{max} (mg g^{-1})**	***BV_b***	***t_b* (h)**	**Ref.**
Iron-modified activated carbon	$Fe(NO_3)_3 \cdot 9H_2O$	As	40-60		5,600-34,000		(Chen, Parette et al. 2007)
Iron-impregnated granular activated carbon (GAC-Fe)	$FeCl_2$	As	100-500	0.305-0.470	313-1494		(Kalaruban, Loganathan et al. 2019)
Granular activated carbon (GAC)		As	100	0.118-0.133	380-388		(Kalaruban, Loganathan et al. 2019)
Granular activated carbon doped with iron (Fe/GAC)	$FeCl_3$	As(V)	180	2.873			(Sigrist, Brusa et al. 2014)

Adsorbent	Treatment	Arsenic species	C_o (µg L^{-1})	Q_{max} (mg g^{-1})	BV_b	t_b (h)	Ref.
Hydrous ferric oxide incorporated onto GAC with phenol formaldehyde resins coating (HFO-PF-coated GAC)	$FeCl_3$/PF	As(V)	1886	0.7117	180	1753	(Zhuang, Hobenshield et al. 2008)
Iron-containing granular activated carbon	$FeCl_2$	As(V) As(III)	57.2 56.1		7500 7500		(Gu, Fang et al. 2005)

2.1.7 Biosorbents

Biosorbents are naturally occurring materials or waste biomass, and their high adsorption capacity and cost-effectiveness make biosorption a promising process in water and wastewater treatment (Igwe and Abia 2006). The group of biomaterials includes aquatic biopolymers, plant biomass, microbial biomass, biochars and agricultural waste (Saqib, Waseem et al. 2013). Column studies have investigated the potential of these materials, with or without pre-treatment or modification, to remove arsenic from aqueous solution in continuous mode (Ghimire, Inoue et al. 2002, Zouboulis and Katsoyiannis 2002, Kamala, Chu et al. 2005, Chen and Chung 2006, Haque, Morrison et al. 2007, Boddu, Abburi et al. 2008, Chen, Chang et al. 2008, Pokhrel and Viraraghavan 2008, Rahaman, Basu et al. 2008, Gupta, Chauhan et al. 2009, Ranjan, Talat et al. 2009, Zhao, Huang et al. 2009, Gupta and Sankararamakrishnan 2010, Sarkar, Pal et al. 2010, Hiroyuki Hoshina 2012, Roy, Mondal et al. 2013, Hu, Ding et al. 2015, Saha and Sarkar 2015, Samad, Fukumoto et al. 2016, Dhoble, Maddigapu et al. 2017, Brion-Roby, Gagnon et al. 2018, Jaiswal, Saxena et al. 2018, Roxanne, Jonathan et al. 2018, Kang, Park et al. 2019, Wei, Wei et al. 2019, Wei, Yu et al. 2019, Ociński and Mazur 2020, Pang, Wang et al. 2020, Zeng, Yu et al. 2020).

2.1.7.1 Aquatic Biomaterials

a) Chitosan

Chitosan (CS) is a natural aminopolysaccharide originated in arthropod exoskeletons (Zeng, Yu et al. 2020) such as crabs and shrimps. The biopolymer is obtained by N-deacetylation of chitin (Ociński and Mazur 2020) and has been applied in heavy metals and arsenic uptake due to its

free amino groups that can serve as sites of coordination binding (Chen and Chung 2006). Chitosan also presents the advantage of being low-cost, biodegradable, renewable and non-toxic (Gupta, Chauhan et al. 2009).

Early experimental column studies with chitosan beads investigated the feasibility of using chitosan without any pretreatment to remove arsenic from wastewater discharged from Gallium arsenide (GaAs) manufacturing in continuous mode (Chen and Chung 2006). Laboratory tests were developed in a glass column with 1.8 cm diameter and 12 cm height with a total packing volume of 30.5 mL, packed with 20 g of chitosan beads of 2.5 mm size. The industrial wastewater contained 2.5 mg L^{-1} of As(III) and 35 mg L^{-1} of As(V) and presented a pH of 4.8. Comparison tests were made with synthetic wastewater containing 10 mg L^{-1} of As(III) or As(V) at pH 5. Recycled chitosan beads were also investigated in continuous mode and presented similar breakthrough time to native chitosan beads. The experiments made with synthetic wastewater at 8 mL min^{-1} resulted in an adsorption capacity of 1.78 and 1.90 mg As g^{-1} bead, for As(III) and As(V), respectively. According to this study, chitosan is a promising adsorbent for arsenic removal from water.

Later, molybdate-impregnated chitosan beads (MICB) were developed to improve arsenic adsorption capacity (Chen, Chang et al. 2008). Laboratory column tests were carried out with synthetic effluent and GaAs manufacturing wastewater with similar characteristics to the previous study (Chen and Chung 2006). The breakthrough time at 30 mL min^{-1} was approximately 7 h for the synthetic wastewater and between 5 h and 8 h for the industrial wastewater. Recycling tests were made, and the adsorption curve remained similar up to 10 cycles of sorption-desorption. MICB adsorption capacity observed with synthetic wastewater was 1.98 and 2.00 mg As g^{-1} MICB for As(III) and As(V), respectively. The adsorption capacities observed for MICB were only slightly higher than the ones observed for chitosan without pretreatment, so the costs of adding molybdate were not justified by an incrementation in the adsorption capacity.

In addition to molybdate impregnation for chitosan beads, studies have proposed other metal or inorganic oxide treatments to improve their arsenic adsorption capacity. Iron oxides are the most common (Gupta, Chauhan et al. 2009, Gupta and Sankararamakrishnan 2010, Dhoble, Maddigapu et al. 2017, Wei, Yu et al. 2019, Ociński and Mazur 2020, Zeng, Yu et al. 2020), followed by aluminum oxides (Boddu, Abburi et al. 2008, Dhoble, Maddigapu et al. 2017), magnesium oxide (Saha and Sarkar 2015), and the combination of iron and manganese oxides (Zeng, Yu et al. 2020).

Among the column studies of chitosan treated with metal oxides, the best arsenic adsorption capacity was observed for chitosan entrapped with Fe-Mn water treatment residual (C-WTR), with an As(III) removal capacity of 32.64 mg g^{-1} of C-WTR even after six cycles of sorption/desorption with 0.5 NaOH solution (Ociński and Mazur 2020).

In addition to the treatment of chitosan with metal oxides, a simple method of protonation of amine groups improved chitosan arsenic adsorption capacity on column tests to a range of 36-50 mg As g^{-1} of chitosan (Brion-Roby, Gagnon et al. 2018, Roxanne, Jonathan et al. 2018), being the highest adsorption capacities among other types of chitosan modifications reported in column studies.

b) Alginate

Alginate is a biopolymer composed of α-l-guluronate and β-d-mannuronate and is a major constituent of the cell wall of seaweed and sea tangle (Liu, Chen et al. 2009, Kang, Park et al. 2019). Alginate acids have a high affinity with divalent cations and produce thermally irreversible and hydrophobic gels (Zouboulis and Katsoyiannis 2002, Hassan, Abdel-Mohsen et al. 2014). Alginate beads are applied to heavy metals and metalloids removal, and their preparation is usually made with calcium as cation (Zouboulis and Katsoyiannis 2002). Arsenic adsorption column studies using alginate treated with metal oxides, such as aluminum oxide (Kang, Park et al. 2019) and iron oxides (Yuan, Yong Hu et al. 2002, Zouboulis and Katsoyiannis 2002, Sarkar, Pal et al. 2010) have been reported.

An alginate-based adsorbent containing calcinated alum sludge from a water treatment facility was developed to enhance surface area and overcome alginate bead limitation of slow adsorption kinetics (Kang, Park et al. 2019). The new adsorbent performed better than a commercial adsorbent (Bayoxide E33) by reaching 10 μg L^{-1} after 200 bed volumes, 50% higher than Bayoxide E33. The initial solution concentration was 200 μg L^{-1}.

Fe(III) crosslinked alginate nanoparticles were also investigated in fixed-bed column experiments for As(V) removal (Singh, Singh et al. 2014). The effect of inlet arsenate concentration (0.5, 1.0 and 1.5 mg L^{-1}), bed height (2, 4 and 6 cm) and flow rate (0.25, 0.50 and 1.0 mL min^{-1}) were studied. The Fe-alginate maximum adsorption capacity of 0.066 mg g^{-1} was achieved with the following dynamic experimental conditions: inlet As(V) solution of 0.5 mg L^{-1}, bed height of 2 cm and flow rate of 0.50 mL min^{-1}.

c) Fish scale

Atlantic cod fish scale has been reported as an alternative biosorbent to remove heavy metals and arsenic from water (Mustafiz, Basu et al. 2002, Basu, Mustafiz et al. 2006, Rahaman, Basu et al. 2008). Column tests were conducted using dried fish scale in a glass column with 2.54 cm diameter and 23.88 cm bed height. The column was fed with a solution of 520 μg L^{-1} As(III) or 342 μg L^{-1} As(V) at a flow rate of 2.0 mL min^{-1}. Breakthrough point (10% Co) was reached after 21.75 h and 25 h for As(III) and As(V), respectively.

2.1.7.2 Agricultural waste

Agricultural waste materials are mainly composed of lignin and cellulose, combined with other components such as hemicellulose, extractives, lipids, proteins, starches, water, hydrocarbons and others (Sud, Mahajan et al. 2008). This type of waste is a potential source of adsorbents for heavy metals and metalloids. The majority of research is directed to cationic heavy metals and few studies have investigated the capacity of various food and agricultural wastes for the biosorption of arsenic (Asere, Stevens et al. 2019).

Carbonized sugarcane bagasse (SCC) is an alternative to active char carbon prepared from agricultural waste material (Roy, Mondal et al. 2013). Column tests were performed to investigate the arsenate and arsenite removal capacities of SCC modified by thioglycolic acid impregnation (Roy, Mondal et al. 2013). Breakthrough curves were generated at different bed heights (11.3 cm to 32.1 cm), flowrates (3.0 to 7.0 mL min^{-1}) and arsenic initial concentration (500 to 1,500 μg L^{-1}) with a pH of 6.0. Experimental and predicted (by Thomas model) adsorption capacities for As(III) and As(V) were found. Maximum adsorption capacities of 0.085 mg g^{-1} and 0.084 mg g^{-1} were reached for As(III) and As(V), respectively, at a flow rate of 3.0 mL min^{-1}, bed height of 32.1 cm and initial concentration of 1,500 μg L^{-1}.

2.1.7.3 Rice-Based Adsorbents

Rice polish, a waste from rice milling industries, was investigated as a potential adsorbent in up-flow fixed bed column studies (Ranjan, Talat et al. 2009). The effect of design parameters, such as bed height (5 to 25 cm), flow rate (1.66 to 8.33 mL min^{-1}) and initial metal ion concentration (100 to 1000 μg L^{-1}), was studied. Maximum uptakes of 0.067 mg g^{-1} for As(III) and 0.079 mg g^{-1} for As(V) were achieved with 25 cm bed height and 30.5 g of rice polish, at 1.66 mL min^{-1} flow rate, fed with a 1000 μg L^{-1} initial arsenic concentration. Desorption-sorption cycles were also investigated, and the recovery efficiency achieved values of approximately 99%.

Good adsorption of arsenic performance was observed for rice waste studies in continuous mode (Ranjan, Talat et al. 2009, Samad, Fukumoto et al. 2016). Considering that rice production is strong in some places where arsenic contamination is a major problem, such as Bangladesh and other Asian countries, rice byproducts can be a low-cost potential solution for arsenic removal from water in these regions.

2.1.7.4 Cotton-Based Adsorbents

Column studies with cotton-based adsorbents were performed after iron modification of the materials (Zhao, Huang et al. 2009, Pang, Wang et al. 2020). A novel adsorbent, Fe(III)-loaded ligand exchange cotton cellulose [Fe(III)LECCA] was synthetized for selective arsenate adsorption (Zhao, Huang et al. 2009). In column tests with 1 mg L^{-1} arsenic aqueous solution, at pH of 7.10, a breakthrough capacity (at 10 µg L^{-1}) of 5.3 mg g^{-1} was achieved with a flow rate of 26 BV h^{-1}. In similar column tests with tap water spiked with As(V), the breakthrough point adsorption capacity was reduced to 65% of the original value.

Fixed-bed column experiments were also performed with another novel adsorbent, consisting of Fe-based metal-organic framework coated onto cotton fiber composites [MIL-88A(Fe)/cotton fibers] (Pang, Wang et al. 2020). A solution with an As(V) concentration of 500 µg L^{-1} was fed at 6.0 mL min^{-1} flow rate to the column with 34 cm length and 1.6 cm diameter. The breakthrough point of 10 µg L^{-1} was achieved after approximately 440 bed volumes.

Another cotton-based adsorbent study in column mode was reported, but instead of iron, zirconium was loaded to the material to improve uptake capacity (Hiroyuki Hoshina 2012). The novel adsorbent was synthesized by radiation-induced graft polymerization (RIGP) of a phosphoric monomer onto nonwoven cotton fabric. Zr(IV) was then loaded to the phosphoric units packed in the column. The new Zr-type adsorbent arsenic removal capacity was investigated in column tests at different pH (1,2,3,5,7 and 9) and different flow rates (200 and 1000 h-1) with an As(V) solution of 1 mg L^{-1}. The maximum adsorption capacity of 0.749 mg g^{-1} was obtained at pH 2 and 1000 h^{-1} flow rate.

Among the agricultural wastes used in dynamic studies for arsenic removal, the cotton-based materials led to better adsorption capacities because of modifications with iron and zirconium. Moreover, iron loading has provided higher adsorption capacity to cotton-based adsorbents than zirconium.

2.1.7.5 Biochar

Biochar is a stable black carbon material produced from a wide range of biomass types (Jung, Kim et al. 2016). The biochar characteristics such as large specific surface area, porous structure, enriched surface functional groups and mineral components, combined with being environmentally friendly, low-cost and effective, make the application of biochar as an adsorbent attractive to researchers (Tan, Liu et al. 2015, Jung, Kim et al. 2016). Recent studies reported the association of iron composites to biochar to improve arsenic adsorption removal in column mode (Hu, Ding et al. 2015, Navarathna, Karunanayake et al. 2019, Wei, Wei et al. 2019).

Biochar derived from hickory chips was impregnated with iron nanoparticles by direct hydrolysis of iron salt and investigated for arsenic adsorption-desorption (Hu, Ding et al. 2015). A column measuring 5 mm in diameter and 12 mm of bed height was filled with 1 g of the iron-impregnated biochar and fed with a 50 mg L^{-1} As(V) solution at 2 mL min^{-1}. Column experimental data were well fitted by the convection-dispersion-reaction (CDER) model. Desorption tests carried out with 0.05 mol L^{-1} NaHCO3 obtained an 85% removal of the retained arsenic.

Magnetized biochar composite (MBC) was prepared by precipitating magnetite primary nanoparticles (Fe_3O_4) on Douglas fir biochar (Navarathna, Karunanayake et al. 2019). Fixed-bed column experiments were performed using a 10 mg L^{-1} As (III) solution at pH 7 at 2 mL min^{-1} flow rate and the breakthrough point was reached after 40 min. Regeneration tests were conducted with 0.5 M KH_2PO_4 at pH 4.5, in three cycles, and results show that restoration rates were 85%, 81% and 76% from the initial adsorption capacity. The desorption efficiency was reduced from 87% to 80% and 76%.

Iron oxide nanoneedles array-decorated biochar fibers (Fe-NN/BFs) were prepared by a hydrothermal method from waste cotton fiber (Wei, Wei et al. 2019). Fixed-bed columns containing 2 g of adsorbent were fed with 275 µg L^{-1} arsenic-spiked natural groundwater at 2.26 mL min^{-1}, at pH 6. For a breakthrough point of 10 µg L^{-1}, the treated volumes for As(V) and As(III) were 1,350 and 350 bed volumes, respectively. For two columns in tandem, the treated volume increased to 2,900 BV for As(V) and 2,500 BV for As(III). The adsorption capacity of the column was 1.80 and 1.55 mg g^{-1} for As(V) and As(III), respectively. Five cycles of regeneration (0.1 M NaOH) were conducted with effective treatment performance.

Magnetic biochar MTB-800 was developed from *Tectona species* (Teak) leaves waste (Verma and Singh 2023). The dry biomass was ground into powder and impregnated with $FeCl_3$. Finally,

biochar was prepared by pyrolysis at 800ºC for 1h. Higher adsorption capacities of 1.87 mg g^{-1} for As(III) and 1.63 mg g^{-1} for As(V) were achieved at the following operational conditions: C_0 = 1 mg L^{-1}, bed height = 6 cm and flow rate of 2.5 mL min^{-1}. After five regeneration cycles using NaOH 0.1M, the adsorption capacity of As(III) and As(V) reduced from 94.92% to 49.55% and from 93.1% to 43.85%, respectively.

2.1.7.6 Fungal Biomass

A recent study investigated the arsenic adsorption capacity of four novel fungal strains in column mode (Jaiswal, Saxena et al. 2018). *Westerdykella* sp. (FNBR_3), *Trichoderma* sp. (FNBR_6), *Lasiodiplodia* sp. (FNBR_13), and *Rhizopus* sp. (FNBR_19) were isolated from agricultural soils containing arsenic in West Bengal, India. Column experiments were performed in a glass column (0.7 cm diameter and 15 cm bed height) packed with alginate beads containing 10 g of immobilized fungal biomass at pH 6, with a flow rate of 8.5 mL min^{-1} and arsenic initial concentration of 200 mg L^{-1}. *Lasiodiplodia* sp. (FNBR_13) led to the highest values of breakthrough time (C = 100 µg L^{-1}) and adsorption capacity: 110 min and 74.88 mg g^{-1}, respectively. The Thomas model was fitted to the experimental results and the highest correlation was exhibited by FNBR_13 experimental data.

In another study, *Aspergillus niger* fungal biomass was treated with iron oxide to remove As(III) and As(V) in continuous mode (Pokhrel and Viraraghavan 2008). A mass of 6.925 g of iron oxide-coated biomass (IOCB) beads were packed in a column with 1.25 cm diameter and 23.7 cm effective bed depth. Different solutions of 100 µg L^{-1} As(III) or As(V) at pH 6 were fed to the column at 3.1 ml min^{-1} flow rate. The breakthrough point of 10 µg L^{-1} for As(V) was achieved after 800 bed volumes for IOCB and after 130 bed volumes for regenerated IOCB (0.25 M NaOH at 10 mL min^{-1}). The As(III) breakthrough point could not be achieved in the first cycle, but it was achieved with regenerated IOCB after 340 bed volumes. The adsorption capacities of IOCB were reported to be 1.08 mg g^{-1} for As(V) and 1.21 mg g^{-1} for As(III).

Fungal biomass can be considered a good source of biosorbents for arsenic removal. However, high values of adsorption capacity reported in the first study (Jaiswal, Saxena et al. 2018) can be explained by the high arsenic initial concentration of 200 mg L^{-1}, 20,000 times higher than the initial arsenic solution in the second study (Pokhrel and Viraraghavan 2008). The second study reported that fungal biomass with iron modification was able to achieve adsorption capacities in continuous mode similar to other biosorbents' removal capacity.

2.1.7.7 Plant Biomass

The arsenic adsorption capacity of sorghum biomass (SB), one of the greatest cereal crops in the world, was investigated in continuous mode (Haque, Morrison et al. 2007). Two columns with 5.4 cm diameter and 40 cm active bed height were fed with a solution containing 5 mg L^{-1} of As(III) at 10 mL min^{-1}. One column was packed with 150 g of non-immobilized sorghum biomass (NISB) and the other one with 140 g of immobilized sorghum biomass (ISB). The maximum adsorption capacities observed for NISB and ISB were, respectively, 2.765 and 2.437 mg g^{-1}.

Preliminary experiments have been conducted with immobilized Garcinia cambogia biomass beads (IGCFIX) to remove As(III) in continuous-flow conditions (Kamala, Chu et al. 2005). A column with 1.6 cm diameter and 7 cm of packed bed height was fed with a 100 mg L^{-1} As(III) solution at a flow rate of 13.3 mL min^{-1}. A regeneration study was carried out with 0.05 M NaOH at 1 mL min^{-1} flow rate, in five cycles. The results achieved point to the feasibility of using IGCFIX in column operation.

Table 2.5 shows the characteristics of dynamic adsorption studies conducted with carbon-based biosorbents. The average performance of biosorbents in column studies was superior to that of traditional types of adsorbents, such as metal (hydr)oxides, ZVI and carbon-based materials. The different categories of biosorbents showed similar results but more studies were conducted with aquatic biomaterials, which can justify their higher feasibility to column studies. Individually, the cod fish scale and chitosan-based materials showed higher maximum adsorption capacities than other biosorbents.

Table 2.5: Comparison of dynamic tests using biosorbents for arsenic removal.

Adsorbent	**Arsenic species**	**C_o (µg L^{-1})**	**t_b (h)**	**Q_{max} (mg g^{-1})**	**BV_b**	**Ref.**
			Aquatic biomaterials			
Chitosan	As(V)	30,000-120,000	424.7-4444.6	36-50		(Brion-Roby, Gagnon et al. 2018)
Chitosan	As(V)	120,000	4.33			(Roxanne, Jonathan et al. 2018)
Chitosan	As(V) As(III)	10,000 10,000		1.9 1.78		(Chen and Chung 2006)
Blue crab chitosan (BC)	As(V)	312	2		~6	(Yao, Jabeur et al. 2024)

Adsorbent	Arsenic species	C_o (μg L^{-1})	t_b (h)	Q_{max} (mg g^{-1})	BV_b	Ref.
Blue crab by-product powder (RM)	As(V)	312	0.45		~4	(Yao, Jabeur et al. 2024)
Molybdate-impregnated chitosan (MICB)	As(V) As(III)	10,000 10,000		1.99 1.96		(Chen, Chang et al. 2008)
Chitosan-based porous magnesia-impregnated alumina (MIPA)	As(V)	300	42-100	17.2		(Saha and Sarkar 2015)
Porous Fe-chitosan beads (P/Fe-CB)	As(III)	975		1.19	3,000	(Wei, Yu et al. 2019)
Iron chitosan spacer granules (ICS)	As(V) As(III)	500-1,000 500-1,000	59.0-106.0 50.5-107.7		210 132	(Gupta and Sankararamakrishnan 2010)
Waste Fe/Mn oxides into chitosan beads (C-WTR)	As(V) As(III) As(III) + As(V)	500 500 500 + 500		13.84-13.97 30.02-32.64	2,700	(Ociński and Mazur 2020)
Magnetic binary oxide particles (MBOP) using chitosan	As(III)	1000	26.15-72	0.436-0.477		(Dhoble, Maddigapu et al. 2017)
Granular adsorbent (GA) using back-wash residue material and chitosan	As(V)	150			210	(Zeng, Yu et al. 2020)
Chitosan-magnetite (ChM) hydrogel	As(V)	10,000		3.84		(Mendizabal, Ríos-Donato et al. 2023)
Chitosan (Ch) hydrogel	As(V)	10,000		1.24		(Mendizabal, Ríos-Donato et al. 2023)
Iron oxide loaded alginate	As(V) As(III)	50		0.0138	230 45	(Zouboulis and Katsoyiannis 2002)
Ferric hydroxide microcapsule	As(III)	100	75 days			(Sarkar, Pal et al. 2010)

Adsorbent	Arsenic species	C_o (µg L^{-1})	t_b (h)	Q_{max} (mg g^{-1})	BV_b	Ref.
loaded calcium alginate (FHMCA)						
Atlantic cod fish scale	As(V)	342-520	21.75-25	4.87-38.36		(Rahaman, Basu et al. 2008)
			Agricultural waste			
Iron(III)-loaded phosphorylated orange juice residue (POJR)	As(V)	15,800			81.4	(Ghimire, Inoue et al. 2002)
Fe-based metal-organic framework/cotton fibers composites	As(III)	500			320-440	(Pang, Wang et al. 2020)
Rice polish	As(V) As(III)	100-10000	3-30.83 2.66-29	0.025-0.079 0.030-0.067		(Ranjan, Talat et al. 2009)
Rice husk	As(III)	50-500		0.016-0.022		(Samad, Fukumoto et al. 2016)
Fe(III)-loaded ligand exchange cotton cellulose adsorbent [Fe(III)LECCA]	As(V)	1,000		5.3	~400	(Zhao, Huang et al. 2009)
Nonwoven cotton fabric	As(V)	1,000		0.749	270-1420	(Hiroyuki Hoshina 2012)
Thioglycolated sugarcane carbon (TSCC)	As(V) As(III)	1,500 1,500		0.084 0.085		(Roy, Mondal et al. 2013)
			Biochar			
Iron-impregnated biochar	As	50,000	0.167			(Hu, Ding et al. 2015)
Magnetite precipitated onto Douglas fir biochar	As(III)	10,000		2.85		(Navarathna, Karunanayake et al. 2019)
Iron oxide nanoneedle array-	As(V) As(III)	275 275		1.80 1.55	1350 350	(Wei, Wei et al. 2019)

Adsorbent	Arsenic species	C_o (µg L^{-1})	t_b (h)	Q_{max} (mg g^{-1})	BV_b	Ref.
decorated biochar fibers (Fe-NN/BFs)						
Magnetic biochar from dry teak leaves (MTB-800)	As(V) As(III)	1,000 1,000		1.63 1.86		(Verma and Singh 2023)
Active manganese dioxide-rice husk biochar	As(III)	5,000	4 (at 250 µgL^{-1})	3.49		(Cuong, Wu et al. 2022)
			Fungal & Plant biomass			
Non-immobilized sorghum biomass (NISB)		5,000	27*	2.765	31 pore volumes [1]	(Haque, Morrison et al. 2007)
Immobilized sorghum biomass (ISB)		5,000	24*	2.437	27 pore volumes [1]	(Haque, Morrison et al. 2007)
Novel fungal strains + alginate beads	As	200,000	0.50-1.83[2]	59.5-74.8		(Jaiswal, Saxena et al. 2018)
Iron oxide-coated fungal biomass (IOCB)	As(V) As(III)	100 100		1.080 1.210[3]	800 340[3]	(Pokhrel and Viraraghavan 2008)

[1]For breakthrough point of 50 µg L^{-1} [2]For breakthrough point of 100 µg L^{-1} [3]Regenerated bed

2.1.8 Industrial Waste and By-products

Looking for industrial waste materials for arsenic uptake and other pollutants removal from water is of great importance to improve sustainability because it can be cost-effective and reduce the waste disposal in industry. Column experiments have shown a good potential for arsenic adsorption using sugar industry waste (Ali, Al-Othman et al. 2014), water treatment solid residuals (Gibbons and Gagnon 2010, Kang, Park et al. 2019), cement (Kundu, Kavalakatt et al. 2004, Kundu and Gupta 2005, Kundu and Gupta 2007), mining residual products (Pereira, Dutra et al. 2007) and, more recently, waste and by-products from scrap metal recycling (Liem-Nguyen, Sjöberg et al. 2020) and steel industry (Shahid, Phearom et al. 2019, Shahid, Phearom et al. 2019, Shahid, Phearom et al. 2020).

Regarding sugar industry waste, column experiments for arsenic removal were developed using, as adsorbent, bagasse fly ash (BFA)(Ali, Al-Othman et al. 2014). The column data were analyzed by bed depth service time (BDST) and Yoon and Nelson models. The arsenate and arsenite removal efficiencies in synthetic influents were 98.9% and 95.6%, and for real arsenic-contaminated water were 91.23% and 87.76%, respectively. The authors concluded that the BFA adsorption column is applicable to natural waters remediation as regards As contamination.

Chemical sludge rich in iron from a water treatment plant (WTP) in the USA was also investigated as a potential adsorbent for arsenic (Gibbons and Gagnon 2010). The materials were rich in iron because the WTP used ferric sulphate as coagulant. Column tests were conducted using the ferric sludge and granular ferric hydroxide (GFH) for comparison purposes. The ferric residual presented a performance similar to GFH and achieved a breakthrough point of 10 µg L^{-1} after 26,400 bed volumes, for a groundwater sample containing 37.7 µg As L^{-1}. Table 2.6 shows characteristics of dynamic adsorption studies using industrial waste and by-products as adsorbents.

IOCC presented an adsorption capacity similar to other traditional adsorbents such as carbon-based materials and metal (hydr)oxides. In terms of arsenic removal efficiency, the iron modified cement (IOCC) doesn´t present advantages compared to the hardened paste of Portland cement (HPPC), even the studies being conducted with different arsenic species. Industrial waste and by-products can be an economic and sustainable way to remove arsenic from water, but further studies should be carried out on their viability for practical applications.

Table 2.6: Comparison of dynamic tests using industrial waste and by-products as adsorbents for arsenic removal.

Adsorbent	**Adsorbent Modification**	**As species**	**C_o (µg L^{-1})**	**Q_{max} (mg g^{-1})**	**As remov. (%)**	**t_b (h)**	**BV_b**	**Ref.**
Bagasse fly ash (BFA)	None	As(V)	50		98.9			(Ali, Al-Othman et al. 2014)
		As(III)	50		95.6			(Ali, Al-Othman et al. 2014)
Water treatment	None	As	37.7				26,400	(Gibbons and

residual solids							Gagnon 2010)
Iron oxide-coated cement (IOCC)	$Fe(NO_3)_3 \cdot 9H_2O$	As(V)	2,000-4,000	3.8852		4.0-41.5	(Kundu and Gupta 2005)
		As(III)	500-2,700	0.1462 - 0.3082	54.04-84.77		(Kundu and Gupta 2007)
Hardened paste of Portland cement (HPPC)	Cement + water	As(V)	500		>90		(Kundu, Kavalakatt et al. 2004)
Stainless steel slags	None	As(V)	10,000		84%		(Liem-Nguyen, Sjöberg et al. 2020)

2.1.9 Nanocomposites

Nano adsorbents are very promising and highly efficient materials for arsenic removal from groundwater, however separation and regeneration are still challenges to their practical application (Lata and Samadder 2016). Nanoparticles are <100 nm size (Christian, Von der Kammer et al. 2008) and different nanomaterials have been tested for arsenic adsorption. Column studies have been conducted with nanoparticles of different materials: alginate (Singh, Singh et al. 2014), aluminum (Önnby, Pakade et al. 2012), carbon (Sharma, Verma et al. 2010, Ali 2018, Wang, Zhang et al. 2019), copper (Reddy, McDonald et al. 2013, Contreras, Henríquez-Vargas et al. 2017), iron (Sarkar, Blaney et al. 2007, Gupta and Ghosh 2009, Morillo, Faccini et al. 2016, Hernández-Flores, Pariona et al. 2018, Wei, Wei et al. 2019), manganese (Luo, Meng et al. 2018), polymers (Savina, English et al. 2011, Önnby, Pakade et al. 2012, Chu 2014), zirconium (Pandi, Lee et al. 2020) and titanium (Hristovski, Baumgardner et al. 2007, Gupta and Ghosh 2009, Danish, Qazi et al. 2013). In order to facilitate reuse and regeneration, the nanoparticles are usually coated onto another material such as glass beads (Danish, Qazi et al. 2013), gel beads (Savina, English et al. 2011, Önnby, Pakade et al. 2012), polystyrene (Chu 2014) and alginate beads (Sarkar, Pal et al. 2010).

Concrete based iron oxide (IO) nanoparticles (NP) were tested in laboratory experiments using a glass column of 2.2 cm of diameter and different bed heights (10, 20 and 30 cm) (Hernández-

Flores, Pariona et al. 2018). Contaminated water containing 10 mg L^{-1} of As(V) was fed constantly at 7.5 mL min^{-1} flow rate. The time of breakthrough for 10 µg L^{-1} of arsenate was found to be 4.1, 6.5 and 8.6 h for 10, 20 and 30 cm of bed height, respectively.

Multi walled carbon nanotubes (CNTs) were also investigated in column adsorption tests for As(III) and As(V) removal (Ali 2018). A glass column containing 2.0 g of CNT and 2.0 g of washed river sand was operated under different flow rates (20, 30 and 40 mL min^{-1}) at pH 6, with an initial arsenic concentration of 40 µg L^{-1}. The optimal flow rate for operation was found to be 30 mL min^{-1} leading to an adsorption capacity of 0.014 mg g^{-1} for As(V) and 0.0135 mg g^{-1} for As(III). The regeneration process was conducted with different eluents and 1.0 M HCl achieved the best results.

A more recent study was conducted with another form of carbon-based sorbent: multi-functionalized magnetic graphene (Wang, Zhang et al. 2019). Adsorption-desorption column tests for As(III) and As(V) were taken with different flow rates, using NaOH and HCl as eluents and results showed an arsenic recovery of approximately 98%.

Table 2.7 presents the results of dynamic adsorption studies conducted with nanocomposites. They are claimed to be a highly efficient option for metals and metalloids adsorption, however the results of tests developed in continuous mode do not prove that yet.

Table 2.7: Comparison of dynamic tests using nanocomposites, GFH and commercial adsorbents for arsenic removal.

Adsorbent	**Arsenic species**	**C_o (µg L^{-1})**	**Q_{max} (mg g^{-1})**	**t_b (h)**	**BV_b**	**Ref.**
			Nanocomposites			
Microwave assisted economic multi walled carbon nanotubes (MWCNTs)	As(V) As(III)	40	0.014 0.0135	50-100		(Ali 2018)
Iron doped phenolic resin based activated carbon micro-nano particles	As(V) As(III)	1,000 1,000-3,000	2.78-3.24 2.60-3.30			(Sharma, Verma et al. 2010)
Cupric oxide (CuO) nanoparticles	As	109		7-15		(Reddy, McDonald et al. 2013)

α-MnO2 nanofibers	As(V) As(III)	200			120 200	(Luo, Meng et al. 2018)
Concrete-maghemite nanocomposites	As(V)	10,000		4.1-8.6		(Hernández-Flores, Pariona et al. 2018)
Metal-doped titania nanoparticles coated glass beads	As	250-1,000	0.477-0.61	1.67-6.5		(Danish, Qazi et al. 2013)
	As(III)	250		1-3.67		(Danish, Qazi et al. 2013)
Zirconium-organic frameworks@biomass-derived porous graphitic nanocomposites (Ui	As(III) As(V)	500 500		1.667 2.167	500 651	(Pandi, Lee et al. 2020)
Granular ferric hydroxide (GFH) and commercial adsorbents						
GFH	As(V)	800	4.92-6.07			(Saldaña-Robles, Damian-Ascencio et al. 2018)
	As	10,000			~500	(Streat, Hellgardt et al. 2008)
	As	500			More than 40,000	(Streat, Hellgardt et al. 2008)
Ferrosorp plus (FP)			0.79		728[1]	(Genç-Fuhrman, Wu et al. 2008)
ArsenX^{np} – a hybrid anion exchanger	As	85			29,000[2]	(Sarkar, Blaney et al. 2007)
Adsorbsia GTO	As	28			3,000-10,000	(Hristovski, Baumgardner et al. 2007)
Iron nanoparticle resin (Lewatit FO36)	As(V)	500	3.229		3,512-4,000	(Boldaji, Nabizadeh et al. 2010)
Fe (III)-phosphorylated resin (Fe-XAD8-DEHPA	As	80		6 (for 3 μg L^{-1})		(Ciopec 2014)

[1]For breakthrough point of 3.75 μg L^{-1} [2]For breakthrough point of 50 μg L^{-1}

2.1.10 Granular ferric hydroxide (GFH) and Commercial adsorbents

Granular ferric hydroxide (GFH) is a well-known, commercially available adsorbent used for arsenic and other water pollutants removal, however, it has some limitations for long time application (Dabizha, Bahr et al. 2020). Column studies have been conducted to investigate specific characteristics of an arsenic adsorption process with GFH (Badruzzaman, Westerhoff et al. 2004, Sperlich, Werner et al. 2005, Genç-Fuhrman, Wu et al. 2008, Sperlich, Schimmelpfennig et al. 2008, Streat, Hellgardt et al. 2008, Streat, Hellgardt et al. 2008, Streat, Hellgardt et al. 2008, Fleming, Eddy et al. 2010, Nguyen, Chen et al. 2011, Saldaña-Robles, Damian-Ascencio et al. 2018).

Rapid small scale tests were performed using three commercially available adsorbents, E33, GFH and Metsorb, to assess the interference of silica, phosphate, vanadate and pH in each of them (Nguyen, Chen et al. 2011). The GFH was found to be the most susceptible to ionic interference. In addition to that, the pH and silica had the most impact in arsenic adsorption comparing to vanadium and phosphate. Other lab-scale study showed that organic matter reduced the adsorption capacity of GFH (Saldaña-Robles, Damian-Ascencio et al. 2018). Real-time pilot scale tests were conducted with GFH treating an inlet arsenic concentration of approximately 1000 $\mu g\ L^{-1}$ at a flow rate of 25 $mL\ min^{-1}$ and X-ray fluorescence (XRF) was validated as a monitoring method for arsenic accumulation through the column (Fleming, Eddy et al. 2010).

Resins are also popular commercial adsorbents due to their excellent hydraulic properties and mechanic resistance (Ciopec 2014). The combinations of resins with metal (hydr)oxides are usually known as hybrid systems. They gather the selectiveness of the metal with the characteristics of the resins to result in more efficient products with better adsorption capacity.

A commercial hybrid anion exchanger named ArsenXnp is formed by the combination of anion exchange resin beads with hydrated ferric oxide (HFO) nanoparticles (Sarkar, Blaney et al. 2007). Field columns packed with ArsenXnp could run more than 20,000 bed volumes before the breakthrough point of 50 $\mu g\ L^{-1}$ of arsenic. The regeneration process after saturation was carried out using 2% NaCl and 2% NaOH and allowed multiple cycles of reuse.

Table 2.7 shows characteristics of dynamic adsorption studies conducted with GFH and commercial adsorbents. Particularly good results were achieved in terms of treated bed volumes, using some alternative materials, such as biosorbents and industrial waste. They can treat similar amounts of contaminated water, in a more sustainable and economic way.

2.1.11 Layered Double Hydroxides (LDH)

Layered double hydroxides (LDH) are a class of anionic clays that has been employed more recently to remove oxyanions such as As(V) and As(III) from aqueous solution (Dias and Fontes 2020). Despite their good adsorption characteristics, the use of LDH in fine powder and its further separation after treatment is still a hindrance for their wide application (Nhat Ha, Kim Phuong et al. 2016). There are various forms of LDH, however few of them have been applied in dynamic tests for arsenic removal.

A zirconium and iron layered double hydroxide (Zn-Fe-LDH) was prepared by a modified co-precipitation method and its arsenic removal capacity was studied in column tests (Lu, Zhu et al. 2015). A column (2.0 cm diameter x 10 cm height) packed with 0.8 g of adsorbent was fed with As(V) solution of 1 mg L^{-1}, at a flow rate of 0.6 mL min^{-1} and pH 7. The handling capacity achieved for breakthrough point of 10 µg L^{-1} was 12.5 L g^{-1} of adsorbent. Desorption tests showed that a solution of 0.5 M NaOH was able to remove 67.8% of As(V) from the adsorbent.

Fixed-bed experiments were also conducted with calcinated Mg-Al-LDH to investigate the effect of particle size, pH, initial As(V) concentration and flow rate in breakthrough curves (Dadwhal, Ostwal et al. 2009). The decrease of particle size, flow rate and initial concentration all caused an increase of breakthrough time.

Results of adsorption studies, conducted with LDH adsorbents in continuous mode, are presented in Table 8. Although LDH are composed of metals with strong affinity to arsenic, the reported column studies did not show interesting results if compared with other metal-containing adsorbents discussed in this article.

Table 2.8: Comparison of dynamic tests using LDH as adsorbents for arsenic removal.

Adsorbent	Arsenic species	C_o (µg L^{-1})	t_b (h)	BV_b	Ref.
Zn-Fe-LDH	As(V)	1,000		~300	(Lu, Zhu et al. 2015)
Mg-Al-Cl-LDH	Total As	506	10	-	(Nhat Ha, Kim Phuong et al. 2016)
Mg-Fe-Cl-LDH	Total As	506	7	-	(Nhat Ha, Kim Phuong et al. 2016)

2.1.12 Antimony adsorption in continuous mode

Few adsorption studies in continuous mode have been reported for antimony removal (Biswas, Inoue et al. 2009, Dorjee, Amarasiriwardena et al. 2014, Lu, Zhu et al. 2015, Ungureanu, Santos et al. 2017, Qiu, Yan et al. 2019, Bacelo, Santos et al. 2022). However, the current research in column adsorption of Sb from water is growing in the last 5 years, on the contrary of research reporting column studies for As removal, which has been reducing in the last 25 years. So, antimony adsorption in aqueous solution might be a potential field of study to explore in the next years.

Different materials were tested for Sb removal in column operation. Granular titanium dioxide (TiO_2) achieved adsorption densities of 0.981 mg Sb g^{-1} for new adsorbent and 0.768-0.905 mg Sb g^{-1} in three regeneration cycles (Qiu, Yan et al. 2019). The addition of nano-zero valent iron (nZVI) to soil columns was reported to increase Sb removal ability of soil (Dorjee, Amarasiriwardena et al. 2014). Ferric-based layered double hydroxide (Zn-Fe-LDH) was reported to achieve good antimony removal results, in a rate of 12,000 L of contaminated water for each kg of Zn-Fe-LDH. Layered double hydroxide mineral, brucite (BRU), was able to treat antimony mining wastewater containing ~170 µg Sb L^{-1}, with maximum adsorption capacity of 0.405 µg g^{-1} (Runtti, Luukkonen et al. 2023).

Antimony removal was also observed in biosorbents: brown seaweeds packed-bed column achieved maximum adsorption capacity of 3.8 mg g^{-1} (Ungureanu, Santos et al. 2017), pine bark tannin resin were able to reach Sb(III) adsorption capacities from 2.7±0.2 to 31±2 mg g^{-1} (Bacelo, Santos et al. 2022), and Fe(III)-loaded saponified orange waste (SOW) gel reduced Sb(V) concentration by almost 99% (Biswas, Inoue et al. 2009).

2.1.12 Conclusions

Much research has been conducted in the past decades to develop adsorption systems for continuous arsenic removal from contaminated water. Different types of materials have been tested and improved to perform better adsorption. Maximum adsorption capacities of 28.96 mg g^{-1} and 74.8 mg g^{-1} were reported mostly by novel adsorbents like binary metal oxides and biosorbents, respectively. Most studies were preliminary and there is still a gap between the identification of novel adsorbents and feasibility studies for practical applications.

Other materials presented similar values of maximum adsorption capacities: 6.07 mg g^{-1} for GFH, 5.00 mg g^{-1} for minerals (mill-scale derived magnetite particles), 3.8852 mg g^{-1} for

industrial waste (iron oxide-coated cement), 3.51 mg g^{-1} for soil and rock (pisolite), 3.30 mg g^{-1} for nanocomposite (iron doped phenolic resin/AC), 3.229 mg g^{-1} for commercial (Lewatit FO36), and 2.873 mg g^{-1} for carbon-based (Fe/GAC),

Biosorbents were employed in most studies published, followed by metal oxides and nanocomposites. There was an increase in the last years in research for low-cost adsorbents such as biosorbents and industrial waste and by-products, which is of high importance to fulfil the gap of efficient and cheap treatment in most of arsenic affected places.

Arsenic adsorption in continuous mode is mostly affected by pH, temperature, flow rate and hydraulic retention time, adsorbent quantity (bed height), adsorbate initial concentration, and the presence of other chemical elements. Iron incorporation is the most common treatment to increase the arsenic adsorption capacity of adsorbent materials, followed by other metals such as aluminium and zirconium.

Further adsorption investigation must be conducted at pilot-scale, which is important to evaluate the application of the adsorbent in full scale, including more studies in regeneration and recovery, which enhance the economical balance of adsorption. Furthermore, the calculation of treatment costs and life cycle assessment (LCA) of the adsorption systems are relevant to be compared with other water treatment techniques.

As arsenic, antimony is also a toxic element which can be remediated by low-cost treatment such as adsorption due to its chemical similarities with arsenic, for which good removal results by adsorption have been demonstrated. Hence, more studies into antimony adsorption should be conducted, mainly into recovery options because of its limited supply in the future. This thesis aims to add in the literature a novel adsorbent, iron-coated cork granulates, to remove antimony in continuous mode.

Overall, this section gathered the most relevant worldwide research into low cost and alternative arsenic and antimony adsorption in dynamic systems, which is important to help to consolidate the available knowledge for sustainable solutions that provide safe access to potable water in contaminated areas. This thesis aims to aid in the literature a novel adsorption system to remove arsenic or antimony in continuous mode using a low cost and alternative adsorbent, iron-coated cork granulates. The effect of operational parameters in the system, such as pH, temperature, flow rate, bed height, initial concentration and water matrix will be assessed.

2.2 Desorption of arsenic and antimony in continuous mode

2.2.1 Introduction

This second section of the literature review aims to establish the state-of-the-art on the desorption of arsenic and antimony desorption from exhausted adsorbents previously used in water treatment. After a certain operation time (which varies depending on the operational conditions, sorbent type, and effluent characteristics) the adsorbent becomes saturated and must be replaced or treated via a regeneration process before it can be reused (Alka, Shahir et al. 2021). Many benefits are associated with the regeneration of saturated adsorbents, including economic savings and reduced environmental impact (Vakili, Deng et al. 2019). In terms of environmental and economic feasibility, the adsorption process is dependent on the reuse of the exhausted adsorbent through regeneration and, in certain circumstances, the recovery of a valuable adsorbate, such as antimony and arsenic (recently inserted in the list of critical materials for supply in Europe (Commission, 2023)), from the saturated bed. When the adsorbent or adsorbate is easily obtainable at low cost, desorption may not be economically viable; nevertheless, desorption can be a more ecologically friendly alternative.

Adsorbent regeneration may be achieved by thermal, chemical, biological, and ozonation processes. Chemical or solvent desorption (DE) is generally viewed as the most cost-effective method (Patel 2021). Like adsorption, desorption can be conducted in batch or continuous (column) mode, and the solvent solution is also known as the eluent. Acids, bases, salts, and complexing agents are different categories of chemicals accessible for use as eluents. A successful desorption process is dependent on the appropriate selection of eluent type and concentration, which is primarily determined by the adsorbent material and the respective adsorption mechanism to the adsorbent (Lata, Singh et al. 2015). This section will focus on chemical desorption, including the eluent effect, regeneration and recovery, challenges, and future perspectives.

2.2.2 Short bibliometrics

A brief bibliometric study on As and Sb adsorption and desorption was carried out in the Web of Science and Scopus databases, in January 2024. The terms “arsenic AND adsorption AND water”, “arsenic AND desorption AND water”, “antimony AND adsorption AND water”, and “antimony AND desorption AND water” were selected. The findings are represented in Figure 2.1.

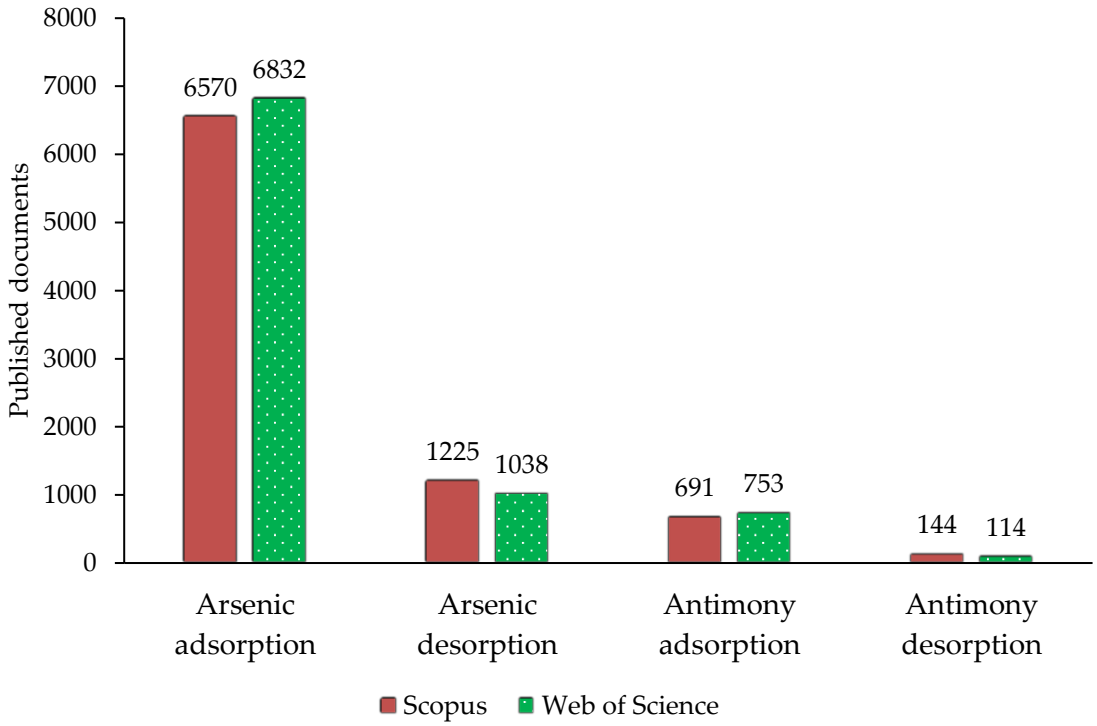


Figure 2.1: Published documents for each term on arsenic and antimony adsorption and desorption from water.

The number of publications on "arsenic AND adsorption AND water" is almost ten times higher than that on "antimony AND adsorption AND water". This might be supported by the fact that arsenic contamination in drinking water is a much older concern than antimony contamination. Arsenic's first regulation in water was established by the U.S. Public Health Service (USPHS) in 1942, with a recommended value of 50 μg L^{-1} (USPHS 1943, Pontius 1994), which was later reduced to 10 μg L^{-1} in 1962 (Smith and Smith 2004). Furthermore, it was included in the first international standard for drinking water, published by the World Health Organization in 1958 with a maximum allowable concentration of 0.2 mg L^{-1} (World Health 1958). Antimony, on the other hand, received its first WHO recommendation over 50 years later, in 1993, of 5 μL^{-1} for drinking water (World Health 1993), which was modified to 20 μg L^{-1} in the 2017 edition (WHO 2017).

Another reason for the higher number of academic papers addressing arsenic adsorption, than those focusing on antimony adsorption, is the larger population impacted by arsenic pollution in drinking water. It is estimated that arsenic-contaminated waters affect more than 230 million people globally, with a substantial part of the population being from developing nations (Shaji, Santosh et al. 2021). Adsorption as a technology for arsenic removal from water is attractive

for these nations since it is considered both inexpensive and effective (Patel 2019, Dudek and Kołodyńska 2022).

Antimony pollution is also a worldwide issue, although the population exposed to antimony-contaminated water has not yet been estimated. Contamination of water resources in the vicinity of shooting-range soils and mining sites with Sb is a problem in countries such as China, the U.S., and Spain, among other economic powers (Li, Zheng et al. 2018, Bolan, Kumar et al. 2022), which should be encouraged to develop and implement more robust and expensive water treatment solutions.

In Figure 2.1, we can also observe the gap between the adsorption and desorption studies. The desorption of arsenic or antimony has been reported approximately 5-6 times less often in academic publications than adsorption, even though desorption is an essential step of the treatment process. Antimony desorption may be even more relevant because the element is widely applied in industry and its recovery may be important because it is identified as being at critical levels of availability in some regions, such as the European continent (Cole-Hamilton 2020). It is expected that the interest on arsenic desorption will rise in the future as it was recently identified as also of critical level of supply in Europe (Commission, 2023).

Figure 2.2 presents the global distribution of publications on the terms “antimony AND desorption AND water” and “arsenic AND desorption AND water”. China has the most publications in both terms, followed by the United States, which has a stronger presence in arsenic desorption. Among the top 20 countries ranking for publications on arsenic desorption we found the most affected countries by arsenic contamination in water: China, the U.S., India, Japan, Pakistan, Argentina, Brazil, Taiwan, Mexico, Vietnam, and Bangladesh.

China has been the largest antimony producer worldwide for 110 years, with more than 60% of global production (in 2019), which is mainly associated with the major mined ore deposits located in the country (Herath, Vithanage et al. 2017, Nishad and Bhaskarapillai 2021). Between 2006 and 2016, China released 1915.58 Gg of antimony into the biosphere, with a recycling rate of just 0.91 % in 2013 (Chu, Mao et al. 2019). This, together with the expanding scientific dominance of China, may help to explain the nation's interest in and leadership in antimony desorption research.

For both arsenic and antimony, three journals published more papers: Journal of Hazardous Materials, Chemosphere, and Science of the Total Environment. In terms of keywords associated to documents found for each expression, it's worth noting that “pH” was highly mentioned for

both "desorption AND arsenic AND water" and "desorption AND antimony AND water". "Groundwater" and "iron" were among the top ten keywords associated to the documents published about "arsenic AND desorption AND water". This was expected, given iron´s significant propensity to bind with arsenic, resulting in the incorporation of this element as the most common alteration of biosorbents to increase arsenic removal rates, as shown in Section 2.1.

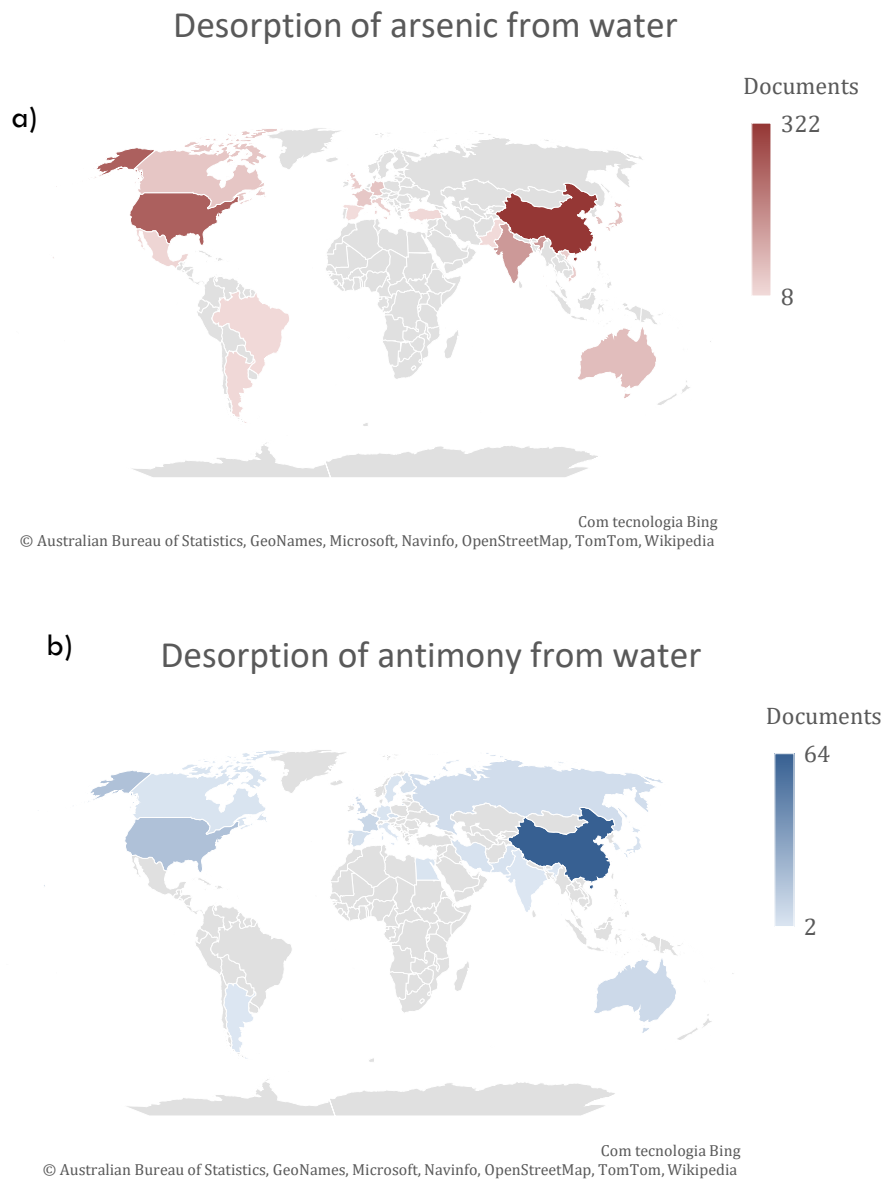


Figure 2.2: Global distribution of academic publications about a) "desorption AND arsenic AND water", and b) "desorption AND antimony AND water".

2.2.3 Adsorption of pnictogens

Antimony and arsenic are toxic elements that can be removed from water by similar low-cost treatment processes due to their chemical similarities; for example, good removal results by adsorption have been demonstrated.

When designing an adsorption system, the adsorbent type is not the only relevant aspect to be considered. The adsorption process can be dependent on the following factors: pH, pHzpc, adsorbent dosage, temperature, pressure, surface area of the adsorbent, and presence of co-existing ions (Zaimee, Sarjadi et al. 2021). Moreover, adsorption in continuous mode might also be affected by other parameters, such as flow rate, hydraulic retention time (HRT), and adsorbate initial concentration. Both Sb and As removal strategies can include the oxidation of the trivalent species, which are harder to adsorb, to the pentavalent species, which has greater affinity for most adsorbents.

Much research has been conducted on arsenic and antimony adsorption by different materials and under various conditions. The most frequent treatment for increasing the arsenic adsorption capacity of adsorbent materials is iron incorporation, followed by the addition of other metals, such as aluminum and zirconium, as shown in section 2.1. The materials developed to adsorb arsenic usually exhibit affinity for antimony removal (Vieira, Pintor et al. 2017, Pintor, Vieira et al. 2018, Bacelo, Santos et al. 2020, Pintor, Vieira et al. 2020, Bacelo, Santos et al. 2022, Kavacık and Dölgen 2023) due to the chemical characteristics shared by the elements. Nano adsorbents, such as carbon nanofibers, carbon nanotubes, and metal-organic frameworks (MOFs), have great potential for removing metalloids from contaminated effluents, however, their small diameter limits their application on a large scale. To overcome this issue, a hybrid aerogel with MOFs embedded in a cellulose nanocrystal matrix has been developed with a diameter of 2 cm (Zhang, Yu et al. 2023). This aerogel was capable of adsorbing high quantities of Sb(V).

Because the resultant composites might inherit the properties of the parent materials while also displaying synergistic effects, the creation of composite adsorbents integrating two or more metal oxides may enhance their adsorption capacities (Zhang, Wu et al. 2023). Not only have binary metal oxides reached significant adsorption capabilities, but so has biosorption. Biosorption has several advantages, such as the use of cheap abundant biomaterials, relatively low operational cost (Senthil Kumar and Tsopbou Ngueagni 2022), and potential lower carbon emissions.

Arsenic and antimony can coexist in contaminated drinking water resources (Gan, Ding et al. 2023). There have been investigations on the effect of coexisting pnictogens (Qiu, Yan et al. 2019, Pintor, Brandão et al. 2021) and the possibility of simultaneous As-Sb removal has been demonstrated (Belozerova, Pechishcheva et al. 2022, Long, Wang et al. 2022, Pintor, Tomasi et al. 2022, Xu, Li et al. 2022). Lately, studies have found removal capacities of adsorption systems operating in continuous mode in the range of 4 to 30 mg g^{-1} of arsenic (Saldaña-Robles, Damian-Ascencio et al. 2018, Ociński and Mazur 2020) and 6 to 31 mg g^{-1} (Iqbal, Saeed et al. 2013, Dabbagh, Mirkamali et al. 2019, Zhu, Huang et al. 2021, Bacelo, Santos et al. 2022) of antimony. Fixed-bed columns operating with both elements have removed As and Sb under World Health Organization drinking water guidelines of 10 μgL-1 and 20 μgL^{-1}, respectively (Lu, Zhu et al. 2015, Qiu, Yan et al. 2019).

Adsorption mechanisms include surface precipitation, physical adsorption, ion exchange, , electrostatic attraction, and functional group complexation (Masindi, Foteinis et al. 2022). The type of interaction between the adsorbate and adsorbent can vary with the type of adsorbent and the element species. The Langmuir and Freundlich equilibrium models, which describe monolayer adsorption onto a homogeneous surface and chemisorption on a heterogeneous surface, respectively, are the most often used models for characterizing As (Yeo, Li et al. 2021) and Sb adsorption (Long, Wang et al. 2020, Peng, Wang et al. 2023).

2.2.4 Desorption parameters

Desorption can be viewed as the opposite of the adsorption process, in which adsorbates are released from the adsorbent surface either by substitution for an ion with a strong affinity for the saturated adsorbent or through chemical interactions with the eluent (Michael, Khalid et al. 2018) as illustrated in Figure 2.3. The optimal eluent is chosen by balancing i) desorption efficiency, ii) regeneration capacity of the adsorbent under treatment, and iii) toxicity and disposal of the eluting solution.

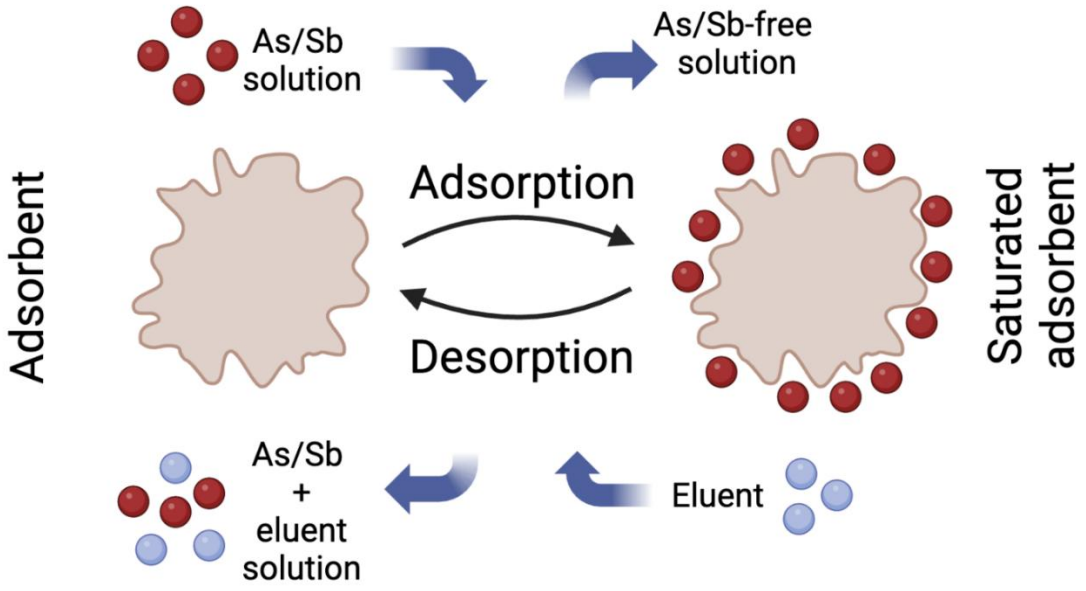


Figure 2.3: Schematic illustration of the adsorption-desorption process of As/Sb in water.

The desorption performance may be assessed by quantifying the desorption capacity, q_d (mg g^{-1}), and the desorption efficiency, d_e (%). The following equations can be used to calculate q_d and d_e.

In batch mode (Patel 2021):

$$q_d = \frac{V * C_d}{m} \tag{2.1}$$

where V is the solution volume (L), C_d is the concentration of adsorbate in the eluent after contacting the adsorbent (mg L^{-1}), and m is the mass of adsorbent (g).

In continuous mode:

$$q_d = \frac{adsorbate\ mass_{out}}{adsorbent\ mass} \tag{2.2}$$

where $adsorbate\ mass_{out}$ is the eluted mass of the adsorbate in the solution (mg), and $adsorbent\ mass$ is the adsorbent mass in the bed (g).

The desorption efficiency can be defined for both modes as follows:

$$d_e = \frac{adsorbate\ mass_{out}}{adsorbate\ mass_{in}} \text{ x } 100 \tag{2.3}$$

where $adsorbate\ mass_{in}$ is the mass of arsenic retained in the saturated adsorbent in the previous adsorption cycle.

The regeneration process can cause a decrease in the adsorption capacity of the adsorbent (q_{loss}), which can be calculated by the expression:

$$q_{loss}\ (\%) = (1 - \frac{q_r}{q_0}) \times 100 \quad (2.4)$$

where q_r is the adsorption capacity after regeneration (mg g^{-1}) and q_0 is the initial adsorption capacity of the fresh adsorbent (mg g^{-1}).

The pH, time of contact or retention time, flow rate, eluent type, concentration of desorbing agent in solution, surface characteristics of the adsorbent, surface coverage, and coexisting ions all influence desorption efficiency, d_e (Tuutijärvi, Vahala et al. 2012). Compared with fresh adsorbents, regenerated adsorbents commonly suffer a reduction in the adsorption parameters, such as adsorption capacity and breakthrough time, compared with the fresh adsorbent. This difference may be due to the degradation of the adsorbent or the presence of undesorbed arsenic/antimony. An increase in arsenic adsorption capacity after 2 to 6 cycles were observed in the literature (Ociński and Mazur 2020), which might be justified by the desorption of the remaining adsorbate from the previous cycles.

2.2.5 Desorption mechanism

Desorption equilibrium and kinetics can be represented by the same theoretical models of adsorption equilibrium (e.g., Langmuir (Langmuir 1918), Freundlich (Freundlich 1907)) and kinetics (e.g., pseudo-first-order, pseudo-second-order, Elovich (Elovich and Larionov 1962)), yet this does not indicate that adsorption kinetics and mechanism are the same as for desorption (Ghosh, Mukiibi et al. 2004). The adsorption and desorption curves are similar in batch mode; however, in continuous mode, the adsorption and desorption profiles are different, as shown in Figure 2.4. The graph from adsorption in continuous mode (Figure 2.4.c) was made using C/C_0 values, which is more usual, but using mg L^{-1} experimental values on y-axis will result in the same shape.

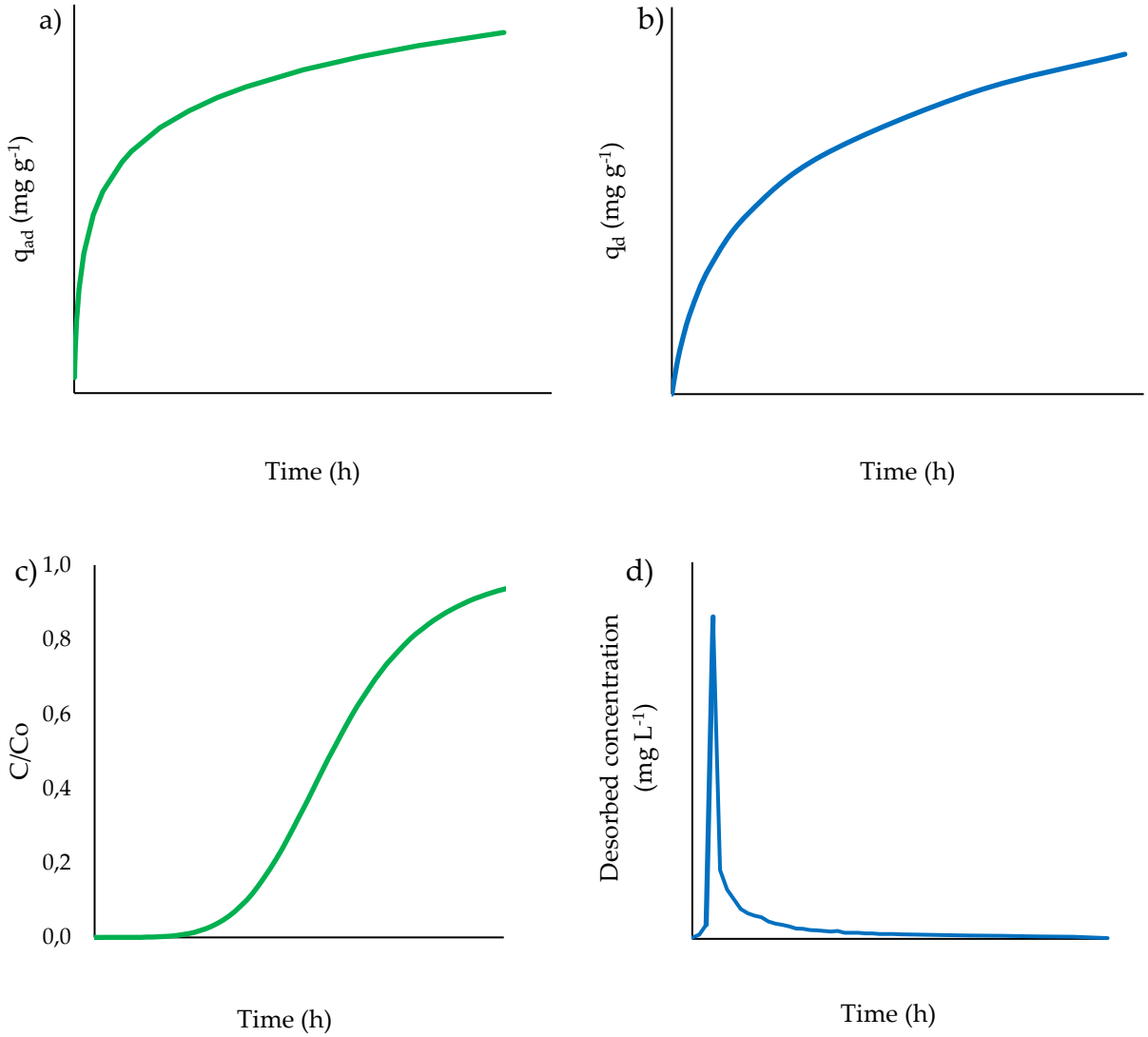


Figure 2.4: Examples of curves of antimony/arsenic a) adsorption and b) desorption in batch mode; and c) adsorption and d) desorption in continuous mode.

Adsorption curves in continuous mode, also known as breakthrough curves, are "s"-shaped, and a range of models can be fitted to the experimental data, such as the Yan model (Yan, Viraraghavan et al. 2001), the Thomas model (Thomas 1944), and the Yoon-Nelson model (Yoon and Nelson 1984). Desorption curves are shaped like a half-bell curve, and no theoretical models currently exist to be applied for describing them.

The study of desorption kinetics is important to predict the possible leaching of pollutants from the spent adsorbent media. Slow desorption kinetics may prevent equilibria from occurring with short elution times (Ghosh, Mukiibi et al. 2004), which could reduce desorption efficiency in column mode and, as a result, the adsorption capacity of the material in subsequent cycles, thereby affecting its potential for reuse.

Arsenic desorption from different adsorbents using 0.1 M NaOH showed similar kinetics, with a rapid phase lasting approximately 4 h, followed by a slower phase lasting 24 h before reaching equilibrium (Wang, Gao et al. 2016, He, Peng et al. 2018). Antimony desorption from rapeseed straw biochar was time-dependent, and biochar that had been coated with Mn was more stable than that without this element (Jia, Zhou et al. 2020). Table 2.9 shows the As/Sb desorption kinetics parameters for different adsorbents.

Table 2.9: Batch desorption kinetics for different adsorbents.

Adsorbent	Adsorbate	Eluent	Desorption model	Desorption parameters	Time required to complete most of the DE	Ref.
Sol-gel maghemite	As(V)	NaOH 0.1 M	Pseudo-second-order	k_2: 0.0005 g mg^{-1} min^{-1} r^2 = 0.985	1 h	(Tuutijärvi, Vahala et al. 2012)
Commercial maghemite	As(V)	NaOH 0.1 M	Pseudo-second-order	k_2: 0.0050 g mg^{-1} min^{-1} r^2 = 0.999	1 h	(Tuutijärvi, Vahala et al. 2012)
Extracellular polymeric substances (EPS)	Sb(V)	Milli-Q water	Pseudo-second-order	k_2: 0.00161 g mg^{-1} h^{-1} r^2 = 0.9977	1 h	(Zhang, Lee et al. 2013)

2.2.6 Desorption of arsenic

The desorption of arsenic and the regeneration performance of different types of adsorbents reported in the literature are summarized in Table 1. The adsorbent types were categorized into four groups: biochar and (modified) biosorbents, nanomaterials, commercial adsorbents, and others.

Table 2.10: Desorption of arsenic and regeneration performance of adsorbents in batch mode.

Adsorbent	Species	Time (h)	Eluents	Desorption efficiency (%)	Cycles	Adsorp. capacity reduction	Ref.
Biochar and (modified) biosorbents							
Al(III) Kapok fibres	As(V)	1	0.01 M HCl	-	5	~33%	(Yeo, Dong et al. 2022)
Fe(III) modified Kapok fiber	As(V)	-	0.1 M HCl	-	4	~38%	(Yeo, Li et al. 2022)

Adsorbent	Species	Time (h)	Eluents	Desorption efficiency (%)	Cycles	Adsorp. capacity reduction	Ref.
Charred orange peel (COP) **Natural orange peel (NOP)**	As(V)	1.5	0.01 M HCl	-	3	10% 26%	(Abid, Niazi et al. 2016)
Fe(III) - biomass of *Staphylococcus xylosus*	As(III) As(V)	0.5 2	0.09 M HCl	100	5	~20% ~40%	(Aryal, Ziagova et al. 2010)
***Garcinia cambogia* plant**	As(III)	0.5	0.05 M NaOH 0.1 M Na_2CO_3 0.2 M NaCl	~99	1	-	(Kamala, Chu et al. 2005)
Green alga (*U. cylindricum*)	As(III)	1	1 M HCl 1 M HNO_3	95 85	10	~2%	(Tuzen, Sarı et al. 2009)
HFO-treated sugarcane bagasse	As(V)	-	30% HCl 1 M NaOH	17 54-85	1	-	(Pehlivan, Tran et al. 2013)
Thiol-functionalized sugarcane bagasse	As(III) As(V)	1	0.01 M HCl	-	5	14% 22%	(Gupta, Vidyarthi et al. 2015)
Iron-impregnated biochar	As(V)	48	0.1 M NaOH	72-60	3	26-37%	(He, Peng et al. 2018)
Polyethylenimine-coated bacterial biosorbent	As(V)	1	0.01 M NaCl 0.01 M Na_2SO_4 0.01 M NaOH	~85-55 ~100-95 100	3 3 3	- - 15%	(Kim, Park et al. 2019)
Water melon rind (WMR) **Citric acid WMR** **Xanthated WMR**	As(III)/As(V)	0.67	0.1 M NaOH	97-20 / 98-50 94-11 / 93-15 98-32 / 96-47	4	-	(Shakoor, Niazi et al. 2018)
Zinc-impregnated lignin biochar (Z-LBC)	As(V)	-	2.5% HCl	-	4	9%	(Park, Lee et al. 2021)

Adsorbent	Species	Time (h)	Eluents	Desorption efficiency (%)	Cycles	Adsorp. capacity reduction	Ref.
Magnetic biochar from Kans grass	As(III) As(V)	14	0.5 M NaOH	68 89	1	-	(Baig, Zhu et al. 2014)
Magnetic wheat straw	As(V)	3	0.1 M NaOH	-	10	>80%	(Tian, Wu et al. 2011)
Hydrated ferric oxide biochar nanohybrids	As(III)	3 x 2	0.5 M NaOH	-	6	~10%	(Zhu, Zhang et al. 2022)
Magnetite-modified water hyacinth biochar	As(V)	12	0.1 M HCl	~80	4	49.2%	(Zhang, Wang et al. 2016)
Ni/Mn-LDHs on pristine biochars (NMMB)	As(V)	48	0.1 M NaOH	81.7	3	2%	(Wang, Gao et al. 2016)
Cross-linked alginate beads (CABs)	As(V)	-	0.3 M NaOH	~85	5	35%	(Raval and Kumar 2022)
Biochar (BC)/nZVZn	As(III) As(V)	0.67	0.2 M NaOH	77-31 78-43	3	-	(Masood ul Hasan, Javed et al. 2023)
Biochar/ Hydroxyapatite (BC/HA-alginate)	As(III) As(V)	0.67	0.2 M NaOH	88-30 64-25	3	-	(Masood ul Hasan, Javed et al. 2023)
Magnetic biochar from dry teak leaves (MTB-800)	As(III) As(V)	2	0.1 M NaOH	-	5	~48% ~53%	(Verma and Singh 2023)
			Nanomaterials				
Chitosan graphene oxide-gadolinium oxide nanorods	As(V)	1	0.1 M NaOH	98-75	6	22%	(Choi, Lingamdinne et al. 2020)
Cross-linked alginate beads impregnated with bilayer-oleic coated magnetite (CAB@BOFe)	As(V)	-	0.3 M NaOH	~11	5	8%	(Raval and Kumar 2022)

Adsorbent	Species	Time (h)	Eluents	Desorption efficiency (%)	Cycles	Adsorp. capacity reduction	Ref.
δ-MnO_2@Fe/Co-MOF-74 nanocomposite	As(III)	6	0.1 M NaOH	-	4	21.1%	(Yang, Zhou et al. 2021)
Graphene nanoplatelets	As(III)	3	2.0 M NaOH 2.0 M KOH	68.35 81.07	1	-	(Nandi, Ghosh et al. 2021)
Magnetic γ-Fe_2O_3 nanoparticles	As(III) As(V)	3	1 M NaOH	-	6	61% 40%	(Lin, Lu et al. 2012)
Sol-gel maghemite nanoparticles	As(V)	48	1 M NaOH	>95	6	5-10%	(Tuutijärvi, Vahala et al. 2012)
Superparamagnetic iron oxide nanoparticles (SPIONs)	As(III)	-	0.1 M NaOH 0.1 M HCl	82 43	8 -	86%	(Asadi Haris, Dabagh et al. 2023)
Electrospun polyethylenimine/polyvinyl chloride nanofiber sheets	As(V)	2	0.02 M NaOH	95	5	9%	(Wang, Kang et al. 2023)
Fe_3O_4@surfactants nanoparticles	As(V)	0.5	1 M NaOH	-	5	15%	(Zhao, Shi et al. 2023)
Fe_3O_4 - polyurethane (PU) foam nanocomposite	As(V) + As(III)	-	0.1 M HCl + 0.1 M NaOH	90-70	5	28%	(Tamaddoni Moghaddam, Ghasemi et al. 2023)
Commercial adsorbents							
Activated carbon – Aquacarb 207 EA	As(V)	72	0.05 – 1 M NaCl 0.5 M $CaCl_2$ 0.5 M $NaNO_3$ 0.5 M NaOH	100 84 100 100	1	<7%	(Di Natale, Erto et al. 2013)
ARM200 (VV)	As	24	6% NaOH	87.2	1	-	(Chen, Sorg et al. 2015)
Commercial maghemite	As(V)	48	1 M NaOH	>95	6	5%	(Tuutijärvi, Vahala

Adsorbent	Species	Time (h)	Eluents	Desorption efficiency (%)	Cycles	Adsorp. capacity reduction	Ref.
							et al. 2012)
E33-G	As	24	6% NaOH	88.1	1	-	(Chen, Sorg et al. 2015)
GFH	As	24	6% NaOH	51.6	1	-	(Chen, Sorg et al. 2015)
Lanthanum-modified iron oxide	As(V)	6	0.05 M NaOH 0.2 M NaOH 1 M NaOH	40.95 83.03 98.78-94.54	1 1 1-3	- - 6%	(Dudek and Kołodyńska 2022)
Nano-zero valent zinc (nZVZn)	As(III) As(V)	0.67	0.2 M NaOH	81-45 84-41	3	-	(Masood ul Hasan, Javed et al. 2023)
			Others				
Amine-doped acrylic ion exchange fiber	As(V)	2	0.1 N HCl + 0.1 N NaOH	-	9	~17%	(Lee, Alvarez et al. 2017)
Iron oxide coated geopolymer microspheres	As(III) As(V)	1	1 M NaOH	72 99	1	-	(Thakur and Armstrong 2021)
Iron-oxide-coated natural rock (IOCNR)	As	6	1 M NaOH	95	1	~49%	(Maji, Kao et al. 2011)
Hausmannite	As(V)	2	Citric acid pH 4 Citric acid pH 5 Citric acid pH 6	~40 ~60 ~67	1	-	(Barreto, Elzinga et al. 2020)
Hematite	As(V)	2	Citric acid pH 4 Citric acid pH 5 Citric acid pH 6	~17 ~46 ~71	1	-	(Barreto, Elzinga et al. 2020)
Ce-Ti hybrid oxide	As(III) As(V)	12	0.5 M NaOH	-	5	28% 19%	(Li, Deng et al. 2010)

Adsorbent	Species	Time (h)	Eluents	Desorption efficiency (%)	Cycles	Adsorp. capacity reduction	Ref.
Alginate beads-encapsulated SPIONs (SPIONs-Alg)	As(III)	-	0.1 M NaOH 0.1 M HCl	91 71	8 -	76%	(Asadi Haris, Dabagh et al. 2023)

The biochar and modified biosorbents could be regenerated to remove arsenic for many cycles. For some biosorbents, such as green algae, the arsenic removal efficiency stayed above 90% after 10 cycles (Tuzen, Sarı et al. 2009). Most of the bio-based materials could be reused for 3-5 cycles with an adsorption capacity loss of about 10-40%. Nanomaterials were reused for around six adsorption-desorption cycles, during which the adsorption loss ranged from 5 to 86%. Commercial adsorbents achieved the lowest average reduction in adsorption capacity of around 6%. This could be due to previous optimization of the products before they were released into the market.

In desorption experiments, As(V) was studied twice as much as As(III). In terms of desorption efficiency, different outcomes were reported for the two species, depending on the type of adsorbent used; it is more common to suffer higher loss of As(V) than As(III) adsorption capacity. After five adsorption-desorption cycles, functionalized sugarcane bagasse showed a 14% reduction in As(III) adsorption capacity, whereas the reduction in As(V) adsorption capacity was 22% (Gupta, Vidyarthi et al. 2015). Similar findings were observed for Fe(III) - biomass of Staphylococcus xylosus (Aryal, Ziagova et al. 2010), although Ce-Ti hybrid oxide, after five adsorption-desorption cycles, had lower arsenite adsorption capacity than arsenate (Li, Deng et al. 2010).

2.2.6.1 Analysis of desorption efficiency by type of eluent

Figure 2.5 shows an overview of the eluents applied for the arsenic desorption studies presented in Table 2.10. The most common types of chemical eluents used to regenerate adsorbents were bases and acids, more specifically NaOH and HCl. Nevertheless, many salts were tested for arsenic removal because they are less aggressive toward material structures. A mixture of chemicals is also common practice for metal desorption (Chaudhary and Farrell 2015, Lee, Alvarez et al. 2017).

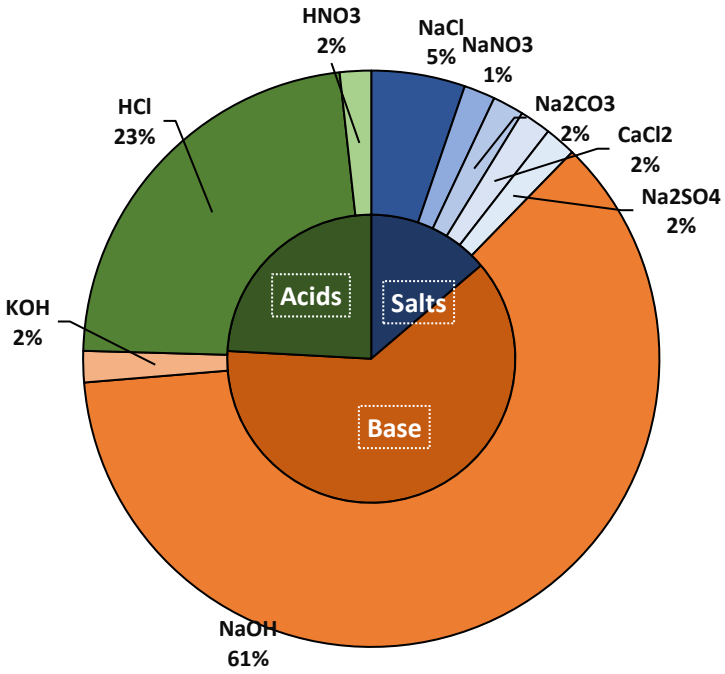


Figure 2.5: Percentage of eluents used for arsenic desorption studies presented in Table 2.10.

2.2.6.1.1 Bases

Sodium hydroxide was the most explored eluent in the regeneration of arsenic-loaded adsorbents. Figure 2.6 shows the desorption efficiency of NaOH by the type of adsorbent. We can observe that 0.1 M was the most applied concentration (pH close to 13), mainly on biochar and (modified) biosorbents, which can be more sensitive to high pH solutions. The efficiency of NaOH in removing As from these materials varied widely, but for nanomaterials and other adsorbents, the desorption efficiency of NaOH ranged between about 70 and 100%.

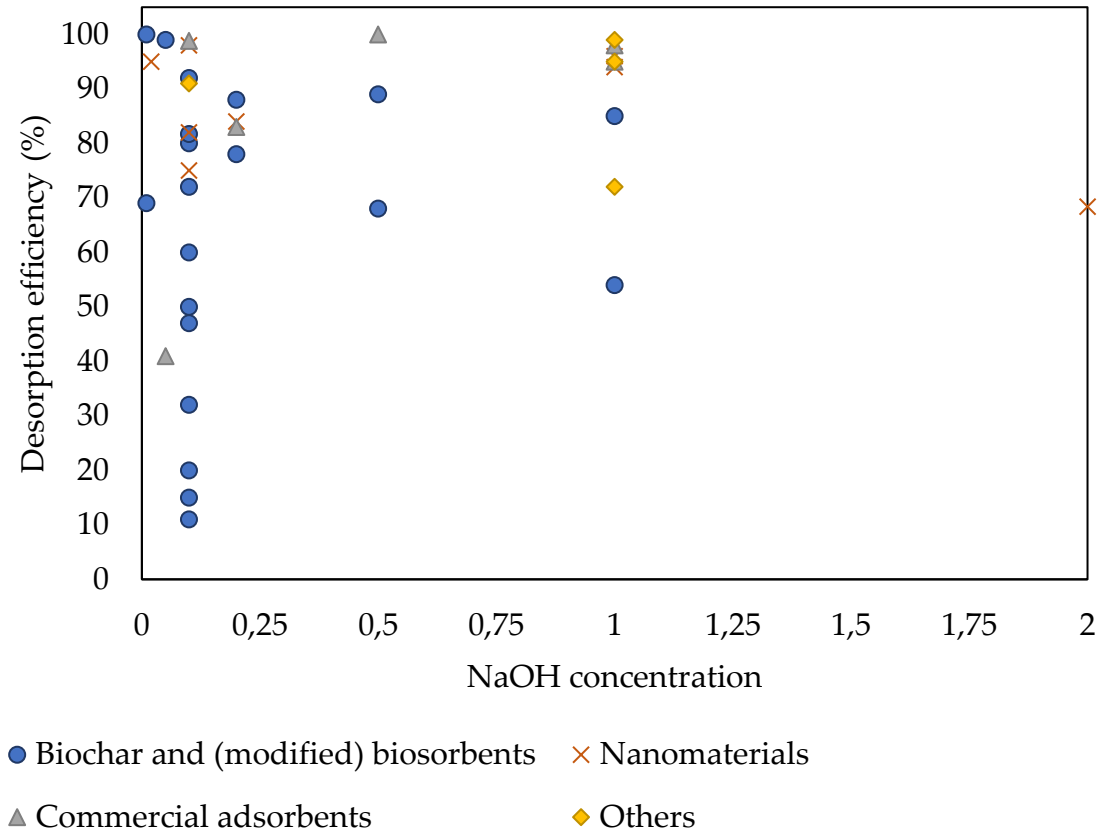


Figure 2.6: Desorption efficiencies of arsenic-loaded adsorbents by NaOH at different concentrations reported in the literature.

The increase in NaOH concentration was not strictly related to the increase in desorption efficiency. Some studies with varying ranges of NaOH concentrations found an optimal concentration of 0.1 M to achieve the highest arsenic desorption (Asadi Haris, Dabagh et al. 2023). An optimal concentration of 2%, between 1% and 6%, has also been reported (Chen, Sorg et al. 2015). The higher performance of NaOH may be related to the repulsion of the adsorbent surface and the more negatively charged arsenate form AsO_4^{3-} at pH values above 11.5 (Ungureanu, Santos et al. 2015). For iron-based adsorbents, NaOH can be even more efficient due to the higher affinity of OH^- to form a bond with Fe^{3+} compared to AsO_4^{3-} (Tuutijärvi, Vahala et al. 2012).

2.2.6.1.2 Acids

The most common acid eluent applied for arsenic desorption is HCl. The application of 0.09 M HCl to desorb both inorganic arsenic species from the Fe(III) - biomass of *Staphylococcus xylosus* was highly efficient in terms of the desorption rate (Aryal, Ziagova et al. 2010). After consecutive adsorption-desorption cycles, the adsorbent exhibited a decrease in adsorption

capacity for both arsenate and arsenite, but the reduction in As(V) capacity was greater. A weaker acid solution of HCl 0.01 M was applied to regenerate orange peel biosorbents for three cycles (Abid, Niazi et al. 2016). A greater reduction in the adsorption capacity of arsenate was observed for natural orange peel (NOP) than for charred orange peel (COP). A more successful acid desorption process was reported for Zinc-impregnated biochar (Z-LBC) using 2.5% HCl, in which the adsorbent could pass through four regeneration cycles with only a slight loss in As(V) removal capacity (Park, Lee et al. 2021).

However, the use of acids as desorbing agent caused high leaching of the iron present in the iron-based adsorbents, compromising the reuse of the regenerated adsorbent in future adsorption cycles.(Ghimire, Inoue et al. 2002, Yeo, Li et al. 2022). The hindrance in the application of acid eluents is sometimes the degradation of the adsorbent; thus, weaker acids, such as organic acids (Zhang, Xie et al. 2021), can be less aggressive, although with lower desorption rates. The iron-based adsorbents may need to reload the iron coating after desorption and before the next adsorption cycle (Yeo, Li et al. 2022).

2.2.6.1.3 Salts

The desorption of arsenic was also reported in the literature using salts such as NaCl, Na_2CO_3, $NaNO_3$, Na_2SO_4, and $CaCl_2$. Arsenic desorption efficiencies of 100% from PEI-coated bacterial biosorbent were achieved using 0.01 M Na_2SO_4 (Kim, Park et al. 2019), and from activated carbons using 0.5 M $NaNO_3$ and 0.5 M NaCl (Di Natale, Erto et al. 2013). In comparison with other chemicals, NaCl has a lower acquisition cost, which makes it a very attractive choice (Di Natale, Erto et al. 2013).

2.2.7 Desorption of antimony

The effect of different chemical eluents on the performance of antimony desorption has also been explored in the literature. Table 2.11summarizes the data reported in the literature for Sb(V) and Sb(III) desorption efficiencies as well as regeneration performance in batch mode for different types of adsorbents: biochar and (modified) biosorbents, nanomaterials, and others.

Table 2.11: Desorption of antimony and regeneration performance of adsorbents in batch operation mode.

Adsorbent	Sb species	Time (h)	Eluents	Desorption efficiency (%)	Desorp. cycles	Adsorption capacity reduction	Ref.
			Biochar and (modified) biosorbents				
Cyanobacteria ***Microcystis***	Sb(V)	24	1 M EDTA 1 M HCl 1 M Citric acid 1 M NaOH	45.94 68.46 51.45 30.55	1	-	(Sun, Yan et al. 2014)
Green bean husk (GBH)	Sb(III)	1	0.1 M HCl	~98.8 – 90	7	~10%	(Iqbal, Saeed et al. 2013)
Iron-modified chitosan [Chifer(III)]	Sb(III)	24	HCl pH 3.5 0.01 M EDTA	78 – 76 68 – 38	3	11.4%	(Lapo, Deme y et al. 2019)
Marine algae *T. conoides*	Sb(III)	1	0.1 M HCl	>99	3	5%	(Vijay aragh avan and Balasu brama nian 2011)
Marine algae *C. sericea*	Sb(III)	4	0.1 M NaOH 0.1 M HCl 0.5 M Na_2HPO_4 0.5 M NaCl	12 17 23 15-45	1 1 1 3	- - - 52%	(Ungur eanu, Filote et al. 2016)
$MnFe_2O_4$-MCM-41-SH	Sb(III)	4	0.1 M Citric acid	-	5	10.9%	(Li and Fu 2020)
Pine bark tannin resin	Sb(III) Sb(V)	48	0.1 M NaOH	27 49	1	-	(Bacel o, Santos et al. 2022)
Tannins from *P. pinaster* bark	Sb(V)	12	0.5 M NaOH	69 – 28	2	-	(Bacel o, Vieira et al. 2018)
Iron-biochar composites (FBC)	Sb(V)	-	0.1 M HCl	-	5	~50%	(Zhan g, Dong

Adsorbent	Sb species	Time (h)	Eluents	Desorption efficiency (%)	Desorp. cycles	Adsorption capacity reduction	Ref.
							et al. 2022)
Amino-functionalized hydrothermal biochar (NMSH)	Sb(V)	-	0.5 M NaOH	-	4	9%	(Deng, Li et al. 2020)
Chitosan-loaded biochar	Sb(III)	-	0.5 M NaOH	-	3	19%	(Chen, Gao et al. 2022)
Pristine biochar	Sb(III)	-	0.5 M NaOH	-	3	30%	(Chen, Gao et al. 2022)
Lichen (*Physcia tribacia*) biomass	Sb(III)	0.5	0.5 M HCl 0.5 M HNO_3	95 78	10 1	20% -	(Uluozlu, Sarı et al. 2010)
La-doped magnetic biochars	Sb(V)	12	0.5 M NaOH + 5 M NaCl	-	6	30-44%	(Wang, Wang et al. 2018)
			Nanomaterials				
Carbon fibers decorated with ferric hydroxide (CF-Fe)	Sb(V)	-	3.0 M NaOH	96.6-76.5	7	4%	(Simsek, Demircivi et al. 2018)
Ce-doped Fe_3O_4	Sb(III)	12	0.5 M NaOH	~100%	3	~0-10%	(Qi, Joshi et al. 2017)
Chitosan-modified pumice (CTS-mPMC)	Sb(III)	0.5	0.5 M HCl	95-70	10	10%	(Sari, Tuzen et al. 2017)
Graphene	Sb(III)	4	0.1 M EDTA	-	5	<20%	(Leng, Guo et al. 2012)
Graphene oxide (GO)	Sb(III)	2	0.1 M EDTA	-	4	14.5%	(Yang, Shi et al. 2015)
Mercapto-functionalized hybrid sorbent	Sb(III)	4	3 M HCl	96.7 at 90°C 81.7 at 60°C	1 1	-	(Fan, Sun et

Adsorbent	Sb species	Time (h)	Eluents	Desorption efficiency (%)	Desorp. cycles	Adsorption capacity reduction	Ref.
				56.4 at 25°C	1		al. 2016)
NH_2-Fe_3O_4-NTA core-shell magnetic nanoparticle sorbents	Sb(III)	10	0.1 M EDTA	-	5	<20%	(Hao, Liu et al. 2019)
Nano-Fe_3O_4 modified red mud	Sb(III)	4	0.5 M HCl 0.5 M NaOH	-	5	~90% <40%	(Peng, Luo et al. 2021)
Polyamide-graphene (PAG) composite	Sb(III)	-	0.5 M HCl	95-80	6	-	(Saleh, Sarı et al. 2017)
Si-doped Fe oxide composites (SFOC$_{10}$)	Sb(V)	8	0.5 M NaCl + 0.5 M NaOH	~85-90	5	<15%	(Yang, Zhou et al. 2021)
Y-tape molecular sieve adsorbent (NaY@Ce)	Sb(III)	12	1 M NaOH	-	4	35%	(Yan, Qiu et al. 2020)
Zirconium porphyrin-based MOF (PCN-222)	Sb(III)	5	0.5 M HCl	-	5	~20%	(Guo, Zhang et al. 2021)
MOF-Y	Sb(V)	24	NaCl	~85	5	32%	(Li, Li et al. 2022)
NH_2-MOF-Y	Sb(V)	24	NaCl	~87	5	32%	(Li, Li et al. 2022)
ZVI decorated carbon nanotubes (CNT – Fe(0))	Sb(III) Sb(V)	4	0.05 M HCl	75 – 65	5	7 – 19%	(Mishra, Dwivedi et al. 2016)
Superparamagnetic nanoparticles Fe@Mg-Al LDH	Sb(III)	-	Acetone Ethanol Methanol HCl Acetone + HCl Ethanol + HCl Methanol + HCl	~60 ~66 ~57 ~68 ~70 63 ~73	1	-	(Motallebi, Moghimi et al. 2022)

Adsorbent	Sb species	Time (h)	Eluents	Desorption efficiency (%)	Desorp. cycles	Adsorption capacity reduction	Ref.
			Others				
Brucite	Sb(III)	2	1 M NaOH 1 M HCl	28.2% 98.6%	1	-	(Runtti, Luukkonen et al. 2023)
Low-cost natural diatomite	Sb(III)	-	0.5 M HCl	-	10	3%	(Sarı, Çıtak et al. 2010)
Hydromagnesite	Sb(III)	2	1 M NaOH 1 M HCl	39.5% 98.7%	1	-	(Runtti, Luukkonen et al. 2023)
Commercial Mg-rich mineral	Sb(III)	2	1 M NaOH 1 M HCl	12.9% 88.7%	1	-	(Runtti, Luukkonen et al. 2023)
MIL-100(Fe)-NH_2	Sb(V)	12	0.1 M NaOH	-	3	~1%	(Cheng, Fang et al. 2023)
Lanthanum-manganese binary oxide	Sb(III) Sb(V)	4	NaOH 2% + NaCl 4% + 20% NaClO	-	5	20% 28%	(Zhang, Wu et al. 2023)
Kaolinite	Sb(V)	12	0.1 M $MgSO_4$	80	1		(Xi, He et al. 2010)
Fe-Mn binary oxides ($FMBO_3$)	Sb(V)	8	1 M NaOH	>80	5	18%	(Yang, Zhou et al. 2018)

Most of the materials used in antimony adsorption-desorption cycles were nanomaterials. They often have greater adsorption capacities, which is advantageous for potential Sb recovery. On average, the antimony desorption efficiency reported in these studies was lower than that reported for arsenic.

Sb(V) desorption from MOF-Y and NH_2-MOF-Y was carried out with different eluents, and the best desorption efficiency was found in the following order: HCl > NaOH > Na_2CO_3 > NaCl > Na_2SO_4 > $NaNO_3$. However, strongly acidic conditions of HCl or strongly alkaline conditions of NaOH and Na_2CO_3 could damage the crystal structure of Y-based MOFs (Li, Li et al. 2022),

and the authors decided to explore adsorption/desorption cycles with the less aggressive eluent NaCl. After five consecutive adsorption-desorption cycles using NaCl, the remaining adsorption capacity was about 68% of the initial one.

Antimonite desorption has been researched almost twice as much as antimonate´s, and some studies have reported different desorption behavior for each species. For example, Sb(III)-loaded lanthanum-manganese binary oxide (L_1M_2BO) could be regenerated more effectively than the same adsorbent loaded with Sb(V) (Zhang, Wu et al. 2023), but Sb(V) recovery rates from pine bark tannin resin were higher than that of Sb(III) (Bacelo, Santos et al. 2022).

All categories of adsorbent could be regenerated at high desorption rates and for many adsorption-desorption cycles. Treatment of adsorbents to improve their adsorption capacity might also improve their regenerability. Iron-biochar composites that went through a higher pyrolysis temperature demonstrated a higher Sb removal performance, even after five adsorption desorption cycles (Zhang, Dong et al. 2022).

2.2.7.1 Analysis of desorption efficiency by type of eluent

A summary of the eluents reported in the literature for Sb desorption is shown in Figure 2.7. The most common eluents applied were HCl, NaOH, NaCl and EDTA. The best desorption efficiencies were achieved by acid solutions.

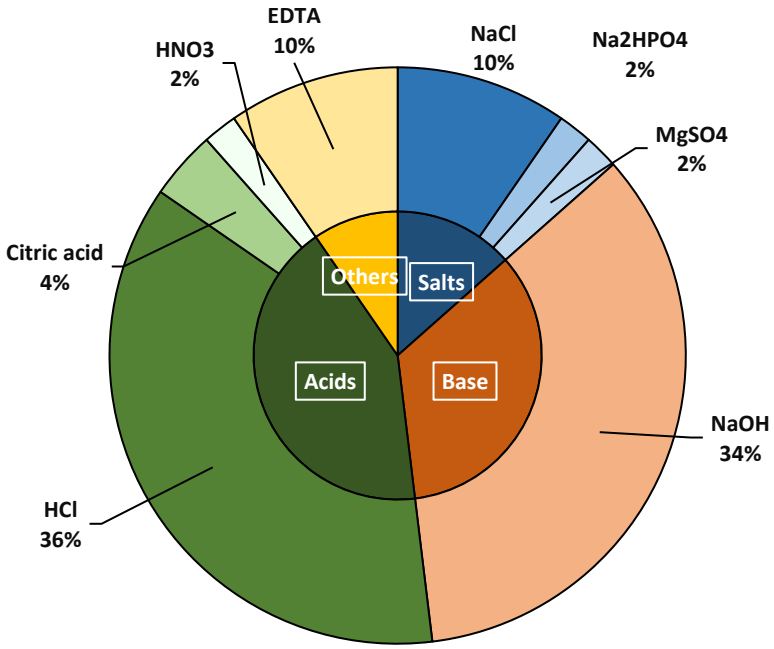


Figure 2.7: Percentage of eluents used for antimony desorption studies presented in Table 2.11.

2.2.7.1.1 Bases

Approximately one third of the studies reported desorption of Sb using alkaline eluent, with NaOH being the only base used. The concentration of the alkaline solution varied from 0.1 to 1 M, with 0.5 M being the most common concentration. The regeneration of Zn-Fe-LDH loaded with As(V) and Sb(V) using 0.5 M NaOH released zinc in the solution (Lu, Zhu et al. 2015). For metal-based adsorbents, elution can be associated with the leaching of the coating and compromise the performance of the adsorbent during future adsorption cycles. Overall, the desorption efficiency of NaOH was not high. However, NaOH has achieved good desorption efficiencies of 92.4% and >80% for some materials, such as carbon fibers decorated with ferric hydroxide (CF-Fe) (Simsek, Demircivi et al. 2018) and Fe-Mn binary oxides (FMBO3) (Yang, Zhou et al. 2018), respectively.

2.2.7.1.2 Acids

Both inorganic and organic acids achieved high Sb desorption rates. However, HCl was the most frequently used eluent and had the highest desorption rates. These high desorption rates may be attributed to the formation of chloro-complexes (Schweitzer and Pesterfield 2010, Runtti, Luukkonen et al. 2023).

For arsenic desorption, NaOH solution was the most frequently used. As opposed to the behavior of Sb, which was best desorbed by acids, alkaline solutions were most effective on As. The differences between the As and Sb desorption mechanisms can be related to their molecular structure. Sb(V) is coordinated with oxygen in an octahedral geometry with a larger ionic radius (Pauling 1933), while As(V) forms a lower spatial structure in a tetrahedral geometry (Simeonidis, Papadopoulou et al. 2017), leading to different adsorption (Pintor, Vieira et al. 2020) and, consequently, desorption mechanisms.

Antimonite recovery from iron-modified chitosan was studied in batch mode using two types of eluent: HCl pH 3.5, and EDTA 0.01 M (Lapo, Demey et al. 2019). Three sorption-desorption cycles were conducted, and HCl was able to maintain a good recovery efficiency of 78 – 76%, but EDTA desorbed less Sb(III), with a noticeable decay occurring between cycles, from 68 to 38%. The acid eluent was also applied for the desorption of Sb(III) from green bean husk (GBH) (Iqbal, Saeed et al. 2013). The recovery efficiency achieved by HCl 0.1 M was very high and stable during seven adsorption-desorption cycles (98.8 – 90%).

The plot of HCl desorption rates versus different concentrations (Figure 2.8) showed that desorption is overall stable with increasing of acid concentration. Although HCl has shown good

results for extracting Sb from saturated media, strong acid solutions can degrade adsorbents. The iron incorporated in adsorbents to increase adsorption capacity is likely to be eluted by acid solutions as reported in some studies (Mei, Xu et al. 2021, Zhang, Dong et al. 2022). Considering that the iron layer is the active binding site for Sb, the adsorbent loses its potential for use in subsequent adsorption-desorption cycles. Low HCl concentrations may be more suited to avoid adsorbent degradation if the HCl concentration has a minimal or no impact on Sb desorption efficiency.

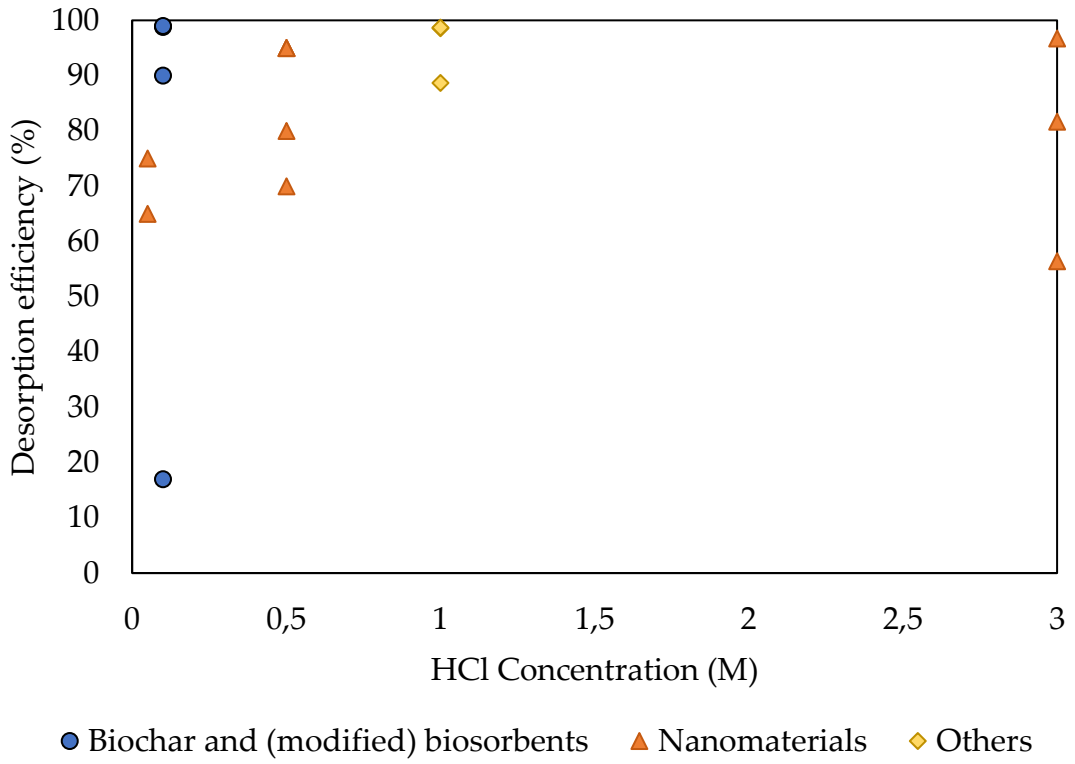


Figure 2.8: Desorption efficiency of antimony-loaded adsorbents by HCl at different concentrations reported in the literature.

2.2.7.1.3 Salts and complexing agents

Salts and complexing agents have been more often explored for Sb desorption than for As desorption. Even though EDTA was used as a desorbing agent in 9% of the studies, very few of them reported desorption efficiency values. Graphene and graphene oxides could be regenerated with 0.1 M EDTA for seven or four cycles, respectively, with a small loss in adsorption capacity (Leng, Guo et al. 2012, Yang, Shi et al. 2015). NaCl solution was also tested as an eluent in 9% of the studies, and it was sometimes associated with other eluents. Desorption efficiency ranged from 15 to 87%. Metal-Organic Frameworks (MOF) adsorbents

could be regenerated with NaCl for five adsorption-desorption cycles with a loss of one-third of the Sb(V) removal efficiency (Li, Li et al. 2022).

2.2.8 Batch *vs* continuous mode desorption

Although numerous investigations on As and Sb desorption have been performed (sections 6 and 7), most of them were carried out in batch mode. Table 3 summarizes the performance of adsorbents regenerated in continuous mode reported in the literature. NaOH solutions of 0.005 M to 1 M were predominantly applied as eluents. Desorption tests using different eluents were carried out on ferric hydroxide-based adsorbents (Chaudhary and Farrell 2015). The regeneration of media could be enhanced by adding NaCl to NaOH regenerating solutions. Arsenic desorption in continuous mode was more reported than that of antimony, with As(V) being the most studied species. Desorption efficiencies were high, perhaps as a result of previous batch mode operation that optimized the applied eluents and their corresponding concentrations. As expected, a decrease in the adsorption capacity of regenerated adsorbents was reported. Thus, investigating methods to minimize the loss of adsorption capacity is important for increasing the viability of desorption for practical usage.

The bed volumes needed for As desorption ranged from 100 to 178. For Sb, the values ranged from 10 to 4000; however, the highest value was obtained from an assay carried out with a very weak solution of 0.005 M NaOH.

Table 2.12: Desorption of As and Sb and regeneration performance of adsorbents in continuous mode.

Adsorbent	Specie	Flow rate (mL/ min)	Eluents	Desorption efficiency (%)	Desorp. cycles	Adsorp. capacity reduction	Bed volumes (BV)	Ref.
Polyethylenimine coated bacterial biosorbent	As(V)	16.7	0.1 M NaOH	99.6-99.8	5	-	-	(Kim, Seo et al. 2020)
Bark-based magnetic iron oxide particle (BMIOP)	As(III)	5	1 M NaOH	-	1	29.71%	-	(Dhoble, Rayalu et al. 2022)
Fiban As5	As(V)	1.38	0.1 M NaOH	85	1	-	125	(Chaudhary and Farrell 2015)

Adsorbent	Specie	Flow rate (mL/ min)	Eluents	Desorption efficiency (%)	Desorp. cycles	Adsorp. capacity reduction	Bed volumes (BV)	Ref.
PAN-Fe	As(V)	1.38	0.1 M NaOH	78	1	-	125	(Chaudhary and Farrell 2015)
FeOOH	As(V)	9.67	0.05 M NaOH	~90	1	~23%	-	(Tresintsi, Simeonidis et al. 2014)
Iron oxide coated sponge (IOCSp)	As(III) As(V)	0.15 m/h	0.3 M NaOH	-	1	9% 10%	100 118	(Nguyen, Vigneswaran et al. 2010)
Iron (oxyhydr)oxide /CNT filters	Sb(III)	1.5	0.005 M NaOH	-	4	27.5%	-	(Liu, Yao et al. 2019)
Quartz sand coated with Fe3O4 and graphene oxide (QFGO)	Sb(III)	10	0.1 M EDTA	-	2	-	~10	(Yang, Shi et al. 2015)

2.2.9 Regeneration and fate of spent adsorbent

One of the main concerns with employing adsorption for water treatment is what happens to the used adsorbent. Waste disposal is a serious issue in the majority of developing nations, and in many cases, the ecotoxic effects of its direct disposal impose a significant barrier to this procedure (Yadav, Saidulu et al. 2022).

It is common to incorporate metals to increase the material´s adsorption capacity. However, to ensure regenerability and prevent metals from leaching into water, methods for making the coating durable and persistent are important (Thakur and Armstrong 2021). When the coating is removed during desorption, recovering (or recycling) the adsorbent by treating it once again with the metal may be an interesting solution. Recycled Al(III)- and Fe(III)-modified kapok fiber (Yeo, Dong et al. 2022, Yeo, Li et al. 2022) have improved adsorption capacities towards arsenic.

The adsorbent, however, loses all of its adsorptive ability after a specific number of regeneration and reuse cycles and should finally be safely sent to a safe destination (Yadav,

Saidulu et al. 2022). Some of these destinations can be immobilization, stabilization, and disposal. In developed countries, common disposal methods include landfilling and incineration; however, nations in economic development still lack the infrastructure to ensure that toxic waste is correctly disposed of, and much fewer safe procedures, such as dumping in backyards, ditches, and lowland areas, are carried out (Yadav, Saidulu et al. 2022). The European Union countries must account for the Directive (EU) 2018/850 of the European Parliament and of the Council of 30 May 2018 amending Directive 1999/31/EC on the landfill of waste. Even safer measures in developed countries can cause environmental problems, such as air pollution in the case of incineration (Yan, Chen et al. 2008). The mixing of biomass-derived spent adsorbents with coal was suggested as a viable option for energy generation in thermal plants, with possible metal recovery from incineration bottom ashes (Mondal and Garg 2017). A life cycle assessment (LCA) compared the four most common strategies for As-rich Fe oxide water treatment residuals (WTRs) and revealed that landfilling had lower toxicity impacts compared to brick stabilization, mixture with organic waste, and open disposal (van Genuchten, Etmannski et al. 2022). It was concluded, however, that landfilling simply converts direct As emissions into an impending As toxicity issue for future generations.

The application of novel adsorbents in real scale also relies upon the possibilities of fate of the contaminated bed. The Toxicity Characteristic Leaching Procedure (TCLP) (SW 1992) is a test that determines whether a waste material such as a spent adsorbent is hazardous or non-hazardous and, consequently, if it may be disposed of in hazardous waste landfills or municipal solid waste landfills. As disposal in a hazardous waste landfill may be 5 to 10 times more expensive than disposal in a municipal solid waste landfill, this categorization is crucial to the final cost of a given media-based treatment system (Impellitteri and Scheckel 2006). The maximum level of arsenic in non-hazardous waste by TCLP is 5 mg L^{-1}. TCLP does not regulate antimony-loaded waste; however, other alternative toxicity tests, such as Soluble Threshold Limit Concentration (STLC) and Total Threshold Limit Concentration (TTLC), set thresholds of 15 mg L^{-1} and 500 mg kg^{-1} for antimony and 5 mg L^{-1} and 500 mg kg^{-1} for arsenic (DTSC). Some TCLP results from arsenic contaminated bed were reported in the literature (Table 2.13).

Table 2.13. TCLP results from arsenic contaminated bed.

Type of adsorbent	Adsorbent	Maximum arsenic leached (mg/L)	Under USEPA limit?	Ref.
Biosorbents	Ferric hydroxide microcapsule-loaded alginate beads (FHMCA)	0.3	Yes	(Sarkar, Pal et al. 2010)
Biosorbent	Iron doped chitosan spacer granules (ICS)	0.02	Yes	(Gupta and Sankararamakrishnan 2010)
Biosorbent	Magnetic binary oxide particles (MBOP)	0.07	Yes	(Dhoble, Maddigapu et al. 2017)
Carbon-based	Iron-containing granular activated carbon	0.09	Yes	(Gu, Fang et al. 2005)
Carbon-based	HFO-PF-Coated GAC	<0.1	Yes	(Zhuang, Hobenshield et al. 2008)
Commercial	ArsenXnp	<1.0	Yes	(Sarkar, Blaney et al. 2007)
Metal (hydr)oxides	Iron mineral-quartz sand	0.4	Yes	(Guo, Stüben et al. 2007)
Mineral	Natural siderite	0.4	Yes	(Guo, Stüben et al. 2007)
Mineral	Granular schwertmannite	0.025	Yes	(Dou, Mohan et al. 2013)
Mineral	Activated siderite-hematite	0.3	Yes	(Guo, Stüben et al. 2008)

2.2.10 Recovery and fate of desorbed solution

To recover an element from an exhausted bed, a large quantity of chemicals is consumed and a secondary effluent is generated (Hu, You et al. 2021). It was estimated that for arsenic removal from treatment systems, desorbed solution disposal might account for 95% of the overall regeneration expenditures if there is not an onsite option for disposing of the regenerant wastewater at the water treatment plant (Sorg, Kolisz et al. 2017). The use of slow flow rates and high eluent concentrations has been suggested to reduce the amount of wastewater generated during the regeneration process (Chaudhary and Farrell 2015).

Very few studies have provided deep investigation on a feasible alternative destination for the metal-loaded solutions. Precipitation of Sb from the solution has been explored, through the addition of Na_2S to an antimony-high-concentrated effluent from desorption (Biswas, Inoue et

al. 2009). More than 98% of the Sb(III) was precipitated and segregated from the solution, which also contained the iron leached from the adsorbent.

More recently, a study explored the secondary use of an antimony desorbing solution by applying it in the production of polyethylene terephthalate (PET) (Liang, Hu et al. 2022). KOH glycol solution was used as a desorbing agent for the Sb(III) saturated adsorbent, and the eluent solution was added to terephthalic acid to produce PET. In addition to the use of Sb-loaded eluent, the study investigated a final application to the saturated adsorbent by converting it into a catalyst for the reduction of nitroarenes.

Antimony recovery is a relevant field of research due to its strong role in industry and limited availability in the future. However, few antimony recovery experiments from adsorption/desorption processes have been reported, and the antimony recovery rates are still lower than those of arsenic.

A UV/sulfite advanced reduction method was proposed to remove arsenic oxyanions from water in the form of elemental arsenic (Wang, Liu et al. 2022). The suggested method might prevent the production of hazardous waste loaded with arsenic in addition to recovering arsenic.

The recovery of arsenic and alkali products from antimony smelting residues was carried out using a novel approach (Long, Zheng et al. 2020). The process, composed of eight steps, was based on the application of CO_2 and $H2SO_4$, achieving an overall 80.6% arsenic recovery efficiency. New methods are urgently needed to recover As from WTRs, convert it into valuable compounds, and reduce stored As toxicity and As emissions (van Genuchten, Etmannski et al. 2022). Arsenic recovery on a large scale is not yet recommended since this process is still not economically feasible and has limited applications (Mondal and Garg 2017). Nevertheless, arsenic recovery might be feasible in the future because it is at risk of supply, according to the European Commission's list of Critical Raw Materials (European, Directorate-General for Internal Market et al. 2023, Wang, Holm et al. 2023).

2.2.11 Challenges

i. Data on arsenic research are more available than Sb ones because of previous research efforts to understand and manage large-scale and long-term As environmental pollution concerns (Wilson, Lockwood et al. 2010). This reflects the higher number of publications on arsenic desorption than on Sb desorption. Nevertheless, there is a high demand for research on antimony desorption and recovery due to its limited availability in the future (Cole-Hamilton 2020) and relevance in a variety of industrial applications.

ii. Most adsorption-desorption experiments reported in the literature were carried out in batch mode, even though real-scale operations in industry usually apply continuous flow mode. Pilot tests are the most costly but crucial for scaling novel adsorbents.
iii. Metal incorporation into adsorbents is important for increasing the adsorption capacity; however, desorption of metalloids can elute the metal coating and compromise the regeneration of the adsorbent for use in further adsorption cycles.
iv. More environmentally friendly materials are being produced for arsenic adsorption than for antimony adsorption. Because of the increased industrial value of antimony, more complex materials are being developed. The commercial applicability of an adsorbent should be determined not only by successful pilot-scale studies and adsorption/desorption feasibility but also by life cycle assessments to analyze the environmental impacts of these materials and whether the gains in adsorption capacity compensate for the environmental impact of production, operation, and disposal.
v. The proper disposal of spent media is a critical environmental concern in the water treatment sector. Finding the end destination for these materials, with a focus on overall environmental benefits, requires careful consideration of numerous factors. Therefore, further research in this field is needed. Meanwhile, a well-maintained landfill remains the most attractive option for the disposal of spent adsorbents after stabilization (Yadav, Saidulu et al. 2022).
vi. TCLP is the standard test for assessing a material´s leachability and toxicity. On the other hand, it has been claimed to have many flaws and to underestimate leachability and, as a result, toxicity (Ghosh, Mukiibi et al. 2004). Therefore, leachability studies of saturated adsorbents should be performed under a variety of experimental conditions to evaluate the stability of new adsorbents (Bai, Tang et al. 2022).

2.2.12 Final remarks

The desorption of arsenic and antimony is an important step in their cost-effective removal from water. The literature data show that the desorption of arsenic has been investigated more than antimony desorption. This difference might be related to the more well-known effect of arsenic on human health. A combination of factors, such as a decrease in Sb availability in the future and its higher economic value, might encourage Sb desorption/recovery studies. Therefore, antimony adsorption/desorption in aqueous solution might be an emerging field of study.

NaOH and HCl are the most often employed desorbing agents for the release of arsenic and antimony, respectively, from saturated adsorbents. Overall, lower desorption efficiencies were

achieved for antimony than for arsenic. This approach might be a sensitive topic when it comes to recovering Sb from desorbing solutions and disposing of toxic media. Understanding the mechanisms and factors affecting arsenic and antimony desorption can help in the development of more effective adsorbents.

Moreover, further studies should be conducted to optimize the separation/recovery process of arsenic and antimony from the desorbed solution. Artificial intelligence is being used to create more reliable models for operational parameter prediction and process optimization, which might increase the viability of desorption.

Finally, finding an economic and environmental balance in the development of new adsorbents and alternative destinations for spent adsorbents at the end-of-life is one of the most important tasks in the field for the following years.

This thesis aims to increase the knowledge on the arsenic and antimony desorption from iron-coated cork granulates, and their recovery potential for industrial potential. Furthermore, it aims to investigate the possible regeneration of iron-coated cork granulates for subsequent adsorption cycles.

2.3 References

(MOH), M. o. H. o. t. P. s. R. o. C. (2006). Chinese National Standards GB 3838-2002: Sanitary Standards for Drinking Water Quality;. S. A. o. C. (SAC). Hongkong, China., China Water Risk:.

Abid, M., N. K. Niazi, I. Bibi, A. Farooqi, Y. S. Ok, A. Kunhikrishnan, F. Ali, S. Ali, A. D. Igalavithana and M. Arshad (2016). "Arsenic(V) biosorption by charred orange peel in aqueous environments." International Journal of Phytoremediation **18**(5): 442-449.

Ali, I. (2018). "Microwave assisted economic synthesis of multi walled carbon nanotubes for arsenic species removal in water: Batch and column operations." Journal of Molecular Liquids **271**: 677-685.

Ali, I., Z. A. Al-Othman, A. Alwarthan, M. Asim and T. A. Khan (2014). "Removal of arsenic species from water by batch and column operations on bagasse fly ash." Environmental Science and Pollution Research **21**(5): 3218-3229.

Alka, S., S. Shahir, N. Ibrahim, M. J. Ndejiko, D.-V. N. Vo and F. A. Manan (2021). "Arsenic removal technologies and future trends: A mini review." Journal of Cleaner Production **278**: 123805.

APCOR. (2020). "Boletim estatístico - Cork 2020." from https://www.apcor.pt/portfolio-posts/boletim-estatistico-2020/#dearflip-df_22474/17/.

Aryal, M., M. Ziagova and M. Liakopoulou-Kyriakides (2010). "Study on arsenic biosorption using Fe(III)-treated biomass of Staphylococcus xylosus." Chemical Engineering Journal **162**(1): 178-185.

Asadi Haris, S., S. Dabagh, H. Mollasalehi and Y. N. Ertas (2023). "Alginate coated superparamagnetic iron oxide nanoparticles as nanocomposite adsorbents for arsenic removal from aqueous solutions." Separation and Purification Technology **310**: 123193.

Asere, T. G., C. V. Stevens and G. Du Laing (2019). "Use of (modified) natural adsorbents for arsenic remediation: A review." Science of The Total Environment **676**: 706-720.

Ayoob, S., A. K. Gupta and P. B. Bhakat (2007). "Analysis of breakthrough developments and modeling of fixed bed adsorption system for As(V) removal from water by modified calcined bauxite (MCB)." Separation and Purification Technology **52**(3): 430-438.

Ayoob, S., A. K. Gupta and P. B. Bhakat (2007). "Performance evaluation of modified calcined bauxite in the sorptive removal of arsenic(III) from aqueous environment." Colloids and Surfaces A: Physicochemical and Engineering Aspects **293**(1): 247-254.

Bacelo, H., S. C. R. Santos and C. M. S. Botelho (2020). "Removal of arsenic from water by an iron-loaded resin prepared from Pinus pinaster bark tannins." Euro-Mediterranean Journal for Environmental Integration **5**(3).

Bacelo, H., S. C. R. Santos, A. Ribeiro, R. A. R. Boaventura and C. M. S. Botelho (2022). "Antimony removal from water by pine bark tannin resin: Batch and fixed-bed adsorption." Journal of Environmental Management **302**: 114100.

Bacelo, H., S. C. R. Santos, A. Ribeiro, R. A. R. Boaventura and C. M. S. Botelho (2022). "Antimony removal from water by pine bark tannin resin: Batch and fixed-bed adsorption." Journal of Environmental Management **302**.

Bacelo, H., B. R. C. Vieira, S. C. R. Santos, R. A. R. Boaventura and C. M. S. Botelho (2018). "Recovery and valorization of tannins from a forest waste as an adsorbent for antimony uptake." Journal of Cleaner Production **198**: 1324-1335.

Badruzzaman, M., P. Westerhoff and D. R. U. Knappe (2004). "Intraparticle diffusion and adsorption of arsenate onto granular ferric hydroxide (GFH)." Water Research **38**(18): 4002-4012.

Bai, Y., X. Tang, L. Sun, W. Yin, G. Hu, M. Liu and Y. Gong (2022). "Application of iron-based materials for removal of antimony and arsenic from water: Sorption properties and mechanism insights." Chemical Engineering Journal **431**: 134143.

Baig, S. A., T. Sheng, Y. Hu, J. Xu and X. Xu (2015). "Arsenic Removal from Natural Water Using Low Cost Granulated Adsorbents: A Review." CLEAN – Soil, Air, Water **43**(1): 13-26.

Baig, S. A., J. Zhu, N. Muhammad, T. Sheng and X. Xu (2014). "Effect of synthesis methods on magnetic Kans grass biochar for enhanced As(III, V) adsorption from aqueous solutions." Biomass and Bioenergy **71**: 299-310.

Barreto, M. S. C., E. J. Elzinga and L. R. F. Alleoni (2020). "Hausmannite as potential As(V) filter. Macroscopic and spectroscopic study of As(V) adsorption and desorption by citric acid." Environmental Pollution **262**: 114196.

Baskan, M. B. and A. Pala (2013). "Batch and Fixed-Bed Column Studies of Arsenic Adsorption on the Natural and Modified Clinoptilolite." Water, Air, & Soil Pollution **225**(1): 1798.

Basu, A., S. Mustafiz, M. R. Islam, N. Bjorndalen, M. S. Rahaman and O. Chaalal (2006). "A COMPREHENSIVE APPROACH FOR MODELING SORPTION OF LEAD AND COBALT IONS THROUGH FISH SCALES AS AN ADSORBENT." Chemical Engineering Communications **193**(5): 580-605.

Belozerova, A. A., N. V. Pechishcheva, S. K. Estemirova and K. Y. Shunyaev (2022). Sorption recovery of arsenic (III) and antimony (III) from solutions using MnO2/C nanocomposite. AIP Conference Proceedings.

Bhakat, P. B., A. K. Gupta and S. Ayoob (2007). "Feasibility analysis of As(III) removal in a continuous flow fixed bed system by modified calcined bauxite (MCB)." Journal of Hazardous Materials **139**(2): 286-292.

Bhakat, P. B., A. K. Gupta, S. Ayoob and S. Kundu (2006). "Investigations on arsenic(V) removal by modified calcined bauxite." Colloids and Surfaces A: Physicochemical and Engineering Aspects **281**(1): 237-245.

Biswas, B. K., J.-i. Inoue, H. Kawakita, K. Ohto and K. Inoue (2009). "Effective removal and recovery of antimony using metal-loaded saponified orange waste." Journal of Hazardous Materials **172**(2): 721-728.

Biterna, M., L. Antonoglou, E. Lazou and D. Voutsa (2010). "Arsenite removal from waters by zero valent iron: Batch and column tests." Chemosphere **78**(1): 7-12.

Biterna, M., A. Arditsoglou, E. Tsikouras and D. Voutsa (2007). "Arsenate removal by zero valent iron: Batch and column tests." Journal of Hazardous Materials **149**(3): 548-552.

Boddu, V. M., K. Abburi, J. L. Talbott, E. D. Smith and R. Haasch (2008). "Removal of arsenic (III) and arsenic (V) from aqueous medium using chitosan-coated biosorbent." Water Research **42**(3): 633-642.

Bolan, N., M. Kumar, E. Singh, A. Kumar, L. Singh, S. Kumar, S. Keerthanan, S. A. Hoang, A. El-Naggar, M. Vithanage, B. Sarkar, H. Wijesekara, S. Diyabalanage, P. Sooriyakumar, A. Vinu, H. Wang, M. B. Kirkham, S. M. Shaheen, J. Rinklebe and K. H. M. Siddique (2022). "Antimony contamination and its risk management in complex environmental settings: A review." Environment International **158**: 106908.

Boldaji, M. R., R. Nabizadeh, M. H. Dehghani, K. Nadafi and A. H. Mahvi (2010). "Evaluating the performance of iron nanoparticle resin in removing arsenate from water." Journal of Environmental Science and Health, Part A **45**(8): 946-950.

Brion-Roby, R., J. Gagnon, J.-S. Deschênes and B. Chabot (2018). "Investigation of fixed bed adsorption column operation parameters using a chitosan material for treatment of arsenate contaminated water." Journal of Environmental Chemical Engineering **6**(1): 505-511.

Bullen, J. C., C. Lapinee, P. Salaün, R. Vilar and D. J. Weiss (2020). "On the application of photocatalyst-sorbent composite materials for arsenic(III) remediation: insights from kinetic adsorption modelling." Journal of Environmental Chemical Engineering: 104033.

Canada, H. (1999). Guidelines for Canadian Drinking Water Quality: Guideline Technical Document – Antimony. Otawwa, Ontario.

Carvalho, P. C. S., A. M. R. Neiva, M. M. V. G. Silva and E. A. F. da Silva (2014). "Geochemical comparison of waters and stream sediments close to abandoned Sb-Au and As-Au mining areas, northern Portugal." Geochemistry **74**(2): 267-283.

Chang, Y.-Y., K.-H. Song and J.-K. Yang (2008). "Removal of As(III) in a column reactor packed with iron-coated sand and manganese-coated sand." Journal of Hazardous Materials **150**(3): 565-572.

Chaudhary, B. K. and J. Farrell (2015). "Understanding Regeneration of Arsenate-Loaded Ferric Hydroxide-Based Adsorbents." Environmental engineering science **32**(4): 353-360.

Chaudhry, S. A., T. A. Khan and I. Ali (2017). "Zirconium oxide-coated sand based batch and column adsorptive removal of arsenic from water: Isotherm, kinetic and thermodynamic studies." Egyptian Journal of Petroleum **26**(2): 553-563.

Chaudhry, S. A., Z. Zaidi and S. I. Siddiqui (2017). "Isotherm, kinetic and thermodynamics of arsenic adsorption onto Iron-Zirconium Binary Oxide-Coated Sand (IZBOCS): Modelling and process optimization." Journal of Molecular Liquids **229**: 230-240.

Chen, A. S. C., T. J. Sorg and L. Wang (2015). "Regeneration of iron-based adsorptive media used for removing arsenic from groundwater." Water Research **77**: 85-97.

Chen, C.-C. and Y.-C. Chung (2006). "Arsenic Removal Using a Biopolymer Chitosan Sorbent." Journal of Environmental Science and Health, Part A **41**(4): 645-658.

Chen, C.-Y., T.-H. Chang, J.-T. Kuo, Y.-F. Chen and Y.-C. Chung (2008). "Characteristics of molybdate-impregnated chitosan beads (MICB) in terms of arsenic removal from water and the application of a MICB-packed column to remove arsenic from wastewater." Bioresource Technology **99**(16): 7487-7494.

Chen, H., Y. Gao, A. El-Naggar, N. K. Niazi, C. Sun, S. M. Shaheen, D. Hou, X. Yang, Z. Tang, Z. Liu, H. Hou, W. Chen, J. Rinklebe, M. Pohořelý and H. Wang (2022). "Enhanced sorption of trivalent antimony by chitosan-loaded biochar in aqueous solutions: Characterization, performance and mechanisms." Journal of Hazardous Materials **425**: 127971.

Chen, R., Z. Zhang, Z. Lei and N. Sugiura (2012). "Preparation of iron-impregnated tablet ceramic adsorbent for arsenate removal from aqueous solutions." Desalination **286**: 56-62.

Chen, W., R. Parette, J. Zou, F. S. Cannon and B. A. Dempsey (2007). "Arsenic removal by iron-modified activated carbon." Water Research **41**(9): 1851-1858.

Cheng, M., Y. Fang, Z. Yang, X. Liu, B. Qiu, T. Zhang, H. Li and W. Zhao (2023). "Grafting amino groups to enhance the adsorption of antimonate by MIL-100(Fe) for from natural water: Performance and mechanism." Chemical Engineering Journal Advances **14**: 100458.

Choi, J.-S., L. P. Lingamdinne, J.-K. Yang, Y.-Y. Chang and J. R. Koduru (2020). "Fabrication of chitosan/graphene oxide-gadolinium nanorods as a novel nanocomposite for arsenic removal from aqueous solutions." Journal of Molecular Liquids **320**: 114410.

Christian, P., F. Von der Kammer, M. Baalousha and T. Hofmann (2008). "Nanoparticles: structure, properties, preparation and behaviour in environmental media." Ecotoxicology **17**(5): 326-343.

Chu, J., J. Mao and M. He (2019). "Anthropogenic antimony flow analysis and evaluation in China." Science of The Total Environment **683**: 659-667.

Chu, K. H. (2014). "Prediction of arsenic breakthrough in a pilot column of polymer-supported nanoparticles." Journal of Water Process Engineering **3**: 117-122.

Cidu, R., R. Biddau, E. Dore and A. Vacca (2013). "Antimony Dispersion at Abandoned Mines in Sardinia, Italy." Procedia Earth and Planetary Science **7**: 171-174.

Ciopec, M. N., Adina; Lupa, Lavinia; Davidescu, Corneliu M.; Negrea, Petru. (2014). "Studies Regarding As(V) Adsorption from Underground Water by Fe-XAD8-DEHPA Impregnated Resin. Equilibrium Sorption and Fixed-Bed Column Tests." Molecules **19**.

Cole-Hamilton, D. (2020). "The Role of Chemists and Chemical Engineers in a Sustainable World." Chemistry – A European Journal **26**(9): 1894-1899.

Cole-Hamilton, D. (2020). "The Role of Chemists and Chemical Engineers in a Sustainable World." Chemistry **26**(9): 1894-1899.

Commission, E., I. Directorate-General for Internal Market, Entrepreunership, SMEs, M. Grohol and C. Veeh (2023). Study on the critical raw materials for the EU 2023 - Final report, Publications Office of the European Union.

Contreras, S., L. Henríquez-Vargas and P. I. Álvarez (2017). "Arsenic transport and adsorption modeling in columns using a copper nanoparticles composite." Journal of Water Process Engineering **19**: 212-219.

Crespo-Alonso, M., V. M. Nurchi, R. Biesuz, G. Alberti, N. Spano, M. I. Pilo and G. Sanna (2013). "Biomass against emerging pollution in wastewater: ability of cork for the removal of ofloxacin from aqueous solutions at different pH." Journal of Environmental Chemical Engineering **1**(4): 1199-1204.

Cuong, D. V., P.-C. Wu, S. Y. H. Liou and C.-H. Hou (2022). "An integrated active biochar filter and capacitive deionization system for high-performance removal of arsenic from groundwater." Journal of Hazardous Materials **423**: 127084.

Dabbagh, R., M.-s. Mirkamali and L. Vafajoo (2019). "Removal of Antimony Metalloid From Synthetic Effluent Using Seaweed as a Low-Cost Natural Sorbent: Adsorption on a Fixed-Bed Column." Journal of Water Chemistry and Technology **41**(1): 21-28.

Dabizha, A., C. Bahr and M. Kersten (2020). "Predicting breakthrough of vanadium in fixed-bed absorbent columns with complex groundwater chemistries: A multi-component granular ferric hydroxide–vanadate–arsenate–phosphate–silicic acid system." Water Research X **9**: 100061.

Dadwhal, M., M. M. Ostwal, P. K. T. Liu, M. Sahimi and T. T. Tsotsis (2009). "Adsorption of Arsenic on Conditioned Layered Double Hydroxides: Column Experiments and Modeling." Industrial & Engineering Chemistry Research **48**(4): 2076-2084.

Danish, M. I., I. A. Qazi, A. Zeb, A. Habib, M. A. Awan and Z. Khan (2013). "Arsenic Removal from Aqueous Solution Using Pure and Metal-Doped Titania Nanoparticles Coated on Glass Beads: Adsorption and Column Studies." Journal of Nanomaterials **2013**: 873694.

de Aguiar, T. R., J. O. A. Guimarães Neto, U. Şen and H. Pereira (2019). "Study of two cork species as natural biosorbents for five selected pesticides in water." Heliyon **5**(1): e01189.

Deliyanni, E. A., D. N. Bakoyannakis, A. I. Zouboulis and E. Peleka (2003). "Removal of Arsenic and Cadmium by Akaganeite Fixed-Beds." Separation Science and Technology **38**(16): 3967-3981.

Dembele, S., A. Akcil and S. Panda (2022). "Technological trends, emerging applications and metallurgical strategies in antimony recovery from stibnite." Minerals Engineering **175**: 107304.

Deng, J., X. Li, X. Wei, Y. Liu, J. Liang, Y. Shao, W. Huang and X. Cheng (2020). "Different adsorption behaviors and mechanisms of a novel amino-functionalized hydrothermal biochar for hexavalent chromium and pentavalent antimony." Bioresource Technology **310**: 123438.

Dhoble, R. M., P. R. Maddigapu, S. S. Rayalu, A. G. Bhole, A. S. Dhoble and S. R. Dhoble (2017). "Removal of arsenic(III) from water by magnetic binary oxide particles (MBOP): Experimental studies on fixed bed column." Journal of Hazardous Materials **322**: 469-478.

Dhoble, R. M., S. Rayalu, A. Kularkar and H. Hajare (2022). "Arsenite removal from drinking water by bark-based magnetic iron oxide particle (BMIOP): a column study." Environmental Science and Pollution Research.

Di Natale, F., A. Erto and A. Lancia (2013). "Desorption of arsenic from exhaust activated carbons used for water purification." Journal of Hazardous Materials **260**: 451-458.

Dias, A. C. and M. P. F. Fontes (2020). "Arsenic (V) removal from water using hydrotalcites as adsorbents: A critical review." Applied Clay Science **191**: 105615.

Dieudonné, A., S. Prévéral, D. Pignol and A. J. M. Stams (2020). "A Sensitive Magnetic Arsenite-Specific Biosensor Hosted in Magnetotactic Bacteria." Applied and Environmental Microbiology **86**(14): e00803-00820.

Dorjee, P., D. Amarasiriwardena and B. Xing (2014). "Antimony adsorption by zero-valent iron nanoparticles (nZVI): Ion chromatography–inductively coupled plasma mass spectrometry (IC–ICP-MS) study." Microchemical Journal **116**: 15-23.

Dou, X., D. Mohan and C. U. Pittman (2013). "Arsenate adsorption on three types of granular schwertmannite." Water Research **47**(9): 2938-2948.

DTSC, D. o. T. S. C. "Persistent and Bioaccumulative Toxic Substances." Retrieved [23/01/2024, from https://dtsc.ca.gov/persistent-and-bioaccumulative-toxic-substances/.

Duarte, A. P. and J. C. Bordado (2015). "Cork – A Renewable Raw Material: Forecast of Industrial Potential and Development Priorities." Frontiers in Materials **2**.

Dudek, S. and D. Kołodyńska (2022). "Arsenic(V) removal on the lanthanum-modified ion exchanger with quaternary ammonium groups based on iron oxide." Journal of Molecular Liquids **347**: 117985.

Duker, A. A., E. J. M. Carranza and M. Hale (2005). "Arsenic geochemistry and health." Environment International **31**(5): 631-641.

Elovich, S. Y. and O. G. Larionov (1962). "Theory of adsorption from nonelectrolyte solutions on solid adsorbents." Bulletin of the Academy of Sciences of the USSR, Division of chemical science **11**(2): 198-203.

EPA, E. P. A. (2002). "National primary drinking water regulations: long term 1 enhanced surface water treatment rule. Final rule." Federal register **67**(9): 1811-1844.

European, C., I. E. Directorate-General for Internal Market, Smes, M. Grohol and C. Veeh (2023). Study on the critical raw materials for the EU 2023 – Final report, Publications Office of the European Union.

European Union, C. (2020). Council Directive 2020/2184 of 16 December 2020, Off. J. Eur. Commun. L: 62.

Fan, H.-T., W. Sun, B. Jiang, Q.-J. Wang, D.-W. Li, C.-C. Huang, K.-J. Wang, Z.-G. Zhang and W.-X. Li (2016). "Adsorption of antimony(III) from aqueous solution by mercapto-functionalized silica-supported organic–inorganic hybrid sorbent: Mechanism insights." Chemical Engineering Journal **286**: 128-138.

Fleming, D. E. B., I. S. Eddy, M. R. Gherase, M. K. Gibbons and G. A. Gagnon (2010). "Real-time monitoring of arsenic filtration by granular ferric hydroxide." Applied Radiation and Isotopes **68**(4): 821-824.

Freundlich, H. (1907). "Über die Adsorption in Lösungen." Zeitschrift für Physikalische Chemie **57U**(1): 385-470.

Fu, H.-Z., M.-H. Wang and Y.-S. Ho (2013). "Mapping of drinking water research: A bibliometric analysis of research output during 1992–2011." Science of The Total Environment **443**: 757-765.

Gan, Y., C. Ding, B. Xu, Z. Liu, S. Zhang, Y. Cui, B. Wu, W. Huang and X. Song (2023). "Antimony (Sb) pollution control by coagulation and membrane filtration in water/wastewater treatment: A comprehensive review." Journal of Hazardous Materials **442**: 130072.

Gandini, A., C. Pascoal Neto and A. J. D. Silvestre (2006). "Suberin: A promising renewable resource for novel macromolecular materials." Progress in Polymer Science **31**(10): 878-892.

Gebel, T. (1997). "Arsenic and antimony: comparative approach on mechanistic toxicology." Chemico-Biological Interactions **107**(3): 131-144.

Genç-Fuhrman, H., P. Wu, Y. Zhou and A. Ledin (2008). "Removal of As, Cd, Cr, Cu, Ni and Zn from polluted water using an iron based sorbent." Desalination **226**(1): 357-370.

Ghimire, K. N., K. Inoue, K. Makino and T. Miyajima (2002). "ADSORPTIVE REMOVAL OF ARSENIC USING ORANGE JUICE RESIDUE." Separation Science and Technology **37**(12): 2785-2799.

Ghosh, A., M. Mukiibi and W. Ela (2004). "TCLP underestimates leaching of arsenic from solid residuals under landfill conditions." Environ Sci Technol **38**(17): 4677-4682.

Gibbons, M. K. and G. A. Gagnon (2010). "Adsorption of arsenic from a Nova Scotia groundwater onto water treatment residual solids." Water Research **44**(19): 5740-5749.

Gibson, L. J., K. E. Easterling and M. F. Ashby (1981). "The structure and mechanics of cork." Proceedings of the Royal Society of London. A. Mathematical and Physical Sciences **377**(1769): 99-117.

Gu, Z., J. Fang and B. Deng (2005). "Preparation and Evaluation of GAC-Based Iron-Containing Adsorbents for Arsenic Removal." Environmental Science & Technology **39**(10): 3833-3843.

Guo, H., D. Stüben and Z. Berner (2007). "Adsorption of arsenic(III) and arsenic(V) from groundwater using natural siderite as the adsorbent." Journal of Colloid and Interface Science **315**(1): 47-53.

Guo, H., D. Stüben and Z. Berner (2007). "Arsenic removal from water using natural iron mineral–quartz sand columns." Science of The Total Environment **377**(2): 142-151.

Guo, H., D. Stüben and Z. Berner (2007). "Removal of arsenic from aqueous solution by natural siderite and hematite." Applied Geochemistry **22**(5): 1039-1051.

Guo, H., D. Stüben, Z. Berner and U. Kramar (2008). "Adsorption of arsenic species from water using activated siderite–hematite column filters." Journal of Hazardous Materials **151**(2): 628-635.

Guo, Y., X. Zhang, N. Xie, R. Guo, Y. Wang, Z. Sun, H. Li, H. Jia, D. Niu and H.-b. Sun (2021). "Investigation of antimony adsorption on a zirconium-porphyrin-based metal–organic framework." Dalton Transactions **50**(39): 13932-13942.

Gupta, A., V. S. Chauhan and N. Sankararamakrishnan (2009). "Preparation and evaluation of iron–chitosan composites for removal of As(III) and As(V) from arsenic contaminated real life groundwater." Water Research **43**(15): 3862-3870.

Gupta, A. and N. Sankararamakrishnan (2010). "Column studies on the evaluation of novel spacer granules for the removal of arsenite and arsenate from contaminated water." Bioresource Technology **101**(7): 2173-2179.

Gupta, A., S. R. Vidyarthi and N. Sankararamakrishnan (2015). "Concurrent removal of As(III) and As(V) using green low cost functionalized biosorbent – Saccharum officinarum bagasse." Journal of Environmental Chemical Engineering **3**(1): 113-121.

Gupta, K. and U. C. Ghosh (2009). "Arsenic removal using hydrous nanostructure iron(III)–titanium(IV) binary mixed oxide from aqueous solution." Journal of Hazardous Materials **161**(2): 884-892.

Hao, H., G. Liu, Y. Wang, B. Shi, K. Han, Y. Zhuang and Y. Kong (2019). "Simultaneous cationic Cu (II)–anionic Sb (III) removal by NH2-Fe3O4-NTA core-shell magnetic nanoparticle sorbents synthesized via a facile one-pot approach." Journal of Hazardous Materials **362**: 246-257.

Hao, L., M. Liu, N. Wang and G. Li (2018). "A critical review on arsenic removal from water using iron-based adsorbents." RSC advances **8**(69): 39545-39560.

Haque, M. N., G. M. Morrison, G. Perrusquía, M. Gutierréz, A. F. Aguilera, I. Cano-Aguilera and J. L. Gardea-Torresdey (2007). "Characteristics of arsenic adsorption to sorghum biomass." Journal of Hazardous Materials **145**(1): 30-35.

Hassan, A. F., A. M. Abdel-Mohsen and H. Elhadidy (2014). "Adsorption of arsenic by activated carbon, calcium alginate and their composite beads." International Journal of Biological Macromolecules **68**: 125-130.

He, R., Z. Peng, H. Lyu, H. Huang, Q. Nan and J. Tang (2018). "Synthesis and characterization of an iron-impregnated biochar for aqueous arsenic removal." Science of The Total Environment **612**: 1177-1186.

He, X., F. Deng, T. Shen, L. Yang, D. Chen, J. Luo, X. Luo, X. Min and F. Wang (2019). "Exceptional adsorption of arsenic by zirconium metal-organic frameworks: Engineering exploration and mechanism insight." Journal of Colloid and Interface Science **539**: 223-234.

Herath, I., M. Vithanage and J. Bundschuh (2017). "Antimony as a global dilemma: Geochemistry, mobility, fate and transport." Environmental Pollution **223**: 545-559.

Hernández-Flores, H., N. Pariona, M. Herrera-Trejo, H. M. Hdz-García and A. I. Mtz-Enriquez (2018). "Concrete/maghemite nanocomposites as novel adsorbents for arsenic removal." Journal of Molecular Structure **1171**: 9-16.

Hiroyuki Hoshina, M. T., Noboru Kasai, Noriaki Seko (2012). "Adsorbent for Arsenic(V) Removal Synthesized by Radiation-Induced Graft Polymerization onto Nonwoven Cotton Fabric." International Journal of Organic Chemistry **Vol. 2** 173-177.

Hristovski, K., A. Baumgardner and P. Westerhoff (2007). "Selecting metal oxide nanomaterials for arsenic removal in fixed bed columns: From nanopowders to aggregated nanoparticle media." Journal of Hazardous Materials **147**(1): 265-274.

Hu, X., Z. Ding, A. R. Zimmerman, S. Wang and B. Gao (2015). "Batch and column sorption of arsenic onto iron-impregnated biochar synthesized through hydrolysis." Water Research **68**: 206-216.

Hu, X., S. You, F. Li and Y. Liu (2021). "Recent advances in antimony removal using carbon-based nanomaterials: A review." Frontiers of Environmental Science & Engineering **16**(4): 48.

Igwe, J. and A. Abia (2006). "A bioseparation process for removing heavy metals from waste water using biosorbents." African journal of biotechnology **5**(12): 1167-1179.

Impellitteri, C. A. and K. G. Scheckel (2006). "The distribution, solid-phase speciation, and desorption/dissolution of As in waste iron-based drinking water treatment residuals." Chemosphere **64**(6): 875-880.

Iqbal, M., A. Saeed and R. G. J. Edyvean (2013). "Bioremoval of antimony(III) from contaminated water using several plant wastes: Optimization of batch and dynamic flow conditions for sorption by green bean husk (Vigna radiata)." Chemical Engineering Journal **225**: 192-201.

Jaiswal, V., S. Saxena, I. Kaur, P. Dubey, S. Nand, M. Naseem, S. B. Singh, P. K. Srivastava and S. K. Barik (2018). "Application of four novel fungal strains to remove arsenic from contaminated water in batch and column modes." Journal of Hazardous Materials **356**: 98-107.

Jang, M., S. H. Min, T. H. Kim and J. K. Park (2006). "Removal of arsenite and arsenate using hydrous ferric oxide incorporated into naturally occurring porous diatomite." Environ Sci Technol **40**(5): 1636-1643.

Jeon, C.-S., K. Baek, J.-K. Park, Y.-K. Oh and S.-D. Lee (2009). "Adsorption characteristics of As(V) on iron-coated zeolite." Journal of Hazardous Materials **163**(2): 804-808.

Jesus, J., R. Nunes da Silva and A. Pintor (2023). "Advances in Cork Use in Adsorption Applications: An Overview of the Last Decade of Research." Separations **10**(7): 390.

Jia, X., J. Zhou, J. Liu, P. Liu, L. Yu, B. Wen and Y. Feng (2020). "The antimony sorption and transport mechanisms in removal experiment by Mn-coated biochar." Science of The Total Environment **724**: 138158.

Jung, K.-W., K. Kim, T.-U. Jeong and K.-H. Ahn (2016). "Influence of pyrolysis temperature on characteristics and phosphate adsorption capability of biochar derived from waste-marine macroalgae (Undaria pinnatifida roots)." Bioresource Technology **200**: 1024-1028.

Kalaruban, M., P. Loganathan, T. V. Nguyen, T. Nur, M. A. Hasan Johir, T. H. Nguyen, M. V. Trinh and S. Vigneswaran (2019). "Iron-impregnated granular activated carbon for arsenic removal: Application to practical column filters." Journal of Environmental Management **239**: 235-243.

Kamala, C. T., K. H. Chu, N. S. Chary, P. K. Pandey, S. L. Ramesh, A. R. Sastry and K. C. Sekhar (2005). "Removal of arsenic(III) from aqueous solutions using fresh and immobilized plant biomass." Water Res **39**(13): 2815-2826.

Kamala, C. T., K. H. Chu, N. S. Chary, P. K. Pandey, S. L. Ramesh, A. R. K. Sastry and K. C. Sekhar (2005). "Removal of arsenic(III) from aqueous solutions using fresh and immobilized plant biomass." Water Research **39**(13): 2815-2826.

Kang, S., S.-M. Park, J.-G. Park and K. Baek (2019). "Enhanced adsorption of arsenic using calcined alginate bead containing alum sludge from water treatment facilities." Journal of Environmental Management **234**: 181-188.

Karki, S., H. Timalsina, S. Budhathoki and S. Budhathoki (2022). "Arsenic removal from groundwater using acid-activated laterite." Groundwater for Sustainable Development **18**: 100769.

Kavacık, B. and D. Dölgen (2023). "Arsenic and antimony removal by using thermal modified treatment plant sludge in a fixed bed column." Journal of the Faculty of Engineering and Architecture of Gazi University **38**(1): 629-638.

Khan, A. H., S. B. Rasul, A. K. M. Munir, M. Habibuddowla, M. Alauddin, S. S. Newaz and A. Hussam (2000). "Appraisal of a simple arsenic removal method for ground water of Bangladesh." Journal of Environmental Science and Health, Part A **35**(7): 1021-1041.

Kim, N., M. Park, Y.-S. Yun and D. Park (2019). "Removal of anionic arsenate by a PEI-coated bacterial biosorbent prepared from fermentation biowaste." Chemosphere **226**: 67-74.

Kim, N., J. H. Seo, Y.-S. Yun and D. Park (2020). "New insight into continuous recirculation-process for treating arsenate using bacterial biosorbent." Bioresource Technology **316**: 123961.

Krika, F., N. Azzouz and M. C. Ncibi (2016). "Adsorptive removal of cadmium from aqueous solution by cork biomass: Equilibrium, dynamic and thermodynamic studies." Arabian Journal of Chemistry **9**: S1077-S1083.

Kundu, S. and A. K. Gupta (2005). "Analysis and modeling of fixed bed column operations on As(V) removal by adsorption onto iron oxide-coated cement (IOCC)." Journal of Colloid and Interface Science **290**(1): 52-60.

Kundu, S. and A. K. Gupta (2007). "As(III) removal from aqueous medium in fixed bed using iron oxide-coated cement (IOCC): Experimental and modeling studies." Chemical Engineering Journal **129**(1): 123-131.

Kundu, S., S. S. Kavalakatt, A. Pal, S. K. Ghosh, M. Mandal and T. Pal (2004). "Removal of arsenic using hardened paste of Portland cement: batch adsorption and column study." Water Research **38**(17): 3780-3790.

Kurt, M. A., Ü. Yıldırım, C. Güler and O. Güven (2021). "Antimony and arsenic contamination in water from antimonite mineralization: a case study from Turhal (Tokat, Northern Turkey)." Environmental Forensics: 1-13.

Langmuir, I. (1918). "THE ADSORPTION OF GASES ON PLANE SURFACES OF GLASS, MICA AND PLATINUM." Journal of the American Chemical Society **40**(9): 1361-1403.

Lapo, B., H. Demey, T. Carchi and A. M. Sastre (2019). "Antimony Removal from Water by a Chitosan-Iron(III)[ChiFer(III)] Biocomposite." Polymers **11**(2).

Lata, S. and S. R. Samadder (2016). "Removal of arsenic from water using nano adsorbents and challenges: A review." Journal of Environmental Management **166**: 387-406.

Lata, S., P. K. Singh and S. R. Samadder (2015). "Regeneration of adsorbents and recovery of heavy metals: a review." International Journal of Environmental Science and Technology **12**(4): 1461-1478.

Lee, C.-G., P. J. J. Alvarez, A. Nam, S.-J. Park, T. Do, U.-S. Choi and S.-H. Lee (2017). "Arsenic(V) removal using an amine-doped acrylic ion exchange fiber: Kinetic, equilibrium, and regeneration studies." Journal of Hazardous Materials **325**: 223-229.

Leng, Y., W. Guo, S. Su, C. Yi and L. Xing (2012). "Removal of antimony(III) from aqueous solution by graphene as an adsorbent." Chemical Engineering Journal **211-212**: 406-411.

Leupin, O. X. and S. J. Hug (2005). "Oxidation and removal of arsenic (III) from aerated groundwater by filtration through sand and zero-valent iron." Water Research **39**(9): 1729-1740.

Lewińska, K., A. Karczewska, M. Siepak and B. Gałka (2018). "The Release of Antimony from Mine Dump Soils in the Presence and Absence of Forest Litter." International journal of environmental research and public health **15**(12): 2631.

Li, J., B. Zheng, Y. He, Y. Zhou, X. Chen, S. Ruan, Y. Yang, C. Dai and L. Tang (2018). "Antimony contamination, consequences and removal techniques: A review." Ecotoxicology and Environmental Safety **156**: 125-134.

Li, Q., R. Li, X. Ma, W. Zhang, B. Sarkar, X. Sun and N. Bolan (2022). "Efficient removal of antimonate from water by yttrium-based metal-organic framework: Adsorbent stability and adsorption mechanism investigation." Colloids and Surfaces A: Physicochemical and Engineering Aspects **633**: 127877.

Li, W. and F. Fu (2020). "Incorporating MnFe2O4 onto the thiol-functionalized MCM-41 for effective capturing of Sb(III) in aqueous media." Microporous and Mesoporous Materials **298**: 110060.

Li, Z., S. Deng, G. Yu, J. Huang and V. C. Lim (2010). "As(V) and As(III) removal from water by a Ce–Ti oxide adsorbent: Behavior and mechanism." Chemical Engineering Journal **161**(1): 106-113.

Li, Z., Q. Yang, Y. Yang, C. Xie and H. Ma (2020). "Hydrogeochemical controls on arsenic contamination potential and health threat in an intensive agricultural area, northern China." Environmental Pollution **256**: 113455.

Liang, J., Z.-N. Hu, X. Zhang, Y. Ai, Y. Wang, K. Ding, J. Gao, J. Wang, D. Niu and H.-b. Sun (2022). "Recovery of antimony using biological waste and stepwise resourcization as catalysts for both polyesterification and transfer hydrogenation." Colloids and Surfaces A: Physicochemical and Engineering Aspects **635**: 128119.

Liem-Nguyen, V., V. Sjöberg, N. P. Dinh, D. H. Huy and S. Karlsson (2020). "Removal mechanism of arsenic (V) by stainless steel slags obtained from scrap metal recycling." Journal of Environmental Chemical Engineering **8**(4): 103833.

Lim, K. T., M. Y. Shukor and H. Wasoh (2014). "Physical, chemical, and biological methods for the removal of arsenic compounds." BioMed research international **2014**: 503784-503784.

Lin, S., D. Lu and Z. Liu (2012). "Removal of arsenic contaminants with magnetic γ-Fe2O3 nanoparticles." Chemical Engineering Journal **211-212**: 46-52.

Liu, Y., S. Chen, L. Zhong and G. Wu (2009). "Preparation of high-stable silver nanoparticle dispersion by using sodium alginate as a stabilizer under gamma radiation." Radiation Physics and Chemistry **78**(4): 251-255.

Liu, Y., J. Yao, F. Liu, C. Shen, F. Li, B. Yang, M. Huang and W. Sand (2019). "Nanoscale iron (oxyhydr) oxide-modified carbon nanotube filter for rapid and effective Sb (III) removal." RSC advances **9**(32): 18196-18204.

Long, H., Y.-j. Zheng, Y.-l. Peng, G.-z. Jin, W.-h. Deng, S.-c. Zhang and H.-b. He (2020). "Separation and recovery of arsenic and alkali products during the treatment of antimony smelting residues." Minerals Engineering **153**: 106379.

Long, X., T. Wang and M. He (2022). "Simultaneous removal of antimony and arsenic by nano-TiO2-crosslinked chitosan (TA-chitosan) beads." Environmental Technology: 1-11.

Long, X., X. Wang, X. Guo and M. He (2020). "A review of removal technology for antimony in aqueous solution." Journal of Environmental Sciences **90**: 189-204.

López-Mesas, M., E. R. Navarrete, F. Carrillo and C. Palet (2011). "Bioseparation of Pb(II) and Cd(II) from aqueous solution using cork waste biomass. Modeling and optimization of the parameters of the biosorption step." Chemical Engineering Journal **174**(1): 9-17.

Lu, H., Z. Zhu, H. Zhang, J. Zhu and Y. Qiu (2015). "Simultaneous removal of arsenate and antimonate in simulated and practical water samples by adsorption onto Zn/Fe layered double hydroxide." Chemical Engineering Journal **276**: 365-375.

Ludwig, R. D., D. J. A. Smyth, D. W. Blowes, L. E. Spink, R. T. Wilkin, D. G. Jewett and C. J. Weisener (2009). "Treatment of Arsenic, Heavy Metals, and Acidity Using a Mixed ZVI-Compost PRB." Environmental Science & Technology **43**(6): 1970-1976.

Luo, J., X. Meng, J. Crittenden, J. Qu, C. Hu, H. Liu and P. Peng (2018). "Arsenic adsorption on α-MnO2 nanofibers and the significance of (100) facet as compared with (110)." Chemical Engineering Journal **331**: 492-500.

Maia, L. C., L. C. Soares and L. V. Alves Gurgel (2021). "A review on the use of lignocellulosic materials for arsenic adsorption." Journal of Environmental Management **288**: 112397.

Maiti, A., S. DasGupta, J. K. Basu and S. De (2008). "Batch and Column Study: Adsorption of Arsenate Using Untreated Laterite as Adsorbent." Industrial & Engineering Chemistry Research **47**(5): 1620-1629.

Maji, S. K., Y.-H. Kao, C.-J. Wang, G.-S. Lu, J.-J. Wu and C.-W. Liu (2012). "Fixed bed adsorption of As(III) on iron-oxide-coated natural rock (IOCNR) and application to real arsenic-bearing groundwater." Chemical Engineering Journal **203**: 285-293.

Maji, S. K., Y.-H. Kao, Y.-B. Wang and C.-W. Liu (2015). "Dynamic column adsorption of As on iron-oxide-coated natural rock (IOCNR) and sludge management." Desalination and Water Treatment **55**(8): 2171-2182.

Maji, S. K., Y. H. Kao and C. W. Liu (2011). "Arsenic removal from real arsenic-bearing groundwater by adsorption on iron-oxide-coated natural rock (IOCNR)." Desalination **280**(1): 72-79.

Maji, S. K., A. Pal and T. Pal (2008). "Arsenic removal from real-life groundwater by adsorption on laterite soil." Journal of Hazardous Materials **151**(2): 811-820.

Maji, S. K., A. Pal, T. Pal and A. Adak (2007). "Modeling and fixed bed column adsorption of As(III) on laterite soil." Separation and Purification Technology **56**(3): 284-290.

Maji, S. K., A. Pal, T. Pal and A. Adak (2007). "Modeling and fixed bed column adsorption of As(V) on laterite soil." Journal of Environmental Science and Health, Part A **42**(11): 1585-1593.

Mallek, M., M. Chtourou, M. Portillo, H. Monclús, K. Walha, A. b. Salah and V. Salvadó (2018). "Granulated cork as biosorbent for the removal of phenol derivatives and emerging contaminants." Journal of Environmental Management **223**: 576-585.

Manna, B. and U. C. Ghosh (2007). "Adsorption of arsenic from aqueous solution on synthetic hydrous stannic oxide." Journal of Hazardous Materials **144**(1): 522-531.

Manna, B. R., S. Dey, S. Debnath and U. C. Ghosh (2003). "Removal of Arsenic from Groundwater using Crystalline Hydrous Ferric Oxide (CHFO)." Water Quality Research Journal **38**(1): 193-210.

Manzo, V., J. Goya-Pacheco, D. Arismendi, M. Becerra-Herrera, A. Castillo-Aguirre, R. Castillo-Felices, M. Rosero-Moreano, E. Carasek and P. Richter (2019). "Cork sheet as a sorptive phase to extract hormones from water by rotating-disk sorptive extraction (RDSE)." Analytica Chimica Acta **1087**: 1-10.

Masindi, V., S. Foteinis, P. Renforth, J. Ndiritu, J. P. Maree, M. Tekere and E. Chatzisymeon (2022). "Challenges and avenues for acid mine drainage treatment, beneficiation, and valorisation in circular economy: A review." Ecological Engineering **183**: 106740.

Masood ul Hasan, I., H. Javed, M. M. Hussain, M. B. Shakoor, I. Bibi, M. Shahid, Farwa, N. Xu, Q. Wei, J. Qiao and N. K. Niazi (2023). "Biochar/nano-zerovalent zinc-based materials for arsenic removal from contaminated water." International Journal of Phytoremediation **25**(9): 1155-1164.

Mei, Y., J. Xu, Y. Zhang, B. Li, S. Fan and H. Xu (2021). "Effect of Fe–N modification on the properties of biochars and their adsorption behavior on tetracycline removal from aqueous solution." Bioresource Technology **325**: 124732.

Melitas, N., J. Wang, M. Conklin, P. O'Day and J. Farrell (2002). "Understanding Soluble Arsenate Removal Kinetics by Zerovalent Iron Media." Environmental Science & Technology **36**(9): 2074-2081.

Mendizabal, E., N. Ríos-Donato, C. F. Jasso-Gastinel and I. P. Verduzco-Navarro (2023). "Removal of Arsenate by Fixed-Bed Columns Using Chitosan-Magnetite Hydrogel Beads and Chitosan Hydrogel Beads: Effect of the Operating Conditions on Column Efficiency." Gels **9**(10): 825.

Michael, F. M., M. Khalid, R. Walvekar, H. Siddiqui and A. B. Balaji (2018). 2 - Surface modification techniques of biodegradable and biocompatible polymers. Biodegradable and Biocompatible Polymer Composites. N. G. Shimpi, Woodhead Publishing: 33-54.

Mishra, S., J. Dwivedi, A. Kumar and N. Sankararamakrishnan (2016). "Removal of antimonite (Sb(iii)) and antimonate (Sb(v)) using zerovalent iron decorated functionalized carbon nanotubes." RSC Advances **6**(98): 95865-95878.

Mondal, M. K. and R. Garg (2017). "A comprehensive review on removal of arsenic using activated carbon prepared from easily available waste materials." Environmental Science and Pollution Research **24**(15): 13295-13306.

Mondal, R., S. Mondal, K. V. Kurada, S. Bhattacharjee, S. Sengupta, M. Mondal, S. Karmakar, S. De and I. M. Griffiths (2019). "Modelling the transport and adsorption dynamics of arsenic in a soil bed filter." Chemical Engineering Science **210**: 115205.

Morillo, D., M. Faccini, D. Amantia, G. Pérez, M. A. García, M. Valiente and L. Aubouy (2016). "Superparamagnetic iron oxide nanoparticle-loaded polyacrylonitrile nanofibers with enhanced arsenate removal performance." Environmental Science: Nano **3**(5): 1165-1173.

Motallebi, R., A. Moghimi, H. Shahbazi and H. Faraji (2022). "Fabrication of superparamagnetic adsorbent based on layered double hydroxide as effective nanoadsorbent for removal of Sb (III) from water samples." IET Nanobiotechnology **16**(2): 33-48.

Müller, V., T. Chavez-Capilla, J. Feldmann and A. Mestrot (2022). "Increasing temperature and flooding enhance arsenic release and biotransformations in Swiss soils." Science of The Total Environment **838**: 156049.

Mustafiz, S., A. Basu, M. R. Islam, A. Dewaidar and O. Chaalal (2002). "A Novel Method for Heavy Metal Removal." Energy Sources **24**(11): 1043-1051.

Nandi, D., S. K. Ghosh, A. Ghosh, S. Siengchin, A. Roy, K. Gupta, J. Parameswaranpillai, A. K. Bhowmick and U. C. Ghosh (2021). "Arsenic removal from water by graphene nanoplatelets prepared from nail waste: A physicochemical study of adsorption based on process optimization, kinetics, isotherm and thermodynamics." Environmental Nanotechnology, Monitoring & Management **16**: 100564.

Natasha, M. Shahid, S. Khalid, N. K. Niazi, B. Murtaza, N. Ahmad, A. Farooq, A. Zakir, M. Imran and G. Abbas (2021). "Health risks of arsenic buildup in soil and food crops after wastewater irrigation." Science of The Total Environment ***772***: 145266.

Navarathna, C. M., A. G. Karunanayake, S. R. Gunatilake, C. U. Pittman, F. Perez, D. Mohan and T. Mlsna (2019). "Removal of Arsenic(III) from water using magnetite precipitated onto Douglas fir biochar." Journal of Environmental Management **250**: 109429.

Nguyen, T. V., S. Vigneswaran, H. H. Ngo and J. Kandasamy (2010). "Arsenic removal by iron oxide coated sponge: Experimental performance and mathematical models." Journal of Hazardous Materials **182**(1): 723-729.

Nguyen, V. L., W.-H. Chen, T. Young and J. Darby (2011). "Effect of interferences on the breakthrough of arsenic: Rapid small scale column tests." Water Research **45**(14): 4069-4080.

Nhat Ha, H. N., N. T. Kim Phuong, T. Boi An, N. T. Mai Tho, T. Ngoc Thang, B. Quang Minh and C. Van Du (2016). "Arsenate removal by layered double hydroxides embedded into spherical polymer beads: Batch and column studies." Journal of Environmental Science and Health, Part A **51**(5): 403-413.

Nishad, P. A. and A. Bhaskarapillai (2021). "Antimony, a pollutant of emerging concern: A review on industrial sources and remediation technologies." Chemosphere **277**: 130252.

Ociński, D. and P. Mazur (2020). "Highly efficient arsenic sorbent based on residual from water deironing – Sorption mechanisms and column studies." Journal of Hazardous Materials **382**: 121062.

Oliveira, G. and A. Costa (2012). "How resilient is Quercus suber L. to cork harvesting? A review and identification of knowledge gaps." Forest Ecology and Management **270**: 257-272.

Önnby, L., V. Pakade, B. Mattiasson and H. Kirsebom (2012). "Polymer composite adsorbents using particles of molecularly imprinted polymers or aluminium oxide nanoparticles for treatment of arsenic contaminated waters." Water Research **46**(13): 4111-4120.

Ouvrard, S., M.-O. Simonnot and M. Sardin (2002). "Reactive Behavior of Natural Manganese Oxides toward the Adsorption of Phosphate and Arsenate." Industrial & Engineering Chemistry Research **41**(11): 2785-2791.

Pandi, K., D.-w. Lee and J. Choi (2020). "Facile synthesis of zirconium-organic frameworks@biomass-derived porous graphitic nanocomposites: Arsenic adsorption performance and mechanism." Journal of Molecular Liquids **314**: 113552.

Pang, D., C.-C. Wang, P. Wang, W. Liu, H. Fu and C. Zhao (2020). "Superior removal of inorganic and organic arsenic pollutants from water with MIL-88A(Fe) decorated on cotton fibers." Chemosphere **254**: 126829.

Park, J.-H., J.-H. Lee, S.-L. Lee, S.-W. Hwang and D.-C. Seo (2021). "Adsorption behavior of arsenic onto lignin-based biochar decorated with zinc." Colloids and Surfaces A: Physicochemical and Engineering Aspects **626**: 127095.

Patel, H. (2019). "Fixed-bed column adsorption study: a comprehensive review." Applied Water Science **9**(3): 1-17.

Patel, H. (2021). "Review on solvent desorption study from exhausted adsorbent." Journal of Saudi Chemical Society **25**(8): 101302.

Pauling, L. (1933). "The Formulas of Antimonic Acid and the Antimonates." Journal of the American Chemical Society **55**(5): 1895-1900.

Pehlivan, E., H. T. Tran, W. K. I. Ouédraogo, C. Schmidt, D. Zachmann and M. Bahadir (2013). "Sugarcane bagasse treated with hydrous ferric oxide as a potential adsorbent for the removal of As(V) from aqueous solutions." Food Chemistry **138**(1): 133-138.

Peng, L., N. Wang, T. Xiao, J. Wang, H. Quan, C. Fu, Q. Kong and X. Zhang (2023). "A critical review on adsorptive removal of antimony from waters: Adsorbent species, interface behavior and interaction mechanism." Chemosphere **327**: 138529.

Peng, Y., L. Luo, S. Luo, K. Peng, Y. Zhou, Q. Mao, J. Yang and Y. Yang (2021). "Efficient Removal of Antimony(III) in Aqueous Phase by Nano-Fe3O4 Modified High-Iron Red Mud: Study on Its Performance and Mechanism." Water **13**(6): 809.

Pereira, P. A. L., A. J. B. Dutra and A. H. Martins (2007). "Adsorptive removal of arsenic from river waters using pisolite." Minerals Engineering **20**(1): 52-59.

Pintor, A. M. A., C. C. Brandão, R. A. R. Boaventura and C. M. S. Botelho (2020). "Multicomponent adsorption of pentavalent As, Sb and P onto iron-coated cork granulates." Journal of Hazardous Materials: 124339.

Pintor, A. M. A., C. C. Brandão, R. A. R. Boaventura and C. M. S. Botelho (2021). "Multicomponent adsorption of pentavalent As, Sb and P onto iron-coated cork granulates." Journal of Hazardous Materials **406**: 124339.

Pintor, A. M. A., C. I. A. Ferreira, J. C. Pereira, P. Correia, S. P. Silva, V. J. P. Vilar, C. M. S. Botelho and R. A. R. Boaventura (2012). "Use of cork powder and granules for the adsorption of pollutants: A review." Water Research **46**(10): 3152-3166.

Pintor, A. M. A., I. T. Tomasi, R. A. R. Boaventura and C. M. S. Botelho (2022). "Establishing the state-of-the-art on the adsorption of coexisting pnictogens in water: A literature review." CHEMOSPHERE **286**.

Pintor, A. M. A., B. R. C. Vieira, R. A. R. Boaventura and C. M. S. Botelho (2020). "Removal of antimony from water by iron-coated cork granulates." Separation and Purification Technology **233**: 116020.

Pintor, A. M. A., B. R. C. Vieira, C. C. Brandão, R. A. R. Boaventura and C. M. S. Botelho (2020). "Complexation mechanisms in arsenic and phosphorus adsorption onto iron-coated cork granulates." Journal of Environmental Chemical Engineering **8**(5): 104184.

Pintor, A. M. A., B. R. C. Vieira, S. C. R. Santos, R. A. R. Boaventura and C. M. S. Botelho (2018). "Arsenate and arsenite adsorption onto iron-coated cork granulates." Sci Total Environ **642**: 1075-1089.

Pintor, A. M. A., B. R. C. Vieira, S. C. R. Santos, R. A. R. Boaventura and C. M. S. Botelho (2018). "Arsenate and arsenite adsorption onto iron-coated cork granulates." Science of The Total Environment **642**: 1075-1089.

Pokhrel, D. and T. Viraraghavan (2008). "Arsenic removal in an iron oxide-coated fungal biomass column: Analysis of breakthrough curves." Bioresource Technology **99**(6): 2067-2071.

Pontius, F. W. (1994). "Crafting a New Arsenic Rule." Journal AWWA **86**(9): 6-104.

Qi, P., Y. Wang, J. Zeng, K. Sui and J. Zhao (2021). "Progress in antimony capturing by superior materials: Mechanisms, properties and perspectives." Chemical Engineering Journal **419**: 130013.

Qi, Z., T. P. Joshi, R. Liu, H. Liu and J. Qu (2017). "Synthesis of Ce(III)-doped Fe3O4 magnetic particles for efficient removal of antimony from aqueous solution." Journal of Hazardous Materials **329**: 193-204.

Qiu, S., L. Yan and C. Jing (2019). "Simultaneous removal of arsenic and antimony from mining wastewater using granular TiO2: Batch and field column studies." Journal of Environmental Sciences **75**: 269-276.

Quansah, R., F. A. Armah, D. K. Essumang, I. Luginaah, E. Clarke, K. Marfoh, S. J. Cobbina, E. Nketiah-Amponsah, P. B. Namujju, S. Obiri and M. Dzodzomenyo (2015). "Association of Arsenic with Adverse Pregnancy Outcomes/Infant Mortality: A Systematic Review and Meta-Analysis." Environmental Health Perspectives **123**(5): 412-421.

Rahaman, M. S., A. Basu and M. R. Islam (2008). "The removal of As(III) and As(V) from aqueous solutions by waste materials." Bioresource Technology **99**(8): 2815-2823.

Ramirez-Muñiz, K., F. Perez-Rodriguez and R. Rangel-Mendez (2018). "Adsorption of arsenic onto an environmental friendly goethite-polyacrylamide composite." Journal of Molecular Liquids **264**: 253-260.

Ranjan, D., M. Talat and S. H. Hasan (2009). "Rice Polish: An Alternative to Conventional Adsorbents for Treating Arsenic Bearing Water by Up-Flow Column Method." Industrial & Engineering Chemistry Research **48**(23): 10180-10185.

Raval, N. P. and M. Kumar (2022). "Development of novel Core–shell impregnated polyuronate composite beads for an eco-efficient removal of arsenic." Bioresource Technology **364**: 127918.

Reddy, K. J., K. J. McDonald and H. King (2013). "A novel arsenic removal process for water using cupric oxide nanoparticles." Journal of Colloid and Interface Science **397**: 96-102.

Rives, J., I. Fernandez-Rodriguez, J. Rieradevall and X. Gabarrell (2013). "Integrated environmental analysis of the main cork products in southern Europe (Catalonia – Spain)." Journal of Cleaner Production **51**: 289-298.

Rosa, M. E., H. Pereira and M. Fortes (1990). "Effects of hot water treatment on the structure and properties of cork." Wood and Fiber Science: 149-164.

Roxanne, B.-R., G. Jonathan, D. Jean-Sébastien and C. Bruno (2018). "Development and treatment procedure of arsenic-contaminated water using a new and green chitosan sorbent: kinetic, isotherm, thermodynamic and dynamic studies." Pure and Applied Chemistry **90**(1): 63-77.

Roy, P., N. K. Mondal, S. Bhattacharya, B. Das and K. Das (2013). "Removal of arsenic(III) and arsenic(V) on chemically modified low-cost adsorbent: batch and column operations." Applied Water Science **3**(1): 293-309.

Runtti, H., T. Luukkonen, S. Tuomikoski, T. Hu, U. Lassi and T. Kangas (2023). "Removal of antimony from model solutions, mine effluent, and textile industry wastewater with Mg-rich mineral adsorbents." Environmental Science and Pollution Research **30**(6): 14139-14154.

Saha, S. and P. Sarkar (2015). "Arsenic mitigation by chitosan based porous magnesia impregnated alumina: performance evaluation in continuous packed bed column." International journal of Environmental Science and Technology **13**.

Saldaña-Robles, A., C. E. Damian-Ascencio, R. J. Guerra-Sanchez, A. L. Saldaña-Robles, N. Saldaña-Robles, A. Gallegos-Muñoz and S. Cano-Andrade (2018). "Effects of the presence of organic matter on the removal of arsenic from groundwater." Journal of Cleaner Production **183**: 720-728.

Saleh, T. A., A. Sarı and M. Tuzen (2017). "Effective adsorption of antimony(III) from aqueous solutions by polyamide-graphene composite as a novel adsorbent." Chemical Engineering Journal **307**: 230-238.

Samad, A., T. Fukumoto, A. Dabwan, H. Katsumata, T. Suzuki, M. Furukawa and S. Knaeco (2016). "Enhanced Removal of Arsenite from Ground Water by Adsorption onto Heat-Treated Rice Husk." Open Journal of Inorganic Non-metallic Materials **06**: 18-23.

Saqib, A. N. S., A. Waseem, A. F. Khan, Q. Mahmood, A. Khan, A. Habib and A. R. Khan (2013). "Arsenic bioremediation by low cost materials derived from Blue Pine (Pinus wallichiana) and Walnut (Juglans regia)." Ecological Engineering **51**: 88-94.

Sarı, A., D. Çıtak and M. Tuzen (2010). "Equilibrium, thermodynamic and kinetic studies on adsorption of Sb(III) from aqueous solution using low-cost natural diatomite." Chemical Engineering Journal **162**(2): 521-527.

Sari, A., M. Tuzen and İ. Kocal (2017). "Application of chitosan-modified pumice for antimony adsorption from aqueous solution." Environmental Progress & Sustainable Energy **36**(6): 1587-1596.

Sarkar, P., P. Pal, D. Bhattacharyay and S. Banerjee (2010). "Removal of arsenic from drinking water by ferric hydroxide microcapsule-loaded alginate beads in packed adsorption column." Journal of Environmental Science and Health, Part A **45**(13): 1750-1757.

Sarkar, S., L. M. Blaney, A. Gupta, D. Ghosh and A. K. SenGupta (2007). "Use of ArsenXnp, a hybrid anion exchanger, for arsenic removal in remote villages in the Indian subcontinent." Reactive and Functional Polymers **67**(12): 1599-1611.

Savina, I. N., C. J. English, R. L. D. Whitby, Y. Zheng, A. Leistner, S. V. Mikhalovsky and A. B. Cundy (2011). "High efficiency removal of dissolved As(III) using iron nanoparticle-embedded macroporous polymer composites." Journal of Hazardous Materials **192**(3): 1002-1008.

Schweitzer, G. K. and L. L. Pesterfield (2010). The aqueous chemistry of the elements, OUP USA.

Şen, A., J. Van den Bulcke, N. Defoirdt, J. Van Acker and H. Pereira (2014). "Thermal behaviour of cork and cork components." Thermochimica Acta **582**: 94-100.

Senthil Kumar, P. and P. Tsopbou Ngueagni (2022). Chapter 15 - Removal of volatile organic carbon and heavy metols through microbial approach. An Innovative Role of Biofiltration in Wastewater Treatment Plants (WWTPs). M. Shah, S. Rodriguez-Couto and J. Biswas, Elsevier: 285-308.

Serfor-Armah, Y., B. J. B. Nyarko, S. B. Dampare and D. Adomako (2006). "Levels of Arsenic and Antimony in Water and Sediment from Prestea, A Gold Mining Town in Ghana and its Environs." Water, Air, and Soil Pollution **175**(1): 181.

Shahid, M. K., S. Phearom and Y.-G. Choi (2019). "Adsorption of arsenic (V) on magnetite-enriched particles separated from the mill scale." Environmental Earth Sciences **78**(3): 65.

Shahid, M. K., S. Phearom and Y.-G. Choi (2019). "Evaluation of arsenate adsorption efficiency of mill-scale derived magnetite particles with column and plug flow reactors." Journal of Water Process Engineering **28**: 260-268.

Shahid, M. K., S. Phearom and Y.-G. Choi (2020). "Packed Bed Column for Adsorption of Arsenic on Mixed-Valent Iron [Fe(II)-Fe(III)] Oxide Synthesized from Industrial Waste." Journal of Hazardous, Toxic, and Radioactive Waste **24**(2): 04020002.

Shaji, E., M. Santosh, K. V. Sarath, P. Prakash, V. Deepchand and B. V. Divya (2021). "Arsenic contamination of groundwater: A global synopsis with focus on the Indian Peninsula." Geoscience Frontiers **12**(3): 101079.

Shakoor, M. B., N. K. Niazi, I. Bibi, M. Shahid, F. Sharif, S. Bashir, S. M. Shaheen, H. Wang, D. C. W. Tsang, Y. S. Ok and J. Rinklebe (2018). "Arsenic removal by natural and chemically modified water melon rind in aqueous solutions and groundwater." Science of The Total Environment **645**: 1444-1455.

Sharma, A., N. Verma, A. Sharma, D. Deva and N. Sankararamakrishnan (2010). "Iron doped phenolic resin based activated carbon micro and nanoparticles by milling: Synthesis, characterization and application in arsenic removal." Chemical Engineering Science **65**(11): 3591-3601.

Sharma, A. K., J. C. Tjell, J. J. Sloth and P. E. Holm (2014). "Review of arsenic contamination, exposure through water and food and low cost mitigation options for rural areas." Applied Geochemistry **41**: 11-33.

Sigrist, M. E., L. Brusa, H. R. Beldomenico, L. Dosso, O. M. Tsendra, M. B. González, C. L. Pieck and C. R. Vera (2014). "Influence of the iron content on the arsenic adsorption capacity of Fe/GAC adsorbents." Journal of Environmental Chemical Engineering **2**(2): 927-934.

Silva, B., M. Martins, M. Rosca, V. Rocha, A. Lago, I. C. Neves and T. Tavares (2020). "Waste-based biosorbents as cost-effective alternatives to commercial adsorbents for the retention of fluoxetine from water." Separation and Purification Technology **235**: 116139.

Silva, S. P., M. A. Sabino, E. M. Fernandes, V. M. Correlo, L. F. Boesel and R. L. Reis (2005). "Cork: properties, capabilities and applications." International Materials Reviews **50**(6): 345-365.

Simeonidis, K., V. Papadopoulou, S. Tresintsi, E. Kokkinos, I. A. Katsoyiannis, A. I. Zouboulis and M. Mitrakas (2017). "Efficiency of Iron-Based Oxy-Hydroxides in Removing Antimony from Groundwater to Levels below the Drinking Water Regulation Limits." Sustainability **9**(2): 238.

Simsek, E. B., P. Demircivi, I. Novak, D. Berek and U. Beker (2018). "Novel composite sorbents based on carbon fibers decorated with ferric hydroxides – simultaneous removal of antimonate and arsenate from aqueous solutions." Water Supply **19**(3): 838-845.

Singh, P., S. K. Singh, J. Bajpai, A. K. Bajpai and R. B. Shrivastava (2014). "Iron crosslinked alginate as novel nanosorbents for removal of arsenic ions and bacteriological contamination from water." Journal of Materials Research and Technology **3**(3): 195-202.

Smedley, P. L. and D. G. Kinniburgh (2002). "A review of the source, behaviour and distribution of arsenic in natural waters." Applied Geochemistry **17**(5): 517-568.

Smichowski, P., Y. Madrid and C. Cámara (1998). "Analytical methods for antimony speciation in waters at trace and ultratrace levels. A review." Fresenius' Journal of Analytical Chemistry **360**(6): 623-629.

Smith, A. H. and M. M. H. Smith (2004). "Arsenic drinking water regulations in developing countries with extensive exposure." Toxicology **198**(1): 39-44.

Sorg, T. J., R. Kolisz, A. S. C. Chen and L. Wang (2017). "Regenerating an Arsenic Removal Iron-Bed Adsorptive Media System, Part 2: Performance and Cost." J Am Water Works Assoc **109**(5): E122-e128.

Sosa, A., M. A. Armienta, A. Aguayo and O. Cruz (2020). "Evaluation of the influence of main groundwater ions on arsenic removal by limestones through column experiments." Science of The Total Environment **727**: 138459.

Sperlich, A., S. Schimmelpfennig, B. Baumgarten, A. Genz, G. Amy, E. Worch and M. Jekel (2008). "Predicting anion breakthrough in granular ferric hydroxide (GFH) adsorption filters." Water Research **42**(8): 2073-2082.

Sperlich, A., A. Werner, A. Genz, G. Amy, E. Worch and M. Jekel (2005). "Breakthrough behavior of granular ferric hydroxide (GFH) fixed-bed adsorption filters: modeling and experimental approaches." Water Research **39**(6): 1190-1198.

Streat, M., K. Hellgardt and N. L. R. Newton (2008). "Hydrous ferric oxide as an adsorbent in water treatment: Part 1. Preparation and physical characterization." Process Safety and Environmental Protection **86**(1): 1-9.

Streat, M., K. Hellgardt and N. L. R. Newton (2008). "Hydrous ferric oxide as an adsorbent in water treatment: Part 2. Adsorption studies." Process Safety and Environmental Protection **86**(1): 11-20.

Streat, M., K. Hellgardt and N. L. R. Newton (2008). "Hydrous ferric oxide as an adsorbent in water treatment: Part 3: Batch and mini-column adsorption of arsenic, phosphorus, fluorine and cadmium ions." Process Safety and Environmental Protection **86**(1): 21-30.

Su, C. and R. W. Puls (2004). "Significance of Iron(II,III) Hydroxycarbonate Green Rust in Arsenic Remediation Using Zerovalent Iron in Laboratory Column Tests." Environmental Science & Technology **38**(19): 5224-5231.

Sud, D., G. Mahajan and M. P. Kaur (2008). "Agricultural waste material as potential adsorbent for sequestering heavy metal ions from aqueous solutions – A review." Bioresource Technology **99**(14): 6017-6027.

Sun, F., Y. Yan, H. Liao, Y. Bai, B. Xing and F. Wu (2014). "Biosorption of antimony(V) by freshwater cyanobacteria Microcystis from Lake Taihu, China: effects of pH and competitive ions." Environmental Science and Pollution Research **21**(9): 5836-5848.

SW, E. (1992). "846. Test Method 1311: Toxicity Characteristic Leaching Procedure, part of Test Methods for Evaluating Solid Waste, Physical/Chemical Methods." Environmental Protection Agency.

Tamaddoni Moghaddam, S., H. Ghasemi, F. B. Hussein and N. Abu-Zahra (2023). "Effect of reaction parameters on Arsenic removal capacity from aqueous solutions using modified magnetic PU foam nanocomposite." Results in Materials **17**: 100373.

Tan, X., Y. Liu, G. Zeng, X. Wang, X. Hu, Y. Gu and Z. Yang (2015). "Application of biochar for the removal of pollutants from aqueous solutions." Chemosphere **125**: 70-85.

Thakur, N. and D. W. Armstrong (2021). "Arsenic sequestration by iron oxide coated geopolymer microspheres." Journal of Cleaner Production **291**: 125931.

Thirunavukkarasu, O. S., T. Viraraghavan, K. S. Subramanian and S. Tanjore (2002). "Organic arsenic removal from drinking water." Urban Water **4**(4): 415-421.

Thomas, H. C. (1944). "Heterogeneous Ion Exchange in a Flowing System." Journal of the American Chemical Society **66**(10): 1664-1666.

Tian, Y., M. Wu, X. Lin, P. Huang and Y. Huang (2011). "Synthesis of magnetic wheat straw for arsenic adsorption." Journal of Hazardous Materials **193**: 10-16.

Tresintsi, S., K. Simeonidis, M. Katsikini, E. C. Paloura, G. Bantsis and M. Mitrakas (2014). "A novel approach for arsenic adsorbents regeneration using MgO." Journal of Hazardous Materials **265**: 217-225.

Tuutijärvi, T., R. Vahala, M. Sillanpää and G. Chen (2012). "Maghemite nanoparticles for As(V) removal: desorption characteristics and adsorbent recovery." Environmental Technology **33**(16): 1927-1936.

Tuzen, M., A. Sarı, D. Mendil, O. D. Uluozlu, M. Soylak and M. Dogan (2009). "Characterization of biosorption process of As(III) on green algae Ulothrix cylindricum." Journal of Hazardous Materials **165**(1): 566-572.

Uluozlu, O. D., A. Sarı and M. Tuzen (2010). "Biosorption of antimony from aqueous solution by lichen (Physcia tribacia) biomass." Chemical Engineering Journal **163**(3): 382-388.

Ungureanu, G., C. Filote, S. C. R. Santos, R. A. R. Boaventura, I. Volf and C. M. S. Botelho (2016). "Antimony oxyanions uptake by green marine macroalgae." Journal of Environmental Chemical Engineering **4**(3): 3441-3450.

Ungureanu, G., S. Santos, R. Boaventura and C. Botelho (2015). "Arsenic and antimony in water and wastewater: Overview of removal techniques with special reference to latest advances in adsorption." Journal of Environmental Management **151**: 326-342.

Ungureanu, G., S. C. R. Santos, I. Volf, R. A. R. Boaventura and C. M. S. Botelho (2017). "Biosorption of antimony oxyanions by brown seaweeds: Batch and column studies." Journal of Environmental Chemical Engineering **5**(4): 3463-3471.

USPHS (1943). "Public Health Service Drinking Water Standards." Public Health Reports (1896-1970) **58**(3): 69-82.

Vakili, M., S. Deng, G. Cagnetta, W. Wang, P. Meng, D. Liu and G. Yu (2019). "Regeneration of chitosan-based adsorbents used in heavy metal adsorption: A review." Separation and Purification Technology **224**: 373-387.

van Genuchten, C. M., T. R. Etmannski, S. Jessen and H. M. Breunig (2022). "LCA of Disposal Practices for Arsenic-Bearing Iron Oxides Reveals the Need for Advanced Arsenic Recovery." Environmental Science & Technology **56**(19): 14109-14119.

Vaz, M. F. and M. Fortes (1998). "Friction properties of cork." Journal of materials science **33**: 2087-2093.

Verma, L. and J. Singh (2023). "Removal of As(III) and As(V) from aqueous solution using engineered biochar: batch and fixed-bed column study." International Journal of Environmental Science and Technology **20**(2): 1961-1980.

Vieira, B. R. C., A. M. A. Pintor, R. A. R. Boaventura, C. M. S. Botelho and S. C. R. Santos (2017). "Arsenic removal from water using iron-coated seaweeds." Journal of Environmental Management **192**: 224-233.

Vijayaraghavan, K. and R. Balasubramanian (2011). "Antimonite Removal Using Marine Algal Species." Industrial & Engineering Chemistry Research **50**(17): 9864-9869.

Villaescusa, I. and J.-C. Bollinger (2008). "Arsenic in drinking water: sources, occurrence and health effects (a review)." Reviews in Environmental Science and Bio/Technology **7**(4): 307-323.

Wang, J., J. Liu, X. Peng, M. He, X. Hu, J. Zhao, F. Zhu, X. Yang and L. Kong (2022). "Reductive removal of As(V) and As(III) from aqueous solution by the UV/sulfite process: Recovery of elemental arsenic." Water Research **223**: 118981.

Wang, J., W. Zhang, Y. Zheng, N. Zhang and C. Zhang (2019). "Multi-functionalization of magnetic graphene by surface-initiated ICAR ATRP mediated by polydopamine chemistry for adsorption and speciation of arsenic." Applied Surface Science **478**: 15-25.

Wang, K., P. E. Holm, U. B. Trettenes, S. R. S. Bandaru, D. van Halem and C. M. van Genuchten (2023). "Molecular-scale characterization of groundwater treatment sludge from around the world: Implications for potential arsenic recovery." Water Research **245**: 120561.

Wang, L., J. Wang, Z. Wang, C. He, W. Lyu, W. Yan and L. Yang (2018). "Enhanced antimonate (Sb(V)) removal from aqueous solution by La-doped magnetic biochars." Chemical Engineering Journal **354**: 623-632.

Wang, Q., C. Luo, Z. Lai, S. Chen, D. He and J. Mu (2022). "Honeycomb-like cork activated carbon with ultra-high adsorption capacity for anionic, cationic and mixed dye: Preparation, performance and mechanism." Bioresource Technology **357**: 127363.

Wang, S., B. Gao and Y. Li (2016). "Enhanced arsenic removal by biochar modified with nickel (Ni) and manganese (Mn) oxyhydroxides." Journal of Industrial and Engineering Chemistry **37**: 361-365.

Wang, Y., L. Sun, T. Han, Y. Si and R. Wang (2016). "Arsenite and arsenate leaching and retention on iron (hydr)oxide-coated sand column." Journal of Soils and Sediments **16**(2): 486-496.

Wang, Z., S. B. Kang, H. J. Yun and S. W. Won (2023). "Efficient removal of arsenate from water using electrospun polyethylenimine/polyvinyl chloride nanofiber sheets." Reactive and Functional Polymers **184**: 105514.

Wei, Y., S. Wei, C. Liu, T. Chen, Y. Tang, J. Ma, K. Yin and S. Luo (2019). "Efficient removal of arsenic from groundwater using iron oxide nanoneedle array-decorated biochar fibers with high Fe utilization and fast adsorption kinetics." Water Research **167**: 115107.

Wei, Y., X. Yu, C. Liu, J. Ma, S. Wei, T. Chen, K. Yin, H. Liu and S. Luo (2019). "Enhanced arsenite removal from water by radially porous Fe-chitosan beads: Adsorption and H2O2 catalytic oxidation." Journal of Hazardous Materials **373**: 97-105.

WHO (2017). Guidelines for drinking-water quality: fourth edition incorporating first addendum. Geneva, World Health Organization.

WHO (2022). Guidelines for drinking-water quality: incorporating the first and second addenda. Geneva, World Health Organization.

Williams, L. E., M. O. Barnett, T. A. Kramer and J. G. Melville (2003). "Adsorption and Transport of Arsenic(V) in Experimental Subsurface Systems." Journal of Environmental Quality **32**(3): 841-850.

Wilson, S. C., P. V. Lockwood, P. M. Ashley and M. Tighe (2010). "The chemistry and behaviour of antimony in the soil environment with comparisons to arsenic: A critical review." Environmental Pollution **158**(5): 1169-1181.

World Health, O. (1958). International standards for drinking-water. Geneva, World Health Organization.

World Health, O. (1993). Guidelines for drinking-water quality: volume 1: recommendations. Geneva, World Health Organization.

Xi, J., M. He and C. Lin (2010). "Adsorption of antimony(V) on kaolinite as a function of pH, ionic strength and humic acid." Environmental Earth Sciences **60**(4): 715-722.

Xu, R., Q. Li, X. Nan, G. Jiang, L. Wang, J. Xiong, Y. Yang, B. Xu and T. Jiang (2022). "Simultaneous removal of antimony(III/V) and arsenic(III/V) from aqueous solution by bacteria–mediated kaolin@Fe–Mn binary (hydr)oxides composites." Applied Clay Science **217**: 106392.

Yadav, M. K., D. Saidulu, P. S. Ghosal, A. Mukherjee and A. K. Gupta (2022). "A review on the management of arsenic-laden spent adsorbent: Insights of global practices, process criticality, and sustainable solutions." Environmental Technology & Innovation **27**: 102500.

Yan, G., T. Viraraghavan and M. Chen (2001). "A new model for heavy metal removal in a biosorption column." Adsorption Science & Technology **19**(1): 25-43.

Yan, R., Z. Qiu, X. Bian, J. Yang, S. Lyu and A. Zhou (2020). "Effective adsorption of antimony from aqueous solution by cerium hydroxide loaded on Y-tape molecular sieve adsorbent: Performance and mechanism." Colloids and Surfaces A: Physicochemical and Engineering Aspects **604**: 125317.

Yan, X.-L., T.-B. Chen, X.-Y. Liao, Z.-C. Huang, J.-R. Pan, T.-D. Hu, C.-J. Nie and H. Xie (2008). "Arsenic Transformation and Volatilization during Incineration of the Hyperaccumulator Pteris vittata L." Environmental Science & Technology **42**(5): 1479-1484.

Yang, B., X. Zhou, Y. Chen, Y. Fang and H. Luo (2021). "Preparation of a spindle δ-MnO2@Fe/Co-MOF-74 for effective adsorption of arsenic from water." Colloids and Surfaces A: Physicochemical and Engineering Aspects **629**: 127378.

Yang, K., C. Zhou, C. Li, S. Dou, X. Li, X. Wang and X. Xu (2021). "Efficient removal of Sb(V) in textile wastewater through novel amorphous Si-doped Fe oxide composites: Phase composition, stability and adsorption mechanism." Chemical Engineering Journal **407**: 127217.

Yang, K., J. Zhou, Z. Lou, X. Zhou, Y. Liu, Y. Li, S. Ali Baig and X. Xu (2018). "Removal of Sb(V) from aqueous solutions using Fe-Mn binary oxides: The influence of iron oxides forms and the role of manganese oxides." Chemical Engineering Journal **354**: 577-588.

Yang, X., Z. Shi and L. Liu (2015). "Adsorption of Sb(III) from aqueous solution by QFGO particles in batch and fixed-bed systems." Chemical Engineering Journal **260**: 444-453.

Yang, X., Z. Shi, M. Yuan and L. Liu (2015). "Adsorption of Trivalent Antimony from Aqueous Solution Using Graphene Oxide: Kinetic and Thermodynamic Studies." Journal of Chemical & Engineering Data **60**(3): 806-813.

Yao, S., F. Jabeur, L. Pontoni, S. Mechri, B. Jaouadi and F. Sannino (2024). "Sustainable removal of arsenic from waters by adsorption on blue crab, Portunus segnis (Forskål, 1775) chitosan-based adsorbents." Environmental Technology & Innovation **33**: 103491.

Yeo, K. F. H., Y. Dong, Y. Yang, C. Li, K. Wu, H. Zhang, Z. Chen, E. B. Atse, L. Yang and W. Wang (2022). "Fast arsenate As(V) adsorption and removal from water using aluminium Al(III) fixed on Kapok fibres." Environmental Pollution **314**: 120236.

Yeo, K. F. H., C. Li, Y. Dong, Y. Yang, K. Wu, H. Zhang, Z. Chen, Y. Gao and W. Wang (2022). "Adsorption performance of Fe(III) modified kapok fiber for As(V) removal from water." Separation and Purification Technology **287**: 120494.

Yeo, K. F. H., C. K. Li, H. Zhang, J. Chen, W. D. Wang and Y. Y. Dong (2021). "Arsenic Removal from Contaminated Water Using Natural Adsorbents: A Review." COATINGS **11**(11).

Yin, H., M. Kong, X. Gu and H. Chen (2017). "Removal of arsenic from water by porous charred granulated attapulgite-supported hydrated iron oxide in bath and column modes." Journal of Cleaner Production **166**: 88-97.

Yoon, Y. H. and J. H. Nelson (1984). "Application of gas adsorption kinetics. I. A theoretical model for respirator cartridge service life." Am Ind Hyg Assoc J **45**(8): 509-516.

Yuan, T., J. Yong Hu, S. L. Ong, Q. F. Luo and W. Jun Ng (2002). "ARSENIC REMOVAL FROM HOUSEHOLD DRINKING WATER BY ADSORPTION." Journal of Environmental Science and Health, Part A **37**(9): 1721-1736.

Zaimee, M. Z., M. S. Sarjadi and M. L. Rahman (2021). "Heavy Metals Removal from Water by Efficient Adsorbents." Water **13**(19).

Zeng, H., Y. Yu, F. Wang, J. Zhang and D. Li (2020). "Arsenic(V) removal by granular adsorbents made from water treatment residuals materials and chitosan." Colloids and Surfaces A: Physicochemical and Engineering Aspects **585**: 124036.

Zhang, C., M. Wu, K. Wu, H. Li and G. Zhang (2023). "Efficient removal of antimonate and antimonite by a novel lanthanum-manganese binary oxide: Performance and mechanism." Journal of Hazardous Materials **442**: 130132.

Zhang, D., D.-J. Lee and X. Pan (2013). "Desorption of Hg(II) and Sb(V) on extracellular polymeric substances: Effects of pH, EDTA, Ca(II) and temperature shocks." Bioresource Technology **128**: 711-715.

Zhang, F., X. Wang, J. Xionghui and L. Ma (2016). "Efficient arsenate removal by magnetite-modified water hyacinth biochar." Environmental Pollution **216**: 575-583.

Zhang, K., K. Yu, X. Luo and S. Luo (2023). "Highly Efficient and Robust Monolith of a Metal–Organic Framework Hybrid Aerogel for the Removal of Antimony from Water." ACS ES&T Engineering **3**(1): 45-56.

Zhang, L., Y. Dong, J. Liu, C. Liu, W. Liu and H. Lin (2022). "The effect of co-pyrolysis temperature for iron-biochar composites on their adsorption behavior of antimonite and antimonate in aqueous solution." Bioresource Technology **347**: 126362.

Zhang, Q. L., Y. C. Lin, X. Chen and N. Y. Gao (2007). "A method for preparing ferric activated carbon composites adsorbents to remove arsenic from drinking water." Journal of Hazardous Materials **148**(3): 671-678.

Zhang, X., N. Xie, Y. Guo, D. Niu, H.-b. Sun and Y. Yang (2021). "Insights into adsorptive removal of antimony contaminants: Functional materials, evaluation and prospective." Journal of Hazardous Materials **418**: 126345.

Zhang, Y., C. Ding, D. Gong, Y. Deng, Y. Huang, J. Zheng, S. Xiong, R. Tang, Y. Wang and L. Su (2021). "A review of the environmental chemical behavior, detection and treatment of antimony." Environmental Technology & Innovation **24**: 102026.

Zhang, Y., E. J. O'Loughlin and M. J. Kwon (2022). "Antimony Redox Processes in the Environment: A Critical Review of Associated Oxidants and Reductants." Journal of Hazardous Materials: 128607.

Zhao, Y., M. Huang, W. Wu and W. Jin (2009). "Synthesis of the cotton cellulose based Fe(III)-loaded adsorbent for arsenic(V) removal from drinking water." Desalination **249**(3): 1006-1011.

Zhao, Y., H. Shi, Z. Du, J. Zhou and F. Yang (2023). "Removal of As(V) from aqueous solution using modified Fe₃O₄ nanoparticles." Royal Society Open Science **10**(1): 220988.

Zhou, J., S. Chen, J. Liu and R. L. Frost (2018). "Adsorption kinetic and species variation of arsenic for As(V) removal by biologically mackinawite (FeS)." Chemical Engineering Journal **354**: 237-244.

Zhu, H., Q. Huang, S. Fu, X. Zhang, Z. Yang, J. Lu, B. Liu, M. Shi, J. Zhang, X. Wen and J. Li (2021). "Removal of Antimony(V) from Drinking Water Using nZVI/AC: Optimization of Batch and Fix Bed Conditions." Toxics **9**(10): 266.

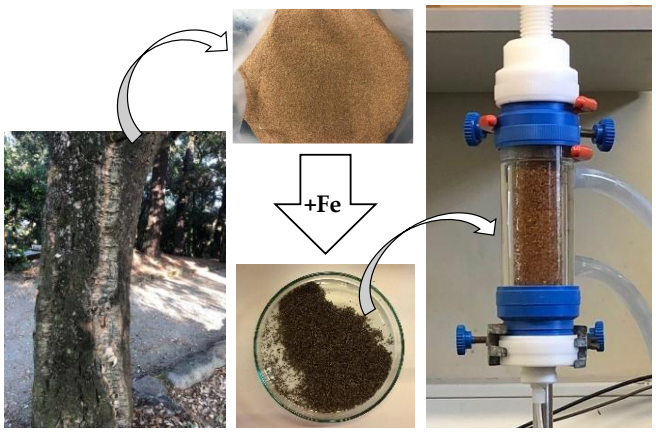
Zhu, T., Y. Zhang, Y. Chen, J.-L. Liu and X.-L. Song (2022). "Synthesis of novel hydrated ferric oxide biochar nanohybrids for efficient arsenic removal from wastewater." Rare Metals **41**(5): 1677-1687.

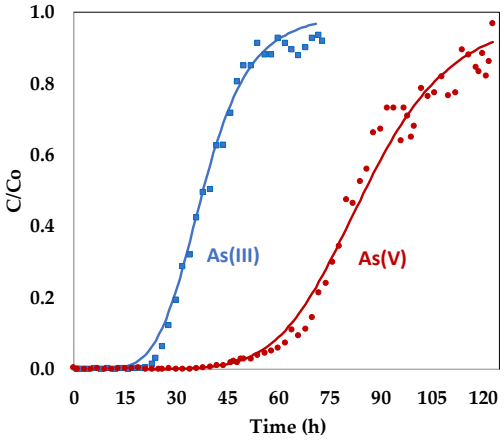
Zhuang, J. M., E. Hobenshield and T. Walsh (2008). "Arsenate sorption by hydrous ferric oxide incorporated onto granular activated carbon with phenol formaldehyde resins coating." Environ Technol **29**(4): 401-411.

Zouboulis, A. I. and I. A. Katsoyiannis (2002). "Arsenic Removal Using Iron Oxide Loaded Alginate Beads." Industrial & Engineering Chemistry Research **41**(24): 6149-6155.

3 REMOVAL OF ARSENIC FROM AQUEOUS SOLUTION BY CONTINUOUS ADSORPTION ONTO IRON-COATED CORK GRANULATES

This chapter is based on: M. A. Carneiro, A. M. A. Pintor, R. A. R. Boaventura and C. M. S. Botelho, *Efficient removal of arsenic from aqueous solution by continuous adsorption onto iron-coated cork granulates*. Journal of Hazardous Materials, 2022: p. 12865.





The search for low-cost technologies for arsenic removal from water is in high demand due to its human toxicity, even at low concentrations. Adsorption can be a cost-effective water treatment technique if applied with inexpensive materials. Arsenic continuous removal by adsorption onto an alternative modified biosorbent, iron-coated cork granulates (ICG), was investigated in this work. Results showed that most experimental parameters of breakthrough curves (BTC) depend on flow rate, bed height, pH, and initial arsenic concentration. The temperature did not significantly affect arsenate removal in continuous mode; however, the adsorption capacity was affected in batch mode. The thermodynamic parameters suggest that the adsorption process is spontaneous and endothermic. The maximum adsorption capacity of ICG for As(V) removal at pH 3 was 4.2±0.3 mg g^{-1}, calculated by Yan model fit, and for As(III) at pH 9 was 1.6±0.2 mg g^{-1}. ICG were able to treat As(V) from 100 µg L-1 to under 10 µg L^{-1} and 50 µg L^{-1} for 895 and 1633 bed volumes, and As(III) for 569 and 861 bed volumes, respectively, both at pH 7. The application of ICG in arsenic oxyanions remediation was found to be effective under various conditions.

3.1 Introduction

In the previous chapters, it has been shown that adsorption is the most cost-effective technology for arsenic removal from water. Moreover, iron impregnation is one of the most common modifications on adsorbents to increase its removal capacity towards oxyanions. Iron-coated cork granulates are modified biosorbents that were previously designed and optimized by the research group and showed promising results when used in batch mode for arsenic adsorption (Pintor, Vieira et al. 2018, Pintor, Brandão et al. 2020, Pintor, Vieira et al. 2020).

In this Chapter, arsenic removal from aqueous solution by ICG in fixed-bed adsorption columns was investigated. The fixed-bed column operational parameters flow rate, temperature, bed height (adsorbent amount) were optimized for As(V) removal using a 2-level 3-factor (2^3) design of experiments (DoE). The effects of pH and arsenic initial concentration on breakthrough curves parameters were also evaluated for As(III) removal. Batch mode experiments were carried out for thermodynamic studies.

3.2 Materials and methods

3.2.1 Materials

The raw cork granulates (RCG) were provided by Corticeira Amorim, S.G.P.S., with a particle size of 0.5-1.0 mm. The iron-coated cork granulates (ICG) were produced as described in a previous study (Pintor, Vieira et al. 2018) and applied in other works (Pintor, Vieira et al. 2018, Pintor, Vieira et al. 2019, Pintor, Vieira et al. 2020, Pintor, Vieira et al. 2020, Pintor, Brandão et al. 2021). In brief, cork granulates were put in contact with a $FeCl_3$ 0.05 M solution of pH 7.0, at 20 g L^{-1}, in a rotating shaker at 20 rpm, for 24 h, at room temperature. Following the coating time, the granulates were washed with distilled water until the iron excess was removed and put to dry for 24 h. The iron content was on average 25 $\pm$ 2 mg g^{-1}.

Arsenic inlet solutions were prepared by diluting, in distilled water, a standard solution of 995 $\pm$ 81 mg As(V) L^{-1}, originated from $HAsNa_2O_4{\cdot}7H_2O$ (Sigma-Aldrich; analytical grade) in 2% HCl, and a standard solution of 939 $\pm$ 35 mg As(III) L^{-1}, originated from As_2O_3 (Acros Organics; 99.5%) in 4% HNO_3. The pH was regulated using 0.1 M, 1 M and 10 M NaOH or HNO_3 solutions.

3.2.2 Analytical Methods

The concentration of arsenic in aqueous solution, both in batch and continuous study, was determined by flame atomic absorption spectrometry (FAAS) for concentrations in the range 5-50 mg L^{-1} and graphite furnace atomic absorption spectrometry (GFAAS) for concentrations ranging from 6.7 to 50 µg L^{-1}. Total dissolved iron was measured by FAAS, in the range 0.25-5 mg L^{-1}.

For As analysis the FAAS equipment (GBC 932 Plus spectrometer) was operated at a wavelength of 193.7 nm, lamp current of 8.0 mA, slit width of 1.0 nm and under nitrous oxide-acetylene flame. The GFAAS equipment was a GBC GF3000, SensAA Dual spectrometer, operating at 193.7 nm, current 8.0 mA, and slit width 1.0 nm, with an 84 s heating program including reading at 2600 °C temperature.

The total dissolved iron was measured by FAAS, at a wavelength of 248.3 nm, lamp current of 5.0 mA, and slit width of 0.2 nm, under air-acetylene flame.

3.2.3 Evaluation of temperature effect in batch operation mode and thermodynamic studies

3.2.3.1 Arsenate adsorption

Despite the fact that recent studies have investigated As(V) adsorption by ICG in batch mode (Pintor, Brandão et al. 2020, Pintor, Vieira et al. 2020), the temperature influence had not yet been assessed. However, this is an important parameter for thermodynamic analysis and the design of a fixed-bed system. The effect of temperature was assessed in As(V) adsorption onto iron-coated cork granulates in batch operation mode by the determination of isotherms at temperatures of 10.0 ± 0.5 °C, 20.0 ± 0.5 °C and 30.0 ± 0.5 °C. As(V) solutions at initial concentrations of 1, 5, 10, 15, 25 and 40 mg L^{-1} were adjusted to pH 3.0 with NaOH and HNO_3. The pH choice was made considering the earlier published results from As(V) adsorption by ICG in batch mode, in which the optimum pH value was observed to be 3.0 (Pintor, Vieira et al. 2018). A volume of 45 mL of As(V) solution was put in contact with the adsorbents at a solid/liquid ratio of 2.5 g L^{-1}, over 48h (Pintor, Vieira et al. 2018) in a rotating shaker (20 rpm). Then, the samples were filtered through cellulose acetate membrane filters (0.45 µm porosity), followed by As quantification. The experiments were done in duplicate (n=2).

The adsorbed amount of As(V) per mass of iron-coated cork granulates (q_{ad}) was calculated according to Eq. (3.1).

$$q_{ad} = \frac{V\,(C_i - C_f)}{m} \quad (3.1)$$

where V is the solution volume (L), C_i and C_f are the initial and final concentrations of the adsorbate (mg L^{-1}), respectively, and m is the mass of adsorbent (g).

The Langmuir (Langmuir 1918) and Freundlich (Freundlich 1907) models in their linearized form (Eq. (3.2) and Eq. (3.3), respectively) were fitted to the experimental data to generate the equilibrium isotherms. The models relate the adsorption capacity of As(V) at equilibrium q_e (mg g^{-1}) with the equilibrium concentration C_e (mg L^{-1}).

$$\frac{C_e}{q_e} = \frac{1}{K_L\, q_{max}} + \frac{C_e}{q_{max}} \quad (3.2)$$

$$log q_e = log K_F + \frac{1}{n} log C_e \quad (3.3)$$

where K_L is the Langmuir constant (L mg^{-1}), K_F is the Freundlich constant ($mg^{(1-1/n)}$ $L^{1/n}$ g^{-1}), q_{max} is the maximum adsorption capacity (mg g^{-1}), and n is a dimensionless parameter related to adsorbent-adsorbate affinity.

The iron content in the final solution was measured to assess the metal leaching from the adsorbent at different temperatures.

3.2.3.2 Thermodynamic studies

The standard Gibbs free energy change (ΔG^0), entropy change (ΔS^0), and enthalpy change (ΔH^0), were estimated to evaluate the adsorption process, using the following equations:

$$\Delta G^0 = -RTLnK_o \quad (3.4)$$

$$\Delta G^0 = \Delta H^0 - T_K \Delta S^0 \quad (3.5)$$

The combination of Eq. (3.4) and Eq. (3.5) leads to:

$$Ln\, K_o = \frac{\Delta S^0}{R} - \frac{\Delta H^0}{RT_K} \quad (3.6)$$

where T_K is the temperature in Kelvin (K), K_0 is the standard equilibrium constant, and R is the gas constant of 8.314 × 10^{-3} kJ mol^{-1} K^{-1}.

3.2.4 Fixed-bed column experiments

Arsenic continuous adsorption assays were taken in a fixed-bed column operating in downward flow due to the low density of the adsorbent. The lab-scale continuous adsorption system consisted of an influent reservoir of 50 L; a glass column (Chromaflex®) with 2.5 cm internal diameter and 15 cm of maximum height; an outlet reservoir of 30 L; a thermostatic bath for temperature control (DIGIT-COOL, J.P. SELECTA), a peristaltic pump for flow rate regulation (VWR); and an automatic sampler (GILSON, FC-203B). Figure 3.1 presents a diagram of the lab-scale experimental structure.

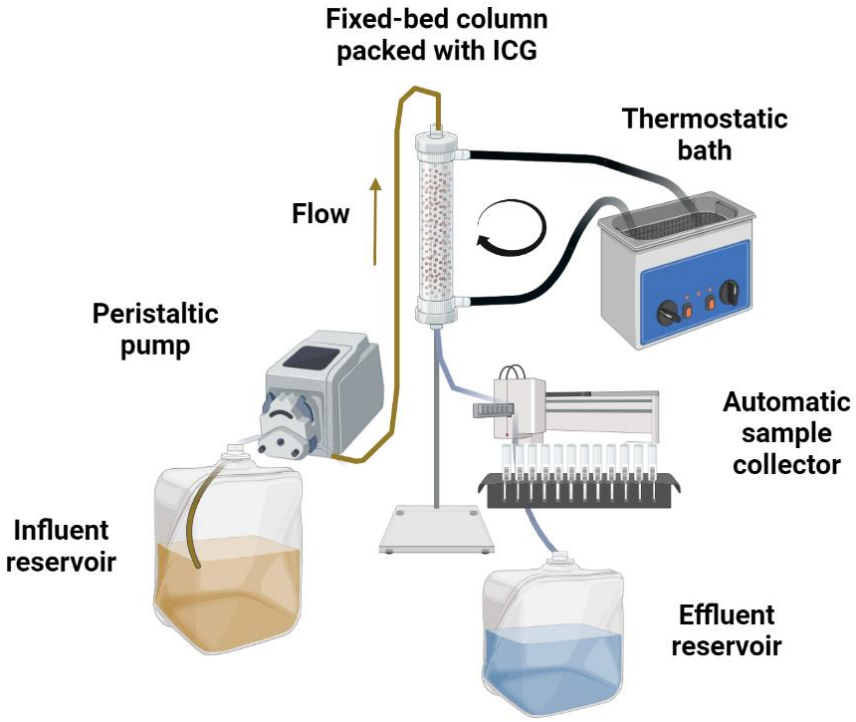


Figure 3.1: Schematic diagram of the lab-scale adsorption system of fixed-bed column.

Before each experiment, the adsorbent was hydrated in distilled water and put into vacuum to remove the air trapped into the pores. The column was packed with the adsorbent and fed by distilled water for 2 h, at similar flow rate of the following experiment.

3.2.4.1 Optimisation of fixed-bed column

A 2-level 3-factor (2^3) design of experiments (DoE) was conducted to investigate the effect of each operational parameter, described in item 2.6. Three factors were selected, each with two

levels: flow rate of 5 mL min $^{-1}$ (-1) and 10 mL min $^{-1}$ (+1); bed height of 6 cm (-1) and 12 cm (+1); and temperature of 10°C (-1) and 30°C (+1). The amount of adsorbent corresponding to bed heights of 6 and 12 cm was 3 and 6 g, respectively.

The flow rate and bed height levels were based on other studies of adsorption column for arsenic removal (Chen and Chung 2006, Sarkar, Pal et al. 2010, Saha and Sarkar 2016, Dhoble, Maddigapu et al. 2017, Brion-Roby, Gagnon et al. 2018, Nguyen, Yacouba et al. 2020). Moreover, the quantity of 3 to 6 g was considered a feasible amount of adsorbent to be produced in lab-scale. The temperature levels were defined regarding the range of groundwater temperature in arsenic affected countries.

In total, eight runs were performed in the fixed-bed column, according to Table 3.1. Each run was repeated once (n=1).

The bed volume (BV) for the column packed up to 6 and 12 cm was 29 and 59 mL, respectively. The iron leached from the adsorbent to the aqueous stream was monitored throughout the experiment, every two hours. The results of the DoE were analyzed using the software *Minitab 19*, including the ANOVA for each characterization parameter.

Table 3.1: Levels of each factor for each fixed-bed column run of the 2^3 factorial design.

Run #	**Flow rate – Q (mL min^{-1})**	**Bed height – Z (cm)**	**Temperature – *T* (°C)**
1	5	6	30
2	10	6	10
3	5	12	10
4	10	12	30
5	10	6	30
6	5	12	30
7	5	6	10
8	10	12	10

3.2.4.2 Analysis of breakthrough curves (BTC)

The fixed-bed column performance was evaluated by breakthrough curves (BTC), which consisted in the plot of the ratio of effluent concentration C (mg L^{-1}) to influent concentration C_o (mg L^{-1}) versus flow time t (min). Breakthrough time (t_b) was fixed as the moment when the effluent concentration reached 10 µg L^{-1}. Saturation time (t_s) was fixed as the moment when the effluent concentration achieved approximately 90% of the initial concentration. Other experimental breakthrough parameters calculated in this work were: adsorption capacity at breakthrough (Iqbal, Saeed et al.); adsorption capacity at the saturation point (q_s); bed volume treated at breakthrough (BV_b); bed volume treated at the saturation point (BV_s); breakthrough volume (V_b) and the saturation volume (Hristovski, Baumgardner et al. 2007) Ungureanu, Santos et al. 2017); arsenic removal at breakthrough (y_b), and arsenic removal at saturation (y_s); the mass transfer zone of the column (Hernández-Flores, Pariona et al. 2018); and, finally, the MTZ/Bed height ratio.

To determine the adsorption capacity, the amount of arsenic loaded in the column $m_{in,t}$ at time t and the amount of unadsorbed arsenic $m_{out,t}$ at time t were calculated (Chatterjee and Schiewer 2011). The amount of mass (g) loaded can be expressed in terms of initial concentration C_o (mg L^{-1}), flow rate Q (L min^{-1}) and time t (min). Then, the amount of arsenic adsorbed in the column $m_{ad,t}$ at time t was calculated as the difference between $m_{in,t}$ and $m_{out,t}$:

$$m_{ad,t} = m_{in,t} - m_{out,t} = C_o Qt - C_o Qt \int_o^{t_b} \left(\frac{C}{Co}\right) dt \quad (3.7)$$

In this way, the adsorption capacity at breakthrough (Iqbal, Saeed et al.) was determined as the total mass of arsenic adsorbed at breakthrough $m_{ad,t}$ divided by the mass of adsorbent in the reactor, M (g):

$$q_b = \frac{m_{ad,t_b}}{M} = \frac{C_o Q \int_o^{t_b} \left(1 - \frac{C}{Co}\right) dt}{M} \quad (3.8)$$

Similarly, the adsorption capacity at saturation (q_S) was determined as:

$$q_s = \frac{m_{ads,t_S}}{M} = \frac{C_o Q \int_o^{t_S} \left(1 - \frac{C}{Co}\right) dt}{M} \quad (3.9)$$

The arsenic removal (y) is the percentage of arsenic mass retained in the adsorbent at a certain time. It was calculated for t_b and t_S as follows:

$$y_b = 1 - \frac{m_{out,t_b}}{m_{in,t_b}} \times 100 \quad (3.10)$$

$$y_s = 1 - \frac{m_{out,t_s}}{m_{in,t_s}} \times 100 \quad (3.11)$$

The mass transfer zone length of the column (Hernández-Flores, Pariona et al.) (cm) was determined by Eq. (3.12), where H is the packed bed height (Ungureanu, Santos et al. 2017). It is an important parameter to consider for the scale-up of the column, related to the efficiency of the adsorption process (Verduzco-Navarro, Rios-Donato et al. 2020).

$$MTZ = H \times \frac{t_s - t_b}{t_s} \quad (3.12)$$

3.2.4.3 Fixed-bed theoretical models

Three models were applied, using nonlinear regression, to describe the experimental breakthrough curves. The fittings were carried out using *Minitab* 19 and *Curve Expert Pro 2.7* software.

a) Thomas model (TH)

Thomas model (Thomas 1944) is a common model for adsorption-desorption without axial dispersion in a fixed-bed column that assumes Langmuir kinetics, expressed by the equation:

$$\frac{C}{C_o} = \frac{1}{1+\exp\left(k_{TH}(q_{TH}m/Q - C_o t)\right)} \quad (3.13)$$

where k_{TH} is the Thomas model constant rate (L min^{-1} mg^{-1}), q_{TH} is the theoretical saturation adsorption capacity (mg g^{-1}), m is the mass of adsorbent in the column (g), Q is the flow rate (L min^{-1}), C_o is the initial adsorbate concentration (mg L^{-1}), t is flow time (min), and C is the concentration of adsorbate at time t (mg L^{-1}).

b) Yoon-Nelson (YN)

The Yoon-Nelson model (Yoon and Nelson 1984) equation is:

$$\frac{C}{C_o} = \frac{\exp\left(k_{YN}*t - \tau_{YN}*k_{YN}\right)}{1+\exp\left(k_{YN}*t - \tau_{YN}*k_{YN}\right)} \quad (3.14)$$

where k_{YN} is the Yoon-Nelson constant rate (min^{-1}), τ_{YN} is the predicted time required for 50% of adsorbate breakthrough ($\frac{C}{C_o} = 0.5$) (min), C_o is the initial adsorbate concentration (mg L^{-1}), t is flow time (min), and C is the concentration of adsorbate at time t (mg L^{-1}).

c) Yan model (YA)

$$\frac{C}{C_o} = 1 - \frac{1}{1+\left(\frac{C_o Q}{q_{Ya} * m} * t\right)^{a_{Ya}}} \quad (3.15)$$

where a_{Ya} is an empirical parameter, q_{Ya} is the theoretical saturation adsorption capacity (mg g^{-1}), m is the mass of adsorbent in the column (g), Q is the flow rate (L min^{-1}), C_o is the initial adsorbate concentration (mg L^{-1}), t is flow time (min), and C is the concentration of adsorbate at time t (mg L^{-1}).

3.2.4.4 Effect of temperature

The influence of temperature on breakthrough curves of As(V) adsorption was analyzed for the range of 10-30ºC. The column operating parameters were: bed height = 12 cm, flow flowrate = 5 mL min^{-1}, initial concentration = 1 mg L^{-1}, and pH = 3.0. These correspond to the optimized configuration found from the results of previous experiments (item 3.2.4.1). Each run was repeated once (n=1).

3.2.4.5 Effect of pH

The pH effect on breakthrough curves was evaluated adjusting pH to values of 3.0, 7.0 and 9.0 for As(V) and 7.0 and 9.0 for As(III). The studies were conducted at a flowrate of 5 mL min^{-1}, a bed height of 12 cm, and an initial concentration of 1 mg L^{-1}, at 20.0 ± 0.3ºC. These are the optimal values previously found for those parameters (item 3.2.4.1). Each run was repeated once (n=1).

3.2.4.6 Effect of initial concentration

The effect of the initial influent concentration in continuous arsenic adsorption was investigated using arsenic solutions of 0.1 and 1.0 mg L^{-1} for each oxidation state. The studies were conducted at a flow rate of 5 mL min^{-1}, 12 cm bed height, pH 7, and a temperature of 20.0 ± 0.3 ºC. Those parameters were obtained from previous optimization experiments (item 3.2.4.1). Each run was repeated once (n=1).

3.3 Results and discussion

3.3.1 Evaluation of temperature effect on batch mode operation and thermodynamic studies

3.3.1.1 Arsenate adsorption

Equilibrium isotherms of arsenate adsorption onto iron-coated cork granulates were obtained at different temperatures. The Langmuir and Freundlich linearized curves for each temperature are displayed in Figure 3.2. The experimental data and the corresponding Langmuir curves can be found in Table 3.2 and Figure 3.3, respectively.

The Langmuir isotherm fits better the equilibrium data (Table 3.5), with correlation coefficients above 0.98. Even though showing a worse fit, Freundlich still presented a good correlation ($r^2 >$ 0.92). Earlier isotherm equilibrium studies of As(V) conducted with ICG at 20ºC at similar conditions (Pintor, Vieira et al. 2018) led to similar results, though Q_{max} was lower: 6.2 ± 0.2 mg g^{-1} in this study and 3.8 ± 0.2 mg g^{-1} in the cited study. This difference can be explained by the variation in the iron content of ICG, the heterogeneity of the material, and particle size, which was previously 0.8-1.0 mm and now 0.5-1.0 mm.

Temperature affects the As(V) adsorption capacity of ICG, indicated by the Langmuir maximum adsorption capacity (Q*max*) and Freundlich constant (K_F). When plotting both parameters versus temperature, a good direct proportionality correlation ($r^2 > 0.97$) was observed between Qmax or K_F and temperature, as shown in Figure 3.4.

Analogous temperature effect on arsenic adsorption was noticed for other iron-modified biosorbents, such as iron oxide impregnated carbon from Tamarind hull (IOITHC) (Maiti, Agarwal et al. 2010), iron modified root powder (Lin, Yang et al. 2018), iron-loaded activated carbon using waste biomass (Liu, Zhang et al. 2010); and other adsorbents such as magnetite nanoparticles (Shipley, Yean et al. 2009). A possible cause for the effect is the increase in the kinetic activity in the solution, causing an increase in the rate of arsenate contact with the adsorbent. Different results, though, were observed for arsenic removal by iron-impregnated granular activated carbon (GAC-Fe), in which a variation of temperature from 30 to 60ºC did not affect the results (Mondal, Balomajumder et al. 2007). The same study considered that arsenic forms more stable bonds with the iron oxides active sites from GAC-Fe, in comparison to GAC, whose removal percentage decreased with the temperature increase. The process proved to be exothermic.

In the equilibrium experiments of As(V), the iron concentration in the equilibrium solution was measured to monitor the iron leached from ICG. The total dissolved iron in equilibrium at 10, 20 and 30°C varied from 0.5±0.2 to 0.9±0.2 mg L^{-1}, 0.8±0.2 to 1.7±0.2 mg L^{-1}, and 1.3± 0.2 to 2.6±0.2 mg L^{-1}, respectively. The iron leached into the solution at equilibrium exceeded the guideline concentration in drinking water of 0.3 mg L-1 (ppm) (World Health 2011) and increased with temperature, which can be a possible disadvantage for the application of ICG on effluents with high temperatures. However, the equilibrium studies were conducted at pH 3, and the acid solution is more favorable for iron leaching than natural waters, whose pH is closer to neutrality.

Table 3.2: Equilibrium model parameters (± standard error of mean).

		T = 10°C	**T = 20°C**	**T = 30°C**
Langmuir	$Qmax$ (mg g^{-1})	5.8 ± 0.2	6.2 ± 0.2	6.9 ± 0.1
	K_L (L mg^{-1})	2 ± 1	6 ± 9	5 ± 2
	r^2	0.997	0.996	0.999
Freundlich	K_F ($mg^{(1-1/n)}$ $L^{1/n}$ g^{-1})	2.5 ± 0.2	4.0 ± 0.1	4.8 ± 0.1
	n	2.9 ± 0.4	5.5 ± 0.9	7.4 ± 0.5
	r^2	0.939	0.929	0.984

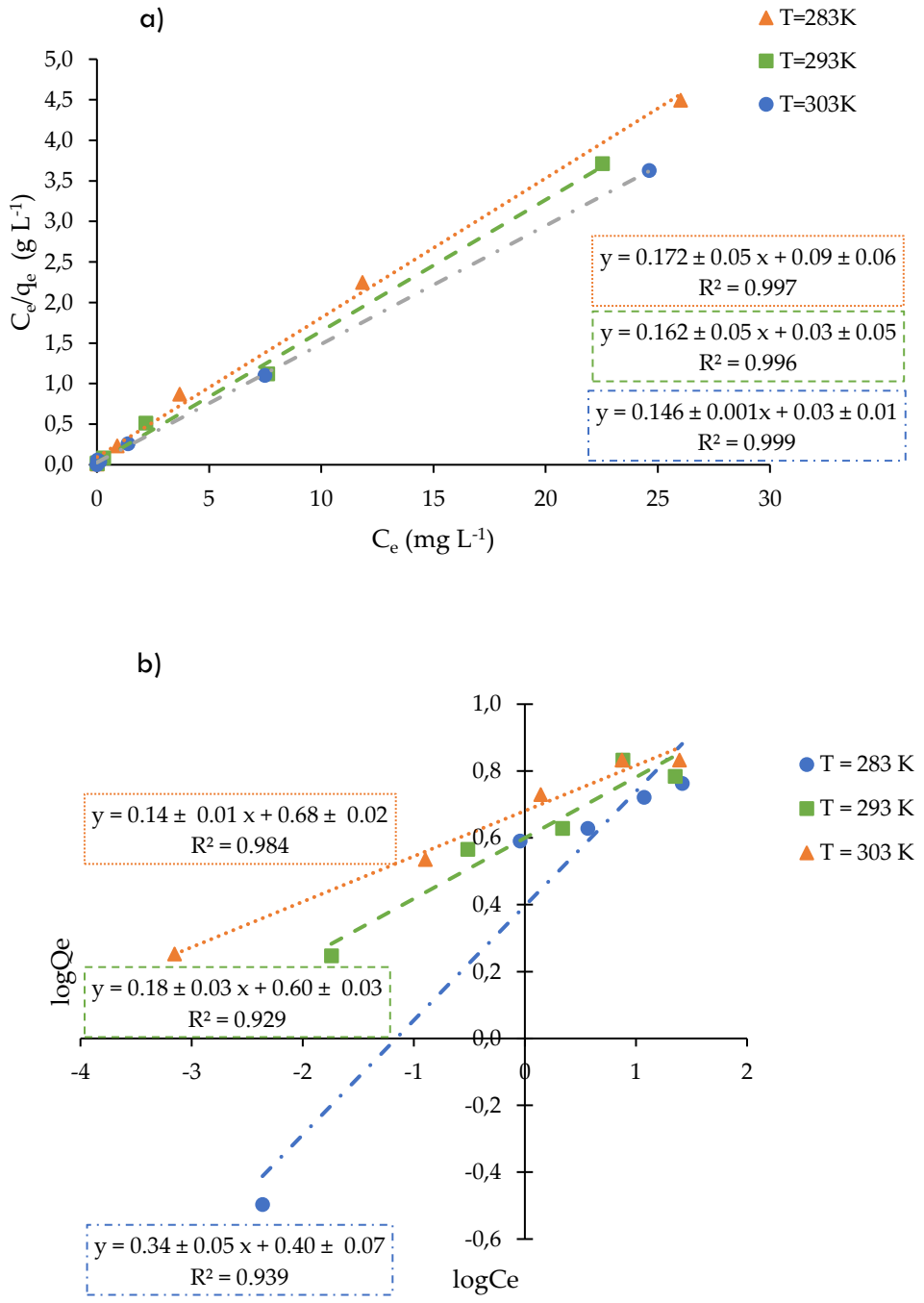


Figure 3.2: Linearized form of a) Langmuir and b) Freundlich (bottom) isotherms, for temperatures of 10, 20 and 30 ºC.

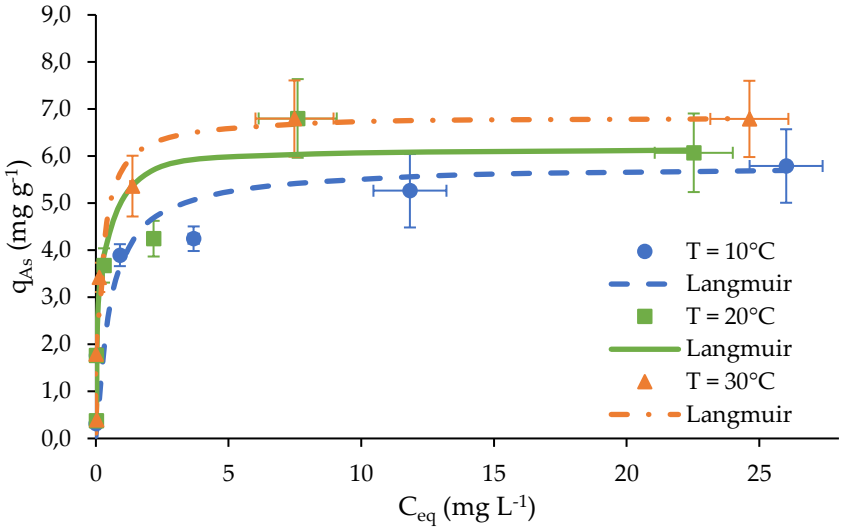


Figure 3.3: Langmuir adsorption isotherms of As(V) on ICG (pH 3.0; S/L ratio = 2.5 g L^{-1}; contact time = 48 h) for temperatures of 10, 20 and 30 °C (Error bars: maximum absolute deviation).

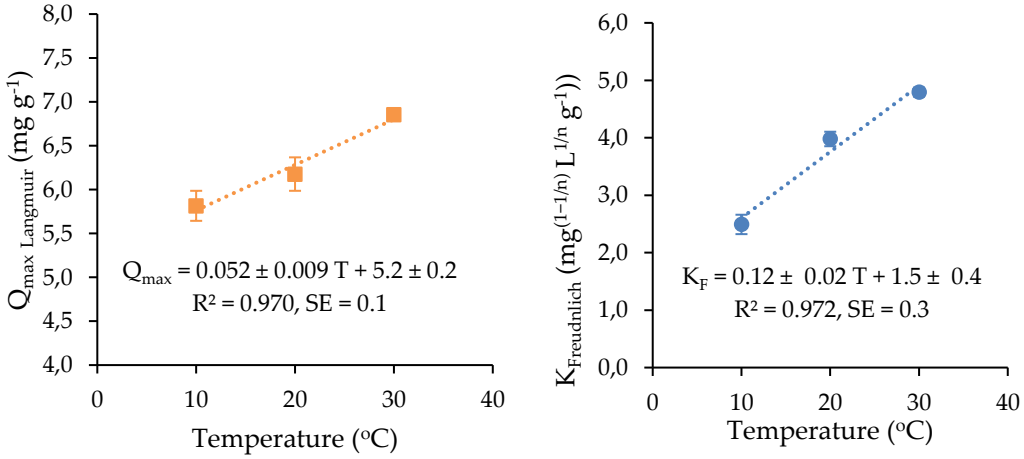


Figure 3.4: Correlation curves between Langmuir maximum adsorption capacity, Qmax (mg g^{-1}) (left) or Freundlich constant, K_F (mg$^{(1-1/n)}$ L$^{1/n}$ g^{-1}) (right) and temperature (°C) (Error bars: standard error of the mean).

3.3.1.2 Thermodynamic studies

The results from the last section (item 3.3.1.1) indicate endothermic adsorption of As(V) onto ICG since adsorption capacity increased with temperature. To better understand that behavior, thermodynamic studies were conducted.

The values of K_o were obtained from the Langmuir model parameter K_L (L mg^{-1}) (Table 3.2). K_o was transformed into a dimensionless constant by multiplying K_L by 10^6 (Milonjić 2007, Nnaji, Agim et al. 2021). The values of ΔH^0 and entropy change ΔS^0 were calculated from the slope and intercept values of the plot $Ln\ K_o$ versus $1/\ T_K$ (Figure 3.5). Table 3.3 presents the thermodynamic parameters.

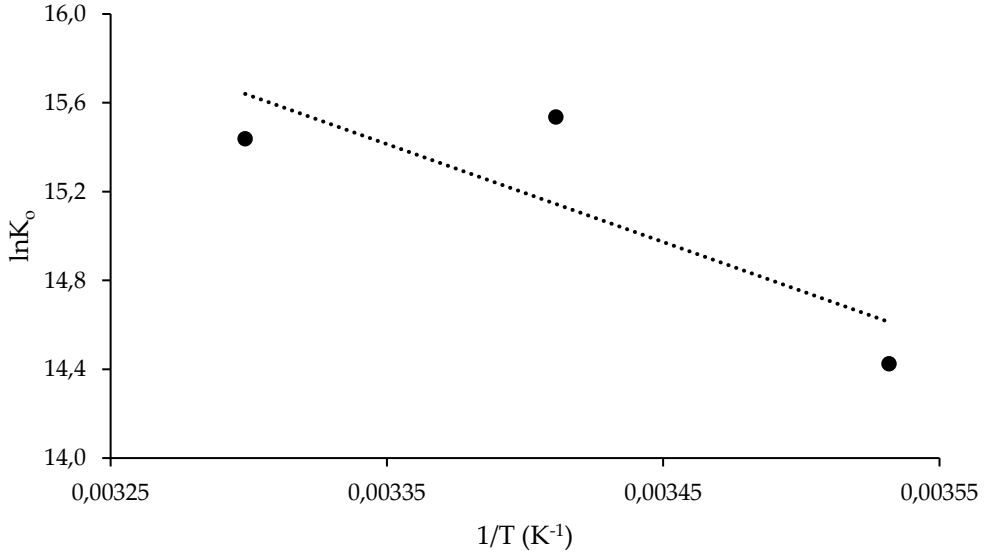


Figure 3.5: $Ln\ K_o$ versus $1/T_K$ graph for the determination of thermodynamic parameters for ICG adsorption (pH 3; S/L ratio = 2.5 g L^{-1}; contact time = 48 h) for temperatures of 10, 20 and 30 °C.

Table 3.3 shows negative values of ΔG^0, which means a spontaneous and feasible process at all three temperatures. In addition, the positive value of ΔH^0 and the decrease of ΔG^0 with increasing temperature confirm that the process is endothermic and becomes more favorable when temperature increases from 10 to 30°C. The positive value of ΔS^0 suggests that the degree of free active sites increased at the solid/liquid interface during arsenate adsorption onto ICG.

Table 3.3: Thermodynamic parameters at various temperatures for As(V) adsorption onto iron-coated cork granulates (S/L = 2.5 g L^{-1}, pH = 3, time = 48 h).

***T* (K)**	**$1/T_K$ (10^{-3})**	$Ln\ K_o$	**ΔG^0 (kJ mol^{-1})**	**ΔH^0 (kJ mol^{-1})**	**ΔS^0 (J mol^{-1} K^{-1})**
283	3.53	14.4	-34 ± 24		
293	3.41	15.5	-37 ± 24	37 ± 24	250 ± 80
303	3.30	15.4	-39 ± 24		

An endothermic process was also the adsorption of arsenate by dried plants (Chiban, Carja et al. 2016), coal mine drainage sludge adsorbent (Kim, Ren et al. 2021), and metal-impregnated biochar (Rahman, Lamb et al. 2021). Nevertheless, the adsorption of arsenic on clay minerals (Mohapatra, Mishra et al. 2007) and on GAC (Mondal, Balomajumder et al. 2007) was found to be an exothermic process, where the temperature increase provided a negative effect in As(V) uptake.

3.3.2 Fixed-bed column adsorption experiments

The capacity of ICG to remove arsenic in continuous mode was investigated at lab-scale fixed-bed column experiments. Several parameters such as bed height, flow rate, temperature, pH and adsorbate initial concentration can influence the adsorption performance and breakthrough curves. Thus, to manage the fixed-bed column in the best way, treatment efficiency was evaluated in different conditions. The results are discussed in the following sections.

3.3.2.1 Optimization of fixed-bed column

The optimization of the fixed-bed column operational parameters, such as bed height, flow rate, and temperature, was planned by a 2^3 full factorial design with eight experiments corresponding to the runs presented in Table 3.1. The time parameters are shown in this work either in hours or in minutes to simplify the comparison with other articles and to provide better visualization of the results.

Table 3.4. Experimental BTC parameters values observed in each column adsorption experiment from 2^3 factorial design.

Run #	t_b (h)	t_s (h)	q_b (mg g^{-1})	q_s (mg g^{-1})	BV_b	BV_s	V_b (L)	V_s (L)	y_b (%)	y_s (%)	*MTZ (cm)*	*MTZ/Bed height*
1	20.6±0.8	85	1.7±0.2	3.5±0.7	229±9	945±87	6.7±0.3	27.8±0.1	99.95 ±0.03	51±6	4.5±0.4	0.76±0.09
2	5.0±0.4	25	0.84±0.08	2.4±0.2	108±14	535±49	3.2±0.3	15.75±0.08	99.75±0.08	57±3	4.8±0.6	0.8±0.1
3	26.3±0.8	78	1.07±0.08	2.1±0.3	146±10	433±25	8.6±0.3	25.5±0.1	99.80±0.05	65±4	8.0±0.4	0.66±0.04
4	20.2±0.4	47	1.7±0.1	2.8±0.3	216±14	503±29	12.8±0.3	29.6±0.1	99.79±0.04	68±3	6.8±0.3	0.57±0.04
5	12.1±0.4	44	2.2±0.1	4.3±0.7	254±25	927±86	7.5±0.3	27.3±0.1	99.99±0.01	54±5	4.4±0.4	0.73±0.09
6	45.3±0.8	122	1.8±0.2	3.4±0.5	252±16	678±39	14.8±0.9	39.9±0.1	99.82±0.03	69±4	7.5±0.3	0.63±0.04
7	18±1	70	1.6±0.2	3.7±0.6	197±23	778±72	5.8±0.4	22.9±0.1	99.67±0.05	57±7	4.5±0.5	0.7±0.1
8	21.5±0.8	71	1.9±0.1	4.4±0.4	226±16	748±43	13.3±0.6	44.1±0.1	99.45±0.08	68±3	8.4±0.5	0.70±0.05

(± standard error of the mean)

In all runs, the initial As(V) concentration was set as 1 mg L^{-1} at a pH = 3, which was found to be the optimal pH value for arsenate batch adsorption onto ICG, according to previously published results (Pintor, Vieira et al. 2018). The effluent samples were collected from the column every one or two hours for arsenate concentration measurement.

Each fixed-bed column run performance was assessed in terms of the experimental breakthrough curve parameters. Table 3.4 presents the values of the BTC experimental parameters for each experiment selected for the 2^3 factorial design.

These eleven variables (except MTZ) were applied as a dependent variable for an ANOVA statistical study. Table 3.5 presents the ANOVA tables with significant ($p < 0.05$) results, and the others ($p > 0.05$) can be found in Table 3.6. The ANOVA results (Table 3.5) allow to conclude that (i) the flow rate factor (Q) significantly influences ($p < 0.05$) the breakthrough time (tb) and the saturation time (t_s), and (ii) the bed height (Z) factor significantly affects ($p < 0.05$) the breakthrough time (t_b), the treated volume at breakthrough (V_b), and the MTZ/Bed height ratio. The main effects plots for each of these parameters are shown in Figure 3.6.

Table 3.5: ANOVA tables with significant ($p < 0.05$) results for the 2^3 factorial design using BTC parameters as response variables: a) breakthrough time (t_b), b) saturation time (t_s); c) treated volume at breakthrough (V_b); and, d) MTZ/Bed height ratio.

a)

Factor	DF	Adj SS	Adj MS	F-Value	P-Value
Q	**1**	**325.7**	**325.7**	**10.4**	**0.03**
Z	**1**	**419.7**	**419.7**	**13.4**	**0.02**
T	1	96.2	96.2	3.1	0.15
Error	4	124.9	31.2		
Total	7	966.6			

b)

Factor	DF	Adj SS	Adj MS	F-Value	P-Value
Q	**1**	**3528.0**	**3528.0**	**11.9**	**0.03**

Z	1	1104.5	1104.5	3.7	0.13
T	1	364.5	364.5	1.2	0.33
Error	4	1186.5	296.6		
Total	7	6183.5			

c)

Factor	**DF**	**Adj SS**	**Adj MS**	**F-Value**	**P-Value**
Q	1	0.1	0.1	0.0	0.90
Z	**1**	**86.6**	**86.6**	**20.3**	**0.01**
T	1	14.9	14.9	3.5	0.14
Error	4	17.0	4.3		
Total	7	118.6			

d)

Factor	**DF**	**Adj SS**	**Adj MS**	**F-Value**	**P-Value**
Q	1	0.000	0.000	0.0	0.96
Z	**1**	**0.03**	**0.03**	**20.5**	**0.01**
T	1	0.006	0.006	4.7	0.10
Error	4	0.005	0.001		
Total	7	0.04			

According to Figure 3.6, it is possible to conclude that, as it would be expected, the flow rate (Q) and the breakthrough time (t_b) are inversely proportional in the studied range, as well as the flow rate and the saturation time (t_s). Therefore, increased values of t_b and t_s are expected in a fixed-bed column run with low values of flow rate. Other studies identified the same effect of flow rate on t_b (Ranjan, Talat et al. 2009, Sawood and Gupta 2020) and t_s (Ranjan, Talat et al. 2009, Singh, Singh et al. 2014) in fixed-bed columns for arsenic removal. The effect of flow

rate in adsorption is related to the residence time, as lower values of flow rate increase the time available for the adsorbate to access the adsorption sites in the adsorbent surface.

As presented in Figure 3.6, bed height (Z) and breakthrough time (t_b) are directly proportional in the studied range, as well as bed height and treated volume at breakthrough (V_b). Therefore, increased values of t_b and V_b are expected in a fixed-bed column with a high bed height. The bed height influences the exhaustion time because it provides more binding sites for the adsorbate to contact with the adsorbent (Ranjan, Talat et al. 2009). The fixed-bed column efficiency is also expressed in terms of MTZ, which should be minimized for best adsorption performance (Mantovaneli, Ferretti et al. 2004), for instance, through flow rate decrease and bed height increase (Díaz-Blancas, Aguilar-Madera et al. 2020). The unutilized bed height can be expressed in terms of MTZ/bed height ratio when comparing different bed height values. The assays with the longest bed height of 12 cm achieved the lowest values of the ratio, $0.57 \leq$ MTZ/Bed height ≤ 0.70. For a bed height of 6 cm we found $0.73 \leq$ MTZ/Bed height ≤ 0.80. This is in accordance with DOE results (Figure 3.6), which show that bed height statistically influences ($p < 0.05$) MTZ/Bed height in an inversely proportional way.

So, from the DOE results of the lab-scale fixed-bed column setup, the optimized flow rate and bed height factors are 5 mL min^{-1} and 12 cm (6 g mass), respectively. As expected, they correspond to the highest empty bed contact time (EBCT) value of 11.8 min. Research on the adsorption kinetics of As(V) at 1 mg L^{-1} onto ICG showed a high adsorption rate in the first 15 minutes (Pintor, Vieira et al. 2020), which confirms that an EBCT of approximately 15 min is required to promote a high rate of arsenic adsorption in continuous mode.

Moreover, DOE results presents that there is not a significant influence ($p < 0.05$) on the column performance as regards the following parameters: adsorption capacity at breakthrough (Iqbal, Saeed et al.), adsorption capacity at the saturation point (q_s), bed volume treated at breakthrough (BV_b), bed volume treated at the saturation point (BV_s), saturation volume (Hristovski, Baumgardner et al.), arsenic removal at breakthrough (y_b), and arsenic removal at saturation (y_s). This means that although the previously defined parameters are preferable, the column can also be operated at less-optimal parameters with effectiveness.

Table 3.6: ANOVA tables design without significant ($p < 0.05$) results, using BTC parameters from the 2^3 factorial design as response variables: a) adsorption capacity at breakthrough (q_b), b) adsorption capacity at saturation (q_s), c) bed volumes at breakthrough (BV_b), d) bed volumes at saturation (BV_s), e) treated volume at saturation (Vs), f) arsenic removal at breakthrough (y_b), and g) arsenic removal at saturation (y_s).

a)

Factor	DF	Adj SS	Adj MS	F-Value	P-Value
Q	**1**	0.03	0.03	0.14	0.73
Z	**1**	0.008	0.008	0.04	0.86
T	1	0.4	0.4	1.99	0.23
Error	4	0.9	0.2		
Total	*7*	1.4			

b)

Factor	DF	Adj SS	Adj MS	F-Value	P-Value
Q	**1**	0.2	0.2	0.2	0.70
Z	**1**	0.2	0.2	0.2	0.70
T	1	0.2	0.2	0.2	0.66
Error	4	4.3	1.1		
Total	*7*	4.9			

c)

Factor	DF	Adj SS	Adj MS	F-Value	P-Value
Q	1	50.0	50.0	0.0	0.89
Z	1	338.0	338.0	0.2	0.72
T	1	9384.5	9384.5	4.2	0.11
Error	4	8911.5	2228.9		
Total	*7*	18,684			

d)

Factor	DF	Adj SS	Adj MS	F-Value	P-Value
Q	1	1839	32960	0.1	0.83

Z	1	84666	84666	2.6	0.18
T	1	39060	39060	1.2	0.34
Error	4	131842	32960		
Total	7	257398			

e)

Factor	DF	Adj SS	Adj MS	F-Value	P-Value
Q	1	0.1	0.1	0.0	0.98
Z	1	256.5	256.5	3.6	0.13
T	1	33.2	33.2	0.5	0.53
Error	4	285.3	71.3		
Total	7	575.1			

f)

Factor	DF	Adj SS	Adj MS	F-Value	P-Value
Q	1	0.006	0.006	0.4	0.55
Z	1	0.1	0.07	5.0	0.09
T	1	0.04	0.04	2.5	0.19
Error	4	0.1	0.0		
Total	7	0.2			

g)

Factor	DF	Adj SS	Adj MS	F-Value	P-Value
Q	1	3.5	3.5	0.1	0.78
Z	1	89.1	89.1	2.3	0.21
T	1	108.8	108.8	2.8	0.17
Error	4	158.4	39.6		
Total	7	359.9			

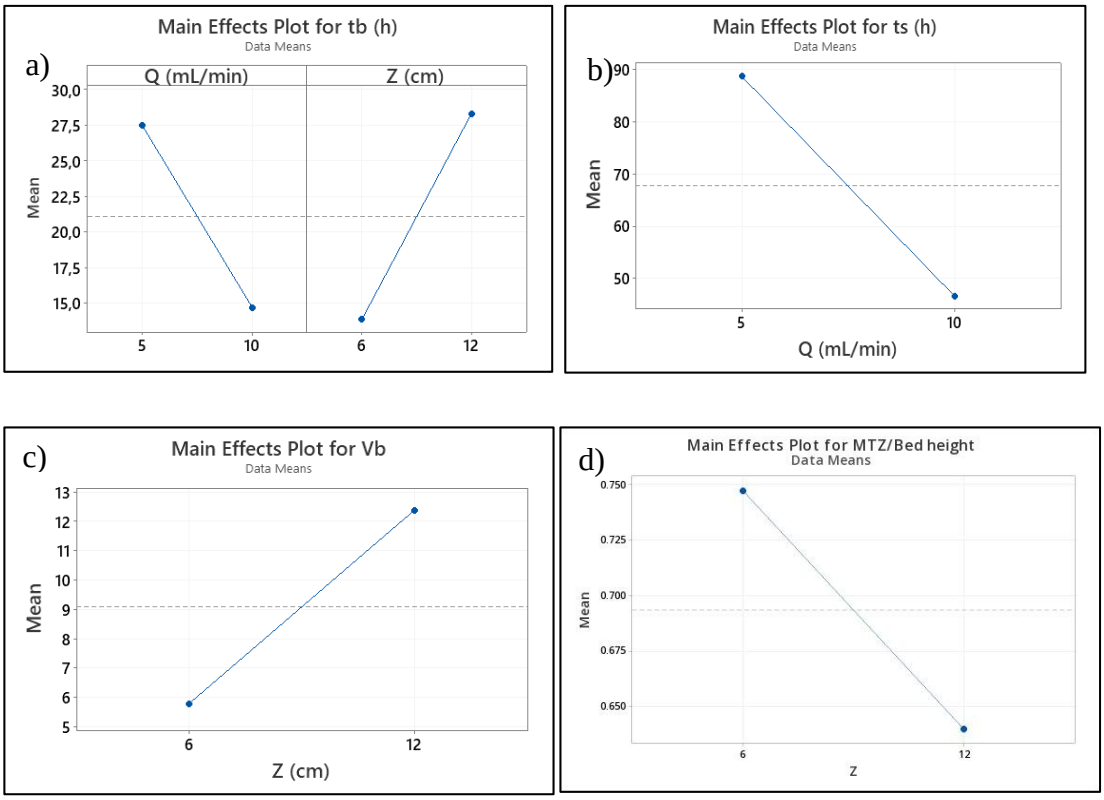


Figure 3.6: Main effect plots for: a) breakthrough time (tb), b) saturation time (ts), c) treated volume at breakthrough (Vb), and d) MTZ/Bed height ratio.

Regardless of the temperature effect observed in batch mode adsorption onto ICG (Figure 3.6)Figure 3.6, this factor did not present a statistically significant influence ($p < 0.05$) on any experimental BTC parameters reported in Table 3.6. Nevertheless, temperature affected the iron amount leached from the adsorbent, as shown in Figure 3.7 (10 and 20ºC) and Figure 3.8 (30ºC). In column assays conducted at pH 3, flow rate of 5 mL min^{-1}, and As(V) initial concentration of 1 mg L^{-1}, the average total iron concentration in the effluent was 0.3±0.1 and 0.5±0.1 mg L^{-1} for experiments at 10 and 20ºC, respectively. Throughout those assays, a smooth decay behavior is observed in the iron concentration, reaching a minimum value at saturation time.

For experiments conducted at 30ºC, an increase in iron leaching was observed approximately until breakthrough time, when it reaches maximum value, followed by a decay until saturation time (Figure 3.8). For the assays with a breakthrough time of 12 h and 45 h, the maximum total iron concentration in the effluent was achieved after 14 h and 42 h operation, respectively. From breakthrough to saturation, there may be a blockage of the iron dissolution due to occupation of the adsorption sites by the arsenic oxyanions or even by small iron-arsenic microprecipitates. These could justify the decrease and, ultimately, absence of Fe in the effluent by saturation time. The adsorption mechanism is better observed in the experiments conducted at 30ºC, which is the

most favorable adsorption temperature in the range of 10 – 30ºC according to the endothermic behavior of ICG arsenic adsorption (item 3.3.1.2).

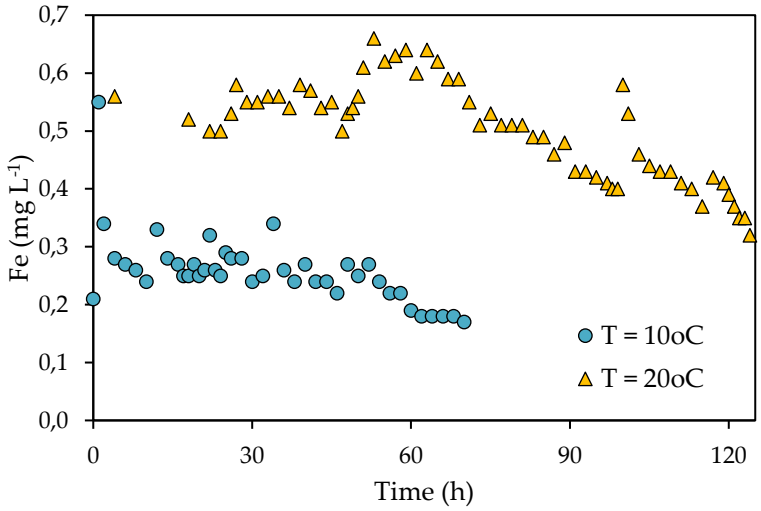


Figure 3.7: Temperature effect in iron leached from ICG in the effluent in fixed-bed column (pH 3; flow rate of 5 mL min^{-1}; Ci (As(V)) = 1 mg L^{-1}).

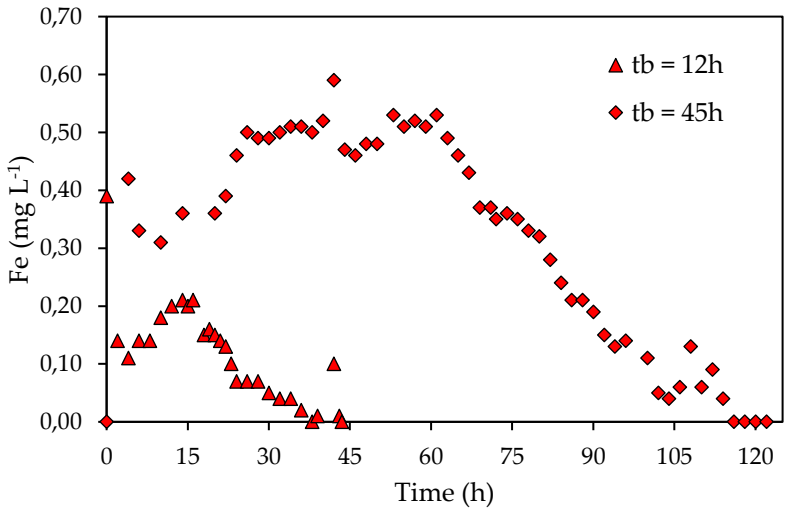


Figure 3.8: Iron leaching behavior through column experiments conducted at 30 ºC (pH: 3; Co As(V): 1 mg L^{-1}).

3.3.2.2 Analysis of breakthrough curves (BTC)

The Thomas (3.13), Yoon-Nelson (3.14), and Yan (3.14) models were fitted to experimental data from 2^3 factorial design fixed-bed column assays (item 3.3.2.1) by nonlinear regression. The results are displayed in

Table 3.7, and BTC's are presented in Figure 3.9. Due to the fact that the Thomas and Yoon-Nelson models are mathematically equivalent (Chu 2020), their correlation parameters and standard

error are equal, as well as the theoretical breakthrough curves. The Yan model better represents the experimental data, considering the higher values of correlation coefficient ($r^2 \geq 0.97$) and lower values of standard error ($SE \leq 0.07$). According to

Table 3.7, theoretical adsorption capacity values from Yan (Q_{YA}) model were slightly smaller than the experimental ones (q_{exp}). Maximum adsorption capacities predicted by the Thomas model were closer to q_{exp}. The divergence in predicted and experimental adsorption parameters can be related to deviations of the model fittings from experimental data at the beginning and at the end of the experimental curve, where saturation is hardly achieved (Jaria, Calisto et al. 2019).

Table 3.7: Parameters of Thomas, Yoon-Nelson and Yan models.

Run	**1**	**2**	**3**	**4**	**5**	**6**	**7**	**8**
				Thomas model				
K_{TH} (10^{-3})	2.0±0.2	6.7±0.7	2.5±0.2	4.4±0.4	5.5±0.7	1.8±0.2	2.5±0.2	2.1± 0.2
q_{TH} (mg g^{-1})	3.3±0.5	2.3±0.5	2.0±0.2	2.7±0.3	3.9±0.6	3.3±0.4	3.6±0.4	4.3± 0.4
q_{exp} (mg g^{-1})	3.5±0.7	2.4±0.2	2.1±0.3	2.8±0.3	4.3±0.7	3.4±0.5	3.7±0.6	4.4±0.4
R^2	0.942	0.961	0.988	0.979	0.968	0.970	0.976	0.971
SE	0.09	0.07	0.04	0.05	0.07	0.06	0.06	0.06
				Yoon-Nelson model				
K_{YN} (10^{-3})	1.5±0.1	5.3±0.5	1.8±0.1	3.6±0.2	4.7±0.4	1.33±0.07	2.1±0.1	1.9± 0.1
t_{YN} 50% (min)	2458±302	815±109	3013±182	1882±177	1320±174	4917±350	2317±192	2852±231
t_{exp} 50% (min)	2255±58	797±11	3001±89	1798±18	1287±17	4730±81	2133±32	2694±60
R^2	0.942	0.961	0.988	0.979	0.968	0.970	0.976	0.971

Run	1	2	3	4	5	6	7	8
SE (m g^{-1})	0.09	0.07	0.04	0.05	0.07	0.06	0.06	0.06
				Yan model				
a_{ya}	3.4±0.2	4.3±0.3	5.4±0.2	6.5±0.3	5.5±0.4	6.2±0.2	4.6±0.2	5.1±0.3
Q_{ya} (mg g^{-1})	3.1±0.3	2.2±0.1	2.0±0.2	2.7±0.2	3.9±0.3	3.2±0.3	3.5±0.3	4.2±0.3
q_{exp} (mg g^{-1})	3.5±0.7	2.4±0.2	2.1±0.3	2.8±0.3	4.3±0.7	3.4±0.5	3.7±0.6	4.4±0.4
SE (mg g^{-1})	0.07	0.05	0.02	0.04	0.05	0.05	0.04	0.05
R^2	0.967	0.980	0.994	0.990	0.980	0.983	0.991	0.981

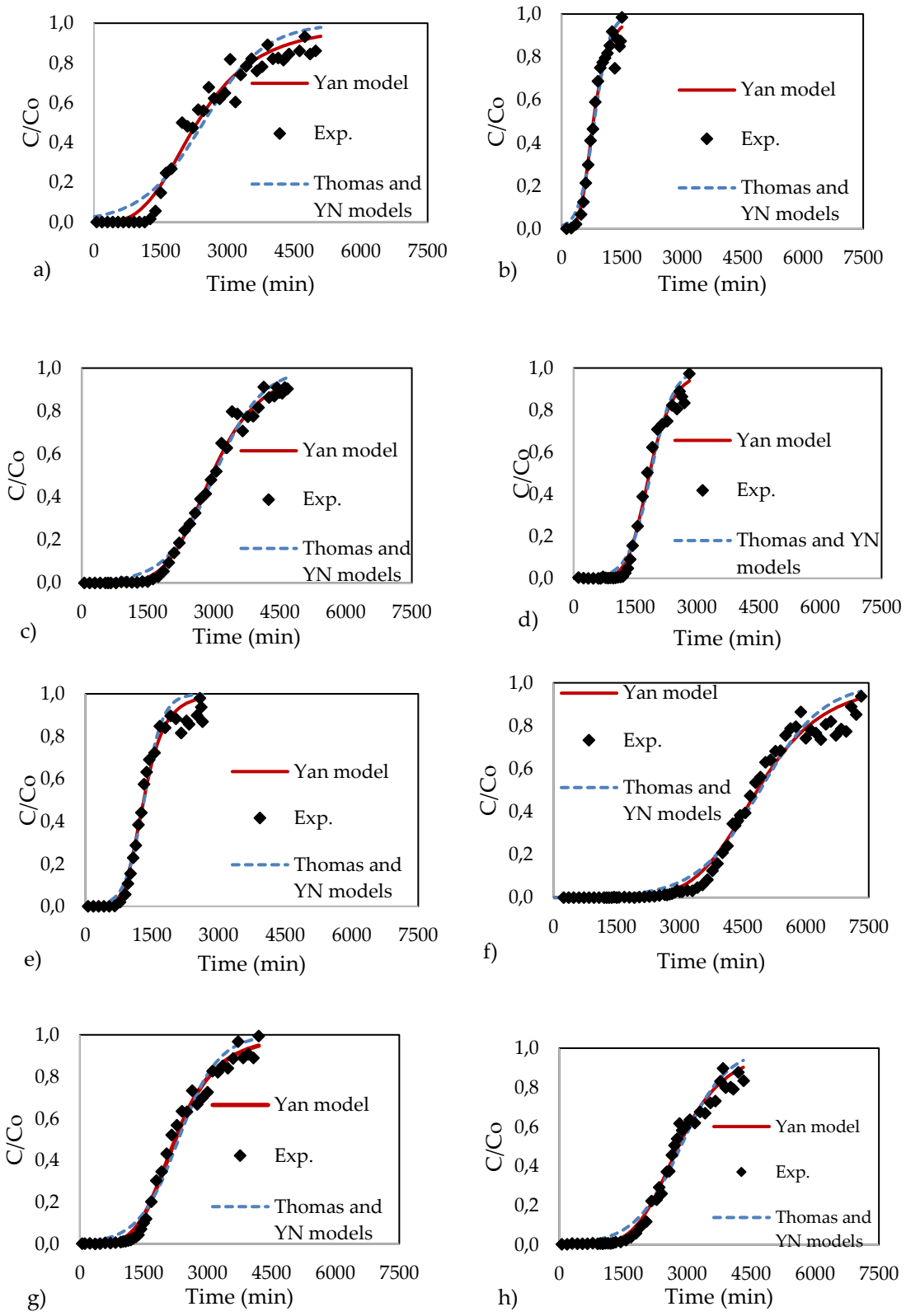


Figure 3.9: Experimental and predicted breakthrough curves obtained for each 2^3 factorial design run, pH = 3 and C_0 = 1 mg L^{-1}: a) run 1, b) run 2, c) run 3, d) run 4, e) run 5, f) run 6, g) run 7, and h) run 8.

3.3.2.3 Effect of temperature

Batch studies revealed that the As(V) adsorption was influenced by temperature in the range 10-30ºC (section 3.3.1). Nevertheless, DOE results (section 3.3.2.1) showed no evidence of a significant temperature effect ($p > 0.05$) in the column performance, for the same temperature range. To obtain an optimal temperature value, an intermediate value of temperature (20ºC) was tested in the optimal conditions of 5 mL min^{-1} flow rate and 12 cm bed height. The breakthrough curves for 20 and 30ºC were very similar, with breakthrough times of 45.6 ± 0.7 h and 45.3 ± 0.8 h, respectively. Figure 3.10 presents the temperature effect in breakthrough curves from the column assays carried out at temperatures 10, 20 and 30ºC. As expected, the assay conducted at 10ºC led to the poorest performance, with a breakthrough time of 26.3 ± 0.8 h.

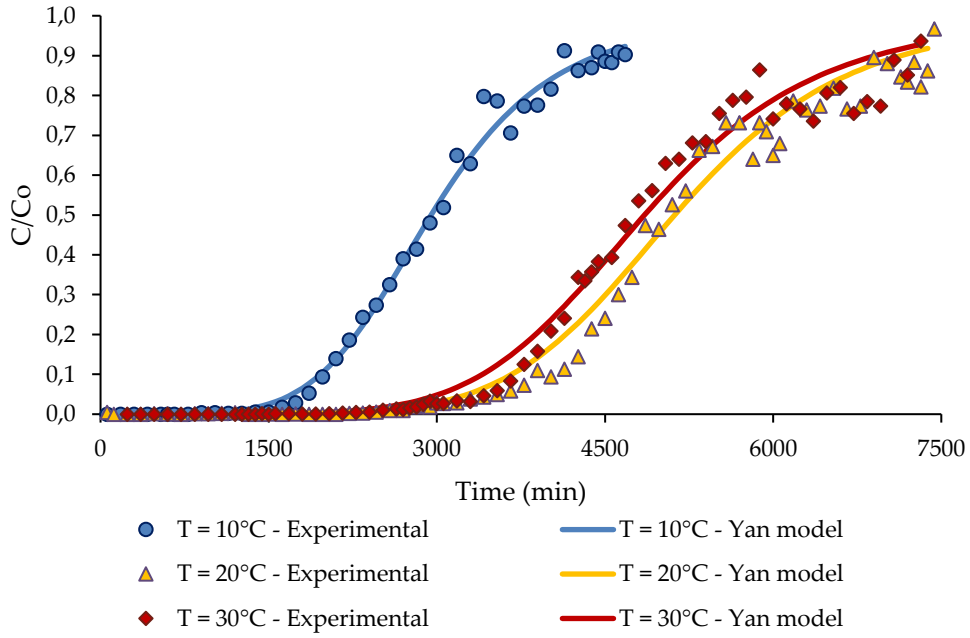


Figure 3.10: Theoretical (Yan model) and experimental breakthrough curves of arsenic adsorption onto ICG at different temperatures: 10, 20 and 30ºC (bed height: 12 cm, flow rate: 5 mL min^{-1}, pH 3.0, $C_{0As(V)}$ 1 mg L^{-1}).

Since the fixed-bed column performances at 20 and 30ºC were close, the temperature of 20ºC was chosen to be applied in the following assays because it is usually closer to environmental conditions.

3.3.2.4 Effect of pH

Previous studies in batch mode showed that As(V) and As(III) adsorption onto ICG is highly dependent on pH (Pintor, Vieira et al. 2018). For As(III), a maximum uptake was obtained at pH 9. Oppositely, for As(V), the increase of pH from 3.0 to 7.0 caused a proportional decrease in adsorption capacity of 50%, from approximately 4.0 mg g^{-1} to 2.0 mg g^{-1} (Pintor, Vieira et al. 2018). In the same study a pH_{PZC} of ICG close to 6 was determined. The inverse trends on arsenate and arsenite uptake observed in batch mode were also observed in continuous mode (Figure 3.11). The experimental and theoretical breakthrough parameters for As(V) and As(III) are found in Table 3.8.

The pH increase caused an inversely proportional effect ($r^2 > 0.9$ on linear regressions) on all BTC parameters for As(V) uptake (Fig. 3.12), except for arsenic removal at breakthrough (y_b), which remained above 99.8%. Adsorption capacity predicted by the Yan model was reduced from 3.8±0.3 to 0.56±0.04 mg g^{-1} with pH increment from 3 to 9. The same increment in pH reduced breakthrough time from 45.6 ± 0.7 h to 7.1 ± 0.5 h (Table 3.8).

The reduction in As(V) adsorption caused by increasing the pH was also reported in other column operation studies using different adsorbents (Nguyen, Yacouba et al. 2020) and justified by the competition of OH^- ion with arsenate ions (K, Tiwari et al. 2020). At pH values lower than the pH_{PZC} of ICG, the positively charged surface of ICG can more efficiently interact with $H_2AsO_4^-$ ions, the contrary of what occurs at high pH, in which the negatively charged ICG surface repulses the more electronegative $HAsO_4^{2-}$ (Pintor, Vieira et al. 2018).

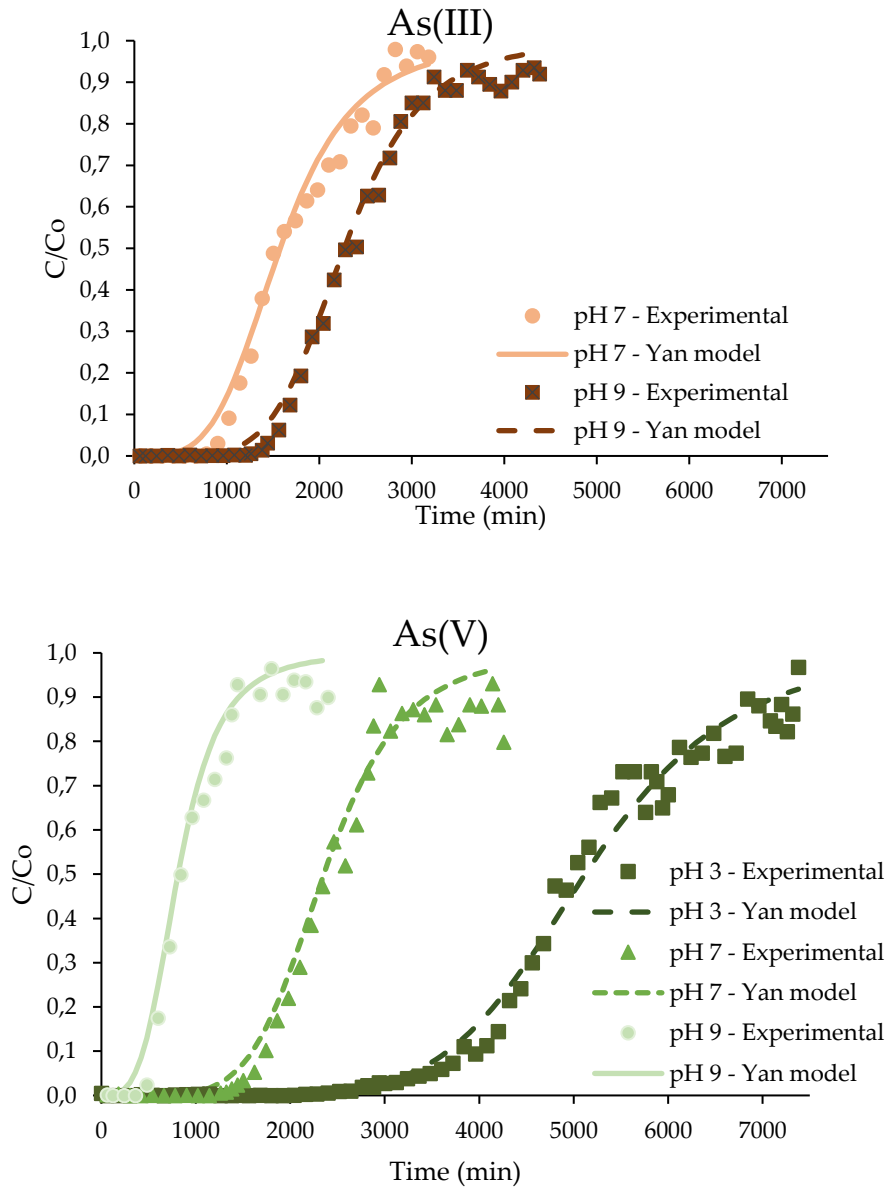


Figure 3.11: Experimental and theoretical (Yan model) breakthrough curves of arsenic adsorption onto ICG for different pH values: a) As(III), pH of 7 and 9; b) As(V) pH of 3, 7 and 9.

In contrast, the increase in pH from 7 to 9 resulted in the rise of As(III) adsorption onto ICG. It was previously observed in the batch results (Pintor, Vieira et al. 2018) that at this pH range, the As(III) is mostly present as neutral arsenious acid (H_3AsO_3), and its adsorption is favorable when the surface of adsorbent is close to neutral, from 6-9, which is close to pH_{PZC} (Maji, Kao et al. 2012, Pintor, Vieira et al. 2018). In addition, it was argued that the beginning of H_3AsO_3 dissociation to $H_2AsO_3^-$ at $pK_a = 9.2$ could induce to an increase in electrostatic repulsion among As(III) and negatively charged adsorbent surface at high values of pH.

Some studies also reported the pH effect on As(III) adsorption, showing analogous trends for arsenite adsorption onto ICG (Maji, Kao et al. 2012, Navarathna, Karunanayake et al. 2019) and others indicate different behavior where As(V) and As(III) are identically influenced by pH (Ali 2018).

The pH has an important effect on the iron leaching from ICG. The concentration of iron leached in the assays carried at pH values of 7 and 9, at 20°C, reached a maximum value of 0.08 mg L^{-1}. In contrast, Fe concentrations of 0.32-0.96 mg L^{-1} were observed in the effluent from the assay at pH 3. However, these values are still much lower than the Fe leached in the batch assay conducted at identical pH and temperature of 20°C (section 3.3.1.1). The fact that a very low concentration of iron was released from ICG reduces the concern raised in section 3.3.1.1 of iron being a hindrance in the application of ICG, considering the adsorbent is more likely to be used at pH conditions of 6-9.

Table 3.10 summarizes literature results from fixed-bed columns operating at an inlet concentration of 1 mg L^{-1}, including the ones obtained in the current study with ICG. The ICG adsorption capacity achieved an excellent value comparing to other modified adsorbents, such as Zr-type adsorbent, iron-mixed mesoporous pellet, and thioglycolated sugarcane carbon. However, in terms of breakthrough time, the values observed for ICG, at similar pH value, were inferior to other iron-based adsorbents, such as magnetic binary oxide particles and iron modified bauxite. It is important to note, however, that the breakthrough time depends highly on the column configuration.

Table 3.8: Experimental and predicted breakthrough parameters of pH effect in As(V) and As(III) adsorption (C_0 = 1 mg L^{-1}, T = 20°C) (± standard error of mean).

	As(V)			**As(III)**	
	pH 3	pH 7	pH 9	pH 7	pH 9

Experimental	t_b (h)	45.6 ± 0.7	22.5 ± 0.6	7.1 ± 0.5	13.7 ± 0.4	22.7 ± 0.7
	t_s (h)	124	70	40	55	73
	q_b (mg g^{-1})	2.0 ± 0.2	1.1 ± 0.1	0.27 ± 0.02	0.54 ± 0.04	0.9 ± 0.1
	q_s (mg g^{-1})	3.9 ± 0.5	2.0 ± 0.3	0.6 ± 0.1	1.2 ± 0.2	1.8 ± 0.4
	BV_b	253 ± 16	125 ± 8	36 ± 3	72 ± 5	116 ± 8
	BV_s	689 ± 40	389 ± 23	204 ± 12	290 ± 17	372 ± 21
	V_b (L)	14.9 ± 0.3	7.4 ± 0.3	2.1 ± 0.1	4.2 ± 0.2	6.8 ± 0.3
	V_s (L)	40.6 ± 0.1	22.9 ± 0.1	12	17.07 ± 0.09	21.90 ± 0.06
	y_b (%)	99.84 ± 0.03	99.90 ± 0.03	99.89 ± 0.05	99.92 ± 0.03	99.93 ± 0.02
	y_s (%)	72 ± 4	60 ± 4	41 ± 5	53 ± 4	61 ± 7
	MTZ (cm)	7.6 ± 0.3	8.1 ± 0.4	9.9 ± 0.8	9.0 ± 0.5	8.3 ± 0.4
	MTZ/Bed height	0.63 ± 0.04	0.68 ± 0.04	0.82 ± 0.07	0.75 ± 0.05	0.69 ± 0.05
Yan Model	Q_{ya} (mg g^{-1})	3.8 ± 0.3	1.9 ± 0.1	0.56 ± 0.04	1.1 ± 0.1	1.6 ± 0.2
	α_{ya}	6.7 ± 0.2	5.8 ± 0.4	4.0 ± 0.4	4.1 ± 0.2	5.6 ± 0.2
	SE (mg g^{-1})	0.04	0.06	0.07	0.04	0.03
	R^2	0.986	0.980	0.972	0.989	0.994
Yoon-Nelson	K_{YN} (10^{-3})	1.31 ± 0.06	2.6 ± 0.2	4.2 ± 0.5	2.5 ± 0.2	2.5 ± 0.1
	t_{YN} 50% (min)	5243 ± 327	2453 ± 271	913 ± 149	1707 ± 166	2375 ± 180
	t_{exp} 50% (min)	5050 ± 107	2374 ± 41	841 ± 24	1528 ± 40	2345 ± 58
	R^2	0.978	0.970	0.962	0.979	0.987
	SE (mg g^{-1})	0.05	0.07	0.08	0.06	0.05

Table 3.9: Fixed-bed column performances reported in other works for As(III) and As(V) removal with an initial concentration of 1 mg L^{-1}.

Adsorbent	Arsenic species	pH	Maximum adsorption capacity (mg g^{-1})	Breakthrough time at 0.01 mg L^{-1} (h)	Ref.
Magnetic binary oxide particles (MBOP) using chitosan	As(III)	7.23	4.67	26	(Dhoble, Maddigapu et al. 2017)
Iron modified calcined bauxite (MCB)	As(III)	6.8±0.4	0.490	50	(Bhakat, Gupta et al. 2007)
Zr-type adsorbent from nonwoven cotton fabric	As(V)	2	0.749	-	(Hoshina, Takahashi et al. 2012)
Iron-mixed mesoporous pellet	As(III)	7±0.1	0.454	11	(Te, Wichitsathian et al. 2018)
	As(V)		0.340	6	
Thioglycolated sugarcane carbon (TSCC)	As(III)	6	0.073	~90	(Roy, Mondal et al. 2013)
	As(V)		0.072		
Agglomerated nanoparticles of Mn-incorporated Fe(III) oxide (MNFO)	As(III)	7.5	3.34	-	(Ghosh, Chakrabarti et al. 2014)
Iron-coated cork granulates (ICG)	As (III)	7	1.2 ± 0.2	13.7 ± 0.4	This study
	As(III)	9	1.8 ± 0.4	22.7 ± 0.7	
	As(V)	3	3.9 ± 0.5	45.6 ± 0.7	
	As(V)	7	2.0 ± 0.3	22.5 ± 0.6	

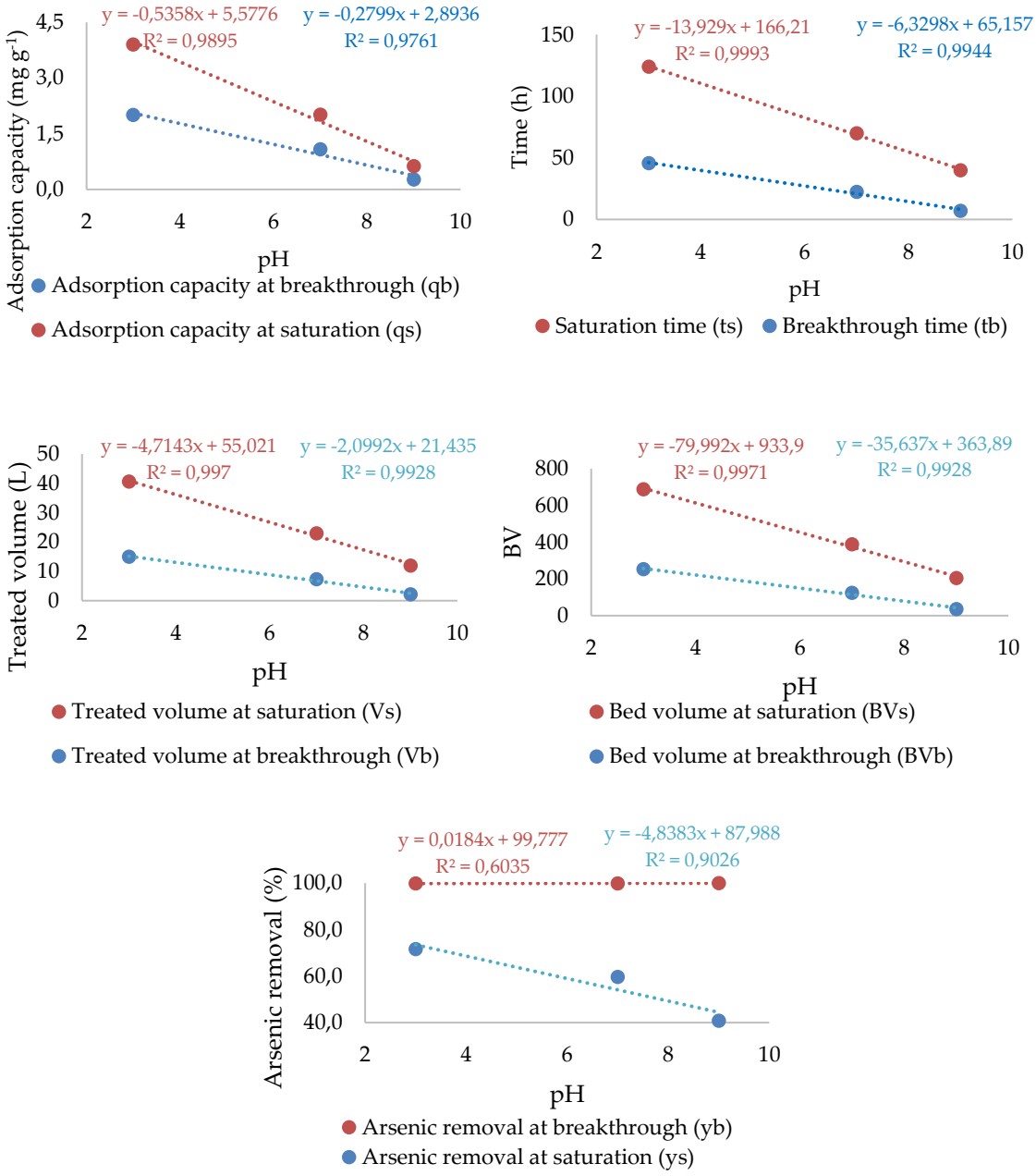


Figure 3.12: pH effect in BTC parameters for As(V) column experiments and trend lines (C_0 = 1 mg L^{-1}; flow rate of 5 mL min^{-1}; bed height of 12 cm; T = 20ºC): a) adsorption capacity (mg g^{-1}), b) adsorption time (h), c) bed volumes, d) treated volume (L),), and e) arsenic removal (%).

Table 3.10: Fixed-bed column performances reported in other works for As(III) and As(V) removal with an initial concentration of 1 mg L^{-1}.

Adsorbent	Arsenic species	pH	Maximum adsorption capacity (mg g^{-1})	Breakthrough time at 0.01 mg L^{-1} (h)	Ref.
Magnetic binary oxide particles (MBOP) using chitosan	As(III)	7.23	4.67	26	(Dhoble, Maddigapu et al. 2017)
Iron modified calcined bauxite (MCB)	As(III)	6.8±0.4	0.490	50	(Bhakat, Gupta et al. 2007)
Zr-type adsorbent from nonwoven cotton fabric	As(V)	2	0.749	-	(Hoshina, Takahashi et al. 2012)
Iron-mixed mesoporous pellet	As(III)	7±0.1	0.454	11	(Te, Wichitsathian et al. 2018)
	As(V)		0.340	6	
Thioglycolated sugarcane carbon (TSCC)	As(III)	6	0.073	~90	(Roy, Mondal et al. 2013)
	As(V)		0.072		
Agglomerated nanoparticles of Mn-incorporated Fe(III) oxide (MNFO)	As(III)	7.5	3.34	-	(Ghosh, Chakrabarti et al. 2014)
Iron-coated cork granulates (ICG)	As (III)	7	1.2 ± 0.2	13.7 ± 0.4	This study
	As(III)	9	1.8 ± 0.4	22.7 ± 0.7	
	As(V)	3	3.9 ± 0.5	45.6 ± 0.7	
	As(V)	7	2.0 ± 0.3	22.5 ± 0.6	

3.3.2.5 Effect of initial concentration

To assess the effect of inlet arsenic concentration in fixed-bed adsorption, new assays were carried out with As(V) and As(III), separately, with initial concentrations of 0.1 and 1 mg L^{-1}, at 20±0.5°C and pH 7.0±0.1. The column tests were conducted at the optimal laboratory-scale column conditions. The results are presented in Table 3.8 and Figure 3.13.

The reduction in inlet concentration of 1.0 to 0.1 mg L^{-1} caused an inversely proportional effect in t_b, t_s, BV_b, BV_s, V_b and V_s, for arsenate adsorption. The adsorption capacity at breakthrough, q_b, reduced from 1.1 mg g^{-1} to 0.8 mg g^{-1} for As(V) and remained unchanged for As(III), as 0.5 mg g^{-1}. The maximum adsorption capacity predicted by the Yan model, Q_{ya}, decreased from 1.9±0.1 to 1.5±0.2 mg g^{-1} and from 1.1±0.1 to 0.8±0.1 mg g^{-1}, for As(V) and As(III), respectively. Even though Q_{ya} values for As(V) are approximately two times higher than Q_{ya} values for As(III), it is still feasible to remove arsenite by ICG adsorption in continuous mode without oxidizing it to arsenate. The column assay operated at 0.1 mg L^{-1} achieved the lowest value of MTZ, of 5.9, with a MTZ/Bed height ratio of 0.49, which confirms the overall good efficiency of the ICG adsorption column for arsenite removal.

From the synthetic arsenic inlet solution used in this work, the ones with the lowest concentration of 0.1 mg L^{-1} at neutral pH value were the closest to real arsenic-contaminated groundwaters used for human consumption, which are usually found at pH 6.5-8 and in the range of 0.1-0.3 mg L^{-1}.

For the As(III) influent at 0.1 mg L^{-1}, effluent concentrations under 10 µg L^{-1} and 50 µg L^{-1} were observed for 569 and 861 bed volumes, respectively. In comparison to other fixed-bed column performances under similar conditions, we achieved better results than Fe-modified GAP (granular attapulgite-supported), which treated 175 and 249 BVs under 10 µg L^{-1} and 50 µg L^{-1}, respectively (Yin, Kong et al. 2017); but not as good as zirconium metal organic frameworks (UiO-66) that treated 1775 BVs before the effluent reached 10 µg L^{-1}.

For the influent with 0.1 mg L^{-1} As(V), the ICG fixed-bed column provided an effluent under 10 µg L^{-1} and 50 µg L^{-1} for 895 and 1633 bed volumes, respectively. The values were higher than those achieved by iron oxide-coated fungal biomass (IOCB) which treated 800 BV before attaining 10 µg L^{-1} at pH 6 (Pokhrel and Viraraghavan 2008); higher also than natural laterite from Thach That (NLTT) when treating approximately 500 BV before breakthrough at 10 µg L^{-1}, at pH 7 (Nguyen, Nguyen et al. 2021); but inferior to the results obtained with GAC-Fe, which reached 10 µg L^{-1} after 1494 BV of treated effluent (Kalaruban, Loganathan et al. 2019).

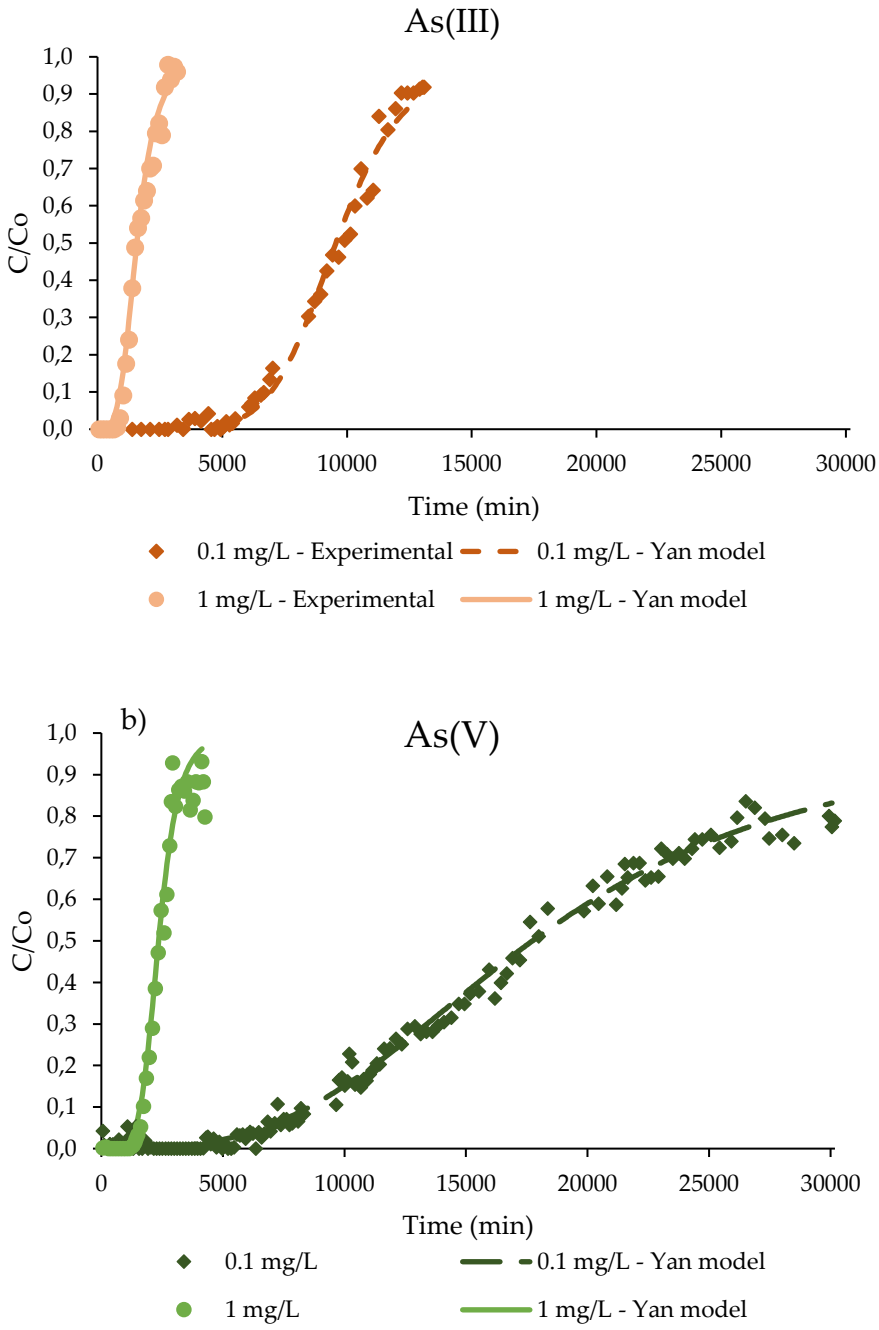


Figure 3.13: Experimental and theoretical (Yan model) breakthrough curves of arsenic adsorption onto ICG with initial concentration values of 0.1 and 1 mg L^{-1} (pH 7 and T = 20°C): a) As(III); b) As(V).

3.4 Conclusions

Iron-coated cork granulates (ICG) were proven to efficiently remove arsenic from aqueous solution at various conditions, including the environmentally relevant conditions of pH 7 and arsenic inlet concentration of 0.1 mg L^{-1}. In these conditions, the effluent exceeded 10 µg L^{-1} and

50 µg L^{-1} only after 895 and 1633 bed volumes, respectively, for As(V), and 569 and 861 bed volumes, respectively, for As(III).

Breakthrough curves were best described by the Yan model with most of the determination coefficients above 0.98, although Thomas and Yoon-Nelson models showed good nonlinear fits. Maximum adsorption capacities in continuous mode predicted by Yan model were 4.2 ±0.3 mg As(V) g^{-1} ICG and 1.6±0.2 mg As(III) g^{-1} ICG for C_o of 1 mg L^{-1}, higher than those obtained in batch experiments for low equilibrium concentration.

Bed height and flow rate provided a statistically significant influence on some BTC experimental parameters; however, no statistically significant effect of temperature was observed in the 10-30 °C range. On the contrary, in batch studies, a directly proportional effect of temperature on isotherm parameters predicted by Langmuir and Freundlich models was observed. A maximum adsorption capacity of 6.9±0.1 mg As(V) g^{-1} ICG at 30°C was calculated using the Langmuir fit. Thermodynamic studies confirmed the adsorption process to be endothermic, spontaneous, and feasible.

In accordance with earlier batch studies, pH variation caused a proportional change in BTC parameters, with 3 and 9 being more favourable pH values for As(V) and As(III), respectively. However, good efficiency was still observed at pH 7 for both species, which is the value recommended for waters with arsenate and arsenite co-contamination. At pH 7, low iron leaching from the adsorbent was also observed. The variation in initial arsenic concentration also influenced the majority of BTC parameters, as expected.

Further work should investigate the removal of arsenic using the ICG fixed-bed column in real waters, such as contaminated groundwater and mining runoff. Forthcoming studies should also explore possibilities for regeneration of the exhausted bed and its sustainable disposal.

3.5 References

Ali, I. (2018). "Microwave assisted economic synthesis of multi walled carbon nanotubes for arsenic species removal in water: Batch and column operations." Journal of Molecular Liquids **271**: 677-685.

Bhakat, P. B., A. K. Gupta and S. Ayoob (2007). "Feasibility analysis of As(III) removal in a continuous flow fixed bed system by modified calcined bauxite (MCB)." Journal of Hazardous Materials **139**(2): 286-292.

Brion-Roby, R., J. Gagnon, J.-S. Deschênes and B. Chabot (2018). "Development and treatment procedure of arsenic-contaminated water using a new and green chitosan sorbent: kinetic, isotherm, thermodynamic and dynamic studies." Pure and Applied Chemistry **90**(1): 63-77.

Chatterjee, A. and S. Schiewer (2011). "Biosorption of Cadmium(II) Ions by Citrus Peels in a Packed Bed Column: Effect of Process Parameters and Comparison of Different Breakthrough Curve Models." CLEAN – Soil, Air, Water **39**(9): 874-881.

Chen, C.-C. and Y.-C. Chung (2006). "Arsenic Removal Using a Biopolymer Chitosan Sorbent." Journal of Environmental Science and Health, Part A **41**(4): 645-658.

Chiban, M., G. Carja, G. Lehutu and F. Sinan (2016). "Equilibrium and thermodynamic studies for the removal of As(V) ions from aqueous solution using dried plants as adsorbents." Arabian Journal of Chemistry **9**: S988-S999.

Chu, K. H. (2020). "Breakthrough curve analysis by simplistic models of fixed bed adsorption: In defense of the century-old Bohart-Adams model." Chemical Engineering Journal **380**: 122513.

Dhoble, R. M., P. R. Maddigapu, S. S. Rayalu, A. G. Bhole, A. S. Dhoble and S. R. Dhoble (2017). "Removal of arsenic(III) from water by magnetic binary oxide particles (MBOP): Experimental studies on fixed bed column." Journal of Hazardous Materials **322**: 469-478.

Díaz-Blancas, V., C. G. Aguilar-Madera, J. V. Flores-Cano, R. Leyva-Ramos, E. Padilla-Ortega and R. Ocampo-Pérez (2020). "Evaluation of mass transfer mechanisms involved during the adsorption of metronidazole on granular activated carbon in fixed bed column." Journal of Water Process Engineering **36**: 101303.

Freundlich, H. (1907). "Über die Adsorption in Lösungen." Zeitschrift für Physikalische Chemie **57U**(1): 385-470.

Ghosh, A., S. Chakrabarti and U. C. Ghosh (2014). "Fixed-bed column performance of Mn-incorporated iron(III) oxide nanoparticle agglomerates on As(III) removal from the spiked groundwater in lab bench scale." Chemical Engineering Journal **248**: 18-26.

Hernández-Flores, H., N. Pariona, M. Herrera-Trejo, H. M. Hdz-García and A. I. Mtz-Enriquez (2018). "Concrete/maghemite nanocomposites as novel adsorbents for arsenic removal." Journal of Molecular Structure **1171**: 9-16.

Hoshina, H., M. Takahashi, N. Kasai and N. Seko (2012). "Adsorbent for Arsenic (V) removal synthesized by radiation-induced graft polymerization onto nonwoven cotton fabric." Int J Org Chem **2**: 173-177.

Hristovski, K., A. Baumgardner and P. Westerhoff (2007). "Selecting metal oxide nanomaterials for arsenic removal in fixed bed columns: From nanopowders to aggregated nanoparticle media." Journal of Hazardous Materials **147**(1): 265-274.

Iqbal, M., A. Saeed and R. G. J. Edyvean (2013). "Bioremoval of antimony(III) from contaminated water using several plant wastes: Optimization of batch and dynamic flow conditions for sorption by green bean husk (Vigna radiata)." Chemical Engineering Journal **225**: 192-201.

Jaria, G., V. Calisto, C. P. Silva, M. V. Gil, M. Otero and V. I. Esteves (2019). "Fixed-bed performance of a waste-derived granular activated carbon for the removal of micropollutants from municipal wastewater." Science of The Total Environment **683**: 699-708.

K, V., A. Tiwari and C. V. Chaudhari (2020). "Mitigation of toxic arsenic (V) from aqueous solution in fixed-bed column using functionally modified bio-polymer." Inorganic and Nano-Metal Chemistry: 1-12.

Kalaruban, M., P. Loganathan, T. V. Nguyen, T. Nur, M. A. Hasan Johir, T. H. Nguyen, M. V. Trinh and S. Vigneswaran (2019). "Iron-impregnated granular activated carbon for arsenic removal: Application to practical column filters." Journal of Environmental Management **239**: 235-243.

Kim, D., Y. Ren, M. Cui, Y. Lee, J. Kim, O. Kwon, W. Ji and J. Khim (2021). "Arsenic adsorption on two types of powdered and beaded coal mine drainage sludge adsorbent." Chemosphere **272**: 129560.

Langmuir, I. (1918). "THE ADSORPTION OF GASES ON PLANE SURFACES OF GLASS, MICA AND PLATINUM." Journal of the American Chemical Society **40**(9): 1361-1403.

Lin, S., H. Yang, Z. Na and K. Lin (2018). "A novel biodegradable arsenic adsorbent by immobilization of iron oxyhydroxide (FeOOH) on the root powder of long-root Eichhornia crassipes." Chemosphere **192**: 258-266.

Liu, Z., F.-S. Zhang and R. Sasai (2010). "Arsenate removal from water using Fe3O4-loaded activated carbon prepared from waste biomass." Chemical Engineering Journal **160**(1): 57-62.

Maiti, A., V. Agarwal, S. De and J. K. Basu (2010). "Removal of As(V) using iron oxide impregnated carbon prepared from Tamarind hull." Journal of Environmental Science and Health, Part A **45**(10): 1207-1216.

Maji, S. K., Y.-H. Kao, C.-J. Wang, G.-S. Lu, J.-J. Wu and C.-W. Liu (2012). "Fixed bed adsorption of As(III) on iron-oxide-coated natural rock (IOCNR) and application to real arsenic-bearing groundwater." Chemical Engineering Journal **203**: 285-293.

Mantovaneli, I., E. Ferretti, M. Simões and C. Silva (2004). "The effect of temperature and flow rate on the clarification of the aqueous Stevia-extract in a fixed-bed column with zeolites." Brazilian Journal of Chemical Engineering **21**(3): 449-458.

Milonjić, S. K. (2007). "A consideration of the correct calculation of thermodynamic parameters of adsorption." Journal of the Serbian chemical society **72**(12): 1363-1367.

Mohapatra, D., D. Mishra, G. R. Chaudhury and R. P. Das (2007). "Arsenic adsorption mechanism on clay minerals and its dependence on temperature." Korean Journal of Chemical Engineering **24**(3): 426-430.

Mondal, P., C. Balomajumder and B. Mohanty (2007). "A laboratory study for the treatment of arsenic, iron, and manganese bearing ground water using Fe3+ impregnated activated carbon: Effects of shaking time, pH and temperature." Journal of Hazardous Materials **144**(1): 420-426.

Navarathna, C. M., A. G. Karunanayake, S. R. Gunatilake, C. U. Pittman, F. Perez, D. Mohan and T. Mlsna (2019). "Removal of Arsenic(III) from water using magnetite precipitated onto Douglas fir biochar." Journal of Environmental Management **250**: 109429.

Nguyen, P. T. T., S. Yacouba, S. Pare and H. M. Bui (2020). "Removal of Arsenic from Groundwater Using Lamdong Laterite as a Natural Adsorbent." Polish Journal of Environmental Studies **29**(2): 1305-1314.

Nguyen, T. H., A. T. Nguyen, P. Loganathan, T. V. Nguyen, S. Vigneswaran, T. H. H. Nguyen and H. N. Tran (2021). "Low-cost laterite-laden household filters for removing arsenic from groundwater in Vietnam and waste management." Process Safety and Environmental Protection **152**: 154-163.

Nnaji, C. C., A. E. Agim, C. N. Mama, P. C. Emenike and N. M. Ogarekpe (2021). "Equilibrium and thermodynamic investigation of biosorption of nickel from water by activated carbon made from palm kernel chaff." Scientific Reports **11**(1): 7808.

Pintor, A., B. Vieira, R. Boaventura and C. Botelho (2019). "Removal of antimony from water by iron-coated cork granulates." Separation and Purification Technology **233**: 116020.

Pintor, A. M. A., C. C. Brandão, R. A. R. Boaventura and C. M. S. Botelho (2020). "Multicomponent adsorption of pentavalent As, Sb and P onto iron-coated cork granulates." Journal of Hazardous Materials: 124339.

Pintor, A. M. A., C. C. Brandão, R. A. R. Boaventura and C. M. S. Botelho (2021). "Multicomponent adsorption of pentavalent As, Sb and P onto iron-coated cork granulates." Journal of Hazardous Materials **406**: 124339.

Pintor, A. M. A., B. R. C. Vieira, R. A. R. Boaventura and C. M. S. Botelho (2020). "Removal of antimony from water by iron-coated cork granulates." Separation and Purification Technology **233**: 116020.

Pintor, A. M. A., B. R. C. Vieira, C. C. Brandão, R. A. R. Boaventura and C. M. S. Botelho (2020). "Complexation mechanisms in arsenic and phosphorus adsorption onto iron-coated cork granulates." Journal of Environmental Chemical Engineering **8**(5): 104184.

Pintor, A. M. A., B. R. C. Vieira, S. C. R. Santos, R. A. R. Boaventura and C. M. S. Botelho (2018). "Arsenate and arsenite adsorption onto iron-coated cork granulates." Science of The Total Environment **642**: 1075-1089.

Pokhrel, D. and T. Viraraghavan (2008). "Arsenic removal in an iron oxide-coated fungal biomass column: Analysis of breakthrough curves." Bioresource Technology **99**(6): 2067-2071.

Rahman, M. A., D. Lamb, M. M. Rahman, M. M. Bahar, P. Sanderson, S. Abbasi, A. S. M. F. Bari and R. Naidu (2021). "Removal of arsenate from contaminated waters by novel zirconium and zirconium-iron modified biochar." Journal of Hazardous Materials **409**: 124488.

Ranjan, D., M. Talat and S. H. Hasan (2009). "Rice Polish: An Alternative to Conventional Adsorbents for Treating Arsenic Bearing Water by Up-Flow Column Method." Industrial & Engineering Chemistry Research **48**(23): 10180-10185.

Roy, P., N. K. Mondal, S. Bhattacharya, B. Das and K. Das (2013). "Removal of arsenic(III) and arsenic(V) on chemically modified low-cost adsorbent: batch and column operations." Applied Water Science **3**(1): 293-309.

Saha, S. and P. Sarkar (2016). "Arsenic mitigation by chitosan-based porous magnesia-impregnated alumina: performance evaluation in continuous packed bed column." International Journal of Environmental Science and Technology **13**(1): 243-256.

Sarkar, P., P. Pal, D. Bhattacharyay and S. Banerjee (2010). "Removal of arsenic from drinking water by ferric hydroxide microcapsule-loaded alginate beads in packed adsorption column." Journal of Environmental Science and Health, Part A **45**(13): 1750-1757.

Sawood, G. M. and S. K. Gupta (2020). "Arsenate adsorption from aqueous solution using iron-loaded Azadirachta indica roots: batch and fixed-bed column study." DESALINATION AND WATER TREATMENT **203**: 292-308.

Shipley, H. J., S. Yean, A. T. Kan and M. B. Tomson (2009). "Adsorption of arsenic to magnetite nanoparticles: Effect of particle concentration, pH, ionic strength, and temperature." Environmental Toxicology and Chemistry **28**(3): 509-515.

Singh, P., S. K. Singh, J. Bajpai, A. K. Bajpai and R. B. Shrivastava (2014). "Iron crosslinked alginate as novel nanosorbents for removal of arsenic ions and bacteriological contamination from water." Journal of Materials Research and Technology **3**(3): 195-202.

Te, B., B. Wichitsathian, C. Yossapol and W. Wonglertarak (2018). "Investigation of Arsenic Removal from Water by Iron-Mixed Mesoporous Pellet in a Continuous Fixed-Bed Column." Water, Air, & Soil Pollution **229**(9): 296.

Thomas, H. C. (1944). "Heterogeneous Ion Exchange in a Flowing System." Journal of the American Chemical Society **66**(10): 1664-1666.

Ungureanu, G., S. C. R. Santos, I. Volf, R. A. R. Boaventura and C. M. S. Botelho (2017). "Biosorption of antimony oxyanions by brown seaweeds: Batch and column studies." Journal of Environmental Chemical Engineering **5**(4): 3463-3471.

Verduzco-Navarro, I. P., N. Rios-Donato, C. F. Jasso-Gastinel, Á. d. J. Martínez-Gómez and E. Mendizábal (2020). "Removal of Cu(II) by Fixed-Bed Columns Using Alg-Ch and Alg-ChS Hydrogel Beads: Effect of Operating Conditions on the Mass Transfer Zone." Polymers **12**(10): 2345.

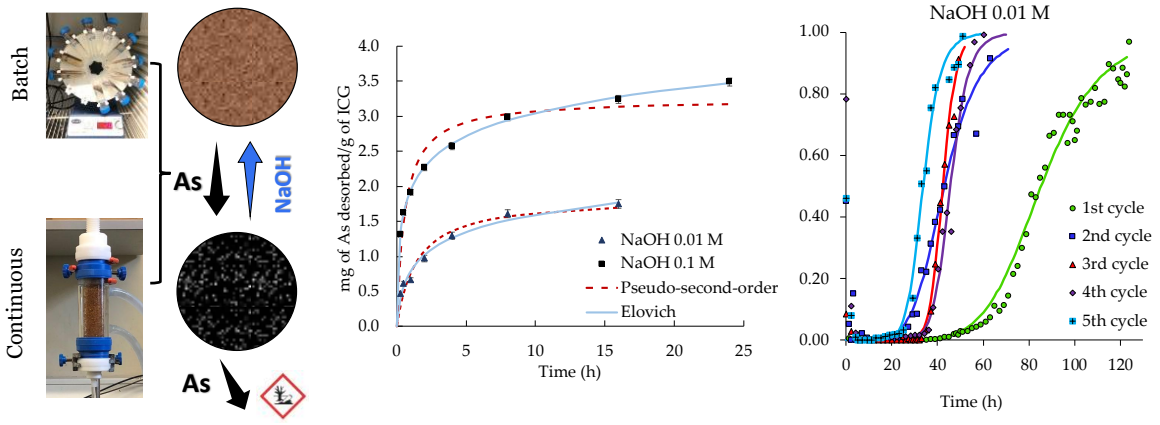
World Health, O. (2011). Guidelines for drinking-water quality. Geneva, World Health Organization.

Yin, H., M. Kong, X. Gu and H. Chen (2017). "Removal of arsenic from water by porous charred granulated attapulgite-supported hydrated iron oxide in bath and column modes." Journal of Cleaner Production **166**: 88-97.

Yoon, Y. H. and J. H. Nelson (1984). "Application of gas adsorption kinetics. I. A theoretical model for respirator cartridge service life." Am Ind Hyg Assoc J **45**(8): 509-516.

4 REGENERATION OF ARSENIC-LOADED IRON-COATED CORK GRANULATES

This chapter is based on: M. A. Carneiro, J. F. R. Coelho, A. M. A. Pintor, R. A. R. Boaventura and C. M. S. Botelho, *Multi-cycle regeneration of arsenic-loaded iron-coated cork granulates for water treatment*. Journal of Water Process Engineering, 2022: p. 103291.



The chemical desorption of arsenic from saturated iron-coated cork granulates (ICG) and the regeneration capacity of this adsorbent for further reuse was investigated in batch and continuous modes. Different types of eluents (bases, acids, salts, and complexing agents) were tested at different concentrations for evaluating their desorption capacity. Moreover, leaching of total organic carbon (TOC), iron content, and characterization by SEM/EDS were used to assess the eluents' attack on the adsorbent structure. The NaOH 0.1 M solution achieved the highest arsenic removal rate from saturated media; however, it was aggressive to the adsorbent structure, as reflected in high TOC values found in the eluate, higher iron leaching from the adsorbent, and higher degradation of cork cellular structure. The Elovich model fitted best ($r^2 > 0.98$) the desorption kinetics when using NaOH as eluent at different concentrations. The less basic solution of NaOH 0.01 M proved to be less aggressive to ICG and allowed media regeneration for at least four adsorption-desorption cycles, while remaining an arsenic adsorption capacity of 1 mg g^{-1} in both batch and continuous modes. ICG´s adsorption capacity was less affected after various cycles than other adsorbents, so this material proved to be potentially applicable on an industrial scale as an alternative green solution for arsenic removal from water. The adsorbent was also successfully applied in continuous mode to remove arsenic from real groundwater and was able to maintain arsenic concentration under 10 µg L^{-1} and 50 µg L^{-1} for 140 and 341 bed volumes respectively. This work provided good insights on arsenic desorption from ICG and its further application in similar real scenarios.

4.1 Introduction

In the previous chapter, iron-coated cork granulates have been successfully applied in continuous mode for adsorption of As from aqueous solution. Still, ICG regeneration capacity has not been yet investigated to evaluate the feasibility of the adsorbent for real application. Desorption and regeneration of any adsorbent play an important role in the adsorption process in ecological and economic terms (Di Natale, Erto et al. 2013). In terms of industrial application, the regeneration over many cycles can be decisive in the choice of the adsorbent (Vakili, Deng et al. 2019). Thus, in developing a new adsorbent, it is important to study its regenerability and the desorption mechanism. This work focuses on the desorption of arsenic from iron-coated cork granulates adsorbents in batch and continuous mode. Moreover, the regenerability of ICG was investigated, and its performance in treating real arsenic-contaminated groundwater was assessed.

The material characterization was performed at different stages of saturation and regeneration by three different methodologies: acid digestion and flame atomic absorption spectroscopy (FAAS) for measuring iron content, scanning electron microscopy (SEM) for visual observation, and energy-dispersive X-ray spectroscopy (EDS) to identify the main elements present in the materials.

4.2 Materials and methods

4.2.1 Materials

The adsorbent, iron-coated cork granulates (ICG), was produced by treating raw cork granulates (RCG) (particle size of 0.5-1.0 mm) with an iron chloride solution, in previously optimized coating conditions (Pintor, Vieira et al. 2018), as described in section 3.2.1.

Arsenic aqueous solutions were diluted in distilled water from a standard solution of 1,069 ± 22 mg As(V) L^{-1} or 987 ± 43 mg As(V) L^{-1}, prepared by dissolution of $HAsNa_2O_4{\cdot}7H_2O$ (Sigma-Aldrich; analytical grade) in 2% HNO_3.

Arsenic-contaminated groundwater was prepared from a matrix of a real groundwater, collected in Northeastern Portugal. The arsenic concentration was elevated to 0.1 mg L^{-1} by spiking with an arsenic commercial standard of 1,000 mg L^{-1} (Chem-Lab).

The eluent solutions were prepared by dissolving in distilled water the following chemicals: sodium hydroxide pearls 99.14% (Labsolve), sodium carbonate anhydrous 99.5% (Merck), nitric

acid 68% (VWR), potassium hydroxide pellets ≥ 85% (Merck), potassium nitrate 99% (Riedel-de-Haen), di-sodium ethylenediaminetetra-acetate (EDTA) > 98.5% (May & Baker), di-sodium hydrogen phosphate dihydrate (VWR).

4.2.1.1 Material characterization

The adsorbents at different stages of saturation and regeneration were characterised by three different methodologies: acid digestion and flame atomic absorption spectroscopy (FAAS) for measuring iron content, scanning electron microscopy (SEM) for visual observation, and energy-dispersive X-ray spectroscopy (EDS) to identify the main elements present in the materials.

The methodology used in a previous study was applied for iron content determination by acid digestion (Pintor, Vieira et al. 2018). In short, the materials were digested using a mixture of HCl 37% (analytical grade, Sigma-Aldrich), HNO_3 68% (analytical grade, VWR) and distilled water for 2 h at 150ºC. The digested solution was filtered and diluted with distilled water, and total iron content was measured by FAAS.

The SEM / EDS exam was performed using a High resolution (Schottky) Environmental Scanning Electron Microscope with X-Ray Microanalysis and Electron Backscattered Diffraction analysis: FEI Quanta 400 FEG ESEM / EDAX Genesis X4M. Samples were coated with a Au/Pd thin film by sputtering using the SPI Module Sputter Coater equipment.

4.2.2 Analysis

For column experiments and kinetics studies, total arsenic concentrations were measured by graphite furnace atomic absorption spectrometry (GFAAS) in the operating range of 6.7–50 µg L^{-1}. For batch experiments, the total arsenic concentration was measured by FAAS in the working range of 5–50 mg L^{-1} (Pintor, Vieira et al. 2018, Pintor, Vieira et al. 2020, Pintor, Brandão et al. 2021) and by inductively coupled plasma-optical emission spectrometry (ICP-OES) in the range of 0.005–10 mg L-1. Total dissolved iron was determined by FAAS and ICP-OES in the ranges of 0.25-5.0 mg L^{-1} and 0.005–10 mg L^{-1}, respectively.

The FAAS and GFAAS equipment used in this work were a GBC 932 Plus and a GBC GF3000, respectively. The ICP-OES apparatus was an ICP-OES Thermo X Series.

The organic matter content of the aqueous solutions was quantified as total organic carbon (TOC) using a Shimadzu Equipment TOC-L.

4.2.3 Batch adsorption-desorption experiments

4.2.3.1 Eluent performance

Different eluents were selected for As(V) desorption: distilled water, NaOH (0.01 M, 0.05 M, 0.1 M, 0.5 M), Na_2CO_3 (0.01 M, 0.1 M, 0.5 M, 1 M, 2 M), HNO_3 (0.1 M), KOH (0.1 M), KNO_3 (0.5 M), EDTA (0.5 M), and Na_2HPO_4 (0.5 M). For each assay, 2.5 g L^{-1} saturated iron-coated cork granulates (3.9 ± 0.5 mg As(V) g^{-1} adsorbent) were put in contact with eluent solutions, in a rotating shaker (Stuart, SB3) at 20 rpm and a controlled temperature of 20.0 ± 0.5 ºC. After 24 h of contact time, the samples were filtered using acetate cellulose filters (0.45 µm pore size) and analyzed for total As concentration by ICP-OES. The As desorbed amount (q_d, mg g^{-1}) was calculated as follows:

$$q_d = \frac{V*C}{m} \quad (4.1)$$

where V is the eluent solution volume (L), C is the As concentration (mg L^{-1}) desorbed to the solution, and m is the mass of saturated adsorbent (g).

The total dissolved iron was measured in the final samples after filtration to determine the extent of iron leaching from the adsorbent.

4.2.3.2 Desorption kinetics

Desorption kinetics were studied for As(V) using NaOH 0.01 and 0.1 mol L^{-1}. Like previous desorption assays, 2.5 g L^{-1} saturated iron-coated cork granulates were put in contact with the basic solution in a rotating shaker at 20 rpm and 20.0 ± 0.5 °C. The contact times were 0.25, 0.5, 1, 2, 4, 8, 16 h for NaOH 0.01 M, and 0.25, 0.5, 1, 2, 4, 8, 16 and 24 h for NaOH 0.1 M. The final solutions were filtered (acetate cellulose filters, 0.45 µm pore size) and analyzed for As by ICP-OES (assays using NaOH 0.1 M) or FAAS/GFAAS (assays using NaOH 0.01 M). The desorbed amount was calculated using Eq. (4.1).

The desorption kinetics were described using the pseudo-first-order model (Lagergren S 1898), the pseudo-second-order model (C.F. Ho and Forster 1996), and Elovich model (Low 1960, Elovich and Larionov 1962) which equations are shown below, respectively. The models were fitted to the experimental values by nonlinear regression, using Curve Expert Pro 2.7 software.

$$q_t = q_e(1 - e^{-k_1 t}) \quad (4.2)$$

$$q_t = \frac{k_2 {q_e}^2 t}{1 + k_2 q_e t} \quad (4.3)$$

$$q_t = \frac{1}{b} \ln (1 + abt) \quad (4.4)$$

where q_t is the adsorbed amount (mg g^{-1}) at time t (h), q_e is the adsorbed amount at equilibrium (mg g^{-1}), k_1 is the pseudo-first-order kinetic constant (h^{-1}), k_2 the pseudo-second-order kinetic constant (g mg^{-1} h^{-1}), a is the initial rate of adsorption (mg g^{-1} h^{-1}) and b is a coverage scale factor (g mg^{-1}) that corresponds to the reciprocal of the coverage at which the adsorption rate has fallen to $1/e$ of its initial value.

4.2.3.3 Adsorption-desorption cycles

Adsorption-desorption cycles were conducted to determine the regenerability of the iron-coated cork granulates. The first cycle was always conducted with fresh ICG and the following cycles with regenerated ICG. For every cycle, an As(V) solution of 40 mg L^{-1} at pH 3.0 or a NaOH eluent solution was put in contact with ICG (S/L ratio 2.5 g L^{-1}) for a certain period in a rotating shaker at 20 rpm and a temperature of 20.0 ± 0.5 °C. Finished the experiment, the adsorbent was separated from the solution and left to dry in an oven overnight. After each desorption cycle, the adsorbent was washed for approximately 2 hours to remove the residual eluent. The final solutions were filtered (acetate cellulose filters, 0.45 µm pore size) and analyzed for As by FAAS. The adsorbed amount (q_{ad}) was calculated by mass balance (Eq. (3.1), and the desorbed amount was calculated by Eq. (4.1).

All the batch assays performed in this work were carried out in duplicate, and the result presented as the average.

4.2.4 Continuous adsorption-desorption experiments

Continuous adsorption-desorption tests were carried out in a lab-scale fixed-bed column, working in a downward flow due to the low density of the adsorbent. The lab-scale continuous adsorption system included a 50 L influent reservoir, a 30 L outlet reservoir, a glass column (Chromaflex®) with a 2.5 cm internal diameter and a maximum height of 15 cm, a peristaltic pump for flow rate regulation (VWR), an automatic sampler (GILSON, FC-203B), and a thermostatic bath for temperature control (DIGIT-COOL, J.P. SELECTA). The operational conditions were optimized in Chapter 3 and were as follows: flow rate - 5 mL min^{-1}, bed height - 12 cm, and temperature - 20 °C, which corresponds to a bed volume of 59 mL and empty bed contact time (EBCT) of 11.8 min. The tests were carried for both arsenic-spiked distilled water (1 mg As(V) L^{-1}) and arsenic-spiked groundwater (0.1 mg As L^{-1}).

The desorption assays were carried out under conditions similar to those of adsorption. The eluent applied was NaOH in concentrations of 0.1 M and 0.01 M. The desorption of arsenic from the exhausted adsorbent was conducted until arsenic concentrations in the eluent were very low. The first cycle was always conducted with fresh ICG and the following cycles with regenerated ICG.

The desorption capacity, Q_d (mg g^{-1}), was calculated as the total amount of arsenic eluted from the saturated adsorbent, divided by the total mass of adsorbent, as follows:

$$Q_d = \frac{M_d}{m} \quad (4.5)$$

where M_d is the As mass (mg) desorbed, and m is the mass of adsorbent (g).

The desorption efficiency (%) was calculated as the ratio between the total of arsenic eluted from the saturated adsorbent (M_d), and the mass of arsenic retained in the saturated adsorbent in the previous adsorption cycle (m_{ad}), as follows:

$$y_d = \frac{M_d}{m_{ad}} \text{ x } 100 \quad (4.6)$$

4.2.5 Analysis breakthrough curves

The performance of the fixed-bed column was evaluated by breakthrough curves (BTC) according to the following experimental parameters: breakthrough time (t_b), saturation time (t_s), bed volumes treated at breakthrough (BV_b), bed volumes treated at the saturation point (BV_s), adsorption capacity at breakthrough (q_b), adsorption capacity at the saturation (q_s); treated volume at breakthrough (V_b), treated volume at saturation (V_s), arsenic removal at breakthrough (y_b), and arsenic removal at saturation (y_s), the mass transfer zone (MTZ) in the column, and the MTZ/Bed height ratio. The calculation of each parameter is described in section 3.2.4.2.

Breakthrough time was defined as that corresponding to the outlet concentration of 10 µg L^{-1}, which is the maximum level permitted in the European Union and the guideline recommended by the World Health Organization (WHO 2017, European Union 2020). Theoretical parameters were obtained by fitting the Yan model to the experimental values by nonlinear regression, using Curve Expert Pro 2.7 software. The Yan model (Yan, Viraraghavan et al. 2001) is an empirical model represented by the equation (3.15).

4.3 Results and discussion

4.3.1 Desorption in batch operation mode

The adsorbent´s regeneration performance was firstly studied in batch operation mode. Lab-scale tests were conducted to evaluate the desorption of arsenic from ICG using several eluents, followed by the study of the effect of different eluent concentrations, and finally, the assessment of regeneration cycles by the application of consecutive adsorption-desorption cycles, using the most suitable eluent.

4.3.1.1 Eluent performance

The desorption of arsenate from ICG was studied by applying different classes of eluents: salts (Na_2CO_3 – 0.1 M and 0.5 M, Na_2HPO_4 – 0.5 M, KNO_3 – 0.5 M), bases (NaOH – 0.1 M and 0.5 M, KOH – 0.1 M), an acid (HNO_3 – 0.1 M), a complexing agent (EDTA – 0.5 M), and distilled water. The distilled water was able to desorb only 4.2%. Figure 4.1 and
Table 4.1 show the desorption efficiency for the other desorbing agents. The bases stood out in comparison to the salts and the acid. Among the bases, NaOH achieved the best desorption efficiencies of 83% and 92%, for concentrations of 0.5 M and 0.1 M, respectively, followed by KOH at 0.1 M (83%). In the class of salts, Na_2CO_3 0.1 M achieved the best elution of 56%. We observed that the acid option was not feasible to be applied in arsenic elution from ICG, not only because of its low desorption capacity (34%) but also for the high extraction of iron from the adsorbent of 9.2 mg Fe g^{-1}, which was approximately 40 times higher than the iron leached in the solution using other eluents. Another iron-based sorbent for arsenic removal had also demonstrated high iron solubility from desorption using an inorganic acid eluent (638 mg L^{-1}) (Bujňáková, Baláž et al. 2013).

The overall arsenic desorption efficiency decreased in the following order: NaOH > KOH > Na_2CO_3 > HNO_3 > Na_2HPO_4 > EDTA > H_2O > KNO_3. For iron leaching from ICG, the increasing order was followed: Na_2CO_3 < H_2O < KNO_3 < Na_2HPO_4 < NaOH < KOH < EDTA < HNO_3.

Table 4.1: Desorption capacity, desorption efficiency, and iron leached for various eluents (± standard error of the mean) .

Eluent	Concentration (M)	Arsenic desorption capacity (mg g^{-1})	Iron leaching (mg g^{-1})	Desorption efficiency (%)	TOC (mg L^{-1})	Final pH of solution
H_2O	-	0.16±0.01	0.04±0.02	(4.2±0.6)	-	3.89
KNO3	0.5	0.07±0.01	0.15±0.02	(1.8±0.4)	-	3.94
NaOH	0.01	2.71±0.04	0.25±0.02	(69±9)	22.26	11.57
NaOH	0.05	3.18±0.05	0.24±0.02	(82±11)	188.05	12.57
NaOH	0.1	3.58±0.05	0.21±0.02	(92±12)	162.55	12.81
NaOH	0.5	3.24±0.05	0.27±0.02	(83±11)	-	13.44
EDTA	0.5	0.51±0.02	0.79±0.02	(13±2)	-	8.71
HNO_3	0.1	1.31±0.02	9.20±0.02	(34±4)	-	-
Na_2CO_3	0.01	1.92±0.04	0.18±0.02	(49±6)	-	10.67
Na_2CO_3	0.1	2.18±0.04	0.05±0.03	(56±7)	-	11.18
Na_2CO_3	0.5	1.87±0.03	0.01±0.02	(48±6)	-	11.44
Na_2CO_3	1.0	1.56±0.03	0.02±0.02	(40±5)	-	11.46
Na_2CO_3	2.0	1.04±0.02	0.05±0.02	(27±4)	-	11.48
Na_2HPO_4	0.5	0.86±0.02	0.16±0.02	(22±3)	48.75	9.06
KOH	0.1	3.22±0.05	0.27±0.02	(83±11)	150.8	12.77

The results showed that desorption efficiency was dependent on pH values (Table 4.1). A pH change in solution affects both arsenate speciation and the surface charge of iron-coated cork granulates. Arsenate is prevalent in solution in the forms H_3AsO_4 (pH<2.2), $H_2AsO_4^-$ (2.2 < pH < 6.9), $HAsO_4^{2-}$ (6.9 < pH > 11.5), and AsO_4^{3-} (pH > 11.5) (Sadiq, Zaidi et al. 1983, Ungureanu, Santos et al. 2015), whereas the iron oxide surface is typically loaded with surface

hydroxyl groups (Fe-OH), and the surface is protonated ($Fe\text{-}OH_2^+$) or deprotonated (Fe-O), depending on the point of zero charge (pH_{PZC}) (Tuutijärvi, Vahala et al. 2012). The pH_{PZC} value for ICG is close to 6 (Pintor, Vieira et al. 2018), and the arsenate loading does not change this value significantly (Pintor, Vieira et al. 2020). Consequently, for all pH levels of the alkaline solutions examined, the surface of ICG is deprotonated and negatively charged, resulting in the release of the negatively charged arsenate molecule (Sarkar, Blaney et al. 2008). A study of the "shared charge" for oxyanions has found that OH^- has the highest affinity to form a bond with Fe^{3+} compared to AsO_4^{3-} and CO_3^{2-} (Tuutijärvi, Vahala et al. 2012), which justifies a higher desorption efficiency for NaOH and KOH solutions. However, KOH 0.1 M solution dissolved more iron than NaOH 0.1 M solution, which may have reduced its desorption efficiency.

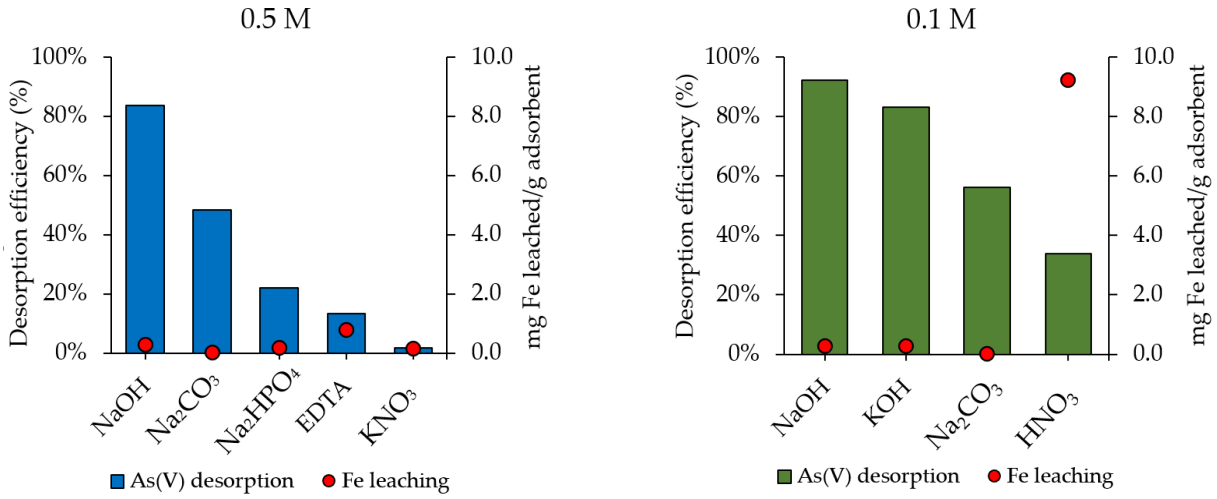


Figure 4.1: Arsenate desorption efficiency and iron leaching from ICG for different eluents and concentrations (S/L ratio of 2.5 g L^{-1}; T = 20°C).

4.3.1.2 Effect of eluent concentration

In this section, a deeper investigation of the effect of eluent concentration was carried out with NaOH and Na_2CO_3, which achieved the best desorption efficiency for the respective class of eluents (section 4.3.1.1) and the lowest iron dissolution. The desorbing efficiency of NaOH solutions was investigated in

the range 0.01 - 0.5 M and that of Na_2CO_3 in the range 0.01 - 2 M. The results are presented in Figure 4.2 and

Table 4.1.

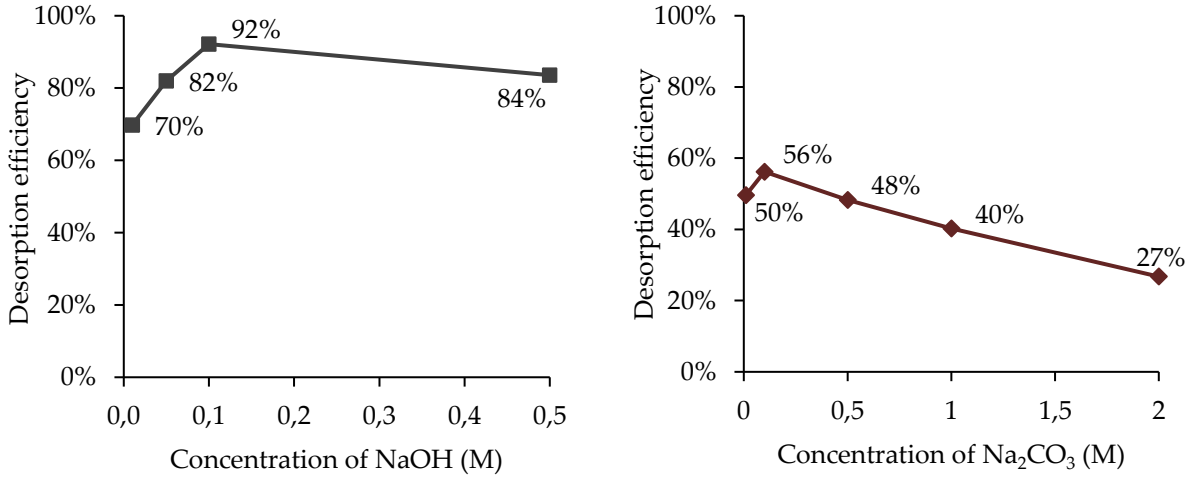


Figure 4.2: Arsenate desorption efficiency using NaOH and Na_2CO_3 solutions at different concentration (S/L ratio - 2.5 g L^{-1}; T = 20ºC).

From Figure 4.2 it can be observed that the variation in eluent concentration causes, firstly, an increase in desorption removal, followed by a decrease. The trend at higher concentrations could be caused by a degradation of the cork structure under strong basic solutions (Machado, Carvalho et al. 2002). Furthermore, a similar tendency was also observed for As(V) desorption from granular ferric hydroxide (GFH) using sodium hydroxide in the range 1% - 6% w/v, with a higher desorption rate achieved for 2% (Chen, Sorg et al. 2015). For commercial adsorbent ARM 200 (VV), the optimum NaOH concentration was found to be 4%, with a desorption efficiency of 87.2% (Chen, Sorg et al. 2015).

The optimal concentration for both NaOH and Na_2CO_3 was found to be 0.1 M. The desorption efficiencies of basic solutions were much higher than that of salt solutions; hence, NaOH was chosen as the optimal eluent for arsenic from ICG. The iron leached from the adsorbent after 24 h in contact with 0.1 M NaOH was 0.21 mg g^{-1}, which is less than 1% of the total iron content of the ICG.

The 92% desorption efficiency of arsenate from ICG by NaOH 0.1 M was higher than that reported for other iron-based adsorbents, such as iron-impregnated biochar, with a desorbing capacity of 72% (He, Peng et al. 2018), and GFH, with 36.5% desorption, for a 1 M concentration (Chen, Sorg et al. 2015).

4.3.1.3 Desorption kinetics

The regeneration of arsenic-loaded adsorbents can produce highly toxic waste. The minimization of both the eluent volume and chemical additions is important, and can be reached by understanding the effects of eluent composition on the equilibrium and kinetics of arsenic desorption (Chaudhary and Farrell 2015). In this section, the kinetics of As(V) desorption from ICG was investigated using NaOH 0.1 M and 0.01 M as desorbing agents. Saturated adsorbents containing 3.9 ± 0.5 mg As(V) g^{-1} and 3.7 ± 0.6 mg As(V) g^{-1} were used for assays with NaOH 0.1 M and NaOH 0.01 M, respectively. The results are presented in Figure 4.3 and Table 4.2.

Desorption using 0.1 M NaOH starts with a rapid increase in the first four hours, followed by a slower second stage (4-24 h). The same trend was also observed in As(V) desorption kinetics on Ni/Mn-LDH-biochar (Wang, Gao et al. 2016) and Fe-biochar (He, Peng et al. 2018) in similar conditions.

The Elovich model fit to the experimental data using NaOH 0.1 M (r^2 = 0.999) and NaOH 0.01 M (r^2 = 0.978) indicates a heterogeneous surface of the adsorbent (Coenen, Gallucci et al. 2019). Results show a slower desorption rate for the 0.01 M NaOH solution. This decrease in desorption rate was expected given the reduction of the available molecules to cleave the arsenate bonds with the adsorbent.

We observed that some samples acquired an orange-yellow colouration, which could indicate a degradation of the adsorbent (Figure 4.4). So, TOC was measured to better understand the impact of eluent on the adsorbent integrity. Both concentrations of sodium hydroxide provoke a disintegration of the adsorbent, which leads to an increase of TOC concentration in the basic solution (Figure 4.5). The stronger basic solution caused significantly higher harm in the ICG, with higher observed TOC concentrations, especially after four hours of contact time. The NaOH 0.01 M solution caused a steep increase in TOC after 16 contact hours. Following TOC results, desorption kinetics for NaOH 0.01 M was studied until 16 h.

At 16 h of contact, the TOC concentration in the solution was 21.4 mg L^{-1} for NaOH 0.01 M, compared to 140.7 mg L^{-1} for NaOH 0.1 M, which is approximately seven times higher. So, the NaOH 0.01 M basic solution was considered more suitable for arsenic desorption from ICG in batch mode, even leading to a lower desorbing capacity.

Table 4.2: Parameters obtained in the fitting of kinetic models to experimental data of desorption kinetics of As(V) from ICG using NaOH (20ºC; S/L = 2.5 g L^{-1}) (± standard error of the mean).

Model	Parameters	0.1 M NaOH	0.01 M NaOH
Pseudo-second-order model	q_e (mg g^{-1})	3.3 ± 0.2	1.9 ± 0.1
	k_2 (g mg^{-1} h^{-1})	0.5 ± 0.1	0.4 ± 0.1
	R^2	0.910	0.945
	SE	0.3	0.1
Elovich	a (mg g^{-1} h^{-1})	26 ± 2	2.7 ± 0.6
	b (g mg^{-1})	2.07 ± 0.03	2.7 ± 0.2
	R^2	0.999	0.978
	SE	0.03	0.08

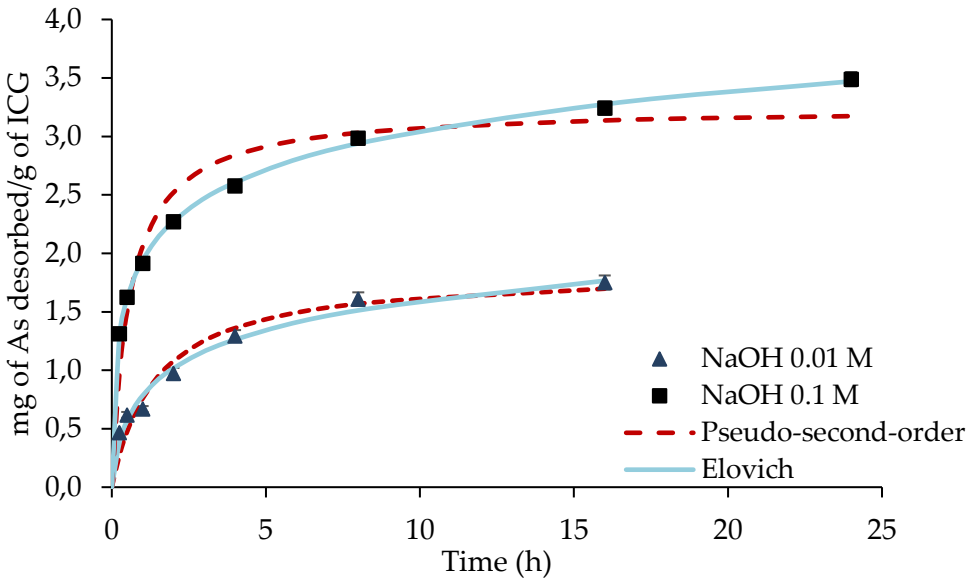


Figure 4.3: Desorption kinetics for arsenate from iron-coated cork granulates using different concentrations of NaOH (20ºC; S/L = 2.5 g L^{-1}) (Error bars: standard errors).

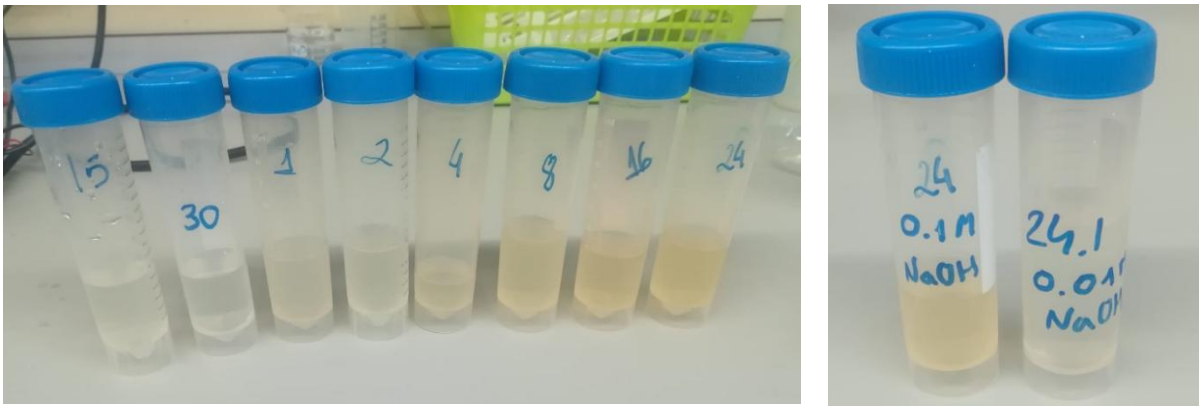


Figure 4.4: Coloration of desorption batch assays samples: a) kinetics of desorption using NaOH 0.1 M (left), b) 24h contact time desorption using NaOH 0.1 M and 0.01 M (right).

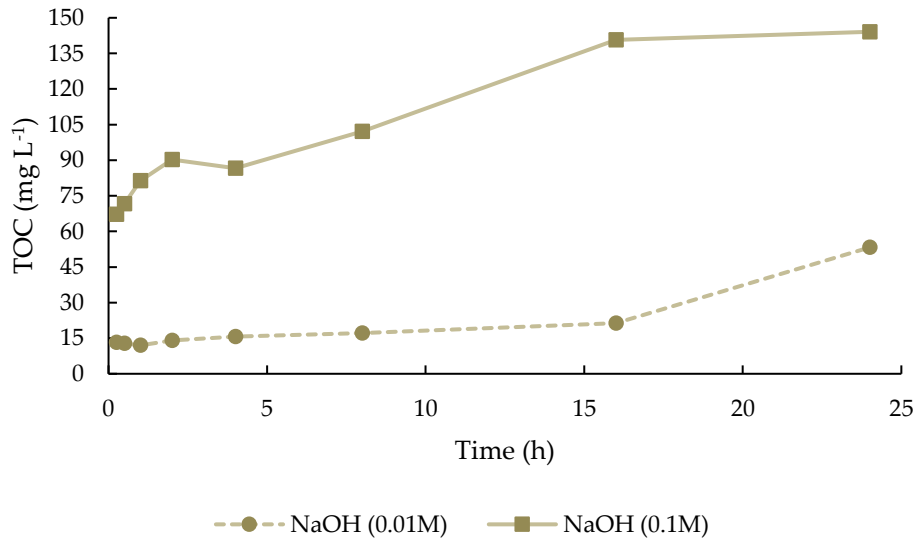


Figure 4.5: Total organic carbon in solution after contacting As-loaded ICG with NaOH.

4.3.1.4 Adsorption-desorption cycles in batch operation mode

The regeneration capacity of the arsenic-loaded adsorbent was investigated in batch mode. For more insights into the effect of eluent concentration, NaOH was applied as eluent in two concentrations: 0.01 M and 0.1 M. The results of adsorption-desorption cycles are presented in Table 4.3.

Even though the desorption rate with NaOH 0.01 M solution was lower than that achieved with NaOH 0.1 M, the weaker basic eluent was able to provide better preservation of adsorption capacity in consecutive adsorption-desorption cycles. The reduction in adsorption capacity after the 1st regeneration was much higher using NaOH 0.1 M than NaOH 0.01 M. The higher TOC values obtained for the NaOH 0.1 M eluent in comparison with NaOH 0.01 M, may help justify these results (Figure 4.5). TOC represents the degradation of the adsorbent properties after

contact with the desorbing agent that attacks the adsorbent structure. The loss in adsorption capacity in the successive cycles can also be related to the remaining arsenic content in the adsorbent (Tresintsi, Simeonidis et al. 2014). It was evident that after highly efficient desorption, such as in the 2nd cycle, the adsorption capacity will be better maintained in the following cycle, as observed between the 2nd and 3rd cycles.

Table 4.3: Performance of ICG on adsorption-desorption cycles using NaOH in batch mode (± standard error of the mean).

		0.01 M		0.1 M	
Cycle	**Assay**	**mg As(V)/ g of ICG**	**Desorption rate (%)**	**mg As(V)/ g of ICG**	**Desorption rate (%)**
1st	Adsorption	5.7 ± 0.2	-	5.0 ± 0.7	-
	Desorption	2.5 ± 0.2	43.1	4.4 ± 0.1	88.2
2nd	Adsorption	1.8 ± 0.1		0.6 ± 0.1	-
	Desorption	1.7 ± 0.2	93.7	-	-
3rd	Adsorption	2.04 ± 0.08			
	Desorption	1.1 ± 0.1	52	-	-
4th	Adsorption	1.0 ± 0.1			
	Desorption				

ICG was able to be regenerated by 0.01 M NaOH, for three cycles, after the first adsorption cycle using fresh ICG. The adsorbent was still able to remove high quantities of arsenic (1.0 mg g^{-1}) even after being exposed to the basic solution. The reduction in adsorption and desorption efficiency through the regeneration cycles was observed in other modified biosorbents, such as modified watermelon rind (Shakoor, Niazi et al. 2018), iron-impregnated biochar (He, Peng et al. 2018), and Fe(III) modified kapok fiber (Yeo, Li et al. 2022).

4.3.2 Adsorption-desorption cycles in a fixed-bed column

4.3.2.1 Arsenic aqueous solution

Lab-scale fixed-bed column assays were conducted using 1 mg As(V) L^{-1} distilled water for the adsorption and NaOH as eluent, in both concentrations of 0.1 M and 0.01 M, to evaluate the

regeneration capacity of ICG in continuous mode. The results obtained in consecutive adsorption-desorption cycles are presented in Figure 4.6 and

Table 4.4.

A trend similar to the batch results was observed in continuous mode. The regenerated ICG presented a lower adsorption capacity in comparison to the fresh ICG, and NaOH 0.01 M could regenerate ICG for more cycles. The breakthrough curves using the regenerated ICG were very much alike, using either NaOH 0.1 M or NaOH 0.01 M.

In the first hours of adsorption with regenerated ICG, a significant concentration of arsenic in the effluent was observed, as shown in Figure 4.6. However, the arsenic release decreased and ceased after a few hours, and then the typical adsorption process was initiated. The Yan model fitted well the adsorption data from all cycles ($r^2 > 0.98$).

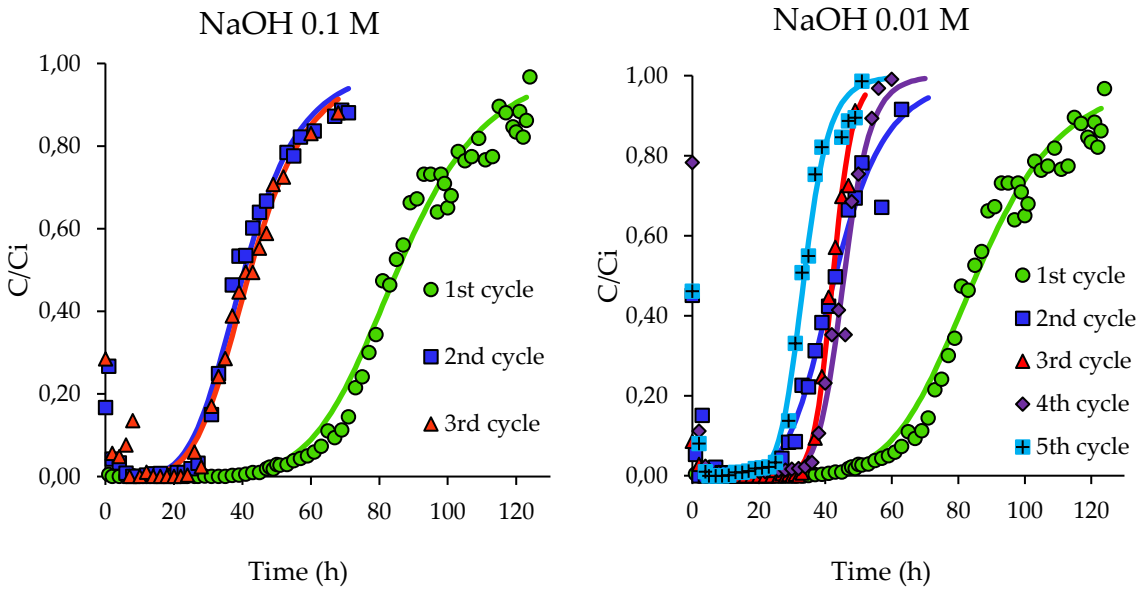


Figure 4.6: Experimental (points) and predicted (lines) breakthrough curves for fresh (1st cycle) and regenerated ICG after NaOH treatment (flow rate 5 mL min^{-1} and 6 g of ICG, C_i = 1 mg As(V) L^{-1}, pH 3.0).

The breakthrough time (t_b) from fresh ICG to regenerated ICG reduced from 46 to 23 h and from 46 to 25 h after treatment with NaOH 0.1 M and 0.01 M, respectively. In the following 3rd, 4th, and 5th adsorption cycles using regenerated ICG by NaOH 0.01 M tb was 34 h, 25 h, and 16 h. Saturation time (t_s) of regenerated ICG ranged from 51 to 63 h and from 68 to 71 h, using NaOH 0.01 M and 0.1 M, respectively. The bed volumes before breakthrough (BV_b) reduced from 253 (fresh ICG) to 147 and 140 after one desorption cycle with NaOH 0.01 M

and 0.1 M, respectively. The BV_b decreased approximately 63% from the 1st to the 5th adsorption cycle using NaOH 0.01 M. A reduction of about 65% was reported from the 1st to the 4th cycle in BV_b of beaded coal mine drainage sludge (BCMDS-YD), using NaOH 0.1 M as desorbing agent (Lee, Ren et al. 2022).

For the adsorption cycles using NaOH 0.1 M regenerated ICG, the treated volume before breakthrough (V_b) was 14.9, 7.0, and 8.2 L. For the adsorption cycles with regeneration carried out with NaOH 0.01 M, ICG was able to treat 14.9, 8.3, 10.5, 7.7, and 5.2 L of water under 10 µg L^{-1} consecutively after desorption cycles.

Fresh ICG achieved adsorption capacities at breakthrough (q_b) and saturation (q_s) of 2.0 and 3.8 mg g^{-1} in continuous mode. The treatment by sodium hydroxide 0.01 M caused a reduction in arsenate uptake after the first regeneration cycle of 30% and 36% in q_b and q_s, respectively. The impact was higher when using NaOH 0.1 M, with a diminution of almost 50% in both q_b and q_s. Figure 4.7 shows the adsorption capacities after each regeneration cycle using NaOH. The q_b of regenerated ICG decayed from 1.3 to 0.8 mg g^{-1} after four regeneration cycles using NaOH 0.01 M. For assays carried with NaOH 0.1 M, the q_b of regenerated ICG kept a constant value of 1.1 mg g^{-1}. Saturation capacities for regenerated ICG varied from 2.4 to 1.6 mg g^{-1} and from 1.9 to 2.0 mg g^{-1} using NaOH 0.01 M and 0.1 M, respectively.

Table 4.4: Experimental and theoretical parameters (Yan model) of arsenate continuous adsorption from arsenic aqueous solution onto fresh (first cycle) and regenerated (other cycles) ICG with NaOH (flow rate 5 mL min^{-1} and 6 g of ICG, C_i = 1 mg As(V) L^{-1}; pH 3.0).

	Parameter	First cycle	Second cycle	Third cycle	Fourth cycle	Fifth cycle
0.01 M	t_b (h)	45.6 ± 0.7	25.1 ± 0.3	33.5 ± 0.4	25 ± 2	16 ± 1
	t_s (h)	124	63	52	60	51
	BV_b	253 ± 16	147 ± 9	185 ± 18	136 ± 17	93 ± 10
	BV_s	689 ± 40	368 ± 22	287 ± 33	325 ± 38	351 ± 21
	V_b (L)	14.9 ± 0.3	8.3 ± 0.4	10.5 ± 0.9	8 ± 1	5.2 ± 0.4
	V_s (L)	40.6 ± 0.1	20.8 ± 0.1	16.2 ± 0.2	18.4 ± 0.2	19.8 ± 0.2
	q_b (mg g^{-1})	2.0 ± 0.2	1.4 ± 0.4	1.3 ± 0.1	1.0 ± 0.1	0.8 ± 0.2
	q_s (mg g^{-1})	3.9 ± 0.5	2.4 ± 1.1	1.6 ± 0.2	1.8 ± 0.2	1.8 ± 0.6
	y_b (%)	99.84 ± 0.03	98.1 ± 0.3	98.5 ± 0.2	95 ± 2	96 ± 1
	y_s (%)	72 ± 4	69 ± 13	81 ± 3	74 ± 4	67 ± 10
	Q_{ya} (mg g^{-1})	3.8 ± 0.3	2.4 ± 0.7	1.6 ± 0.2	1.9 ± 0.2	1.8 ± 0.4
	a_{ya}	6.7 ± 0.2	5.6 ± 0.4	14.4 ± 1.4	11.5 ± 1.0	9.0 ± 0.8
	SE (mg g^{-1})	0.04	0.05	0.05	0.05	0.04
	R^2	0.986	0.977	0.984	0.983	0.988
0.1 M	t_b (h)	45.6 ± 0.7	23.2 ± 0.6	24.3 ± 0.9	-	-
	t_s (h)	124	71	68	-	-
	BV_b	253 ± 16	123 ± 8	145 ± 15	-	-
	BV_s	689 ± 40	377 ± 22	405 ± 44	-	-
	V_b (L)	14.9 ± 0.3	7.0 ± 0.2	8.2 ± 0.4	-	-
	V_s (L)	40.6 ± 0.1	21.3 ± 0.1	22.8 ± 0.3	-	-
	q_b (mg g^{-1})	2.0 ± 0.2	1.08 ± 0.05	1.0 ± 0.1	-	-
	q_s (mg g^{-1})	3.9 ± 0.5	2.0 ± 0.2	1.9 ± 0.4	-	-
	y_b (%)	99.84 ± 0.03	97.3 ± 0.3	96 ± 1	-	-
	y_s (%)	72 ± 4	60 ± 3	64 ± 6	-	-
	Q_{ya} (mg g^{-1})	3.8 ± 0.3	1.9 ± 0.1	1.9 ± 0.2	-	-
	a_{ya}	6.7 ± 0.2	4.9 ± 0.3	5.0 ± 0.3	-	-
	SE (mg g^{-1})	0.04	0.05	0.04	-	-

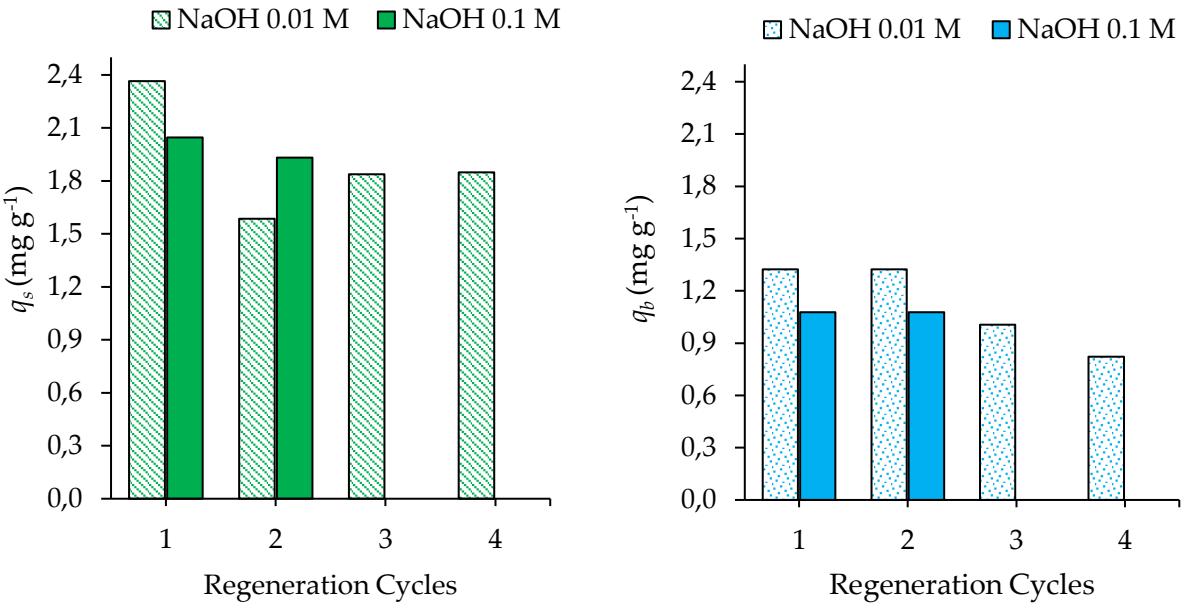


Figure 4.7: Adsorption capacities of regenerated ICG, using NaOH 0.1 M and 0.01 M, in successive adsorption-desorption cycles in continuous mode (flow rate 5 mL min^{-1} and 6 g of ICG): a) at saturation (left), b) at breakthrough (right).

The performance of breakthrough curves from fresh ICG to regenerated ICG by NaOH 0.01 M was essentially affected, with a reduction in almost all parameters (t_b, t_s, BV_b, BV_s, q_b, q_s, V_b, V_s, y_b, y_s) except two, MTZ and MTZ/bed height. The values of these parameters for the fixed-bed column assay using fresh ICG were 7.6 cm and 0.63, respectively, whereas for regenerated ICG using NaOH 0.01 M, they reduced to 6.9 and 0.60, 4.1 and 0.36, 6.7 and 0.58, respectively, for the 2nd, 3rd, and 4th cycles of adsorption. The shortening in these parameters means an improvement in the fixed-bed column efficiency overall by increasing the utilized bed height. The adsorption cycles using NaOH 0.1 M and the last adsorption cycle (5th) using NaOH 0.01 M presented lower fixed-bed performance, like the assay carried with fresh ICG. The fact that the fixed-bed column was more efficient through most of the adsorption cycles with regenerated ICG using NaOH 0.01 M suggests that the reduction of adsorption efficiency observed after desorption is caused by the residual arsenic content in the adsorbent.

This effect can be observed in the breakthrough curves (Figure 4.6), in which BTCs after NaOH 0.01 M treatment are steeper than BTC at 1st adsorption cycle (fresh ICG) and BTCs from regeneration cycles with NaOH 0.1 M.

The desorption efficiency through the regeneration cycles was 62%, 113% and 130% for 1st, 2nd, and 3rd desorption cycles, respectively, using NaOH 0.1 M. For the weaker basic solution,

the desorption efficiencies were 74%, 77%, 139%, and 103% for the 1st, 2nd, 3rd, and 4th cycles, respectively. The desorption parameters are presented in
Table 4.5. The desorption capacity varied from 1.8 to 2.5 mg g^{-1} and 2.3 to 2.7 mg g^{-1} for NaOH 0.01 M and 0.1 M, respectively. The desorption capacities using the stronger basic solution were slightly higher, as observed in batch mode (4.3.1.2). The efficiencies above 100% in some of the later desorption cycles can be explained by the desorption of residual arsenic from previous cycles.

Table 4.5: Parameters from desorption cycles of ICG regeneration after continuous adsorption with arsenic aqueous solution.

	Parameter	First cycle	Second cycle	Third cycle	Fourth cycle
0.01 M	*Qd (mg g^{-1})*	2.5 ± 0.2	1.8 ± 0.2	2.2 ± 0.1	1.9 ± 0.1
	Yd (%)	74 ± 12	76 ± 9	135 ± 5	107 ± 4
	BV_d	178 ± 15	148 ± 16	140 ± 9	112 ± 7
	V (L)	10.0 ± 0.6	8.4 ± 0.7	7.9 ± 0.2	6.3 ± 0.2
0.1 M	*Qd (mg g^{-1})*	2.7 ± 0.1	2.3 ± 0.2	2.5 ± 0.8	-
	Yd (%)	62 ± 6	113 ± 12	130 ± 41	-
	BV_d	19 ± 1	24 ± 2	24 ± 2	-
	V (L)	1.10 ± 0.04	1.3 ± 0.1	0.77 ± 0.02	-

The desorption profiles for both basic solutions are displayed in Figure 4.8. The desorption using NaOH 0.1 M was faster than NaOH 0.01 M. The stronger basic solution was able to desorb the arsenic from the adsorbent in 3 h, but the weaker base required more than 20 h to achieve a good desorption efficiency. This means a consumption of approximately 19 BV and 1 L of eluent using NaOH 0.1 M and about 145 BV and 8.1 L of eluent using NaOH 0.01 M. The maximum concentrations of arsenic eluted were 173.7 mg L^{-1} at 0.1 h and 30.3 mg L^{-1} at 0.5 h, for NaOH 0.1 M and 0.01 M, respectively. The maximum concentrations increased after each desorption cycle in both scenarios, suggesting that the arsenic adsorbed on the regenerated ICG was not bound as strongly to the adsorbent.

A different trend was reported in other studies where a decay in maximum concentrations of arsenic was observed after each desorption cycle (Gupta, Chauhan et al. 2009, Lee, Ren et al. 2022). Lee et al. (2022) reported a maximum concentration of approximately 40 mg L^{-1} of arsenic in the eluted solution after 0.2 h, 0.33 h and 0.5 h, respectively, after 1st, 2nd, and 3rd desorption cycle of saturated BCMDS, using NaOH 0.1 M. For iron-chitosan composites saturated with an inlet solution of 0.5 mg As L^{-1} the maximum concentrations of arsenic in desorption ranged from approximately 3.2 to 0.8 mg L^{-1}, using NaOH 0.1 M (Gupta, Chauhan et al. 2009). The

highest leached arsenic concentration of roughly 25 mg L^{-1} was also observed in the first minutes of desorption of Fe-impregnated biochar using $NaHCO_3$ (Hu, Ding et al. 2015). For sulfate-modified iron oxide-coated sand (SMIOCS), the maximum concentration of arsenic in the NaOH 0.2 M desorption solution was 5.7 mg L^{-1} after 1.5 h (Vaishya and Gupta 2006).

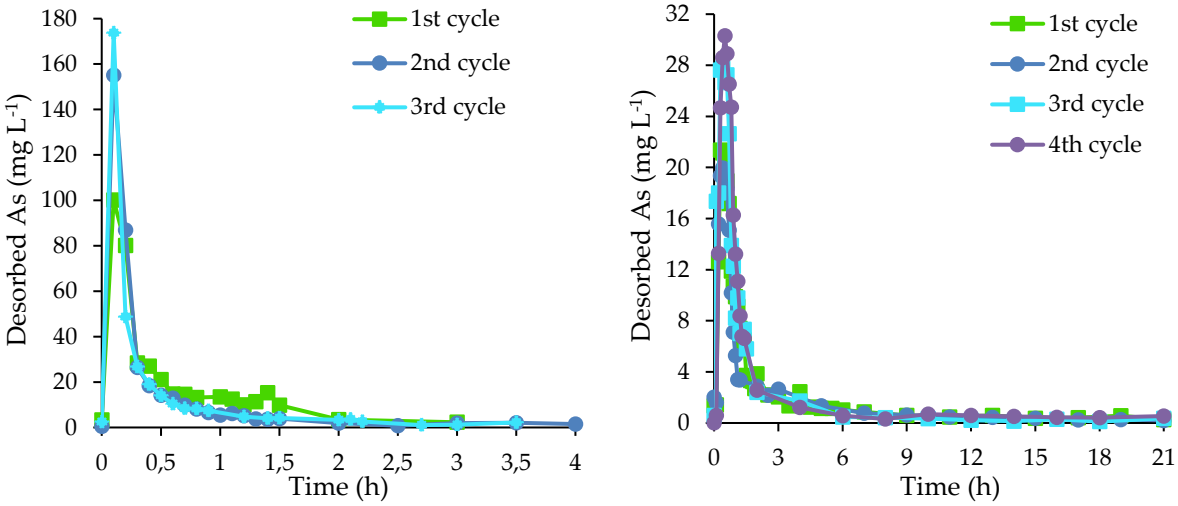


Figure 4.8: Desorption profile using: 0.1 M NaOH (left), 0.01 M NaOH (right).

During regeneration cycles, the TOC and iron content in the samples were monitored. A colouration was observed in the samples after NaOH 0.1 M treatment (Figure 4.9), similarly to batch desorption (Figure 4.4). Figure 4.10 presents the boxplot graph for the TOC of samples from desorption in continuous mode. The TOC measured in the samples from each desorption cycle was on average 10.1, 11.6, 11.1, and 11.4 mg L^{-1} for 1st, 2nd, 3rd, and 4th cycles, respectively, using NaOH 0.01 M. For 1st, 2nd, and 3rd cycles of desorption using NaOH 0.1 M the average values were 109.2, 69.2, and 43.5 mg L^{-1}, respectively. The results showed a proportional increase in TOC values similar to the reported results in batch (Figure 4.5), of about 4-10 times higher concentration with NaOH 0.1 M than 0.01 M. The TOC values decayed through desorption cycles after treatment with NaOH 0.1 M, but the application of the weaker base kept TOC values almost constant through the desorption runs.

TOC results confirm the higher degradation in the ICG after treatment with NaOH 0.1 M, which justifies the limited application of the stronger basic solution for only 3 cycles in continuous mode and two cycles in batch mode (item 4.3.1.4). In regeneration studies conducted with iron-chitosan composites, TOC values ranging from 10.2 to 12.2 mg L^{-1} in the desorption effluent after two regeneration cycles with 0.1 M NaOH have been reported and considered to be acceptable values (Gupta, Chauhan et al. 2009).

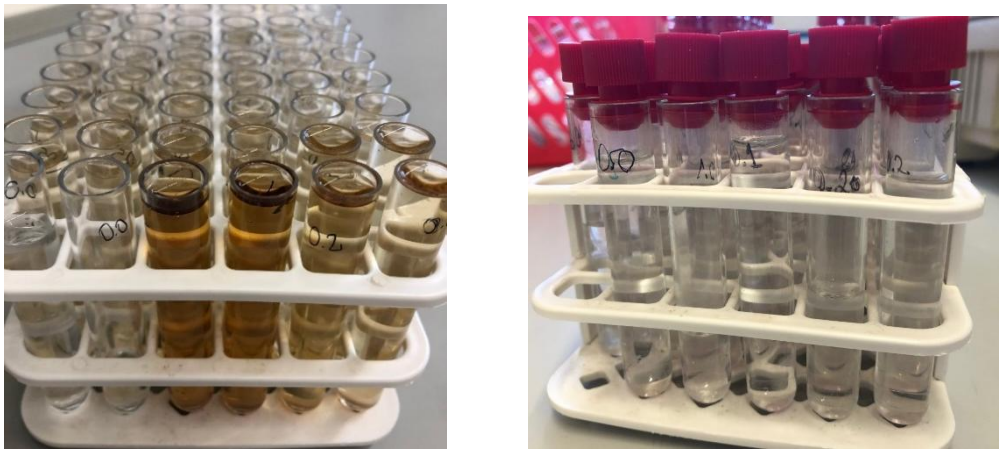


Figure 4.9: Continuous desorption samples for NaOH 0.1 M (left) and 0.01 M (right).

The adsorbent degradation can also be expressed in terms of iron leached from ICG after desorption, as the iron layer in the adsorbent is essential to keep the arsenic removal capacity in the following regeneration cycles. Figure 4.11 shows the iron leached in each desorption cycle carried out with NaOH. The maximum concentration of iron was higher for NaOH 0.1 M than for NaOH 0.01 M treatment.

Table 4.6: Iron leaching from each adsorption-desorption cycle in continuous mode using NaOH 0.1 M and NaOH 0.01M.

		0.01 M			0.1 M		
Cycle	**Assay**	**mg Fe**	**Assay duration (h)**	**mg Fe / assay duration (mg h^{-1})**	**mg Fe**	**Assay duration (h)**	**mg Fe / assay duration (mg h^{-1})**
1st	Adsorption (Fresh ICG)	0.0	124	0.00	0.0	169	0.00
	Desorption	0.5	24	0.02	0.4	3	0.12
2nd	Adsorption	15.4	63	0.24	13.0	71	0.18
	Desorption	0.1	12	0.01	0.6	4	0.14
3rd	Adsorption	6.8	52	0.13	17.9	68	0.26
	Desorption	0.2	22	0.01	0.6	3	0.20
4th	Adsorption	10.8	60	0.18	-	-	-
	Desorption	0.6	21	0.03	-	-	-
5th	Adsorption	10.2	51	0.20	-	-	-
	Desorption	-			-	-	-

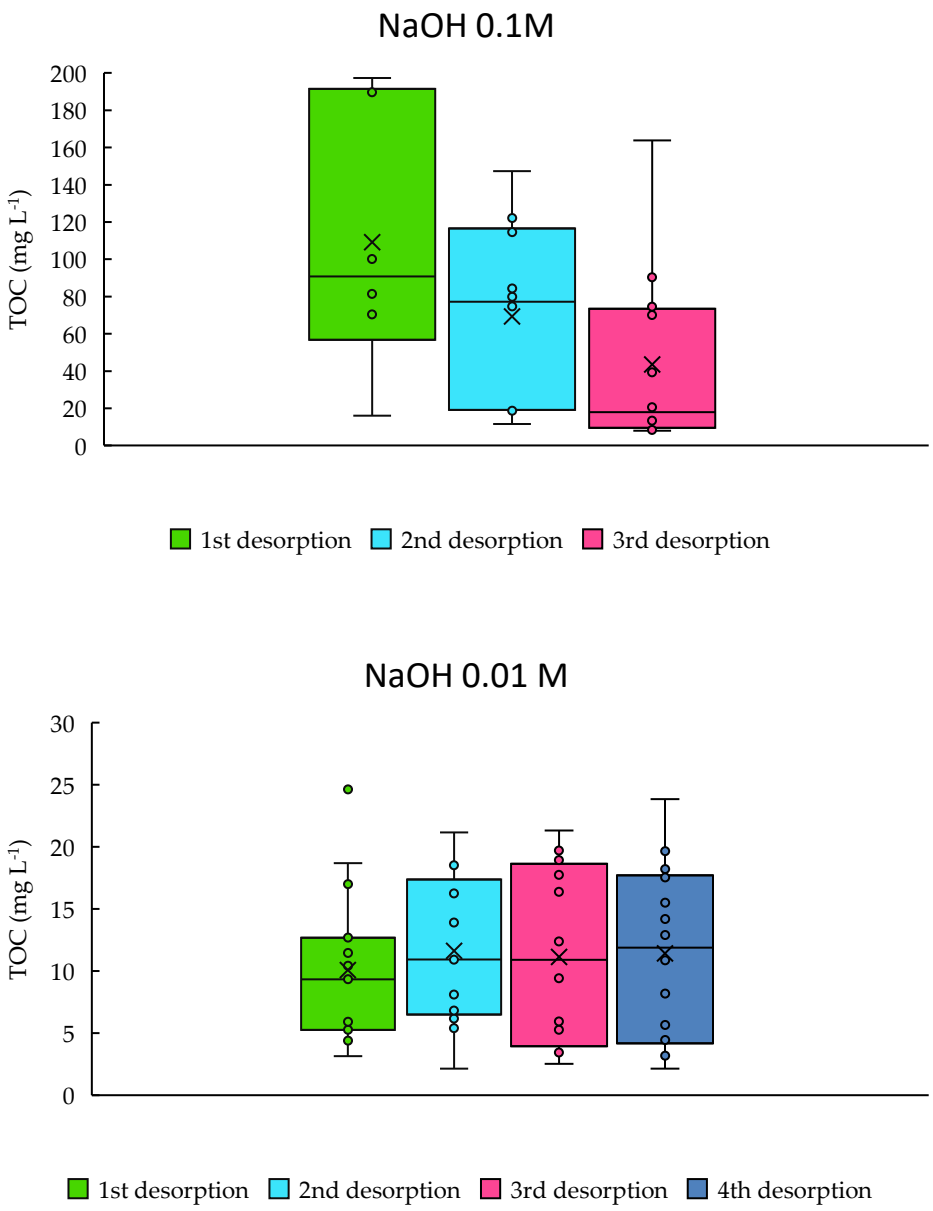


Figure 4.10: Boxplot graph of total organic carbon for desorption cycles in continuous mode, using 0.1 M NaOH (top) and 0.01 M NaOH (bottom).

The calculation of the iron leached in each assay was carried out by measuring the area below the curve of iron leaching versus time for each adsorption/desorption cycle. The results are presented in Table 4.6. It was observed a higher iron leaching in adsorption than in desorption cycles. However, using NaOH 0.1 M, the rate of iron leaching in desorption was also high (Table 4.6). This indicates that NaOH 0.1 M was more aggressive to the adsorbent than NaOH 0.01 M.

The increase in iron leaching related to an increase in NaOH concentration was also reported (Chaudhary and Farrell 2015) in regeneration studies of ferric hydroxide-based adsorbents.

The authors attributed the iron leaching to the formation of $Fe(OH)_2^+$ ions. The consequent decrease in the adsorbent active site is tied to a decline in the regenerated adsorbent´s performance.

The iron content was quantified in the fresh adsorbent and after 3 and 5 continuous cycles with desorption using NaOH 0.1 M and NaOH 0.01 M, respectively, to assess the degradation of the active sites in the adsorbent. Two methods were used: calculation of area below curve using experimental adsorption/desorption data and results from acid digestion of a saturated sample of adsorbent followed by FAAS (Table 4.7). By calculating the iron mass balance through experimental data of iron leaching, a reduction of 19% and 25% of iron content (mg Fe g^{-1} ICG) was found after all adsorption-desorption cycles using NaOH 0.1 M and NaOH 0.01 M, respectively, considering the remaining iron mass and the initial adsorbent mass of 6 g. A higher reduction in iron content was expected in the material treated with NaOH 0.01 M because it went through more adsorption/desorption cycles. By acid digestion, the reduction in iron loading on regenerated ICG was 4% and 18%, for NaOH 0.1 M and NaOH 0.01 M, respectively (Table 4.7). The difference in the iron content reduction found by each determination method can be explained by the mass loss in the cork structure, which was previously verified by TOC measurements. A more substantial mass loss is confirmed using NaOH 0.1 M due to the higher difference in the iron content values found by each method (4% to 19%) compared to NaOH 0.01 M (18% to 25%).

Figure 4.12 shows SEM micrographs of fresh ICG, and ICG treated with NaOH 0.01 M and 0.1 M, in continuous mode, after 5 and 3 cycles of operation, respectively. It is possible to note that regenerated ICG have cellular structural deformation compared to fresh ICG. The ICG treated with NaOH 0.01 M (Figure 4.12.a) show thinning of the cell walls but maintain the layered structure of the cells present in fresh ICG. However, the ICG treated with NaOH 0.1 M (Figure 4.12.b) show further degradation, with wrinkled cells and an unstructured cellular arrangement (Figure 4.12.c). Even after alkaline treatment, iron is still present in both samples in its original heterogeneous distribution, though at lower concentrations. EDS analysis of the materials is presented in Figure 4.13. The elements Fe, C, O are the most abundant in all samples and As are presented in the treated samples.

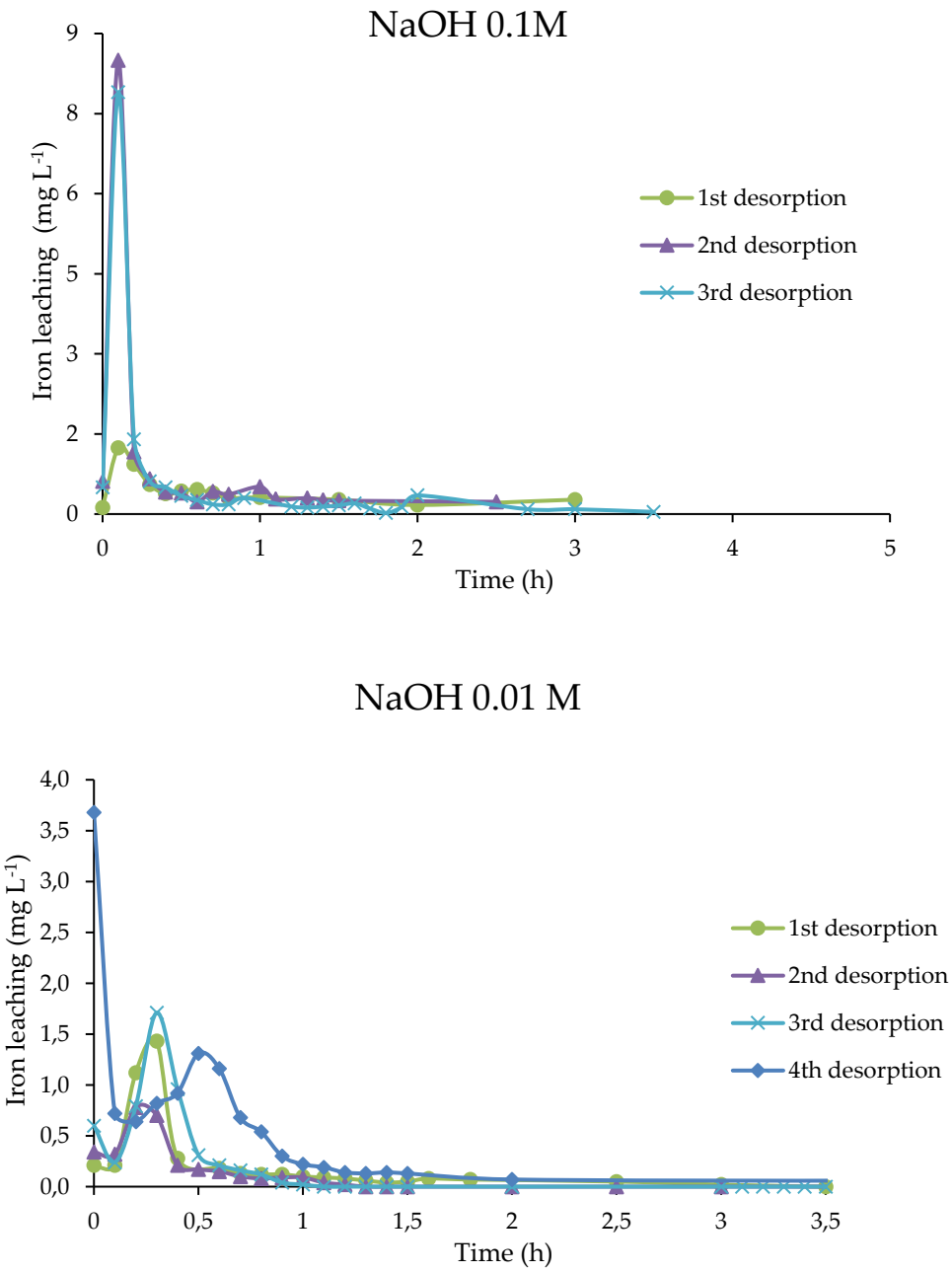


Figure 4.11: Iron leaching from desorption cycles in continuous mode, using 0.1 M NaOH (top) and 0.01 M NaOH (bottom).

Table 4.7: Iron content of ICG before and after adsorption-desorption cycles in continuous mode using NaOH, measured by FAAS after acid digestion.

Sample	Iron composition (mg g^{-1})		Reduction
	Before	After	(%)
ICG treated with NaOH 0.1 M	28 ± 1	26 ± 1	4

(Three adsorption cycles and three desorption cycles)			
ICG treated with NaOH 0.01 M (Five adsorption cycles and four desorption cycles)	23 ± 1	19 ± 1	18

Table 4.8 presents the effect of regeneration in different adsorbents. Generally, the adsorbent suffers a loss of adsorption capacity, which on regenerated ICG was lower than the loss suffered by iron oxide-coated biomass (IOCB) after one desorption cycle. However, other adsorbents such as commercial ArsenX^{np}, Lewatit FO36, and biosorbent rice polish could pass through desorption with a minor drop in adsorption capacity. The reduction in adsorption capacity can be related to the incomplete recovery of arsenic from the bed media or the modification in the adsorbent´s properties after treatment under high pH values (Chaudhary and Farrell 2015).

Table 4.8: Comparison between new and regenerated adsorbents for As(V) removal in continuous mode.

Adsorbent	**Cycle**	**Initial As concentration ($\mu g\ L^{-1}$)**	**Saturation capacity ($mg\ g^{-1}$)**	**Breakthrough time (h)**	**Estimated loss on adsorption capacity (%)**	**Ref.**
	1st	100	0.47	-	40.4	

Iron oxide-coated biomass (IOCB)	2nd	100	0.28	-		(Pokhrel and Viraraghavan 2008)
ArsenXnp	1st	200	~6.2	-	11.3	(Sarkar, Blaney et al. 2007)
	2nd	200	~5.5	-		
Lewatit FO36	1st	500	3.229	-	12.48	(Boldaji, Nabizadeh et al. 2010)
	2nd	500	2.826	-		
Rice polish	1st	1,000	0.079	18	16.5	(Ranjan, Talat et al. 2009)
	2nd	1,000	0.066	17		
Iron-coated cork granulates (ICG)	1st	1,000	3.8	46	36.8	This study
	2nd	1,000	2.4	25		

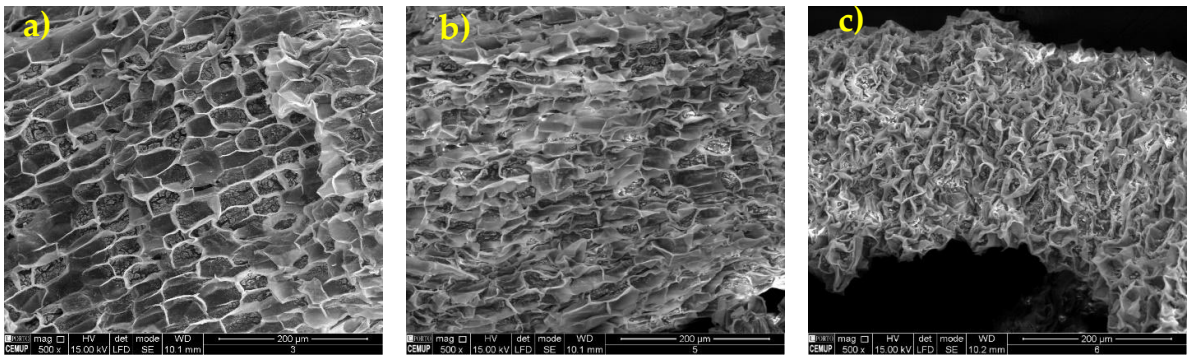


Figure 4.12: SEM micrographs of: a) iron-coated cork granulates, 500x magnification, b) iron-coated cork granulates treated with NaOH 0.01 M, 500x magnification; c) iron-coated cork granulates treated with NaOH 0.1 M, 500x magnification

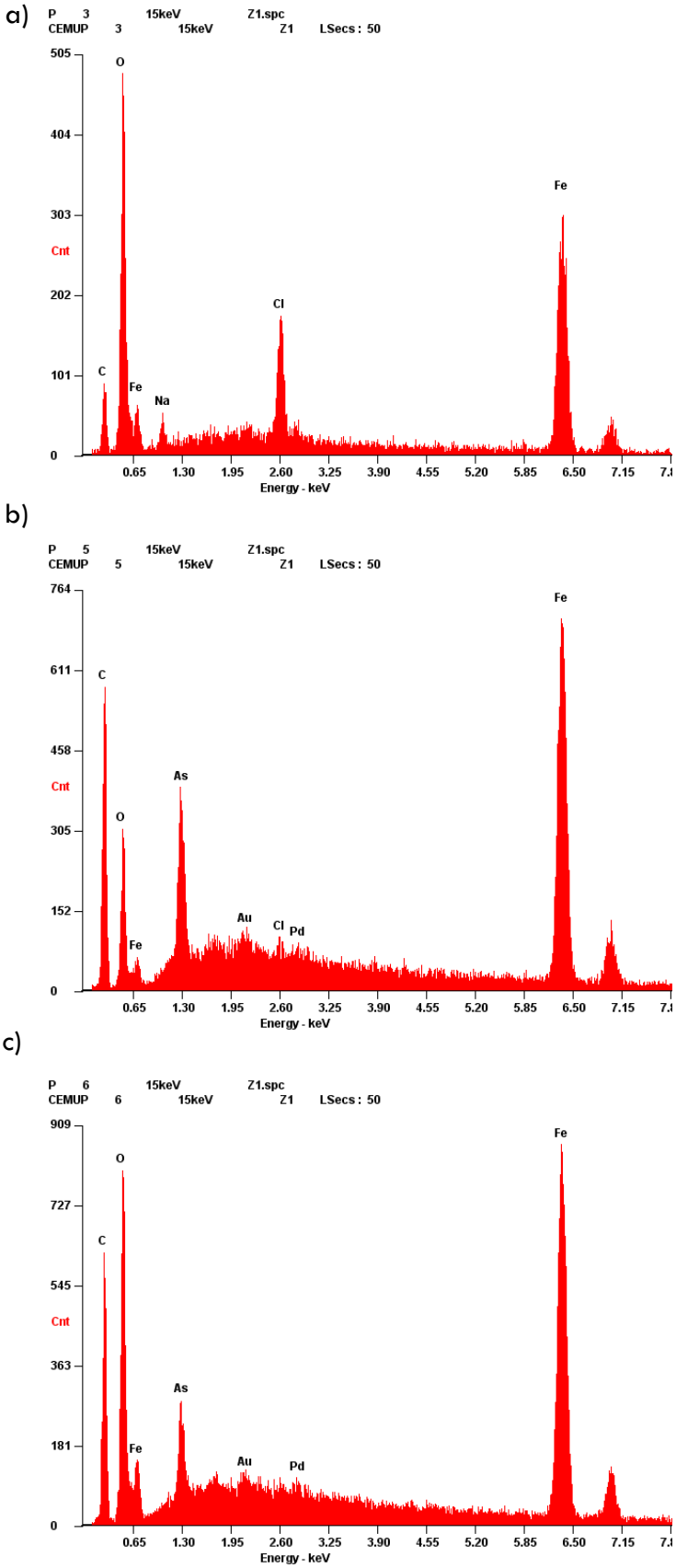


Figure 4.13: EDS analysis of a) iron-coated cork granulates, b) iron-coated cork granulates treated with NaOH 0.01 M, c) iron-coated cork granulates treated with NaOH 0.1 M.

4.3.2.2 Arsenic-contaminated groundwater

Studies were conducted with natural groundwater contaminated with arsenic to evaluate the applicability of ICG in a real scenario. The groundwater characterisation is shown in Table 4.9.

Table 4.9: Characteristics of the groundwater sample collected in Northeastern Portugal.

Parameter	**Concentration (mg L^{-1})**
Total solids	320 ± 10
Total dissolved solids	310 ± 2
Arsenic	0.020 ± 0.001
NO_3^-	ND (<0.8)
SO_4^{2-}	40.2 ± 0.2
PO_4^{3-} (as P)	ND (< 0.03)
TOC	4 ± 1
Iron	ND (<0.09)
Boron	0.06 ± 0.05
Lithium	0.10 ± 0.01
Magnesium	10.6 ± 0.2
Manganese	0.3 ± 0.1
Potassium	2.61 ± 0.03
Sodium	ND (<0.2)
Calcium	ND (<0.15)
Zinc	ND (<0.15)

Adsorption-desorption cycles were carried out in continuous mode using real-spiked groundwater with 0.1 mg L^{-1} of total As at the natural pH of the water of 7.09 ± 0.01. The desorption experiments were carried out with 0.1 M NaOH. The results are shown in Figure 4.14, Figure 4.15 and Table 4.10.

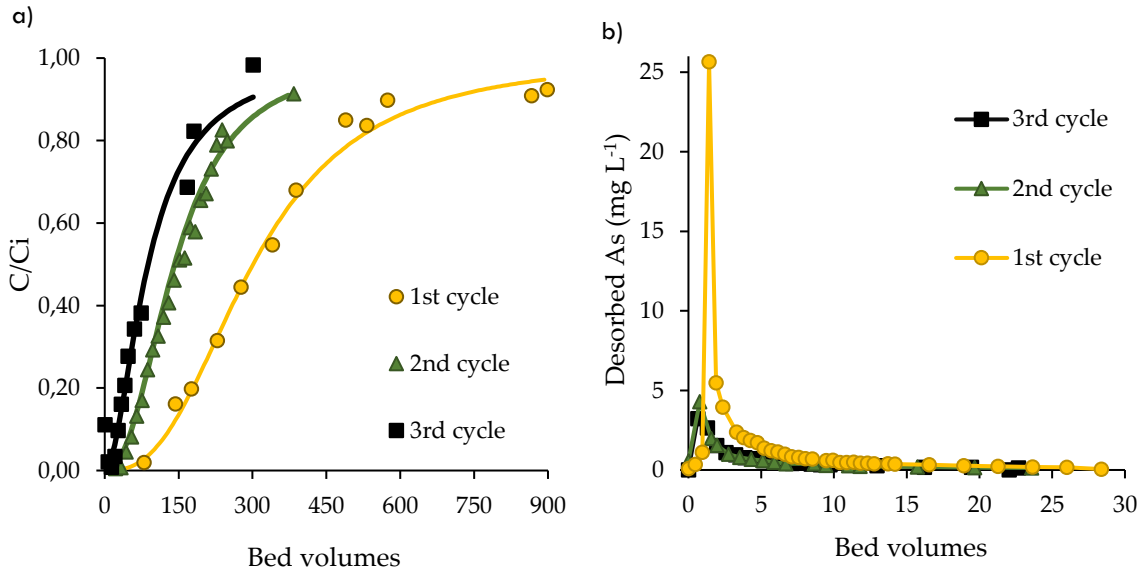


Figure 4.14: Adsorption-desorption cycles: a) Experimental (points) and predicted (lines) breakthrough curves for new (1st cycle) and regenerated (2nd and 3rd cycles) ICG using real-spiked groundwater (flow rate 5 mL min^{-1} and 6 g of ICG), b) desorption profiles for three cycles using 0.1 M NaOH.

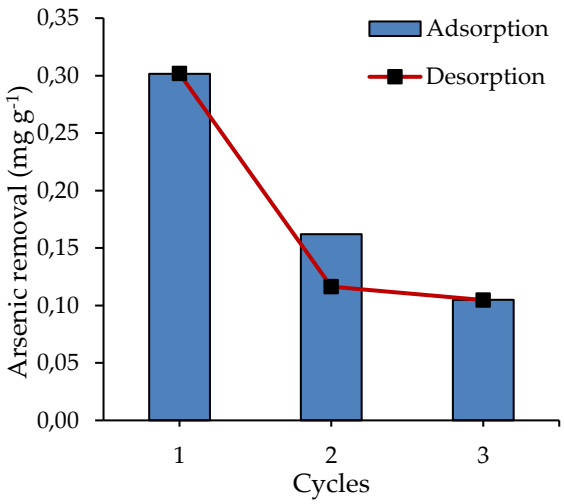


Figure 4.15: Adsorbed and desorbed amount of As in three adsorption-desorption cycles by ICG using As-spiked groundwater (flow rate of 5 mL min^{-1}; 6 g of ICG; 20ºC; C_i = 0.1 mg L^{-1}).

Table 4.10: Experimental and predicted breakthrough parameters of arsenic adsorption from real groundwater onto fresh (first cycle) and regenerated (second and third cycle) ICG (± standard error of mean).

		Parameter	First cycle	Second cycle	Third cycle
Experimental	Breakthrough at 10 µg L^{-1}	t_b (h)	26 ± 2	10.7 ± 0.8	4.3 ± 0.6
		q_b (mg g^{-1})	0.12 ± 0.01	0.054 ± 0.004	0.025 ± 0.004
		BV_b	140 ± 13	58 ± 6	29 ± 5
		V_b (L)	7.9 ± 0.5	3.3 ± 0.3	1.6 ± 0.3
		y_b (%)	99.2 ± 0.6	98.3 ± 0.2	98.6 ± 0.3
	Breakthrough at 50 µg L^{-1}	t_b (h)	64 ± 2	27.6 ± 0.8	18.0 ± 0.8
		q_b (mg g^{-1})	0.23 ± 0.02	0.12 ± 0.01	0.09 ± 0.01
		BV_b	341 ± 25	132 ± 10	120 ± 13
		V_b (L)	19 ± 0.8	7.5 ± 0.3	6.8 ± 0.6
		y_b (%)	87 ± 1	83 ± 1	89 ± 2
	Saturation at C/C$_0$ = ~0.90	t_s (h)	169	71	45
		q_s (mg g^{-1})	0.30 ± 0.05	0.16 ± 0.01	0.10 ± 0.09
		BV_s	898 ± 58	384 ±25	301 ± 30
		V_s (L)	50.7 ± 0.1	21.7 ± 0.1	17.0 ± 1.4
		y_s (%)	39 ± 5	45 ± 4	39 ± 4
		MTZ (cm)	9.7	9.8	10.4
		MTZ/Bed height	0.84	0.85	0.90
Yan Model		Q_{ya} (mg g^{-1})	0.26 ± 0.01	0.14 ± 0.01	0.08 ± 0.01
		a_{ya}	2.7 ± 0.1	2.4 ± 0.1	1.8 ± 0.1
		SE (mg g^{-1})	0.03	0.03	0.04
		r^2	0.992	0.993	0.984

The breakthrough time and the arsenic removal efficiency before breakthrough (y_b) were 26 h and 99.2 %, respectively, using fresh ICG. The Yan model fitted best the breakthrough curve (r^2 = 0.992) with a predicted adsorption capacity of 0.26 ± 0.01 mg g^{-1}. ICG adsorption capacities from fixed-bed column studies using synthetic solutions (similar operational conditions) were 1.5 ± 0.2 mg g^{-1} for As(V) and 0.8 ± 0.1 mg g^{-1} for As(III) (Chapter 3). The reduction of arsenic adsorption capacity by ICG can be related to the presence of interferents, such as sulfates (concentration of 40.2 ± 0.2 mg L^{-1}). Sulfate was identified to reduce As(III) removal by zerovalent iron (Su and Puls 2001), zirconium-based material (ZrPACM-43) (Mandal, Sahu et al. 2013), and hydrous ferric oxide (HFO) (Inam, Khan et al. 2021), more specifically in the pH range from 4 to 7 (Wilkie and Hering 1996). The competitive effect of sulfate was also observed in As(V) adsorption by FHO (Wilkie and Hering 1996, Inam, Khan et al. 2021), by activated modified biochar (Alam, Shaikh et al. 2018), and by Fe(III) modified kapok fiber (Yeo, Li et al.

2022). The water applied in this study could either have As(V), As(III) or both species because As(III) could be already present in groundwater spiked with a general arsenic standard.

It is found in the literature that several alternative adsorbents were investigated in the removal of arsenic from real groundwater (spiked or not), as the results are shown in

Table 4.11. It is possible to note that the adsorbents showed very similar results, with no outlier in terms of adsorption of real groundwater performance. The comparison between various adsorbents' performance is difficult because each assay was carried out in different experimental conditions, such as EBCT and initial arsenic concentration. Nevertheless, slightly better results were found in studies with iron-oxide-coated natural rock (IOCNR), iron-chitosan granules (ICB), and iron-coated cork granulates (ICG) in terms of BV_s before the breakthrough.

ICG saturated with arsenic were regenerated for further adsorption tests. The results show that the adsorbent loses 50% of its arsenic uptake capacity after each regeneration cycle but can still remove arsenic under 10 µg L^{-1} during three adsorption-desorption cycles. The adsorption rate before the breakthrough, y_b, was above 98% in the three cycles. Nonetheless, the BV_b reduced 60% after one regeneration cycle, from 140 to 58. This behavior was observed in other adsorbents such as iron-chitosan granules (ICB) and iron-chitosan flakes (ICF), in which regeneration by NaOH 0.1 M caused a reduction of approximately 60% and 70% in BVb, respectively, for the treatment of groundwater spiked with As(V) (Gupta, Chauhan et al. 2009).

The desorption efficiency after 1st, 2nd and 3rd cycles was 100%, 72% and 103.2%, respectively. Lower desorption efficiencies were observed in commercial iron-based media such as granular ferric hydrogen (GFH) and ARM200 (LVS), treated with NaOH 1 M, of 26% and 39%, respectively (Chen, Sorg et al. 2015). The presence of chemical interferents such as silica was suggested as the possible cause for low arsenic desorption.

Table 4.11: Performance of alternative adsorbents on the removal of arsenic from real (spiked) groundwater in a fixed-bed column.

Adsorbent	Bed height (cm)	EBCT (min)	Initial As concentration (µg L^{-1})	Bed volumes before the breakthrough	Breakthrough time (h)	Ref.
Iron-oxide-coated natural rock (IOCNR)	10	~3.9	40	~244	16	(Maji, Kao et al. 2012)
Laterite soil	10	~4.1	330	~100	6.75	(Maji, Pal et al. 2008)
Iron chitosan spacer granules (ICS)	10	~19	179	30	~10	(Gupta and Sankararamakrishnan 2010)
	20	~38	179	45	~29	
	30	~57	179	64	~61	
XCF (xanthated chitosan flakes)	30	~57	200	99	94	(Gupta, Yunus et al. 2012)
Iron-chitosan granules (ICB)	30	~53	500	147	130	(Gupta, Chauhan et al. 2009)
Iron-coated cork granulates (ICG)	12	11	100	140	26	This study

The desorption profile of each cycle (Figure 4.14.b) shows that maximum concentrations of arsenic eluted from the exhausted bed reduced through each cycle, from 25 to 3 mg L^{-1}. The desorption time was reduced from 6 to 3 h. In total, 2.9 L of desorption effluent was produced for the treatment of 12.8 L of groundwater under 10 µg L^{-1}. The total volume treated until the saturation point was 89.4 L.

The iron concentration In the effluent from the adsorption and desorption cycles was inferior to the EU standard in drinking water of 0.2 mg L^{-1} (European Union 2020) (Figure 4.16), indicating the non-leachability of iron from the adsorbent as earlier observed at neutral pH, which is according to the results found in Chapter 3 from adsorption tests in continuous mode at neutral pH.

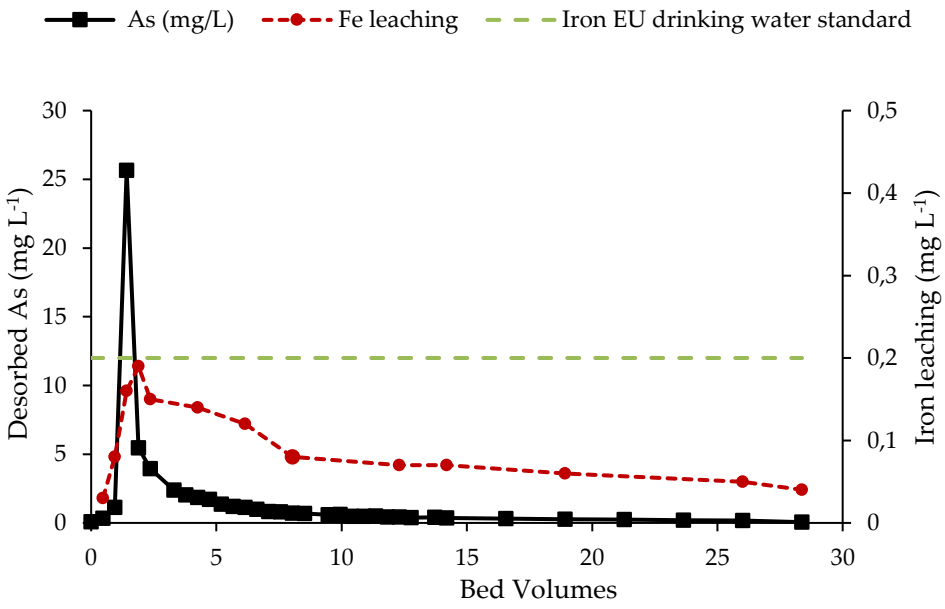


Figure 4.16: Arsenic and iron concentrations from desorption of saturated ICG after real water treatment.

The results suggest that the adsorbent can be recycled in a real application. However, better results might be obtained by a weaker base, such as 0.01 mol L^{-1} NaOH, which achieved the best regeneration performance with synthetic water in batch (item 3.1.4) and continuous mode (item 3.2.1). However, in continuous mode, the desorption using NaOH 0.01 M should take longer and produce a higher volume of waste when compared to NaOH 0.1 M. It is important to take those parameters (desorption capacity, desorption time, and volume of eluting solution) into consideration to decide which desorbing agent is more appropriate.

4.4 Conclusions

In this Chapter, the desorption of arsenic from saturated iron-coated cork granulates and the performance of regenerated ICG to remove arsenic from water were investigated. From batch tests it was concluded that basic solutions achieved higher desorption efficiency than salts and acid. The best desorption rate of 92% was observed using NaOH 0.1 M. The increase in the concentration of sodium hydroxide from 0.01 M to 0.5 M showed an increase in desorption of arsenic until 0.1 M, followed by a reduction. Even though the optimum desorption efficiency in batch mode was obtained using NaOH 0.1 M, the 0.01 M concentration was less aggressive to the adsorbent and permitted ICG to be regenerated for up to four cycles with a residual adsorption capacity above 1 mg g^{-1} in both batch and continuous mode.

Total organic carbon and iron leaching were 5-10 times higher in desorption with NaOH 0.1 M than NaOH 0.01 M The stronger degradation of ICG with NaOH 0.1 M was also confirmed by an observation of cell wall collapse in SEM micrographs. The low resistance of the structure resulted in limited performance of regenerated ICG treated with the stronger basic eluent.

As regards adsorption and desorption capacity, the best results were achieved in continuous mode in comparison to batch mode. Adsorption capacity reduced from 3.8 $\pm$ 0.3 to 1.8 $\pm$ 0.4 mg g^{-1} from 1st to 5th adsorption cycle in continuous mode, in contrast to the reduction from 5.7 $\pm$ 0.2 to 1.0 $\pm$ 0.1 mg g^{-1} in batch mode, after NaOH 0.01 M treatment.

Fixed-bed column tests conducted with arsenic-contaminated groundwater showed the feasibility of the application of ICG in real waters, which makes it an attractive green adsorbent for commercial purposes.

This Chapter provided good insights into arsenic desorption from ICG and the application of ICG for adsorption in real scenarios. In Chapter 6, a deeper study on the effect of the groundwater matrices in the arsenic removal capacity will be presented to justify the difference in performance observed between the treatment of synthetic and natural waters.

4.5 References

Alam, M. A., W. A. Shaikh, M. O. Alam, T. Bhattacharya, S. Chakraborty, B. Show and I. Saha (2018). "Adsorption of As (III) and As (V) from aqueous solution by modified Cassia fistula (golden shower) biochar." Applied Water Science **8**(7): 198.

Boldaji, M. R., R. Nabizadeh, M. H. Dehghani, K. Nadafi and A. H. Mahvi (2010). "Evaluating the performance of iron nanoparticle resin in removing arsenate from water." Journal of Environmental Science and Health, Part A **45**(8): 946-950.

Bujňáková, Z., P. Baláž, A. Zorkovská, M. J. Sayagués, J. Kováč and M. Timko (2013). "Arsenic sorption by nanocrystalline magnetite: An example of environmentally promising interface with geosphere." Journal of Hazardous Materials **262**: 1204-1212.

C.F. Ho, Y. S., Wase, D.A.J. and C. Forster (1996). "Removal of lead ions from aqueous solution using sphagnum moss peat as adsorbent." Water SA **22**(3): 219-224.

Chaudhary, B. K. and J. Farrell (2015). "Understanding Regeneration of Arsenate-Loaded Ferric Hydroxide-Based Adsorbents." Environmental engineering science **32**(4): 353-360.

Chen, A. S. C., T. J. Sorg and L. Wang (2015). "Regeneration of iron-based adsorptive media used for removing arsenic from groundwater." Water Research **77**: 85-97.

Coenen, K., F. Gallucci, E. Hensen and M. van Sint Annaland (2019). "Kinetic model for adsorption and desorption of H2O and CO2 on hydrotalcite-based adsorbents." Chemical Engineering Journal **355**: 520-531.

Di Natale, F., A. Erto and A. Lancia (2013). "Desorption of arsenic from exhaust activated carbons used for water purification." Journal of Hazardous Materials **260**: 451-458.

Elovich, S. Y. and O. G. Larionov (1962). "Theory of adsorption from nonelectrolyte solutions on solid adsorbents." Bulletin of the Academy of Sciences of the USSR, Division of chemical science **11**(2): 198-203.

European Union, C. (2020). Council Directive 2020/2184 of 16 December 2020, Off. J. Eur. Commun. L: 62.

Gupta, A., V. S. Chauhan and N. Sankararamakrishnan (2009). "Preparation and evaluation of iron–chitosan composites for removal of As(III) and As(V) from arsenic contaminated real life groundwater." Water Research **43**(15): 3862-3870.

Gupta, A. and N. Sankararamakrishnan (2010). "Column studies on the evaluation of novel spacer granules for the removal of arsenite and arsenate from contaminated water." Bioresource Technology **101**(7): 2173-2179.

Gupta, A., M. Yunus and N. Sankararamakrishnan (2012). "Equilibrium and dynamic studies of the removal of As(III) and As(V) from contaminated aqueous systems using a functionalized biopolymer." Journal of Chemical Technology & Biotechnology **87**(4): 546-552.

He, R., Z. Peng, H. Lyu, H. Huang, Q. Nan and J. Tang (2018). "Synthesis and characterization of an iron-impregnated biochar for aqueous arsenic removal." Science of The Total Environment **612**: 1177-1186.

Hu, X., Z. Ding, A. R. Zimmerman, S. Wang and B. Gao (2015). "Batch and column sorption of arsenic onto iron-impregnated biochar synthesized through hydrolysis." Water Research **68**: 206-216.

Inam, M. A., R. Khan, K. H. Lee, M. Akram, Z. Ahmed, K. G. Lee and Y. M. Wie (2021). "Adsorption Capacities of Iron Hydroxide for Arsenate and Arsenite Removal from Water by Chemical Coagulation: Kinetics, Thermodynamics and Equilibrium Studies." Molecules (Basel, Switzerland) **26**(22): 7046.

Lagergren S, K. (1898). "About the Theory of So-called Adsorption of Soluble Substances." Sven. Vetenskapsakad. Handingarl **24**: 1-39.

Lee, Y., Y. Ren, M. Cui, Y. Zhou, O. Kwon, J. Ko and J. Khim (2022). "Arsenic adsorption study in acid mine drainage using fixed bed column by novel beaded adsorbent." Chemosphere **291**: 132894.

Low, M. J. D. (1960). "Kinetics of Chemisorption of Gases on Solids." Chemical Reviews **60**(3): 267-312.

Machado, R., J. R. Carvalho and M. Joana Neiva Correia (2002). "Removal of trivalent chromium (III) from solution by biosorption in cork powder." Journal of Chemical Technology & Biotechnology: International Research in Process, Environmental & Clean Technology **77**(12): 1340-1348.

Maji, S. K., Y.-H. Kao, C.-J. Wang, G.-S. Lu, J.-J. Wu and C.-W. Liu (2012). "Fixed bed adsorption of As(III) on iron-oxide-coated natural rock (IOCNR) and application to real arsenic-bearing groundwater." Chemical Engineering Journal **203**: 285-293.

Maji, S. K., A. Pal and T. Pal (2008). "Arsenic removal from real-life groundwater by adsorption on laterite soil." Journal of Hazardous Materials **151**(2): 811-820.

Mandal, S., M. K. Sahu and R. K. Patel (2013). "Adsorption studies of arsenic(III) removal from water by zirconium polyacrylamide hybrid material (ZrPACM-43)." Water Resources and Industry **4**: 51-67.

Pintor, A. M. A., C. C. Brandão, R. A. R. Boaventura and C. M. S. Botelho (2021). "Multicomponent adsorption of pentavalent As, Sb and P onto iron-coated cork granulates." Journal of Hazardous Materials **406**: 124339.

Pintor, A. M. A., B. R. C. Vieira, C. C. Brandão, R. A. R. Boaventura and C. M. S. Botelho (2020). "Complexation mechanisms in arsenic and phosphorus adsorption onto iron-coated cork granulates." Journal of Environmental Chemical Engineering **8**(5): 104184.

Pintor, A. M. A., B. R. C. Vieira, S. C. R. Santos, R. A. R. Boaventura and C. M. S. Botelho (2018). "Arsenate and arsenite adsorption onto iron-coated cork granulates." Science of The Total Environment **642**: 1075-1089.

Pokhrel, D. and T. Viraraghavan (2008). "Arsenic removal in an iron oxide-coated fungal biomass column: Analysis of breakthrough curves." Bioresource Technology **99**(6): 2067-2071.

Ranjan, D., M. Talat and S. H. Hasan (2009). "Rice Polish: An Alternative to Conventional Adsorbents for Treating Arsenic Bearing Water by Up-Flow Column Method." Industrial & Engineering Chemistry Research **48**(23): 10180-10185.

Sadiq, M., T. H. Zaidi and A. A. Mian (1983). "Environmental behavior of arsenic in soils: Theoretical." Water, Air, & Soil Pollution **20**(4): 369-377.

Sarkar, S., L. M. Blaney, A. Gupta, D. Ghosh and A. K. SenGupta (2007). "Use of ArsenXnp, a hybrid anion exchanger, for arsenic removal in remote villages in the Indian subcontinent." Reactive and Functional Polymers **67**(12): 1599-1611.

Sarkar, S., L. M. Blaney, A. Gupta, D. Ghosh and A. K. SenGupta (2008). "Arsenic Removal from Groundwater and Its Safe Containment in a Rural Environment: Validation of a Sustainable Approach." Environmental Science & Technology **42**(12): 4268-4273.

Shakoor, M. B., N. K. Niazi, I. Bibi, M. Shahid, F. Sharif, S. Bashir, S. M. Shaheen, H. Wang, D. C. W. Tsang, Y. S. Ok and J. Rinklebe (2018). "Arsenic removal by natural and chemically modified water melon rind in aqueous solutions and groundwater." Science of The Total Environment **645**: 1444-1455.

Su, C. and R. W. Puls (2001). "Arsenate and Arsenite Removal by Zerovalent Iron: Effects of Phosphate, Silicate, Carbonate, Borate, Sulfate, Chromate, Molybdate, and Nitrate, Relative to Chloride." Environmental Science & Technology **35**(22): 4562-4568.

Tresintsi, S., K. Simeonidis, M. Katsikini, E. C. Paloura, G. Bantsis and M. Mitrakas (2014). "A novel approach for arsenic adsorbents regeneration using MgO." Journal of Hazardous Materials **265**: 217-225.

Tuutijärvi, T., R. Vahala, M. Sillanpää and G. Chen (2012). "Maghemite nanoparticles for As(V) removal: desorption characteristics and adsorbent recovery." Environmental Technology **33**(16): 1927-1936.

Ungureanu, G., S. Santos, R. Boaventura and C. Botelho (2015). "Arsenic and antimony in water and wastewater: Overview of removal techniques with special reference to latest advances in adsorption." Journal of Environmental Management **151**: 326-342.

Vaishya, R. C. and S. K. Gupta (2006). "Arsenic(V) Removal by Sulfate Modified Iron Oxide-Coated Sand (SMIOCS) in a Fixed Bed Column." Water Quality Research Journal **41**(2): 157-163.

Vakili, M., S. Deng, G. Cagnetta, W. Wang, P. Meng, D. Liu and G. Yu (2019). "Regeneration of chitosan-based adsorbents used in heavy metal adsorption: A review." Separation and Purification Technology **224**: 373-387.

Wang, S., B. Gao and Y. Li (2016). "Enhanced arsenic removal by biochar modified with nickel (Ni) and manganese (Mn) oxyhydroxides." Journal of Industrial and Engineering Chemistry **37**: 361-365.

WHO (2017). Guidelines for drinking-water quality: fourth edition incorporating first addendum. Geneva, World Health Organization.

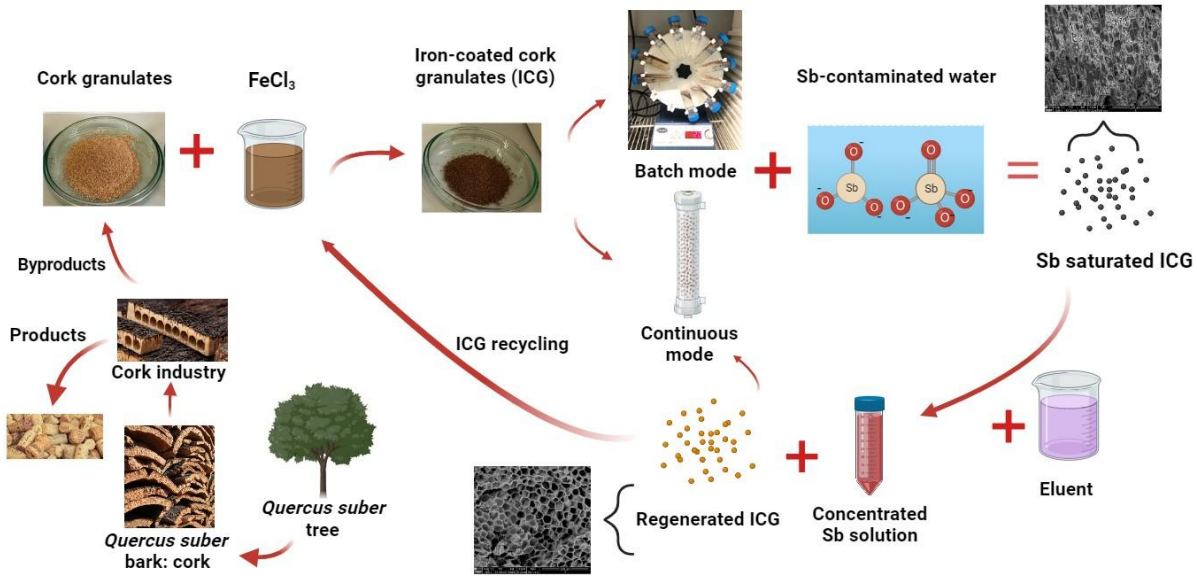
Wilkie, J. A. and J. G. Hering (1996). Adsorption of arsenic onto hydrous ferric oxide: Effects of adsorbate/adsorbent ratios and co-occurring solutes. Colloids and Surfaces A: Physicochemical and Engineering Aspects.

Yan, G., T. Viraraghavan and M. Chen (2001). "A New Model for Heavy Metal Removal in a Biosorption Column." Adsorption Science & Technology **19**(1): 25-43.

Yeo, K. F. H., C. Li, Y. Dong, Y. Yang, K. Wu, H. Zhang, Z. Chen, Y. Gao and W. Wang (2022). "Adsorption performance of Fe(III) modified kapok fiber for As(V) removal from water." Separation and Purification Technology **287**: 120494.

5 ANTIMONY ADSORPTION AND DESORPTION: BATCH AND CONTINUOUS MODE STUDIES

This chapter is based on: Carneiro, M. A., Silva, T. A., Teixeira, P. J. S., Boaventura, R. A. R., Botelho, C. M. S., & Pintor, A. M. A. (2024). *New insights on antimony removal and recovery from water and wastewater using iron-coated cork granulates: Desorption on batch and fixed-bed column systems*. Chemical Engineering Science, 296, 120207. Doi:https://doi.org/10.1016/j.ces.2024.120207



This work investigated Sb adsorption-desorption using iron-coated cork granulates (ICG) in both batch and continuous modes to evaluate the material´s adsorption and regeneration performance, as well as the possibility of antimony recovery. A fixed-bed column filled with ICG, demonstrated maximum adsorption capacities of 13 ± 2 mg g^{-1} and 10 ± 1 mg g^{-1} for Sb(III) and Sb(V), respectively, at pH 3. ICG was able to remove Sb within the WHO guideline of 20 µg L^{-1} at pH 6. Among the different classes of eluents tested for Sb(V) desorption, the acids achieved the highest desorption rates – 81 ± 9% and 66 ± 8% for HCl 1M and ascorbic acid 0.1M, respectively. The desorption kinetics showed that HCl 1 M reached equilibrium in 4 h, but ascorbic acid 0.1 M took 16 h. This work presents an ecological emerging solution for antimony removal and recovery from water and wastewater.

5.1 Introduction

In the previous chapters, it has been shown that iron-coated cork granulates are good adsorbents for arsenic removal from water in continuous mode (Chapter 3). Moreover, the regeneration of the saturated media was possible through five and three adsorption-desorption cycles from aqueous solution and groundwater matrix, respectively (Chapter 4). In addition, arsenic recovery from the saturated media via As-loaded eluent was demonstrated in the previous chapter.

The removal of antimony from aqueous solution was also found to be feasible in batch mode, according to early studies in the research group (Pintor, Brandão et al. 2020, Pintor, Vieira et al. 2020). Hence, this work investigated the antimony adsorption in aqueous solution by ICG, and the subsequent desorption in batch and continuous modes aiming at both drinking water and wastewater treatment, and resource recovery.

The material characterization was performed before and after desorption using acid digestion and flame atomic absorption spectroscopy (FAAS) for measuring iron content, scanning electron microscopy (SEM) for visual observation, and energy-dispersive X-ray spectroscopy (EDS) to identify the main elements present in the materials.

5.2 Materials and methods

5.2.1 Materials

Stock solutions of Sb(III) were produced by diluting antimony trichloride (SbCl3) (ACS reagent, Acrós Organics) in 0.1% (v/v) HCl. Stock solutions of Sb(V) were produced by diluting potassium hexahydroxoantimonate ($KSb(OH)_6$) (Aldrich) in distilled water. A distilled water dilution of the stock solutions was performed to achieve the desired working concentration.

The desorption eluents were prepared by diluting the following chemicals in distilled water: sodium hydroxide (NaOH) pearls 99.14% (Labsolve), sodium carbonate anhydrous Na2CO3 99.5% (Merck), disodium ethylenediaminetetraacetate (EDTA) > 98.5% (May & Baker), nitric acid (HNO_3) 68% (VWR), HCl 37% (VWR), citric acid (99.5-102.0)% (Panreac), ascorbic acid (VWR), tartaric acid (Merck), and NaCl (Merck).

Iron-coated cork granulates (ICG) were manufactured as described in section 3.2.1.

5.2.2 Analytical Methods

Antimony

The concentration of Sb(III) / Sb(V) was determined by measuring total antimony by flame atomic absorption spectrometry (FAAS) (GBC 932 Plus) between 2–50 mg L^{-1} and graphite furnace atomic absorption spectrometry (GFAAS) (GBC GF 3000, SenAA Dual) between 20-100 µg L^{-1}. The operating conditions for both spectrometers were 8 mA lamp current, 217.6 nm wavelength and 0.2 nm slit width. In GFAAS, a Ni solution of 50 mg L−1 (prepared from a commercial standard) was used as a chemical matrix modifier.

5.2.2.2 Iron

Iron concentrations were determined by measuring total iron concentration by FAAS (GBC 932 Plus) in the range of 0.25–5 mg L^{-1} under an air-acetylene flame, a slit width of 0.2 nm, at 8 mA lamp current and a wavelength of 248.3 nm.

5.2.3 Adsorption in continuous mode

The lab-scale system employed for the adsorption of Sb(V) and Sb(III) onto iron-coated cork granules in continuous mode consisted of various components. These included a glass column (Chromaflex®) (diameter = 2.5 cm and length = 15 cm), an influent reservoir with a capacity of 50 L, an effluent reservoir with a capacity of 30 L, a peristaltic pump (Hei-FLOW Advantage 01, Heidolph), a thermostatic bath (DIGIT-COOL, J.P. SELECTA), and an automatic sample collector (GILSON, FC-203B). A representation of the lab-scale adsorption system is shown in Figure 3.1.

The fixed-bed column was operated in a downward flow due to the adsorbent's low density. ICG were hydrated in distilled water and vacuumed before each experiment to minimize the air trapped in the pores. Next, the adsorbent was added to the column, which was then operated for two hours with distilled water under the same operational conditions previously optimized for arsenic removal in Chapter 3: 5 mL min^{-1} of flow rate (FR), 12 cm of bed height (6 g of ICG), and 20°C of temperature. The experimental breakthrough parameters were calculated using the equations mentioned Chapter 3.

The Yan model (Yan, Viraraghavan et al. 2001) (Eq. (3.15) was fitted to the experimental results and the theoretical parameters were obtained.

5.2.4 Adsorption on a batch operation mode

Batch adsorption of antimony was carried out using a mixing rotator (SB3, Stuart) operating at 20 rpm within a thermostatic cabinet operating at 20.0 ± 0.5 °C, with a solid-to-liquid (S/L) ratio of 2.5 g L^{-1}. After contact, the adsorbent was separated by filtering it through cellulose acetate membrane filters (0.45 µm pore size), and the concentration of antimony was measured in the solution. More details on batch methodological procedures were described in previous works (Pintor, Vieira et al. 2020, Pintor, Brandão et al. 2021). The total iron concentration was additionally determined to observe the release of iron from the adsorbent.

Equilibrium experiments were performed for Sb(III) at pH 3, with a fixed initial concentration of 10 mg L^{-1}. The S/L was varied at values of 0.5, 1.0, 2.0, 3.0, 4.0 and 5.0 g L^{-1}. The contact time for the experiments was fixed as 24 h.

The adsorption kinetics was evaluated for Sb(III) at pH 3.0, with initial concentrations of 1 and 15 mg L^{-1}, for contact times of 0.25, 0.5, 1, 2, 4, 8, 16 and 24 h; and 0.25, 0.5, 1, 2, 4, 8, 16, 24 and 48 h, respectively.

The adsorbed amount after each experiment, q_{ad}, was obtained using an equation of mass balance (Eq. (3.1).

5.2.4.1 Kinetic models

Both adsorption and desorption kinetic data were assessed using the pseudo-first-order model (Eq. (4.2)), pseudo-second-order model (Eq. (4.3)), and Elovich model (Eq. (4.4)) Non-linear regression analysis was performed using CurveExpert Professional v. 2.6.4 to fit the kinetic models to the experimental results.

5.2.5 Desorption in batch mode

Desorption tests were conducted using different eluents at different concentrations to remove Sb(V) from the saturated ICG. Only the Sb(V) species was tested because it is the most prevalent oxidation state of the element in water. The eluents used as follows: base – NaOH (0.1 M and 0.5 M); acid – HCl (from 0.1 M to 1 M), tartaric acid (0.5 M), citric acid (from 0.1 M to 1 M), ascorbic acid (from 0.001 M to 1 M); salt and complexing agents – NaCl (0.5 M), Na_2CO_3 (0.5 M), and EDTA (0.5 M); and distilled water. The assays were carried out using antimony saturated-ICG containing 10 ± 1 mg Sb(V)/g ICG. The contact time in desorption tests was 24

h. Figure 5.1 illustrates a schematic diagram of the adsorption and desorption assays carried out in batch mode.

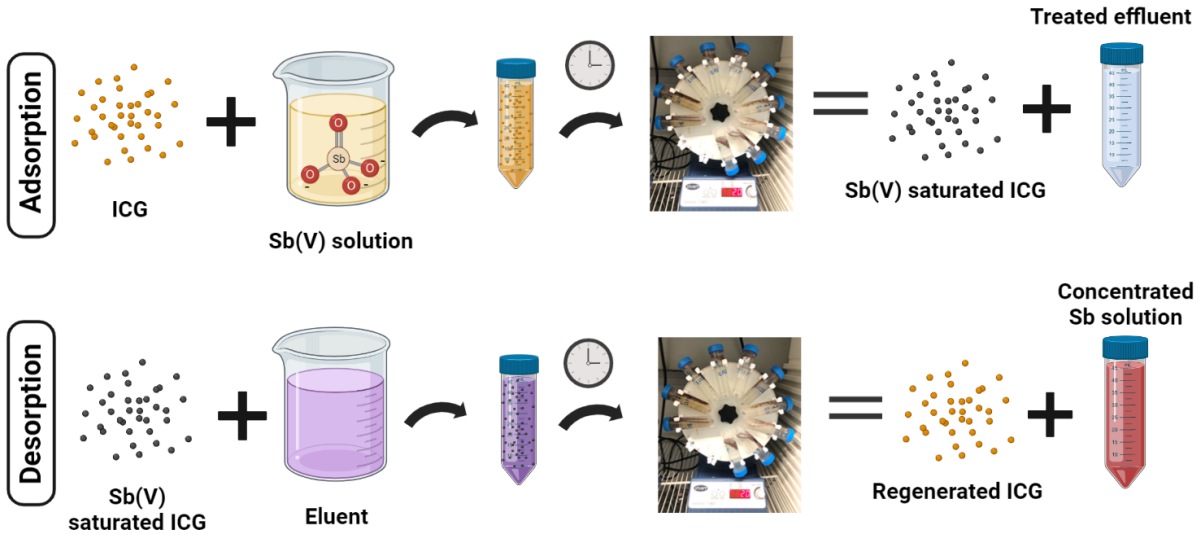


Figure 5.1: Representation of lab-scale batch operating mode of antimony adsorption and desorption onto iron-coated cork granules.

Ascorbic acid 0.1 M and HCl 1 M were used as eluents to study the desorption kinetics of Sb(V). For that, 0.25, 0.5, 1, 2, 4, 8, 16 and 24 h were the contact times. The assays were carried out using antimony saturated-ICG containing 10 ± 1 mg Sb(V)/g ICG, at a fixed temperature of 20.0 ± 0.5 °C and a S/L ratio of 2.5 g L^{-1}.

A mixing rotator was used to agitate the solutions at a speed of 20 rpm. Following the previously specified contact times, filtration was carried out with a 0.45 µm acetate cellulose filter. Subsequently, the filtrated solution was analyzed for the total concentration of Sb by FAAS. The desorbed amount of Sb (q_d, mg g^{-1}) was calculated according to Eq. (4.1.

To determine the amount of iron that leached from the adsorbent, the total amount of dissolved iron in the solutions mentioned above was determined using FAAS.

5.2.6 Desorption in continuous mode

Cycles of adsorption and desorption were performed to evaluate how effectively regenerated ICG can remove Sb(V) from an aqueous solution. For adsorption, the column was fed by a solution of 5 mg L^{-1} of Sb(V) at the operating conditions described in section 2.4. After bed saturation, the column was fed by ascorbic acid 0.1 M in the same operating conditions of adsorption. After desorption was complete, distilled water was pumped by the column at the same flow rate to remove the acid.

5.2.7 Adsorption in continuous mode using recycled iron-coated cork granulates

After two adsorption-desorption cycles in continuous mode using ascorbic acid 0.1 M as eluent, as described in section 5.2.6, the ICG was recycled by undergoing a new iron coating. The desorbed ICG were put in contact with a FeCl3 0.05 M solution of pH 7.0, for 24 h, then washed with distilled water until the iron excess was removed, as described in section 5.2.1. Then, another adsorption cycle was carried out under the conditions described in section 5.2.3 to assess the performance of the recycled adsorbent.

5.2.8 Material characterization

Few studies explore the material changes before and after desorption. In this work, the material was characterized by iron content and SEM—EDS to evaluate the effect of desorption on its chemical and structural properties.

5.2.8.1 Acid digestion

The iron content of the ICG was assessed before and after regeneration. Each adsorbent material was digested in glass tubes connected to condensers with a mixture of 5.0 mL distilled water, 4.0 mL HNO3 65% (analytical grade, VWR), and 12.0 mL HCl 37% (analytical grade, VWR). The total dissolved iron was determined by FAAS after the digested solution had been filtered and diluted with distilled water. The iron content was calculated by mass balance.

5.2.8.2 SEM-EDS

Scanning electron microscopy coupled with energy-dispersive X-ray spectroscopy (SEM-EDS) was used to determine the surface morphology and elemental components of the adsorbent. The SEM / EDS analysis was conducted using a High resolution (Schottky) Environmental Scanning Electron Microscope with X-Ray Microanalysis and Electron Backscattered Diffraction analysis: FEI Quanta 400 FEG ESEM / EDAX Genesis X4M.

Using the SPI Module Sputter Coater equipment, samples were coated with an Au/Pd thin film by sputtering.

5.3 Results and discussion

5.3.1 Adsorption in continuous mode

5.3.1.1 Effect of pH

The breakthrough curves at pH 3.0 and 6.0 were compared for each inorganic antimony species. These pH values were selected because they were considered optimal for the adsorption of Sb(V) and Sb(III), respectively, in a previous study in discontinuous mode (Pintor, Vieira et al. 2020). The studies were conducted at an initial concentration of 1 mg L^{-1} and a temperature of 20ºC. The experimental results and Yan model predictions are shown in Figure 5.2 and Table 5.1.

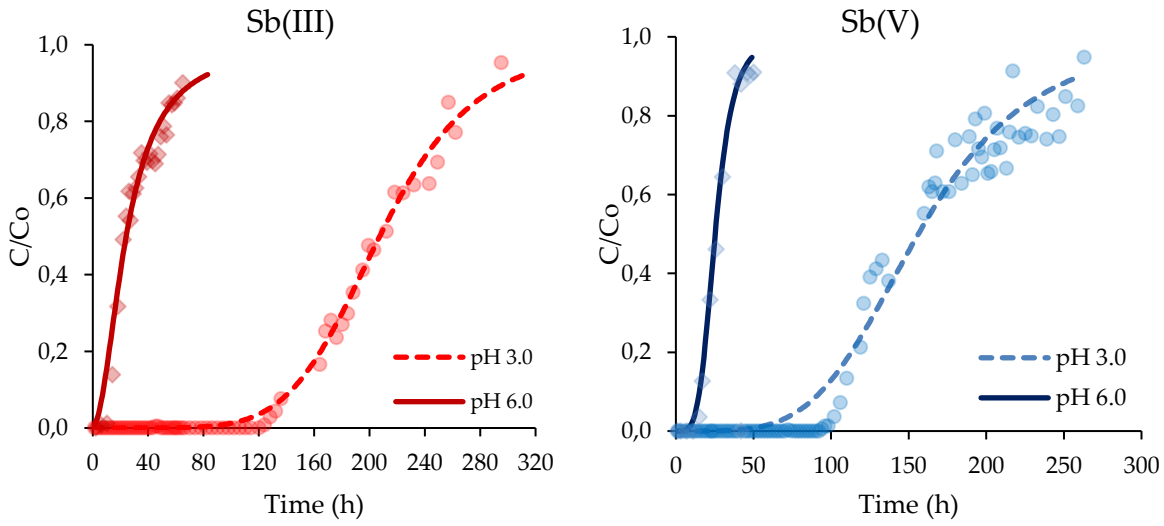


Figure 5.2: pH effect on the Sb(III) and Sb(V) removal in the fixed-bed column (dots = experimental data, lines = Yan model predicted curves) (Inlet Sb(III)/Sb(V) concentration 1 mg L^{-1}; Bed height: 12 cm; Flow rate: 5 mL min^{-1}; Temperature: 20ºC).

Table 5.1: Experimental and predicted breakthrough parameters on pH effect in Sb(III) and Sb(V) adsorption (Ci = 1 mg L^{-1}, T = 20ºC, FR = 5 mL min^{-1}; Bed height = 12 cm) (±standard error of the mean).

		Sb(III)		**Sb(V)**	
Experimental		pH 3	pH 6	pH 3	pH 6
	t_b (h)	126 ± 0.4	10.3 ± 0.2	98 ± 0.4	12.8 ± 0.3
	t_s (h)	295	65	263	50
	q_b (mg g^{-1})	7.9 ± 0.9	0.49 ± 0.03	6.2 ± 0.6	0.84 ± 0.06
	q_s (mg g^{-1})	13 ± 2	1.5 ± 0.2	10 ± 1	2.0 ± 0.2
	BV_b	639 ± 11	52 ± 1	501± 9	68 ± 2
	BV_s	1502 ± 87	331±19	1339 ± 77	265 ±15
	V_b (L)	37.7 ± 0.7	3.09 ± 0.08	29.5 ± 0.5	4.0 ± 0.1
	V_s (L)	88.5 ± 0.2	19.50 ± 0.06	78.9 ± 0.1	15.6 ± 0.1
	y_b (%)	99.973 ± 0.006	99.45 ± 0.08	99.2 ± 0.1	99.95 ± 0.01
	y_s (%)	71 ± 5	48 ± 4	63 ± 4	62 ± 4
	MTZ (cm)	6.9 ± 0.3	10.1 ± 0.5	7.5 ± 0.3	8.9 ± 0.4
	MTZ/Bed height	0.57 ± 0.03	0.84 ± 0.05	0.63 ± 0.04	0.74 ± 0.05
Yan Model	Q_{ya} (mg g^{-1})	13.0 ± 1.5	1.2 ± 0.1	9.9 ± 0.9	1.7 ± 0.1
	a_{ya}	6.1 ± 0.3	2.1 ± 0.1	4.3 ± 0.2	4.5 ± 0.3
	SE (mg g^{-1})	0.04	0.05	0.06	0.04
	R^2	0.984	0.953	0.972	0.990

Adsorption of both antimony species was higher at pH 3, compared to the almost neutral solution at pH 6. For Sb(V), this pH effect follows batch equilibrium and kinetic studies shown in earlier research work, but for Sb(III), it was expected that adsorption would remain constant throughout a wide range of pH (Pintor, Vieira et al. 2020). Other results reported in the literature for iron-based adsorbents for Sb(V) indicated optimal pH values ranging from 3 to 5, with a significant decrease as pH increases above 5 (Deng, Jin et al. 2017). These results indicate that ICG may be a great candidate for treating acid effluents, such as acid mine drainage (Manaka, Yanase et al. 2007, Guo, Fu et al. 2018, Cappuyns, Van Campen et al. 2021).

Furthermore, the effect of pH reduction from 6 to 3 was more evident for Sb(III) removal than for Sb(V) removal, as seen in Figure 5.2. The maximum Sb(III) and Sb(V) adsorption capacities achieved were 13 $\pm$ 2 mg g^{-1} and 10 $\pm$ 1 mg g^{-1}, respectively, at pH 3. Meanwhile, the reduction in adsorption capacity from pH 3 to pH 6 was 89% and 80% for Sb(III) and Sb(V), respectively (Table 1). These findings are according to the literature that shows Sb adsorption to be speciation and pH-dependent (Bai, Tang et al. 2022, Dündar, Mehenktaş et al. 2022). However, it was not expected for this material, given the batch adsorption results referred earlier. Other studies have found a stronger Sb(V) than Sb(III) affinity toward green seaweed at pH 2 (Ungureanu, Filote et al. 2016). The optimal pH value for Sb(V) adsorption by Microcystis biomass was found to be 2.5-3.0 (Sun, Yan et al. 2014).

The ICG maximum removal capacity of Sb(III) In continuous mode was superior to that of quartz sand coated with Fe_3O_4 and graphene oxide (QFGO) of 2.88 – 6.09 mg g^{-1} as estimated by the Thomas model (Yang, Shi et al. 2015), brown seaweeds of 3.56 $\pm$ 0.06 mg g^{-1} as estimated by the Yan model (Ungureanu, Santos et al. 2017); but inferior to that of pine bark tannin resin of 31 $\pm$ 2 mg g^{-1} as estimated by the Yan model (Bacelo, Santos et al. 2022). Table 5.2 presents the maximum adsorption capacities reported in the literature.

Table 5.2: Comparison between adsorption of antimony in fixed-bed columns.

	Species	pH	C_i (mg L^{-1})	Flow rate (mL min^{-1})	Bed height (cm)	Maximum adsorption capacity (mg g^{-1})	Ref.
Brown seaweeds	Sb(III)	7	25	4	17	3.56 ± 0.06	(Ungureanu, Santos et al. 2017)
Granular titanium dioxide (TiO_2)	Sb(V)	8.2	0.24	1.5	16	0.981	(Qiu, Yan et al. 2019)
Pine bark tannin resin	Sb(III)	6	9	3	10.5	31 ± 2	(Bacelo, Santos et al. 2022)
Quartz sand coated with Fe_3O_4 and graphene oxide (QFGO)	Sb(III)	7	40	8	10	6.03	(Yang, Shi et al. 2015)
Layered double hydroxide mineral, brucite (BRU)	Sb(III)	7.2	0.17	5.83	9.9	0.0004	(Runtti, Luukkonen et al. 2023)
Nanoscale zero-valent iron (Fe0) supported on activated carbon (nZVI/AC)	Sb(V)	7	1	5	20	0.6275	(Zhu, Huang et al. 2021)
Fe-Mn binary oxides ($FMBO_3$)	Sb(V)	7	0.2	3.75	8.2	3.12	(Yang, Liu et al. 2019)
Bayoxide E33 (GFH)	Sb(III)	7	0.1	54.4	11.3	2.11	(Sazakli, Zouvelou et al. 2014)
Iron-coated cork granulates (ICG)	Sb(III)	3	1	5	12	13.0 ± 1.5	This study
	Sb(V)	3	1	5	12	9.9 ± 0.9	

5.3.2 Adsorption in batch mode

The pH effect on Sb(III) and Sb(V) adsorption onto ICG was previously investigated by this research group (Pintor, Vieira et al. 2020). In this study, the uptake of Sb(III) was stable in the range of 4-10, achieving a maximum adsorption capacity of 5.8 mg g^{-1} at pH 6.

Nonetheless, the investigation on the effect of pH in Sb(III) adsorption in continuous mode showed that the best adsorption capacity was found at pH 3 (Table 5.1). In order to confirm the best

results of Sb(III) uptake onto ICG at pH 3, equilibrium and kinetics studies were conducted at this pH.

5.3.2.1 Equilibrium studies

The adsorption equilibrium of Sb(III) onto ICG was investigated at pH 3 and the results are shown in Figure 5.3 and Table 5.3.

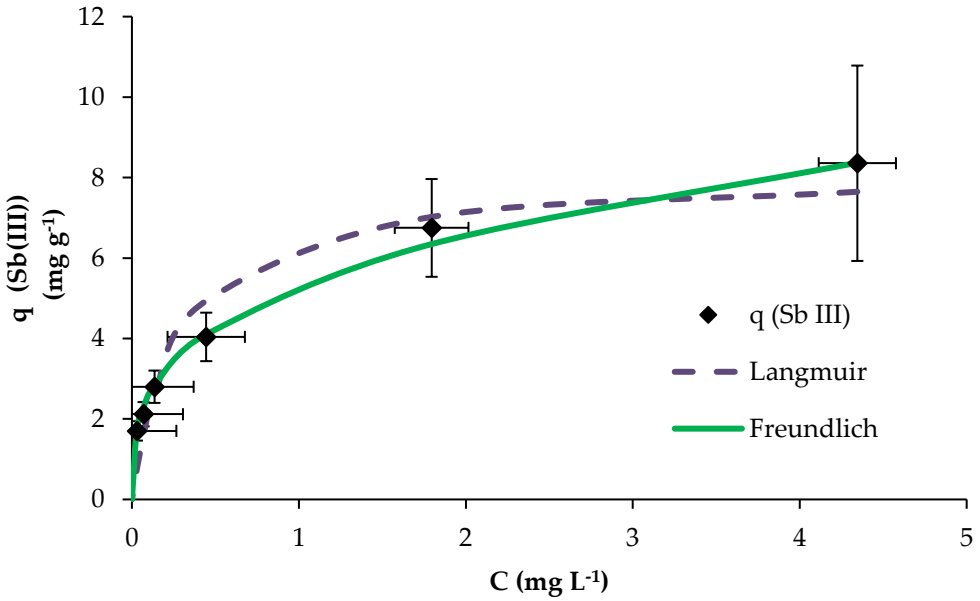


Figure 5.3: Adsorption equilibrium of Sb(III) on iron-coated cork granulates: experimental and model-fitting data (pH 3.0; 2.5 g L^{-1}; 24 h; 20ºC) (Error bars: maximum absolute deviation).

Table 5.3: Equilibrium model parameters for Sb(III) at pH 3.0 (C_i = 10 mg L^{-1}) (± standard error of the mean).

		T = 20ºC
Langmuir	Q_{max} (mg g^{-1})	8.2 ± 0.7
	K_L (L mg^{-1})	3 ± 1
	R^2	0.937
	SE	0.7
Freundlich	K_F ($mg^{(1-1/n)} L^{1/n} g^{-1}$)	5.3 ± 0.2
	n	3.2 ± 0.3
	R^2	0.982
	SE	0.4

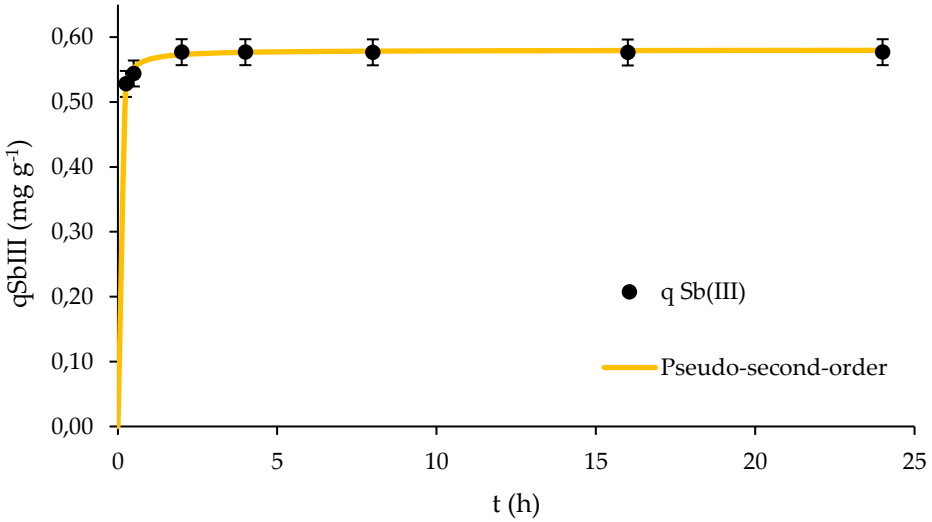
The Freundlich model presented a better fit to the experimental data like earlier equilibrium experiments conducted with Sb(III) onto iron-coated cork granulates (Pintor, Vieira et al. 2020). The Langmuir model showed a satisfactory fit and allowed us to estimate the maximum adsorption capacity as 8.2 ± 0.7 mg g^{-1}. This is over 40% higher than the Langmuir estimate for Sb(III) removal reported for pH 6 as 5.8 ± 0.5 mg g^{-1} (Pintor, Vieira et al. 2020). Hence, an increase in pH from 3 to 6 has a negative impact on the ICG´s Sb(III) adsorption capacity.

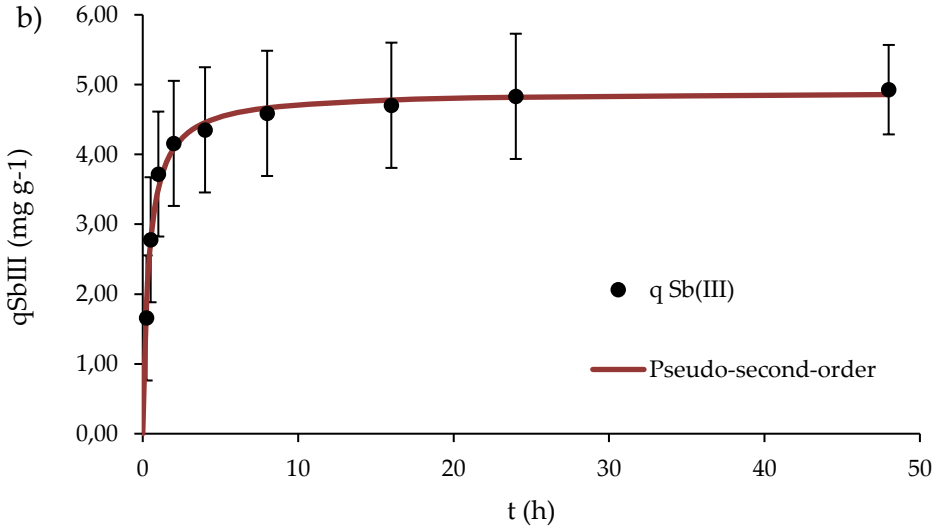
Similar results were reported in studies showing that Sb(III) adsorption in zero-valent iron decreased from 15.3 mg g^{-1} to 10.9 mg g^{-1} as pH increased from 3-10 (Zhang, Jiang et al. 2019) and from ~70% to ~30% as pH increased from 4-10 (Liu, Feng et al. 2020). However, the opposite behavior was also observed when an increase in pH caused an increase in adsorption capacity (Zou, Liu et al. 2016, Ungureanu, Santos et al. 2017, Bacelo, Vieira et al. 2018, Bacelo, Santos et al. 2022). Also, no influence on Sb(III) removal was observed in the pH ranges from 2 to 12 (Verbinnen, Block et al. 2013) or 3 to 9 (Yang, Shi et al. 2015) for other iron-based adsorbents.

The193egateve effect of pH increase on Sb(III) removal onto ICG can be caused by a higher concentration of H^+ in acidic solutions, which benefits the adsorption processes that may be taking part in the Sb(III) complexation with iron oxide surface groups (Guo, Wu et al. 2014, Pintor, Vieira et al. 2020).

5.3.2.2 Kinetic studies

The kinetics models were fitted to the experimental results, however, only the pseudo-second order model led to satisfactory results (Figure 5.4 and Table 5.4). This indicates the occurrence of chemisorption, which is generally observed in iron-based adsorbents (Deng, Jin et al. 2017). A previous study (Pintor, Vieira et al. 2020) showed that the kinetics of Sb(III) adsorption at pH 6 (C_i = 10 mg L^{-1}) was very well described by the pseudo-second-order and Elovich models, with a kinetic constant k_2 value of 0.12 ± 0.03 g mg^{-1} h^{-1}. This value was lower than the k_2 found in this study of 0.51 ± 0.05 g mg^{-1} h^{-1} (C_i = 15 mg L^{-1}), which indicates faster adsorption at pH 3.0 compared to pH 6.0.


0,60
0,50
0,40
0,30
0,20
0,10
0,00
qSbIII (mg g-1)
0
5
10
15
20
25
t (h)
q Sb(III)
Pseudo-second-order


b)
6,00
5,00
4,00
3,00
2,00
1,00
0,00
qSbIII (mg g-1)
0
10
20
30
40
50
t (h)
q Sb(III)
Pseudo-second-order

Sb(III) adsorption kinetics initially presents a high adsorption rate for both initial concentration assays. For the lower concentration, Sb(III) equilibrium was achieved after 2 h. Still, in the first 15 min, the adsorption capacity of 0.53 ± 0.02 mg g^{-1} was very close (more than 90%) to the equilibrium adsorption capacity of 0.580 ± 0.003 mg $g^{-}1$ (Table 5.4). For higher concentrations, the kinetics was slower. The equilibrium was achieved after 48 h, leading to an adsorption capacity of 4.90 ± 0.07 mg g^{-1}, but after 4 h, the Sb(III) uptake was almost in equilibrium (90%) with an adsorption capacity of 4.4 ± 0.9 mg g^{-1}. The initial concentration increase from 1 to 15 mg L^{-1} resulted in an approximately 8-fold increase in adsorption capacity at equilibrium.

With other biosorbents, antimonite adsorption proceeded very rapidly. For example, in brown seaweeds, the equilibrium was also reached after 2 h but with good adsorption in the first 15 minutes ($0.022 \pm 0.002 < k_2 < 0.41 \pm 0.03$) (Ungureanu, Santos et al. 2017). By cyanobacterium *Synechocystis sp.*, almost 50% of the adsorption was achieved in 30 min, and equilibrium was reached after 1 h ($k_2 = 0.052$) (Zhang, Pan et al. 2011). In the first 20 minutes, antimonite was rapidly removed by iron-oxide-cottonwood biochar, and equilibrium was obtained after one hour (Zhang, Dong et al. 2022).

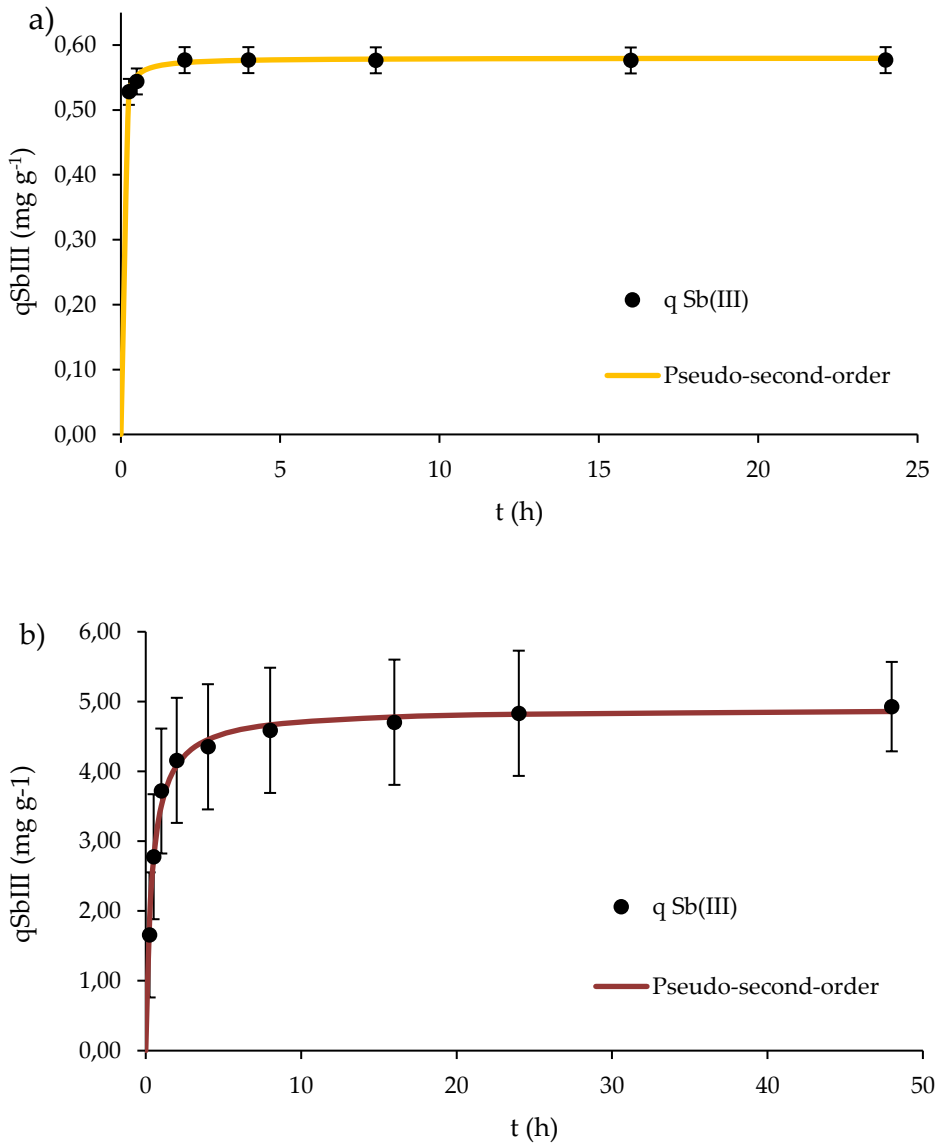


Figure 5.4: Adsorption kinetics (S/L = 2.5 g L^{-1}, 20ºC, pH 3) with experimental and fitted pseudo-second-order model of Sb(III) for initial concentration of: a) 1 mg L^{-1} and b) 15 mg L^{-1}.

Table 5.4: Parameters from pseudo-first-order, pseudo-second-order and Elovich fitting to experimental data of adsorption kinetics of Sb(III) onto iron-coated cork granulates (pH 3; 20°C; S/L = 2.5 g L^{-1}) (± standard error of the mean).

		C_i = 1 mg L^{-1}	C_i = 15 mg L^{-1}
Pseudo-second-order model	q_e (mg g^{-1})	0.580 ± 0.003	4.90 ± 0.07
	k_2 (g mg^{-1} h^{-1})	68 ± 9	0.51 ± 0.05
	R^2	0.914	0.986
	SE	0.006	0.1
Pseudo-first-order model	q_e (mg g^{-1})	0.573 ± 0.004	4.63 ± 0.09
	k_1 (h^{-1})	9.8 ± 0.9	1.7 ± 0.2
	R^2	0.727	0.965
	SE	0.01	0.2
Elovich	α (mg g^{-1} h^{-1})	-	83 ± 65
	b (g mg^{-1})	-	1.5 ± 0.2
	R^2	-	0.883
	SE	-	0.4

5.3.3 Desorption in batch mode

In the study of desorption, only Sb(V) was examined, as it is the most prevalent oxidation state in the environment. Several eluents were tested, at varying concentrations, in batch mode. The findings are summarized in Figure 5.5 and Table 5.5. The acids outperformed the base and the

salts, indicating Sb(V) desorption from ICG to be more favorable at very low pH levels. In Sb(V) desorption from cyanobacteria, acid eluents such as HCl 1 M (68.46%) and citric acid 1 M (51.45%) were found to be more efficient than NaOH 1 M (30.55%) (Sun, Yan et al. 2014). Oppositely, the Sb(V) desorption from pine bark tannin resin was found to be higher using a basic solution of NaOH 0.1 M than using acid solutions of HCl (0.04 – 0.5 M) (Bacelo, Santos et al. 2022). Another study reported desorption rates of 65-75% for ZVI decorated carbon nanotubes (CNT – Fe(0)) using HCl 0.05 M (Mishra, Dwivedi et al. 2016).

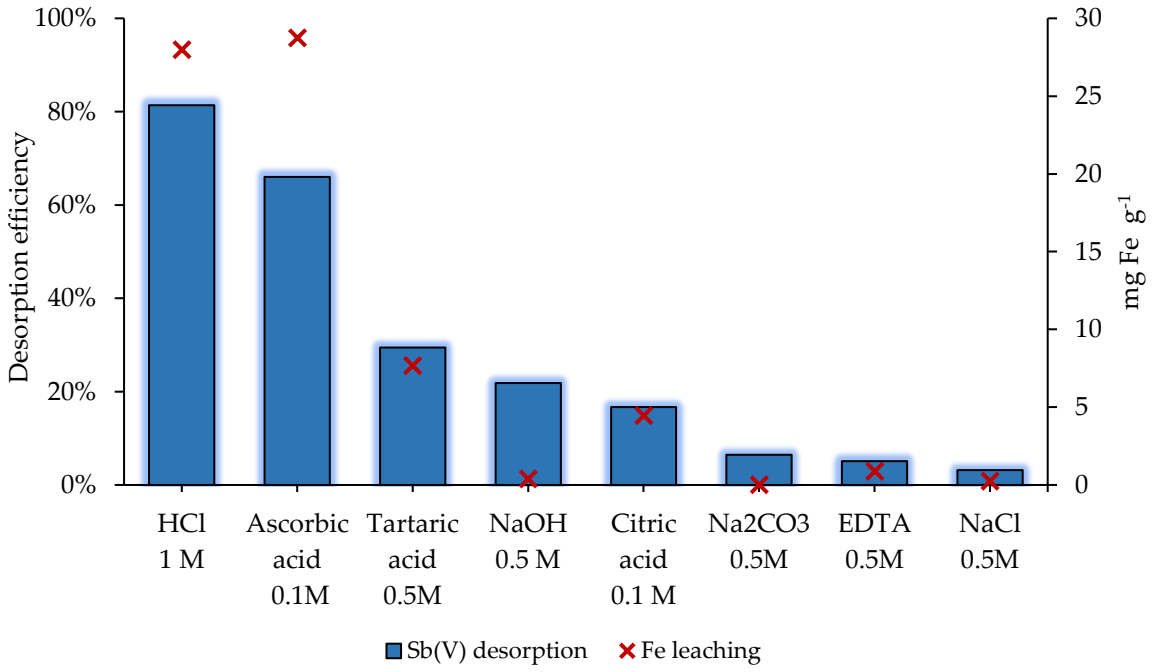


Figure 5.5: Desorption efficiency of Sb(V) from ICG in batch mode and iron leaching for each eluent (S/L = 2.5 g L-1; 20ºC; 10 ± 1 mg Sb(V)/g ICG; Initial iron loading = 29 ± 3 mg Fe/g ICG).

Table 5.5: Experimental data of desorption of Sb(V) in batch mode from iron-coated cork granulates using different eluents (S/L = 2.5 g L^{-1}; 20ºC; 10 ± 1 mg Sb(V)/g ICG).

Eluent	Concentration (M)	mg Sb(V)/g ICG	Iron leached (mg g^{-1})	Desorption efficiency (%)	Initial pH	Final pH
H_2O	-	0.00	0.00	0.00	-	4.21
NaCl	0.5	0.3 ± 0.4	0.25 ± 0.07	3 ± 4	-	4.31
EDTA	0.5	0.5 ± 0.4	0.87 ± 0.07	5 ± 4	-	8.17
NaOH	0.1	1.5 ± 0.4	0.16 ± 0.07	14 ± 4	-	12.67
NaOH	0.5	2.3 ± 0.4	0.38 ± 0.07	22 ± 4	13.36	13.46
Na_2CO_3	0.5	0.7 ± 0.4	0.03 ± 0.07	6 ± 4	10.92	10.95
Tartaric acid	0.5	3.1 ± 0.4	7.7 ± 0.4	29 ± 5	1.86	1.85
Citric acid	0.1	1.7 ± 0.5	4.5 ± 0.9	17 ± 5	2.18	2.17
Citric acid	0.5	1.6 ± 0.5	5.1 ± 0.9	16 ± 5	1.86	1.75
Citric acid	1	1.4 ± 0.5	4.9 ± 0.9	13 ± 5	1.55	1.55
Ascorbic acid	0.001	1.5 ± 0.4	2.8 ± 0.2	14 ± 4	3.84	4.01
Ascorbic acid	0.005	4.9 ± 0.4	15.2 ± 0.8	47 ± 6	3.39	3.76
Ascorbic acid	0.01	6.1 ± 0.4	21.0 ± 0.9	58 ± 7	3.23	3.53
Ascorbic acid	0.05	6.9 ± 0.4	24.7 ± 0.9	66 ± 7	2.89	3.06
Ascorbic acid	0.1	6.9 ± 0.5	28.7 ± 1.9	66 ± 8	2.72	2.83
Ascorbic acid	0.5	6.7 ± 0.4	11.8 ± 0.7	64 ± 7	2.35	2.39
Ascorbic acid	1	6.0 ± 0.5	26.8 ± 1.9	58 ± 7	2.13	2.17
HCl	0.1	0.8 ± 0.4	3.2 ± 0.4	8 ± 4	-	1.51
HCl	0.5	5.9 ± 0.4	21.6 ± 0.8	56 ± 7	0.72	0.67
HCl	1	8.5 ± 0.4	28 ± 1	81 ± 9	0.42	0.82

The influence of eluent concentration on desorption was investigated for HCl, ascorbic acid, and citric acid. Each eluent behaved differently (Figure 5.6). Between 0.1 to 1 M, the citric acid desorption efficiency remained nearly constant. Differently, the ascorbic acid efficiency rapidly increased from 0.001 to 0.05 M, reaching a maximum value of 66 ± 8 % at 0.1 M, and started to decrease from 0.1 M to 1 M. In the concentration range of 0.1 M to 1 M, HCl showed a different trend with a rise in efficiency until 81 ± 9 % but a propensity to reach a curve inflection at higher concentrations.

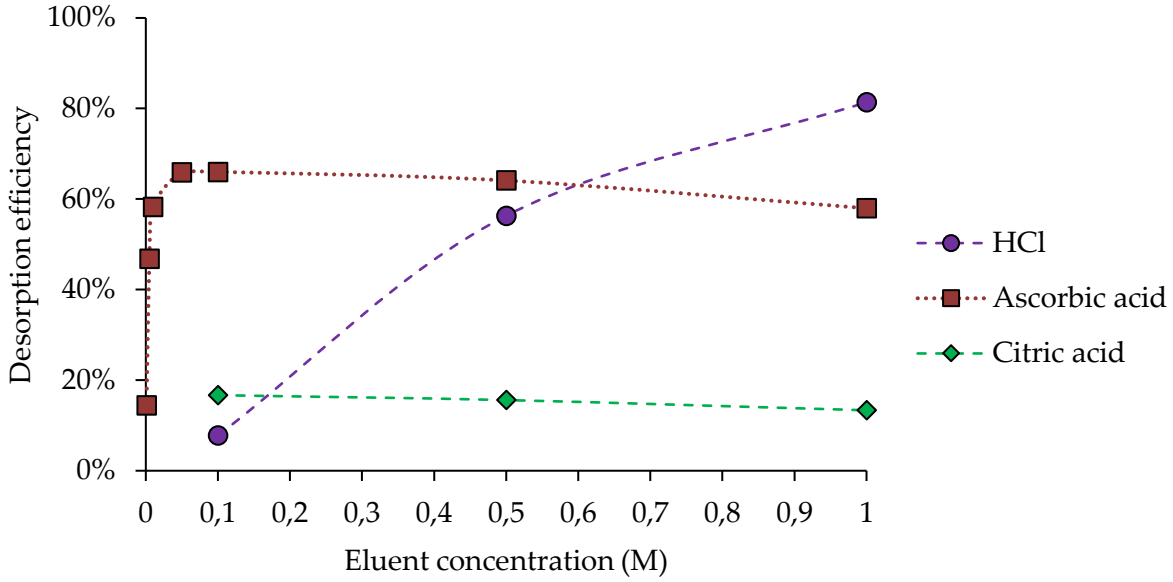


Figure 5.6: Desorption efficiency of Sb(V) versus eluent´s concentration (S/L = 2.5 g L^{-1}; 20ºC; 10 ± 1 mg Sb(V)/g ICG).

The Sb(V) desorption kinetics was studied using the eluents with the highest desorption efficiency at their most efficient concentration: ascorbic acid 0.1 M and HCl 1 M. The results from kinetic model fittings are shown in

Table 5.6 and Figure 5.7. The pseudo-first-order model was the best fit for the experimental data for both desorbing agents, based on the observation of the correlation coefficient (R^2) and the standard error (SE), followed by the pseudo-second-order model and the Elovich model. The difference between each model fitting was higher when the inorganic acid was used.

Table 5.6: Parameters obtained in the fitting of kinetic models to experimental data of desorption kinetics of Sb(V) from ICG.

Model	Parameters	HCl	Ascorbic acid
Pseudo-first-order	q_e (mg g^{-1})	5.7 ± 0.2	5.8 ± 0.3
	k_1 (h^{-1})	0.86 ± 0.05	0.22 ± 0.03
	R^2	0.994	0.976
	SE	0.2	0.4
Pseudo-second-order	q_e (mg g^{-1})	6.3 ± 0.3	7.0 ± 0.5
	k_2 (g mg^{-1} h^{-1})	0.18 ± 0.04	0.03 ± 0.01
	R^2	0.963	0.973
	SE	0.4	0.4
Elovich	a (mg g^{-1} h^{-1})	20 ± 14	2.4 ± 0.7
	b (g mg^{-1})	0.9 ± 0.2	0.57 ± 0.09
	R^2	0.852	0.963
	SE	0.8	0.4

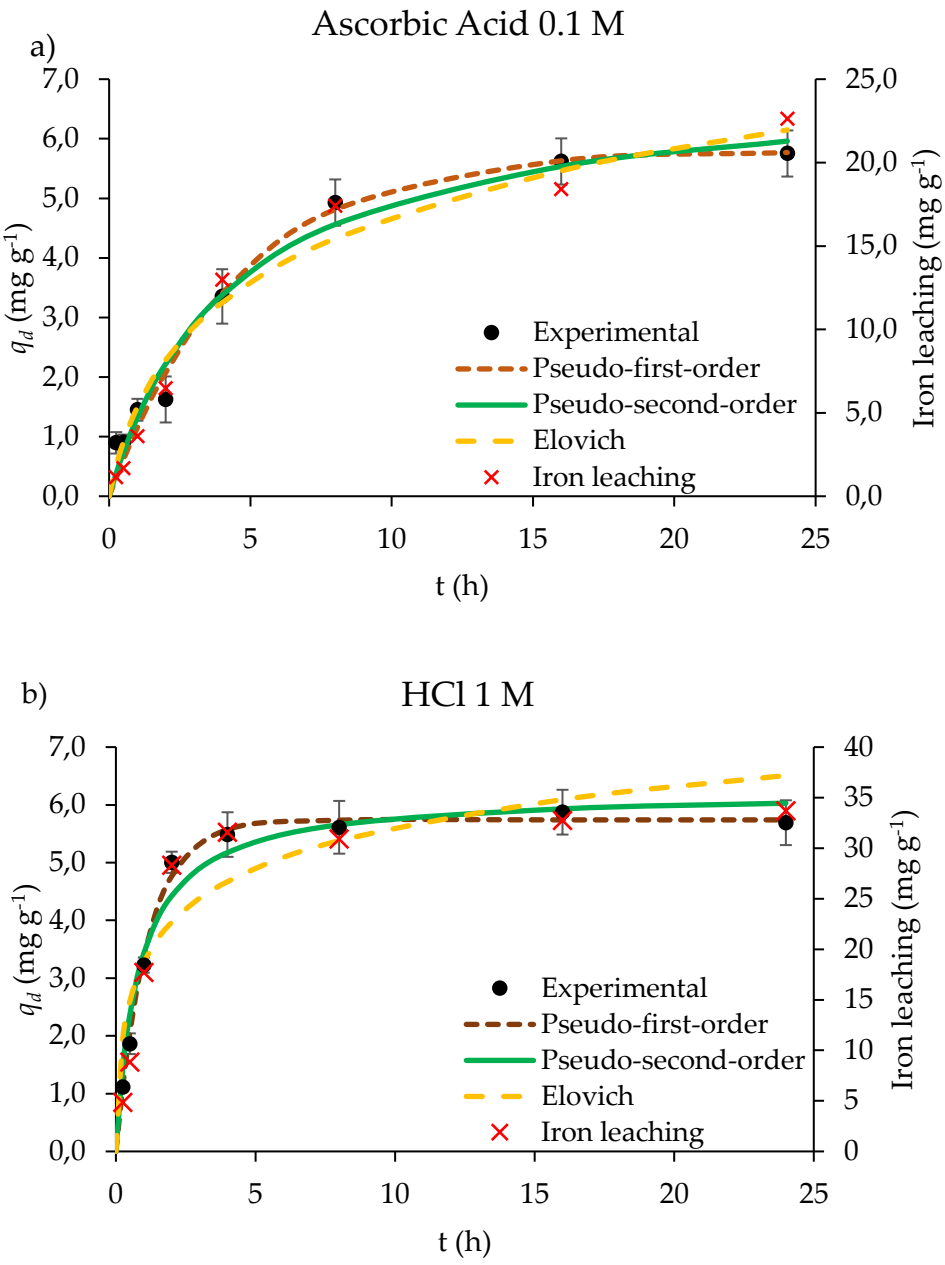


Figure 5.7: Desorption kinetics of Sb(V) by a) ascorbic acid 0.1 M and b) HCl 1 M (S/L = 2.5 g L^{-1}; 20ºC, 10 ± 1 mg Sb(V)/g ICG): experimental data and fits to pseudo-first-order, pseudo-second-order and Elovich models.

Pseudo-first-order model estimations showed that both acids had comparable maximum desorption capacities (q_d) of 5.9 and 5.8 mg Sb(V) g^{-1} for HCl 1 M and ascorbic acid 0.1 M, respectively. However, the curve shapes differed, the curve of HCl 1 M being steeper than the curve of ascorbic acid. This difference in the curves' shapes is reflected in the contact time required to achieve roughly the maximum q_d, which was 16 h and 4 h for ascorbic acid 0.1 M

and HCl 1 M, respectively. The kinetic constant k1 of 0.86 ± 0.05 h^{-1} was also about four times higher for HCl 1 M than that for ascorbic acid 0.1 M of 0.22 ± 0.03 h^{-1}.

The maximum concentration of iron leached in the desorbed solution when using ascorbic acid 0.1 M and HCl 1 M was 23 ± 2 mg g^{-1} and 34 ± 2 mg g^{-1}, respectively, corresponding to approximately 70 and 100% of the iron content in the adsorbent. As hydrochloric acid is more aggressive, the eluent chosen for desorption in continuous mode was the ascorbic acid 0.1 M.

The results revealed that the iron, together with the Sb(V), was desorbed from ICG, possibly posing a barrier to the application of the adsorbent in multiple adsorption cycles. The results differed from As(V) desorption from ICG, in which the basic eluents allowed for the highest desorption rates, and the iron coating was preserved sufficiently to withstand 3 and 5 adsorption/desorption cycles using NaOH 0.1 M and 0.01 M, respectively (Chapter 4).

The increased efficiency of HCl in removing Sb(V) can be attributed to Fe dissolution, and as a result, the removal of previously adsorbed Sb(V) complexed to iron. Runtti et al. (2022) suggest that the higher performance of HCl over NaOH to desorb Sb(V) from Mg-rich mineral adsorbents might be attributed to the forming of chloro-complexes. The affinity of Sb(V) to organic acids such as ascorbic acid, can be justified by the formation of neutral or cationic complexes, while the affinity of Sb(V) towards tartaric acid can be related to the formation of Sb(V)-tartrate complex (Thangaraj and Bhaskarapillai 2020). The finding of this work is in line with the literature, in which citric acid was found to have lower effect on Sb release, compared to tartatric acid (Hu and He 2017).

The NaOH solutions that have proven to be effective eluents for As(V) from ICG were ineffective for desorbing Sb(V) from ICG. Variations in the interaction between arsenate and OH- and antimonate and OH^- in alkaline solutions can explain these differences. Antimony has a lower negative charge at high pH values (-1) compared to arsenic (-3) (Ungureanu, Santos et al. 2015). When the ICG surface charge becomes negative at alkaline pH values (its pHpzc is 6 (Pintor, Vieira et al. 2018)), that can cause a more repulsive effect on arsenate, which might not be observed for antimonate. Another difference between antimony and arsenic that might be related to their different interaction with NaOH is the molecular structure. Sb(V) is arranged with oxygen in an octahedral geometry, while As(V) forms a lower spatial structure in a tetrahedral geometry (Simeonidis, Papadopoulou et al. 2017), leading to different adsorption (Pintor, Vieira et al. 2020) and, consequently, desorption mechanisms.

5.3.4 Desorption in continuous mode

We performed three adsorption-desorption cycles using 0.1 M ascorbic acid as a desorbing agent. Fresh ICG, regenerated ICG (after Sb desorption) and recycled ICG (after iron reloading) were used in the first, second and third adsorption cycles, respectively. The results are shown in Figure 5.8 and Table 5.7.

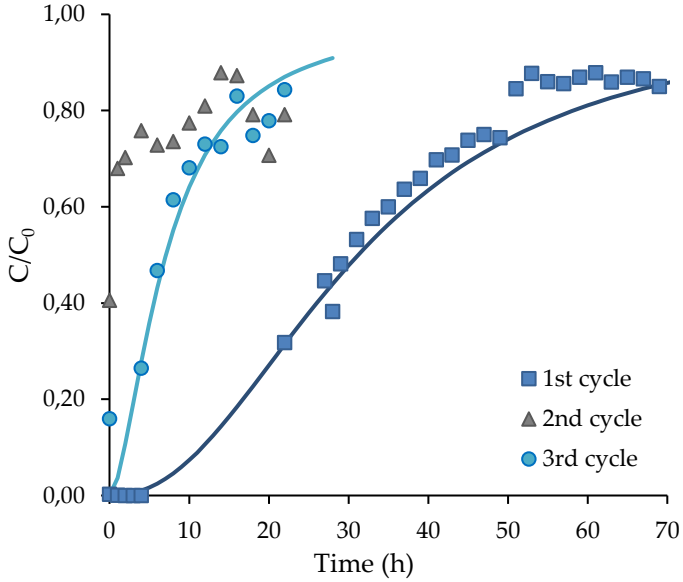


Figure 5.8: Experimental and predicted (Yan model) breakthrough curves for Sb(V) adsorption from fresh ICG, regenerated ICG (after Sb desorption) and recycled ICG (after Fe reloading) (Ci = 5 mg L^{-1}; pH = 3.0, FR = 5 mL min^{-1}, 6 g of ICG, T = 20° C).

Table 5.7: Experimental and predicted parameters (Yan model) of antimonate continuous adsorption using fresh ICG (1st cycle), regenerated ICG (2nd cycle), and recycled ICG (3rd cycle) (± standard error of the mean).

	Parameter	First cycle	Second cycle	Third cycle
Experimental	t_s (h)	69	22	22
	BV_s	367 ± 22	122 ± 7	111 ± 7
	V_s (L)	20.7 ± 0.1	6.9 ± 0.1	6.2 ± 0.1
	q_s (mg g^{-1})	8.0 ± 0.6	1.4 ± 0.4	1.9 ± 0.8
Predicted	Q_{ya} (mg g^{-1})	7.5 ± 0.3	-	1.4 ± 0.2
	α_{ya}	2.7 ± 0.1	-	1.7 ± 0.2
	SE (mg g^{-1})	0.03	-	0.06
	R^2	0.990		0.966

The fresh ICG achieved a saturation adsorption capacity (q_s), according to the Yan model, of 7.5 ± 0.3 mg Sb(V) g^{-1}. Following adsorption, a desorption cycle was conducted for 7 h using ascorbic acid 0.1 M, resulting in a desorption capacity of 6.6 ± 0.2 mg Sb(V) g^{-1} (88 ± 4 %). Nevertheless, the iron leaching observed in batch desorption studies was also observed in continuous mode, with an iron removal of approximately 27.0 ± 0.8 mg Fe g^{-1}, 87 ± 4 % of the original iron content in the adsorbent. Following desorption, another AD cycle was carried out, and as expected, the Sb(V) removal by the adsorbent was no longer feasible. This is a result of the absence of active sites from the iron coating leached in the previous desorption assay.

A new iron coating was carried out to regenerate and recycle the adsorbent. An AD cycle was run with recycled ICG, and a saturation adsorption capacity of 1.4 mg Sb(V) g^{-1} (Yan model) was achieved, about 80% lower than the value obtained with fresh ICG. Another study using Fe(III) modified kapok fiber after adsorption/desorption cycles (using HCl as eluent), further reinvigorated with iron, showed a reduction in arsenic removal of 55% compared to the one found using fresh adsorbent (Yeo, Li et al. 2022). The authors suggested this might have been caused by damage in the structure of the natural adsorbent. For this reason, material characterization studies were carried out on ICG before and after adsorption and regeneration to understand possible modifications on the cork material that caused recycling to be ineffective.

5.3.5 Analysis of fresh, regenerated and recycled adsorbent

The iron content from fresh and recycled ICG was determined by acid digestion followed by FAAS. Results showed that recycled ICG had an iron loading of 13 ± 1 mg g^{-1}, which was 58 ± 4% lower than the iron loading of fresh ICG (31 ± 1 mg g^{-1}). Therefore, the decrease in iron content in the adsorbent likely relates to the lower performance of the recycled adsorbents in terms of Sb(V) uptake.

SEM was used to compare the morphology and structure of the iron-coated cork granulates before and after desorption. Figure 5.9 shows SEM micrographs of the ICG and recycled ICG after Sb(V) adsorption, and ICG after desorption using ascorbic acid 0.1 M and HCl 1 M. The Sb(V)-loaded ICG (Figure 5.9ab) does not show a visual modification in comparison to fresh ICG (before adsorption) as shown in Chapter 4 and reported by Pintor, Vieira et al. (2018), with visible iron deposits and structured cell walls laid in “bricks”. In contrast, recycled ICG has a different cell structure, with wrinkled cells and fewer iron deposits (Figure 5.9c and d). This

structural alteration, accompanied by a reduction in iron content, explains the lower efficiency of the recycled material in adsorbing antimonate.

The iron layer is nearly eliminated in the samples after one adsorption-desorption cycle. However, it is still detectable in the ICG desorbed with ascorbic acid 0.1 M (Figure 5.9e). Overall, it seems the wall composition was not altered after desorption, but the adsorbent structure became less compact, with the cells more open, which might be the reason influencing iron fixation. SEM micrographs of ICG samples after treatments with NaOH 0.1 M and NaOH 0.01 M revealed a stronger degradation in the adsorbent structure (Chapter 4). Nonetheless, the alkaline treatment did not remove as much iron from the cork cells as the acid eluents (Figure 5.9ef).

The EDS results of ICG before and after desorption determined from the SEM images are shown (Figure 5.10). Before desorption, the most abundant elements in ICG are Sb and Fe, with lower peaks of C and O. As predicted, Sb and Fe are much less present in the samples after desorption, with C and O remaining as the most abundant elements of the organic adsorbent.

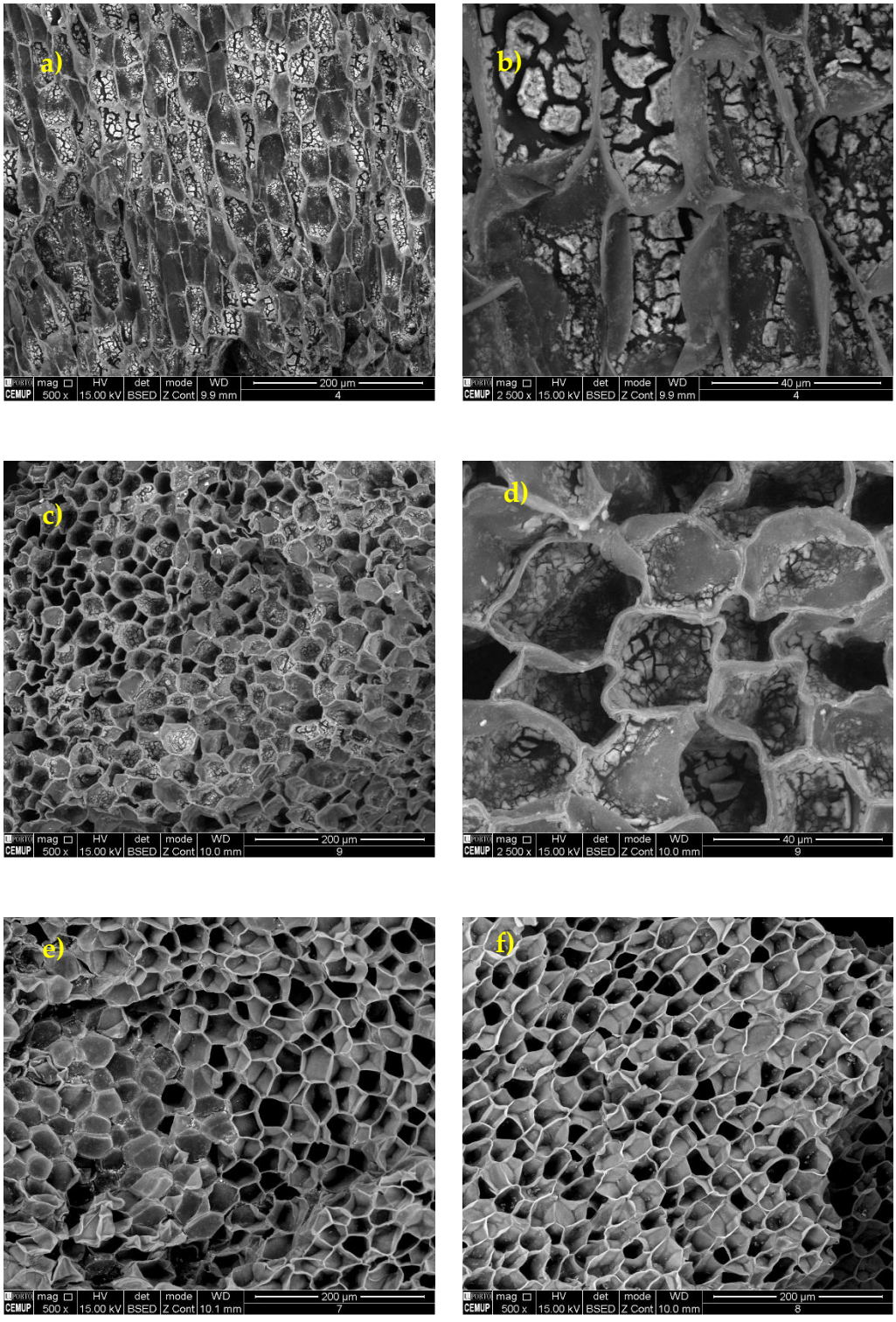


Figure 5.9: SEM micrographs of: ICG after Sb(V) adsorption, a) 500x magnification, and b) 2500x magnification; recycled ICG after Sb(V) adsorption, c) 500x magnification, and d) 2500x magnification; ICG after Sb(V) desorption e) with acid ascorbic 0.1 M, 500x magnification and f) with HCl 1 M, 500x magnification.

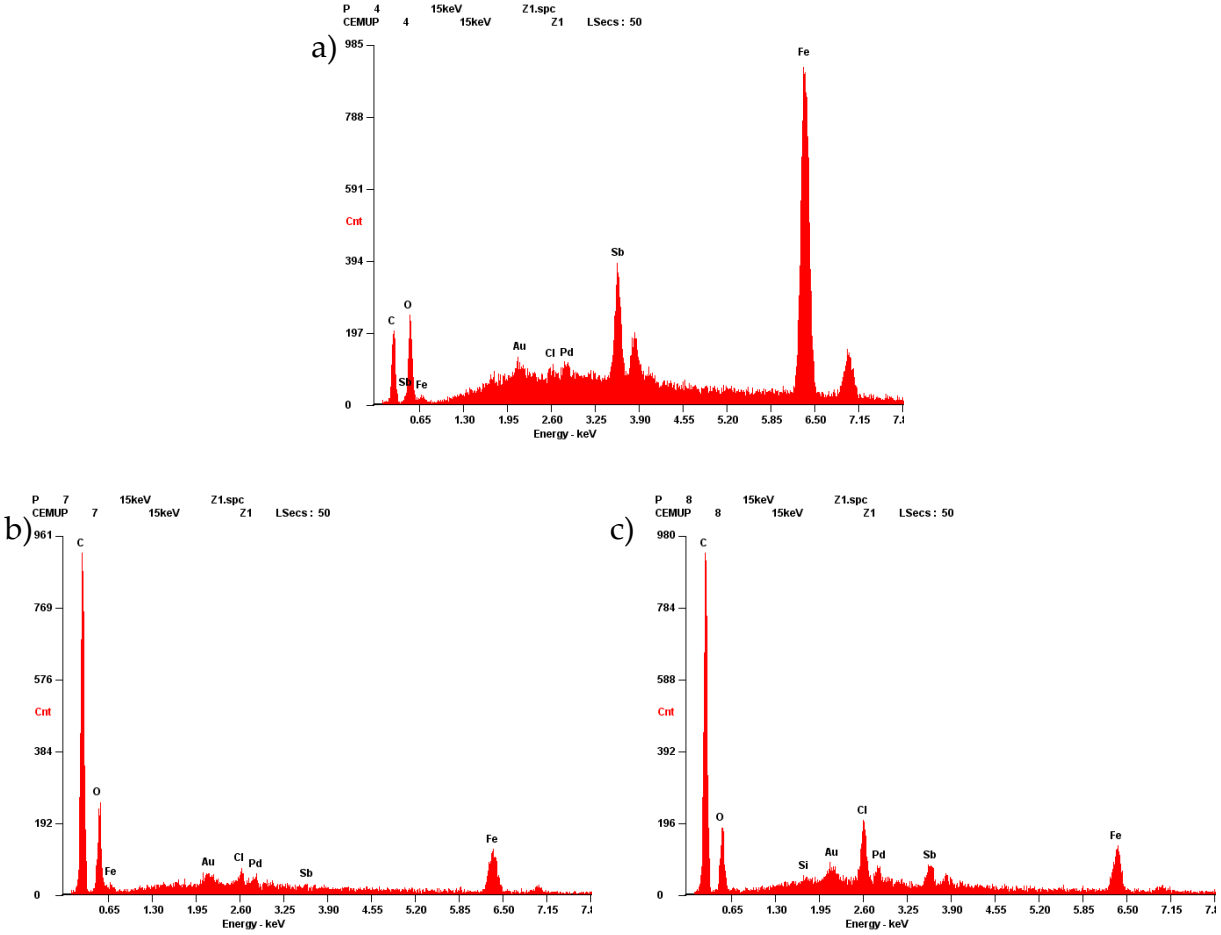


Figure 5.10: EDS analysis of a) Sb(V)-loaded ICG before desorption, b) ICG after desorption with ascorbic acid 0.1 M, c) ICG after desorption with HCl 1 M.

5.4 Conclusions

This Chapter evaluated the scaling up of antimony adsorption using iron-coated cork granulates (ICG), a carbon-neutral material for antimony removal. In continuous mode, the adsorption capacities were 13 ± 2 mg g^{-1} and 10 ± 1 mg g^{-1} for Sb(III) and Sb(V), respectively. However, pH sensitivity reduced performance at higher pH levels, suggesting ICG's preference for treating acid effluents such as acid mine drainage. Acids were effective for Sb desorption from ICG compared to NaOH, salts, or complexing agents. However, iron leaching during desorption impacted the reuse of ICG. Further research should be carried out using real water matrices to identify the interference of other contaminants in the antimony adsorption. For scaling-up the

technology, improvements on the recovery/extraction techniques and environmental impact evaluations are necessary.

5.5 References

Bacelo, H., S. C. R. Santos, A. Ribeiro, R. A. R. Boaventura and C. M. S. Botelho (2022). "Antimony removal from water by pine bark tannin resin: Batch and fixed-bed adsorption." Journal of Environmental Management **302**: 114100.

Bacelo, H., B. R. C. Vieira, S. C. R. Santos, R. A. R. Boaventura and C. M. S. Botelho (2018). "Recovery and valorization of tannins from a forest waste as an adsorbent for antimony uptake." Journal of Cleaner Production **198**: 1324-1335.

Bai, Y., X. Tang, L. Sun, W. Yin, G. Hu, M. Liu and Y. Gong (2022). "Application of iron-based materials for removal of antimony and arsenic from water: Sorption properties and mechanism insights." Chemical Engineering Journal **431**: 134143.

Cappuyns, V., A. Van Campen and J. Helser (2021). "Antimony leaching from soils and mine waste from the Mau Due antimony mine, North-Vietnam." Journal of Geochemical Exploration **220**: 106663.

Deng, R.-J., C.-S. Jin, B.-Z. Ren, B.-L. Hou and A. S. Hursthouse (2017). "The Potential for the Treatment of Antimony-Containing Wastewater by Iron-Based Adsorbents." Water **9**(10): 794.

Dündar, O. A., C. Mehenktaş and Ö. Arar (2022). "Removal of Antimony(III) and Antimony(V) from water samples through water-soluble polymer-enhanced ultrafiltration." Environmental Research **215**: 114324.

Guo, W., Z. Fu, H. Wang, F. Song, F. Wu and J. P. Giesy (2018). "Environmental geochemical and spatial/temporal behavior of total and speciation of antimony in typical contaminated aquatic environment from Xikuangshan, China." Microchemical Journal **137**: 181-189.

Guo, X., Z. Wu, M. He, X. Meng, X. Jin, N. Qiu and J. Zhang (2014). "Adsorption of antimony onto iron oxyhydroxides: Adsorption behavior and surface structure." Journal of Hazardous Materials **276**: 339-345.

Hu, X. and M. He (2017). "Organic ligand-induced dissolution kinetics of antimony trioxide." Journal of Environmental Sciences **56**: 87-94.

Liu, S., H. Feng, L. Tang, H. Dong, J. Wang, J. Yu, C. Feng, Y. Liu, T. Luo and T. Ni (2020). "Removal of Sb(III) by sulfidated nanoscale zerovalent iron: The mechanism and impact of environmental conditions." Science of The Total Environment **736**: 139629.

Manaka, M., N. Yanase, T. Sato and K. Fukushi (2007). "Natural attenuation of antimony in mine drainage water." GEOCHEMICAL JOURNAL **41**(1): 17-27.

Mishra, S., J. Dwivedi, A. Kumar and N. Sankararamakrishnan (2016). "Removal of antimonite (Sb(iii)) and antimonate (Sb(v)) using zerovalent iron decorated functionalized carbon nanotubes." RSC Advances **6**(98): 95865-95878.

Pintor, A. M. A., C. C. Brandão, R. A. R. Boaventura and C. M. S. Botelho (2020). "Multicomponent adsorption of pentavalent As, Sb and P onto iron-coated cork granulates." Journal of Hazardous Materials: 124339.

Pintor, A. M. A., C. C. Brandão, R. A. R. Boaventura and C. M. S. Botelho (2021). "Multicomponent adsorption of pentavalent As, Sb and P onto iron-coated cork granulates." Journal of Hazardous Materials **406**: 124339.

Pintor, A. M. A., B. R. C. Vieira, R. A. R. Boaventura and C. M. S. Botelho (2020). "Removal of antimony from water by iron-coated cork granulates." Separation and Purification Technology **233**: 116020.

Pintor, A. M. A., B. R. C. Vieira, S. C. R. Santos, R. A. R. Boaventura and C. M. S. Botelho (2018). "Arsenate and arsenite adsorption onto iron-coated cork granulates." Science of The Total Environment **642**: 1075-1089.

Qiu, S., L. Yan and C. Jing (2019). "Simultaneous removal of arsenic and antimony from mining wastewater using granular TiO2: Batch and field column studies." Journal of Environmental Sciences **75**: 269-276.

Runtti, H., T. Luukkonen, S. Tuomikoski, T. Hu, U. Lassi and T. Kangas (2022). "Removal of antimony from model solutions, mine effluent, and textile industry wastewater with Mg-rich mineral adsorbents." Environmental Science and Pollution Research.

Runtti, H., T. Luukkonen, S. Tuomikoski, T. Hu, U. Lassi and T. Kangas (2023). "Removal of antimony from model solutions, mine effluent, and textile industry wastewater with Mg-rich mineral adsorbents." Environmental Science and Pollution Research **30**(6): 14139-14154.

Sazakli, E., S. V. Zouvelou, I. Kalavrouziotis and M. Leotsinidis (2014). "Arsenic and antimony removal from drinking water by adsorption on granular ferric oxide." Water Science and Technology **71**(4): 622-629.

Simeonidis, K., V. Papadopoulou, S. Tresintsi, E. Kokkinos, I. A. Katsoyiannis, A. I. Zouboulis and M. Mitrakas (2017). "Efficiency of Iron-Based Oxy-Hydroxides in Removing Antimony from Groundwater to Levels below the Drinking Water Regulation Limits." Sustainability **9**(2): 238.

Sun, F., Y. Yan, H. Liao, Y. Bai, B. Xing and F. Wu (2014). "Biosorption of antimony(V) by freshwater cyanobacteria Microcystis from Lake Taihu, China: effects of pH and competitive ions." Environmental Science and Pollution Research **21**(9): 5836-5848.

Thangaraj, V. and A. Bhaskarapillai (2020). "Organic acids modify the binding selectivity of crosslinked poly(ionic liquid) between Sb(III) and Sb(V)." Materials Today Communications **25**: 101507.

Ungureanu, G., C. Filote, S. C. R. Santos, R. A. R. Boaventura, I. Volf and C. M. S. Botelho (2016). "Antimony oxyanions uptake by green marine macroalgae." Journal of Environmental Chemical Engineering **4**(3): 3441-3450.

Ungureanu, G., S. Santos, R. Boaventura and C. Botelho (2015). "Arsenic and antimony in water and wastewater: Overview of removal techniques with special reference to latest advances in adsorption." Journal of Environmental Management **151**: 326-342.

Ungureanu, G., S. C. R. Santos, I. Volf, R. A. R. Boaventura and C. M. S. Botelho (2017). "Biosorption of antimony oxyanions by brown seaweeds: Batch and column studies." Journal of Environmental Chemical Engineering **5**(4): 3463-3471.

Verbinnen, B., C. Block, P. Lievens, A. Van Brecht and C. Vandecasteele (2013). "Simultaneous removal of molybdenum, antimony and selenium oxyanions from wastewater by adsorption on supported magnetite." Waste and Biomass Valorization **4**(3): 635-645.

Yan, G., T. Viraraghavan and M. Chen (2001). "A New Model for Heavy Metal Removal in a Biosorption Column." Adsorption Science & Technology **19**(1): 25-43.

Yang, K., Y. Liu, Y. Li, Z. Cao, C. Zhou, Z. Wang, X. Zhou, S. A. Baig and X. Xu (2019). "Applications and characteristics of Fe-Mn binary oxides for Sb(V) removal in textile wastewater: Selective adsorption and the fixed-bed column study." Chemosphere **232**: 254-263.

Yang, X., Z. Shi and L. Liu (2015). "Adsorption of Sb(III) from aqueous solution by QFGO particles in batch and fixed-bed systems." Chemical Engineering Journal **260**: 444-453.

Yeo, K. F. H., C. Li, Y. Dong, Y. Yang, K. Wu, H. Zhang, Z. Chen, Y. Gao and W. Wang (2022). "Adsorption performance of Fe(III) modified kapok fiber for As(V) removal from water." Separation and Purification Technology **287**: 120494.

Zhang, C., H. Jiang, Y. Deng and A. Wang (2019). "Adsorption performance of antimony by modified iron powder." RSC Advances **9**(54): 31645-31653.

Zhang, D., X. Pan, L. Zhao and G. Mu (2011). "Biosorption of antimony (Sb) by the cyanobacterium Synechocystis sp." Pol J Environ Stud **20**: 1353-1358.

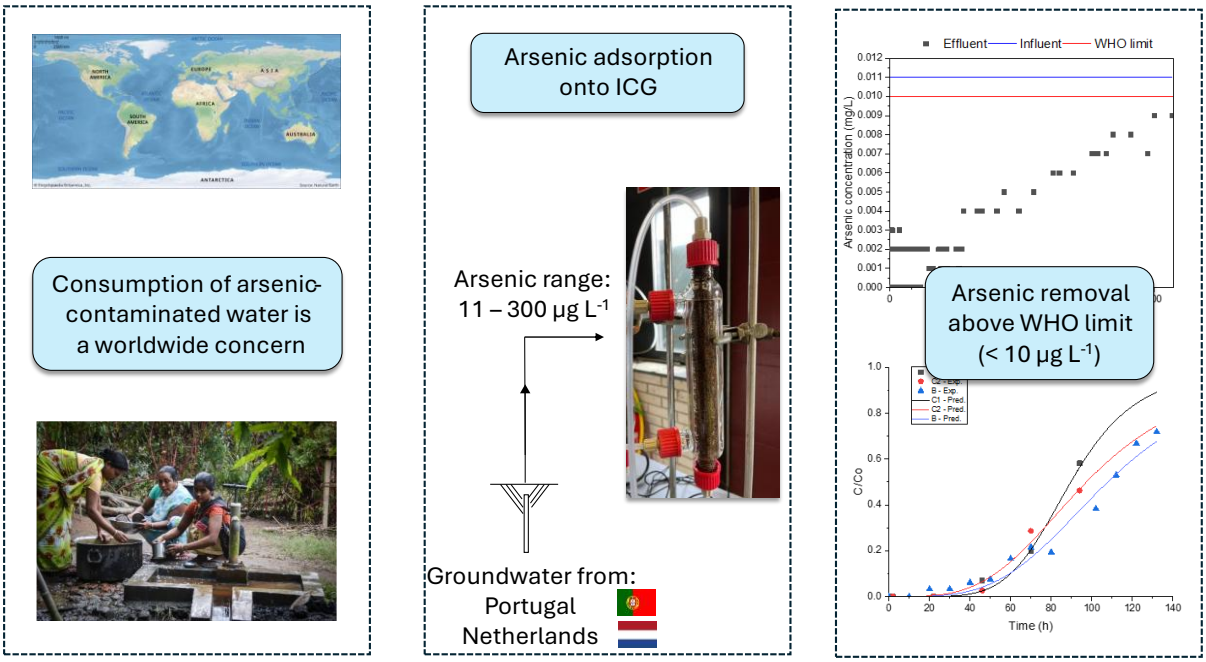
Zhang, L., Y. Dong, J. Liu, C. Liu, W. Liu and H. Lin (2022). "The effect of co-pyrolysis temperature for iron-biochar composites on their adsorption behavior of antimonite and antimonate in aqueous solution." Bioresource Technology **347**: 126362.

Zhu, H., Q. Huang, S. Fu, X. Zhang, Z. Yang, J. Lu, B. Liu, M. Shi, J. Zhang, X. Wen and J. Li (2021). "Removal of Antimony(V) from Drinking Water Using nZVI/AC: Optimization of Batch and Fix Bed Conditions." Toxics **9**(10): 266.

Zou, J.-P., H.-L. Liu, J. Luo, Q.-J. Xing, H.-M. Du, X.-H. Jiang, X.-B. Luo, S.-L. Luo and S. L. Suib (2016). "Three-Dimensional Reduced Graphene Oxide Coupled with Mn3O4 for Highly Efficient Removal of Sb(III) and Sb(V) from Water." ACS Applied Materials & Interfaces **8**(28): 18140-18149.

6 ARSENIC REMOVAL FROM DIFFERENT GROUNDWATER MATRICES

This chapter is based on: M. A. Carneiro, L. L. F. Agostinho, R. A. R. Boaventura, C. M. S. Botelho and A. M. A. Pintor. *Advances in the treatment of arsenic-contaminated groundwater by the adsorption onto iron-coated cork granulates on fixed-bed column*. Groundwater for Sustainable Development (under review).



Iron-coated cork granulates (ICG) are an emerging adsorbent successfully tested in continuous mode for the removal of arsenic and other oxyanions in water. Novel adsorbents are being reported in the literature showing good arsenic adsorption capacities in aqueous solution, however, many fail to achieve arsenic removal under legal limits for water intended for human consumption when treating natural water samples with a complex matrix. The present study investigates the impact of different groundwater (GW) matrices, from wells in Portugal and The Netherlands, on arsenic adsorption onto iron-coated cork granulates. Groundwater (As-spiked or not) was treated in lab-scale fixed-bed columns from initial concentrations (11 - 300 µg L^{-1}) until the arsenic WHO guideline and European Union Directive 2020/2184 of 10 µg L^{-1}. The effect of an oxidation-filtration pretreatment was also investigated.

The ICG demonstrated the capacity to treat real groundwater across a wide range of arsenic concentrations under10 µg L^{-1}. The ICG performed better in the GW matrix from The Netherlands than that from Portugal. That could be attributed to the elevated concentrations of nitrate in the Portuguese matrix, which might have a stronger competitiveness with the arsenic oxyanions for the ferric sites in the adsorbent, compared to the more abundant chloride in the Dutch matrix. Moreover, the pretreatment using the aeration/sand filter reactor improved the arsenic removal in the Dutch matrix, and it reached values of breakthrough time, treated volume at breakthrough and bed volumes at breakthrough of 39 ± 5 h, 12 ± 2 L, 202 ± 27 and, respectively, for an initial concentration of 300 ± 10 µg L^{-1}. This study showed that the use of low-cost environmentally friendly iron-coated cork granulates to remove arsenic from groundwater is feasible at different concentrations in different water matrices.

6.1 Introduction

As the adsorbent can be responsible for 70% of the operational costs of an adsorption system for water treatment (Dotto and McKay 2020), the search for low-cost adsorbents is highly relevant in the water sector (Bhattacharya, Talukdar et al. 2023). Novel adsorbents are being reported in the literature with good adsorption capacities for a specific element in aqueous solution. However, many fail to achieve arsenic removal under legal limits when treating real water samples with a complex matrix, which is still a major weak point in literature (Dotto and McKay 2020, Bhattacharya, Talukdar et al. 2023, Sharma, Singh et al. 2023).

In Chapter 4, iron-coated cork granulates were able to reduce arsenic concentration under WHO limits from arsenic-spiked groundwater matrix from Portugal. In this Chapter, the impact of different groundwater matrices, from wells in Portugal and in the Netherlands was investigated.

6.2 Materials and methods

6.2.1 Adsorbent preparation

The adsorption assays from Chapters 3, 4 and 5 were carried out using iron-coated cork granulates (ICG) produced, as described by Pintor et al. (2018), by putting cork granulates (0.5-1.0 mm) in contact with a 0.05M $FeCl_3$ solution for 24h in 50 mL tubes, at a S/L = 20 g/L and a controlled temperature of 20ºC. For this Chapter, the method from Pintor et al. (2018) was adapted, so that the iron-coated cork granulates could be produced in a larger amount, increasing the maximum production capacity by 13x. The parameters for the small and medium capacity of ICG production on a lab scale are described in Table 6.1. The rotating shakers for each scale are shown in Figure 6.1.

Table 6.1: Parameters of iron-coated cork granulates production in lab scale.

	Small scale	**Medium scale**
Rotating shaker device	Stuart, SB3	Ovan, R8-HD E
Rotation (rpm)	20	20
Flask volume (L)	0.05	2
Total volume (L)	1.2	16
Solid/Liquid rate (g/L)	20	20
Coating solution concentration (mol/L)	0.05	0.05
Coating solution pH	7.0	7.0
Coating time (h)	24	2, 4, 6, 16 and 24
Temperature (°C)	20	room
Maximum mass of ICG produced (g)	21.6	288



Figure 6.1: Rotator mixers with 16L (left) and 1.2 L capacity (right).

The effect of coating times equal to 2, 4, 6, 16 and 24 hours on iron content and arsenic adsorption capacity of the ICG were investigated. The iron loading was measured by acid digestion followed by Fe detection in FAAS. The adsorption capacity was tested by measuring the remaining arsenic after a 40 mg L^{-1} arsenate solution (prepared by diluting, in distilled water, a standard solution of 995 ± 81 mg As(V) L^{-1}, originated from $HAsNa_2O_4{\cdot}7H_2O$ (Sigma-Aldrich; analytical grade) in 2% HCl) was put in contact with ICG at a 2.5 g/L solid-liquid rate in 50 mL flasks for 48h. Total organic carbon was measured in the solution after 48h (Shimadzu Equipment TOC-L).

To investigate the effect of reusing the coating solution, the same 0.05 M $FeCl_3$ solution was used for four consecutive coating cycles of 2h each.

6.2.2 Fixed-bed adsorption column studies in Portugal

6.2.2.1 Feeding water

The feeding water was 100 L of groundwater collected from a well in Northern Portugal in February 2023. The groundwater characterization is shown in
Table 6.2.

Table 6.2: Groundwater composition from Portuguese well.

Parameters	Value	Unit	Analytical Method
pH	6.95		Electrode
Conductivity	238-261	µS cm^{-1}	Multiparametric probe
Dissolved oxygen	2.5 – 4.6	mg L^{-1} DO	Multiparametric probe
Total solids	125 ± 14	mg L^{-1}	Gravimetric
Total dissolved solids	125 ± 14	mg L^{-1}	Gravimetric
Total suspended solids	ND	m mg L^{-1}g L^{-1}	Gravimetric
TOC (Total organic carbon)	2.3 ± 0.2	mg L^{-1}	Catalytic Oxidation and IR detection
Calcium	7.14	mg L^{-1}	ICP-AES
Copper	53	µg L^{-1}	ICP-AES
Iron	0.024	mg L^{-1}	ICP-AES
Potassium	1.84	mg L^{-1}	ICP-AES
Magnesium	2.16	mg L^{-1}	ICP-AES
Sodium	15	mg L^{-1}	ICP-AES
Lead	1	µg L^{-1}	ICP-AES
Aluminum	25	µg L^{-1}	ICP-AES
Boron	5	µg L^{-1}	ICP-AES
Cadmium	ND	µg L^{-1}	ICP-AES
Chromium	1	µg L^{-1}	ICP-AES
Manganese	ND	µg L^{-1}	ICP-AES

Parameters	Value	Unit	Analytical Method
Nickel	ND	µg L^{-1}	ICP-AES
Zinc	61	µg L^{-1}	ICP-AES
Arsenic	11	µg L^{-1}	ICP-AES
Lithium	9	µg L^{-1}	ICP-AES
NO_3^-	30	mg L^{-1}	Glass Electrode
Cl^-	20.4	mg L^{-1}	Argentometric
PO_4^{3-}	0.12	mg P L^{-1}	Colorimetric with ascorbic acid
SO_4^{2-}	ND	mg L^{-1}	Turbidimetric

6.2.2.2 Experimental set-up

The continuous adsorption experiments were conducted in a lab installation at the Laboratory of Separation and Reaction Engineering – Laboratory of Catalysis and Materials (LSRE-LCM) (Faculty of Engineering of The University of Porto, Portugal). The lab-scale adsorption system was the same as described in Chapter 3 (Figure 3.1) with the following operating parameters - flow rate: 5 mL min^{-1}, bed height: 12 cm, diameter: 2.5 cm, adsorbent mass: 6 g, temperature: 20 °C, bed volume: 59 mL, empty bed contact time (EBCT): 12 min. The fixed-bed column was operated using downward flow due to the low density of the adsorbent.

6.2.3 Fixed-bed adsorption column studies in The Netherlands

6.2.3.1 Feeding water

The fixed-bed column assays were carried out using groundwater pumped from a well with about 40 meters depth located in the Water Application Center (Van Hall Larenstein University of Applied Sciences, The Netherlands). Assays were conducted using both raw/untreated and treated groundwater after a pretreatment system for iron removal. The composition of the groundwater before and after the pretreatment is shown in

Table 6.3. Table 6.4 shows the analytical methods applied to determine each parameter.

A total arsenic solution of 1,000 mg L^{-1} (ICP standard – VWR/PROLABO) was diluted in demineralized water to prepare the 0.5 mg L^{-1} mother solution for the groundwater spiking. Nitric acid 68% (VWR) was used for sample conservation.

Table 6.3: Groundwater composition from the Dutch well, before (untreated) and after (treated) the pretreatment for iron removal in April 2023.

Parameters	Value (µg L^{-1})		Efficiency removal (%)	Guidelines/Limits for drinking water (µg L^{-1})		
	Untreated groundwater	Treated groundwater		WHO (WHO 2022)	EU (European Union 2020)	Netherlands (Netherlands 2023)
Calcium	237,000	23,700	90			
Copper	1.35	1.35	-	2,000	2,000	2,000
Iron	4770	197	95.9	300	200	200
Potassium	29,800	30,300	-1.7			
Magnesium	98,200	98,600	-0.4			
Sodium	540,000	546,000	-1.1	50,000	200,000	150,000
Silver	<0.50	<0.50	-	100		
Barium	627	546	12.9	1300		
Beryllium	<0.10	<0.10	-			
Molybdenum	<0.50	<0.50	-			
Lead	<2.00	2.54	>27	10	10	5
Rubidium	72.9	76.5	-4.9			
Aluminium	<5.00	<5.00	-	100-200	200	200
Boron	243	245	-0.8	2400	1,500	1,500
Cadmium	0.24	<0.20	>16.7	3	5	5
Cobalt	1.66	<1.00	>39.8			
Chromium	<5.00	<5.00	-	50	25	50
Manganese	389	407	-4.6	80	50	50
Nickel	<1.00	<1.00	-	70	20	20
Phosphorus	677	130	80.8			

Parameters	Value (µg L^{-1})		Efficiency removal (%)	Guidelines/Limits for drinking water (µg L^{-1})		
	Untreated groundwater	Treated groundwater		WHO (WHO 2022)	EU (European Union 2020)	Netherlands (Netherlands 2023)
Sulfur	2120	2090	1.4			
Selenium	<5.00	<5.00	-	40	20	20
Silicon	13,200	12,700	3.8			
Tin	<1.00	<1.00	-			
Zinc	6.30	2.29	63.6			3,000
Arsenic	<5.00	<5.0	-	10	10	10
Cerium	<10.0	<10.0	-			
Lithium	25.3	25.9	-2.4			
Lanthanum	<1.00	<1.00	-			
Zirconium	<5.00	<5.00	-			
Strontium	1,040	1,030	1.0			
Tungsten	<10.0	<10.0	-			
Ammonia	2,511	1,276	49.2	-	500	200
NO_2^-	0.000	64	< -63	3,000	500	100
Nt	0.000	624	< -62300			
NO_3^-	0.000	560	< -55900	50,000	50,000	50,000
Cl^-	1,096.724	1,103.127	-0.6	-	250,000	150,000
PO_4^{3-}	502	81	83.9			
SO_4^{2-}	0.000	0.000	-	-	250,000	150,000

Table 6.4: Parameters and methods for the experiments in The Netherlands.

Parameter	**Method**	**Unit**
pH	pH/Ion meter	-
Conductivity	(SevenCompact S220 Mettler Toledo)	mV
Arsenic	Modified Gutzeit test (Semi-quantitative test strips Quantofix® Arsen 10)	mg/L
As, Mn, Fe, Ca, Cu, K, Mg, Na, Ag, Ba, Be, Mo, Pb, Rb, Al, B, Cd, Cobalt, Cr, Ni, P, S, Se, Si, Sn, Zn, Ce, Li, La, Sr, W	ICP-OES (Inductively coupled plasma optical emission spectrometry, Perkin Elmer Optima 5300 DV)	µg/L
Ammonia, NO_2-, Nt, NO_3^-, Cl^-, PO_3^{4-}, SO_4^{2-}	Discrete analyzer spectrophotometry (Aquakem 250, Thermo Scientific)	mg/L

6.2.3.2 Groundwater pretreatment

Large amounts of drinking water in The Netherlands are obtained from underground sources, in which the concentration of iron can reach several tens of milligrams per liter. Whereas 0.2 mg L^{-1} is considered acceptable by the European Commission standards (European Union 2020), the WHO guideline is 0.3 mg L^{-1} (WHO 2022). Iron is found in groundwater as a result of rain percolating through sand, rocks, and other minerals (Chaturvedi and Dave 2012). In general, the iron concentration found in groundwater does not affect human health. Its primary problems include taste, visual effects, clogging, corrosion of iron pipes, and residual iron-based coagulants (Chaturvedi and Dave 2012). Iron occurs naturally in water in soluble form as ferrous iron (bivalent iron in dissolved form Fe(II) or $Fe(OH)^+$) or complexed form as ferric iron (trivalent iron: Fe(III) met in the precipitate $Fe(OH)_3$) (Chaturvedi and Dave 2012). As ferric iron is less soluble than divalent iron, it can be removed by filtration (Sharma, Petrusevski et al. 2003). Many systems apply oxidation-filtration technologies to remove iron from groundwater, by transforming the soluble form to the insoluble form.

The first stage of the iron removal process involves the oxidation by spraying of bivalent iron with oxygen from the air. The chemical reactions were presented in the literature (Sharma, Petrusevski et al. 2003, van de Griend, Warrener et al. 2022). In this process, an electron is lost from the divalent iron to the oxygen, creating ferric iron and water (Eq. (6.1)). Upon reaction with water, ferric iron precipitates as iron hydroxide, $Fe(OH)_3$ (Eq. (6.2)). The summary of the reactions is shown in Eq. (6.3):

$$Fe^{2+} + \frac{1}{4}O_2 + H^+ \rightarrow Fe^{3+} + \frac{1}{2}H_2O \quad (6.1)$$

$$Fe^{3+} + 3H_2O \rightarrow Fe(OH)_3 \downarrow + 3H^+ \quad (6.2)$$

$$Fe^{2+} + \frac{1}{4}O_2 + 2\frac{1}{2}H_2O \rightarrow Fe(OH)_3 \downarrow + 2H^+ \quad (6.3)$$

After oxidation, the iron hydroxide formed is removed by a rapid sand filtration step. The assays were conducted using either raw groundwater and treated groundwater (

Table 6.3). The treatment of the groundwater consists of an iron removal system (REMON industries, Marum, Holland) based on oxidation-filtration. The pilot installation is set in the Water Application Center at the Van Hall Larestein (Leeuwarden, Netherlands) (Figure 6.2). The pilot system aims to remove the iron by oxidation followed by filtration of the iron particles formed by the conversion of Fe^{2+} in $Fe(OH)_3$, as shown in the equations (6.1), (6.2) and (6.3). After the aeration step, filtration takes place on sand particles with a diameter of 0.5-1.5 mm and a speed varying between 5 to 15 m/h.



Figure 6.2: Oxidation-filtration system to remove iron from the groundwater in the Water Application Center: front view(left) and top view (right).

6.2.3.3 Experimental set-up

The lab set-up was installed in the Water Application Center (Figure 6.3). The arsenic adsorption assays were carried out in two identical glass columns to run the two run in parallel for each assay 1 and 2 (Table 6.4). The arsenic removal system was operated in different conditions: 1) using untreated or untreated groundwater spiked with arsenic, and 2) operating in continuous adsorption only during the day (turning the system on in the morning and shutting it down during the night), and 3) having sample collected manually and/or using automatic sampler.

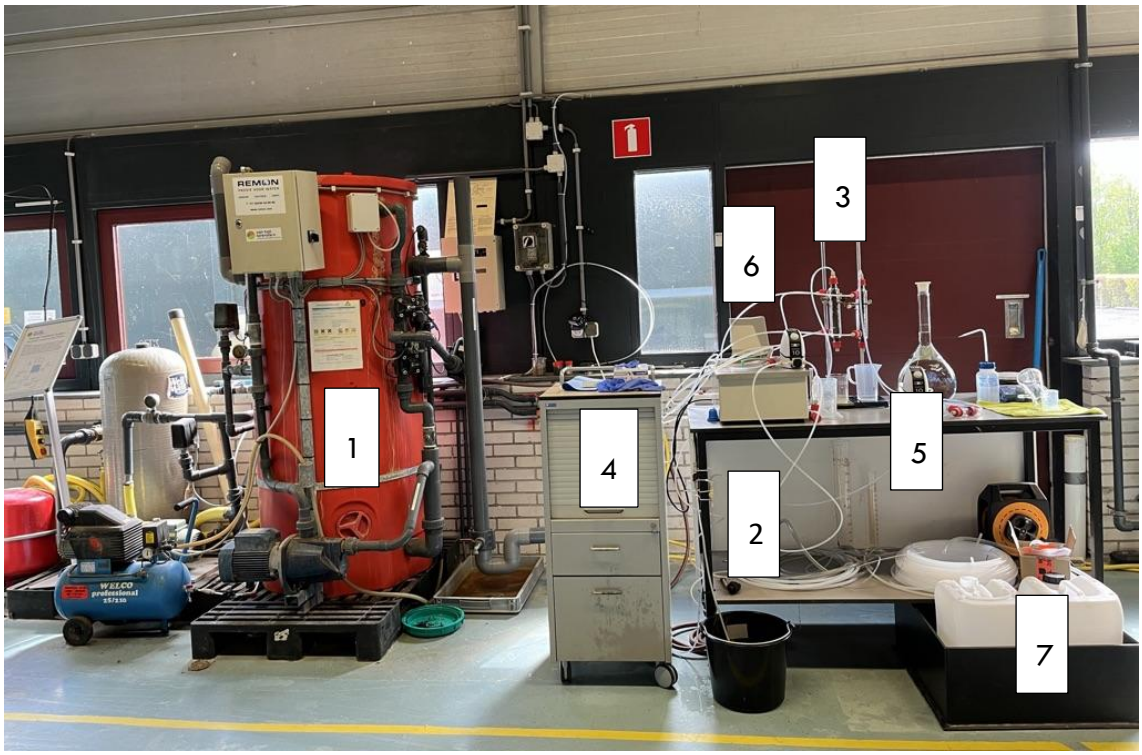


Figure 6.3: Lab installation at the Water Application Center for arsenic adsorption from groundwater in a fixed-bed column.

Table 6.4. Conditions of the adsorption columns assays.

Assay	Adsorption column	Feed	Operation	Sampling
1	Filter A	Raw groundwater	Continuous with daily interruptions	Manual
(Fig. 3a)	Filter B			
2	Filter C1	Treated groundwater	Continuous without interruptions	
(Fig. 3b)	Filter C2			Automatic

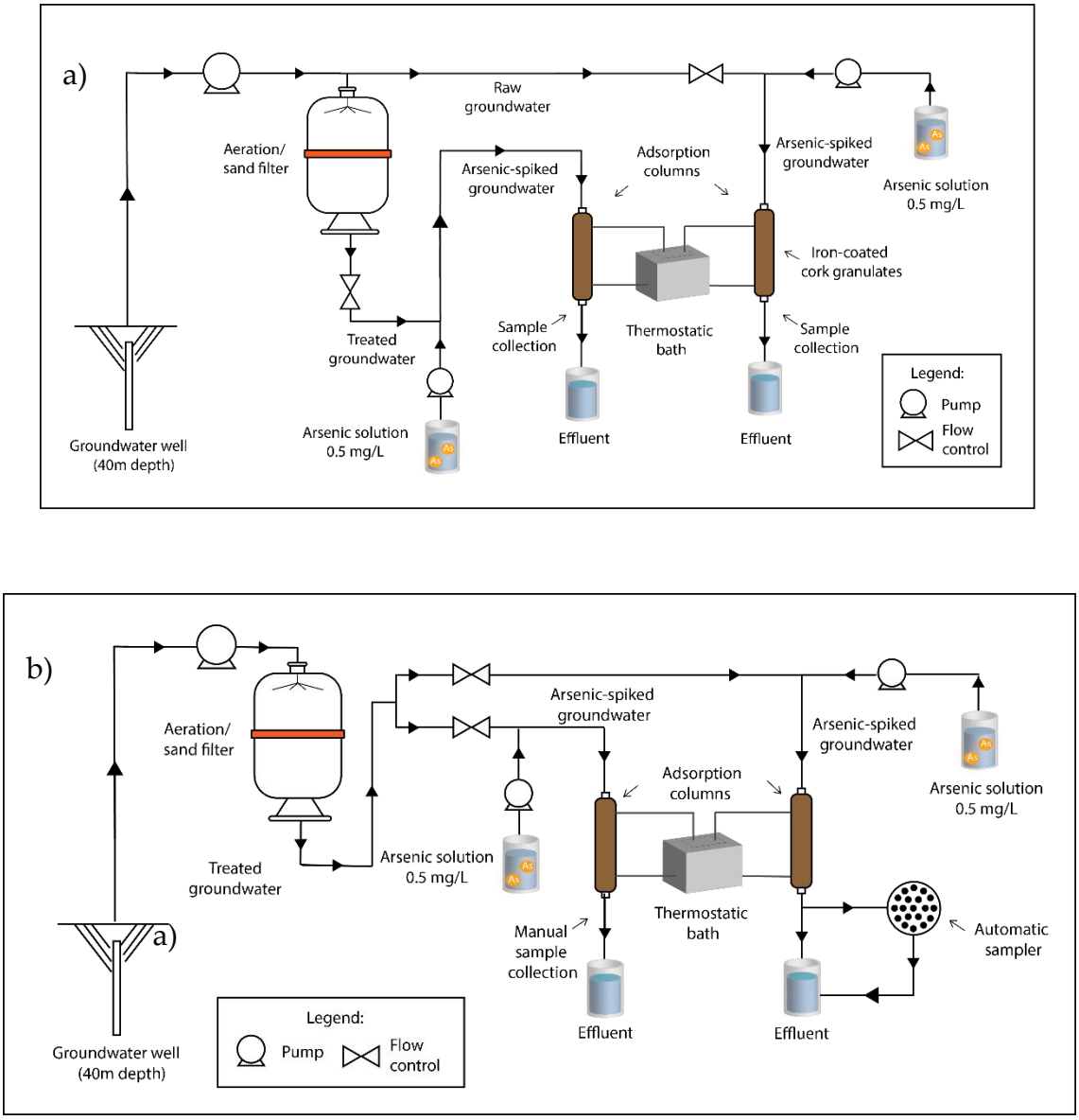


Figure 6.4: Scheme of continuous adsorption system for arsenic removal from groundwater onto iron-coated cork granulates at the Water Application Center (The Netherlands): a) assay 1, b) assay 2.

The lab-scale adsorption system consisted of 1) a groundwater feeding system (well, pump and pipes), 2) flow controllers, 3) adsorption columns filled with ICG, 4) reservoir containing arsenic mother solution, 5) arsenic dosing pumps, 6) thermostatic bath, 7) reservoir for effluent. The fixed-bed columns were operated using downward flow due to the low density of the adsorbent. Each column was filled with 6 g of iron-coated cork granulates, operated using a flow rate of 5 mL min^{-1}, a bed height of 25.5 cm (internal diameter = 1.7 cm), a bed volume of 58 mL, and an empty bed contact time (EBCT) of 12 min. A thermostatic bath circulated water in the columns to maintain a minimum temperature of 20°C. The maximum temperature reached 24°C on

warmer days. Before starting the experiment, the feed water matrix, without the arsenic spiking, was passed through the filter columns for 2h hours. An arsenic solution of 0.5 mg L^{-1} was spiked to achieve an inlet concentration of 0.3 mg L^{-1} using a peristaltic pump.

6.2.3.4 pE x pH diagram

The stability of many solutes in water is highly dependent on pE and pH. The Pourbaix diagrams are used to describe the behavior of those solutes in water environments as a function of redox potential and pH. A pE-pH diagram for iron was created based on the simplified pE-pH diagram for iron in water (Manahan 2017).

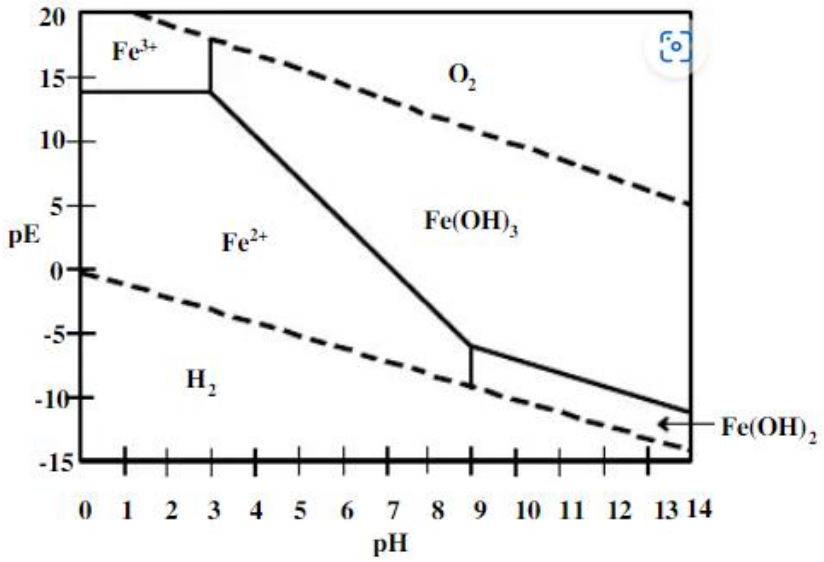


Figure 6.5: Simplified pE-pH diagram for iron in water (Manahan 2017).

To convert the conductivity in pE, the equation below was applied:

$$pE = \frac{Eh \times \mathrm{F}}{2.303 \times R \times T} \qquad (6.4)$$

where,

Eh is the Electrical potential (V), F is the Faraday constant = 23061 (cal/V), R is the Gas constant = 1.987 (cal/degree) and T is the Temperature (K).

The pH and pE values for each column are shown in Table 6.5. The pE was calculated according to Eq. (6.4). All temperatures were 293.15 (T = 20ºC).

Table 6.5: pH, conductivity and pE values.

Column A			Column B		
pH	pE	Cond. (mV)	pH	pE	Cond. (mV)
7.595	-0.880	-51.2	7.734	-0.988	-57.5
7.461	-0.784	-45.6	7.623	-0.970	-56.4
7.235	-0.543	-31.6	7.935	-1.267	-73.7
7.373	-0.674	-39.2	7.517	-0.815	-47.4
7.406	-0.707	-41.1	7.596	-0.882	-51.3
7.293	-0.626	-36.4	7.488	-0.780	-45.4
7.281	-0.590	-34.3	7.558	-0.846	-49.2
7.535	-0.825	-48	7.567	-0.851	-49.5
7.459	-0.775	-45.1	7.622	-0.933	-54.3
7.448	-0.751	-43.7	7.625	-0.916	-53.3
7.604	-0.916	-53.3	7.618	-0.932	-54.2
7.481	-0.789	-45.9	7.623	-0.932	-54.2
7.325	-0.634	-36.9	7.694	-0.997	-58
7.255	-0.643	-37.4	7.609	-0.990	-57.6

6.2.3.5 Dissolved oxygen and flow rate campaign

The study of the relationship between water temperature and dissolved oxygen can provide more insight for assessing water quality (Tan, Zhang et al. 2022). A short campaign was carried out to observe the dissolved oxygen (DO) and flow rate (FR) variation from the treated groundwater. A multichannel oxygen meter (OXY-4 SMA, G3, PreSens®) was used for the automatic recording of DO values in an interval of 30 s, for 1400 minutes. A MIK compact magnetic-inductive flow meter (Kobold) with a digital display, in a working range of 0.16 – 3.2 L/min was used for manual acquisition of flow rate. An initial flow rate of 1 L/min was set. Figure 6.6. shows the experimental setup for DO and FR monitoring.

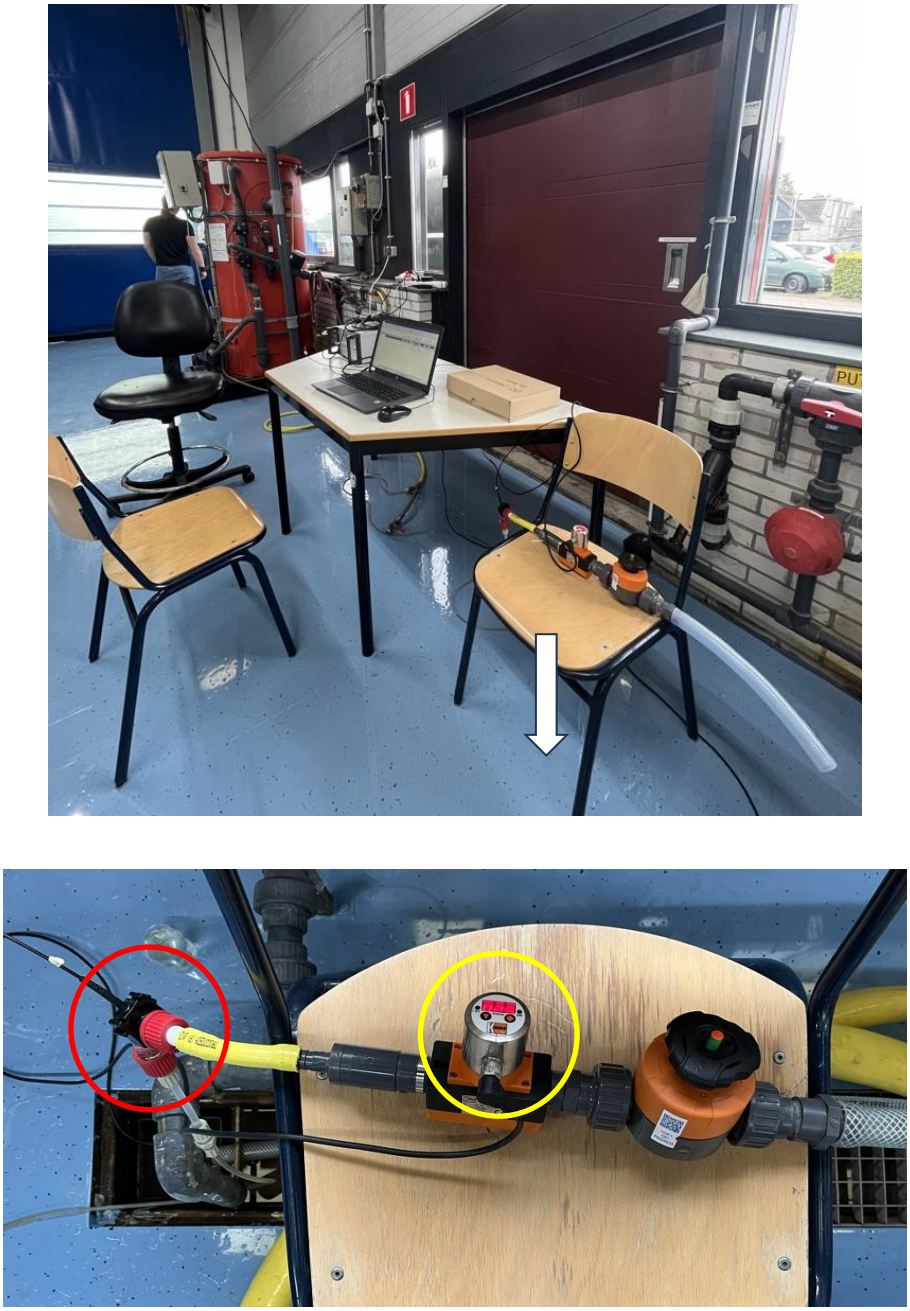


Figure 6.6: DO (red circle) and flow meters (yellow circle) to monitoring the treated groundwater.

6.2.4 Analysis of breakthrough curves

The breakthrough curves (BTC) were created by plotting the quotient of effluent and influent arsenic concentration versus the time. BTCs were characterized in terms of breakthrough time (t_b), bed volumes treated at breakthrough (BVb), adsorption capacity at breakthrough (q_b), treated volume at breakthrough (V_b), arsenic removal at breakthrough (y_b), the mass transfer zone (MTZ) in the column, and the MTZ/Bed height ratio. Each parameter´s calculation was addressed in Chapter 3.

Breakthrough time was defined as the time required to reach the effluent concentration of 10 μg L^{-1}, which is the maximum level allowed by the European Union and the recommended guideline by the World Health Organization (European Union 2020, WHO 2022). Theoretical parameters were determined by fitting the Yan model to the experimental values by nonlinear regression, using Curve Expert Pro 2.7 software. The Yan model is an empirical model represented by the equation (3.15).

6.2.5 Adsorbent digestion

An acid digestion was carried out at the adsorbent before and after each adsorption experiment. In brief, 150 mg of dry ICG was put to digest at 150°C for two hours in an acid solution containing 5 mL of distilled water, 4 mL of HNO3 68% and 12 mL of HCL 37%. Each sample was digested in replicate and the results were given by the average of the two results. The iron, manganese and arsenic concentrations were measured using ICP-OES.

6.3 Results and discussion

6.3.1 Effect of coating time and solution reuse in the adsorbent performance

The study found that the higher iron loading onto ICG was achieved at 16h of coating, followed by 24h. As a result, the ICG coated during these intervals showed higher adsorption capacity for arsenic (
Table 6.6). The study also found that recycling the iron solution was not feasible, as the ICG iron content was reduced by 50% in the second cycle. However, in the subsequent cycles the iron content remained constant (Table 6.7). The results are summarized in Figure 6.7.

Table 6.6: Comparison of different coating times for ICG preparation.

Coating time (h)	Iron loading (mg/g)	qAs (mg/g)	TOC (mg/L)
2	21.5 ± 0.7	3.2	13.13
4	21.7 ± 0.8	-	-
6	21.5 ± 0.8	-	-
16	35 ± 1	6.7	12.92
24	27 ± 3	5.5	14.54

Table 6.7: Reuse of coating solution to produce ICG.

Coating solution usage cycle (t =2 h)	ICG iron content (mg g^{1})
1st	21.5
2nd	11.2
3rd	11.8
4th	10.8

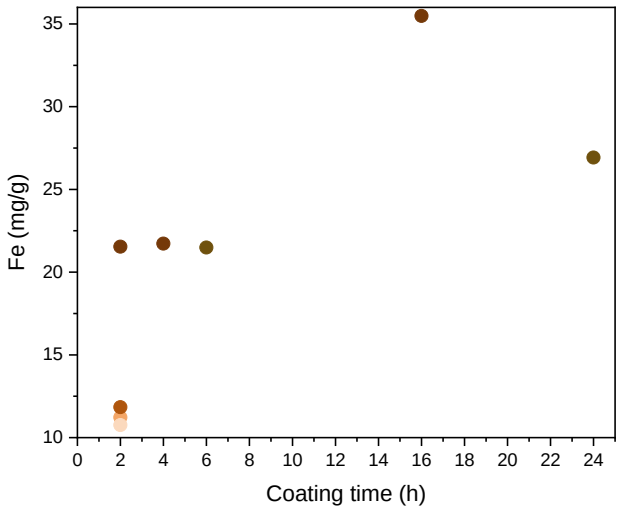


Figure 6.7: Iron impregnation in the iron-coated cork granulates at different coating times using fresh ( )and recycled FeCl3 solution: 2nd recycling ( ), 3rd ( ) and 4th ( ) recycling cycles.

Throughout the coating cycles, the color of the reused coating solution changed from brown to black. That indicates that a redox reaction occurred, converting the iron state in the solution from ferric (Fe^{3+}) oxide to ferrous (Fe^{2+}) oxide. As the mixing equipment was exposed to light in the laboratory, a photochemical reduction of ferric to ferrous iron may have occurred (Laglera and van den Berg 2007, Lueder, Jørgensen et al. 2020). The photochemical reduction of Fe(III) ions in aqueous solution can be influenced by irradiation wavelength, pH of the solution and other factors (Feng and Nansheng 2000). Further experiments under other conditions might be conducted to confirm the influence of those factors in the recycling of the ICG iron coating solution.

6.3.2 Fixed-bed adsorption column studies in Portugal

The raw water arsenic concentration found for these experiments (11 µg L^{-1}) in the groundwater well was above the WHO limit but inferior to the reported in other groundwater from Portugal of 20 µg L^{-1} (Chapter 4) or in other European Union countries such as Italy, with an average of 14.4 µg L^{-1} (Parrone, Ghergo et al. 2020), Cyprus with max. concentrations of 41 µg L^{-1} (Christodoulidou, Charalambous et al. 2012), and Croatia where average arsenic concentrations increased in deeper wells from 27 to 205 µg L^{-1} on well depths > 50 m (Romić, Habuda-Stanić et al. 2011).

The concentrations also changes seasonaly, with summer being the time of the year with the highest values due to the low levels of precipitation (Romić, Habuda-Stanić et al. 2011). Given the fact that the samples collected for this study were done during a reported high precitpitation winter in northeast Portugal, these levels may likely rise over the summer.

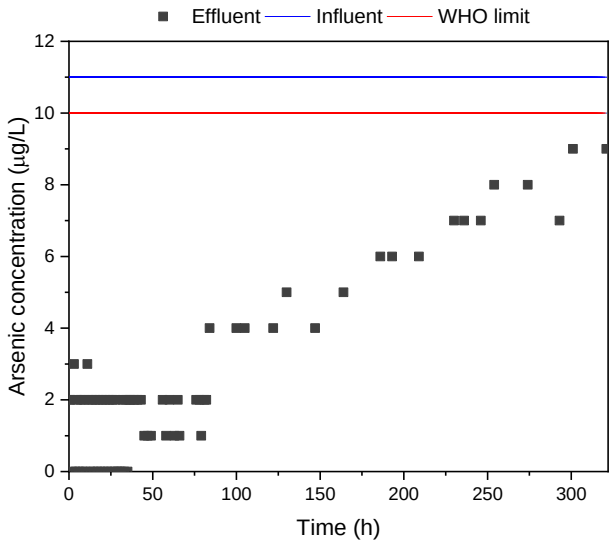


Figure 6.8: Arsenic concentration in the fixed-bed column effluent (adsorbent mass = 6g, flow rate = 5 $mL.min^{-1}$, temperature = 20°C).

The arsenic effluent concentration was kept under 10 µg L^{-1} during 321 h and 1706 ± 78 bed volumes (Figure 6.8). Other metals concentration was also monitored (Zn, Mn, Fe). In the early hours of the experiment, there was a rise in the effluent concentrations of manganese, lead and iron (Figure 6.9). The effluent concentration in the first two cases exceeded the WHO limits. The zinc concentration also increased over time (Figure 6.9), although there is no established guideline for its presence in drinking water.

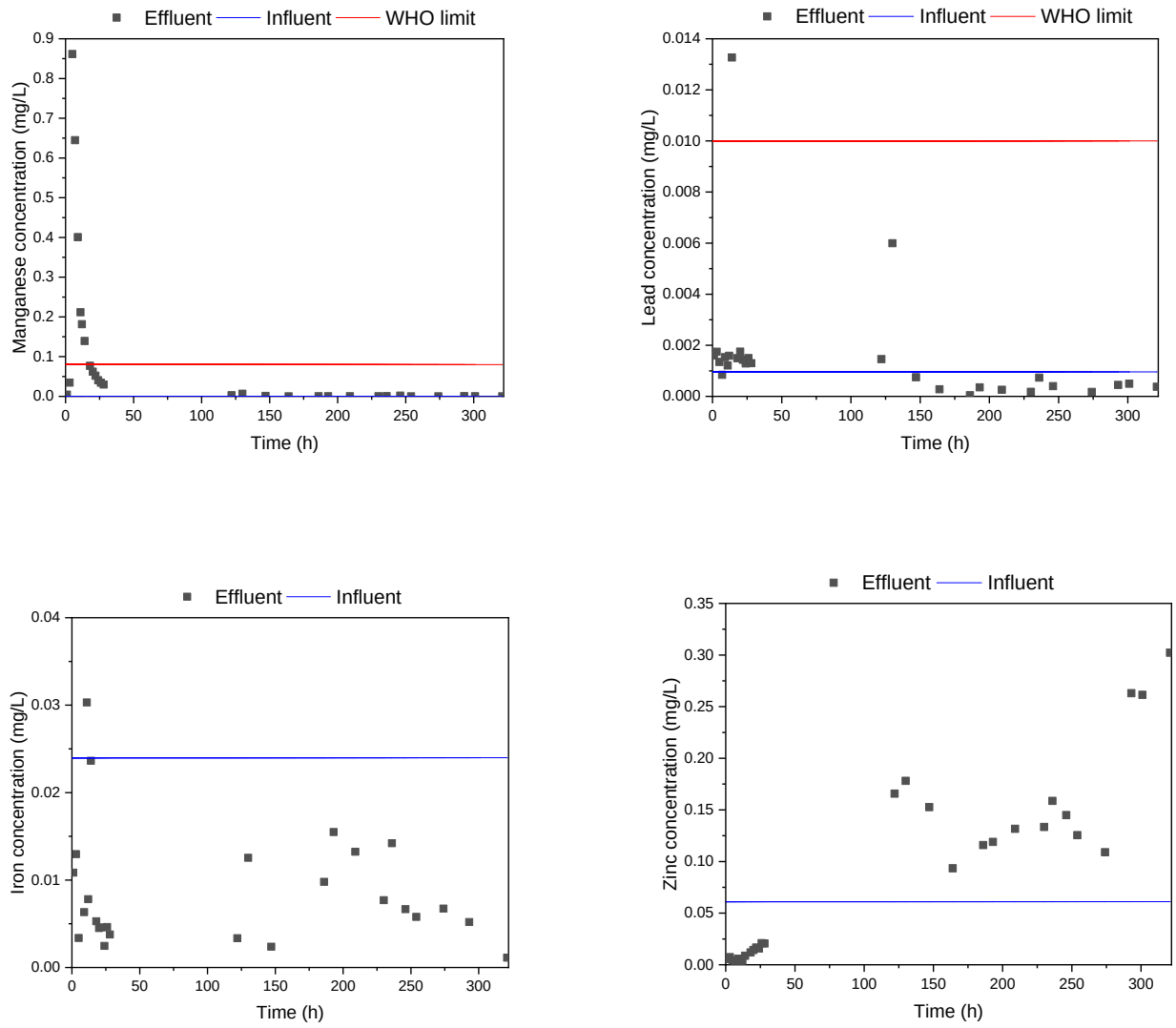


Figure 6.9: Influent and effluent concentrations of a) manganese, b) lead, c) iron, and d) zinc in the fixed-bed column (adsorbent mass = 6g, flow rate = 5 mL.min^{-1}, temperature = 20ºC).

6.3.3 Fixed-bed adsorption column studies in The Netherlands

6.3.3.1 pH and conductivity

The effluent pH and conductivity were monitored throughout the duration of the assay. The pH from filters B, C1, and C2 using treated groundwater was higher than the pH from Filter A, using untreated groundwater (Figure 6.10). The pH average values were 7.61 ± 0.07, 7.61 ± 0.06, 7.52 ± 0.07, and 7.4 ± 0.1, respectively. The increase in the pH is justified by the higher presence of hydroxyl groups from the iron hydroxide formed in the oxidation-precipitation pretreatment.

A similar behavior was observed in the effluent conductivities' values, which were lower in Filter A fed by raw GW compared to Filter B, fed with the treated GW. The average conductivity

values for filters A, B, C1, and C2 for -37 ± 5 mV, -54 ± 4 mV, -53 ± 3, and -47 ± 4 mV, respectively. Another study also observed an increase in both the pH and oxygen redox potential after aeration of natural groundwater (Annaduzzaman, Rietveld et al. 2021).

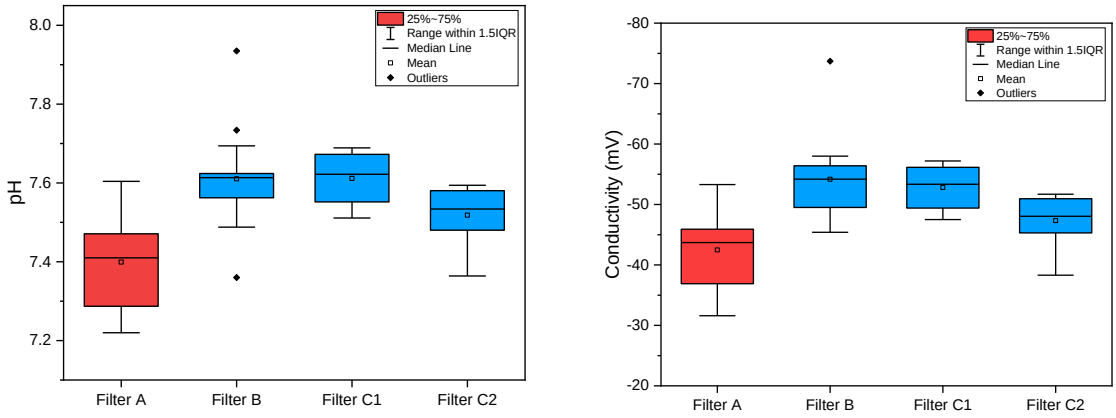


Figure 6.10: Boxplot of pH (left) and conductivity (right) from the assays using untread groundwater (red) and treated groundwater (blue).

6.3.3.2 Iron

The pretreatment system, composed of aeration followed by a sand filter, was critical in reducing the iron concentration from the groundwater (Figure 6.11), but the values after treatment were still higher than the WHO and the European Commission limit for drinking water of 0.3 mg L^{-1} and 0.2 mg L^{-1}, respectively. To complement the system, the adsorption column, filled with ICG, was able to remove the iron under the legal limits in filters B, C1 and C2 (Figure 6.9).

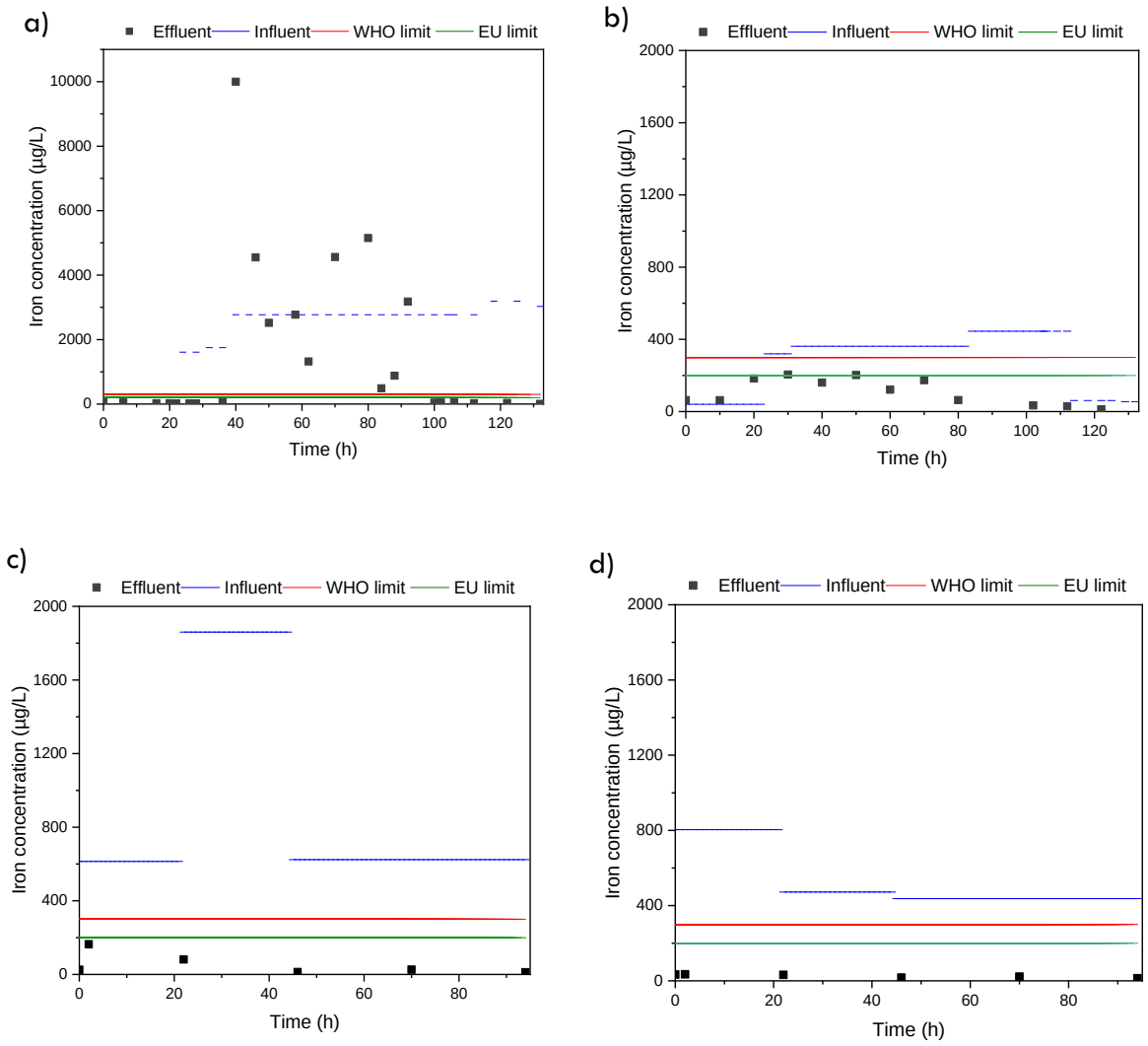


Figure 6.11: Inlet and outlet total iron concentration versus time for a) Filter A, b) Filter B, c) Filter C1, and d) Filter C2.

Iron deposition was observed in the effluent tubes of filter A, indicating the presence of ferric oxide Figure 6.12. The pH, conductivity and pE data (Table 6.8) from the adsorption columns were implemented in pE-pH diagrams to identify the predominant iron species in the groundwater before and after the aeration/sand filter treatment. The effluent pH ranged from 7 to 8, and the pE ranged from 0 to 2, which are placed in the boundary between Fe^{2+} and $Fe(OH)_3$ formation (Figure 6.13). It can be seen that iron is present in both oxidation states (Fe^{2+} and $Fe^{3+}/Fe(OH)_3$) in the effluents from filters A and B. However, the ferric oxide (Fe^{3+}) is more predominant in Filter A while ferrous oxide (Fe^{2+}) is more predominant in Filter B.

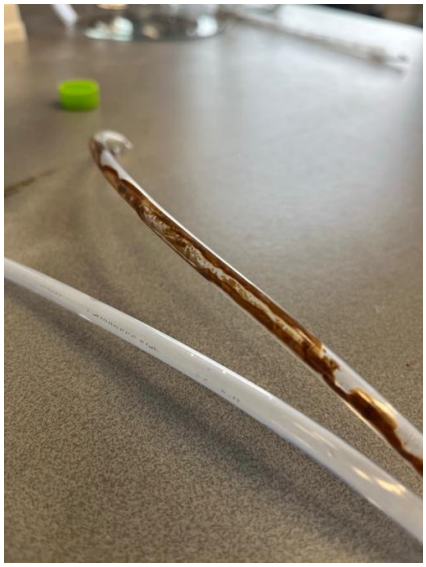


Figure 6.12: Iron deposits in the outlet tubes from Filter A.

Table 6.8: pH, conductivity and pE values.

Column A			Column B		
pH	pE	Cond. (mV)	pH	pE	Cond. (mV)
7.595	-0.880	-51.2	7.734	-0.988	-57.5
7.461	-0.784	-45.6	7.623	-0.970	-56.4
7.235	-0.543	-31.6	7.935	-1.267	-73.7
7.373	-0.674	-39.2	7.517	-0.815	-47.4
7.406	-0.707	-41.1	7.596	-0.882	-51.3
7.293	-0.626	-36.4	7.488	-0.780	-45.4
7.281	-0.590	-34.3	7.558	-0.846	-49.2
7.535	-0.825	-48	7.567	-0.851	-49.5
7.459	-0.775	-45.1	7.622	-0.933	-54.3
7.448	-0.751	-43.7	7.625	-0.916	-53.3
7.604	-0.916	-53.3	7.618	-0.932	-54.2
7.481	-0.789	-45.9	7.623	-0.932	-54.2
7.325	-0.634	-36.9	7.694	-0.997	-58
7.255	-0.643	-37.4	7.609	-0.990	-57.6

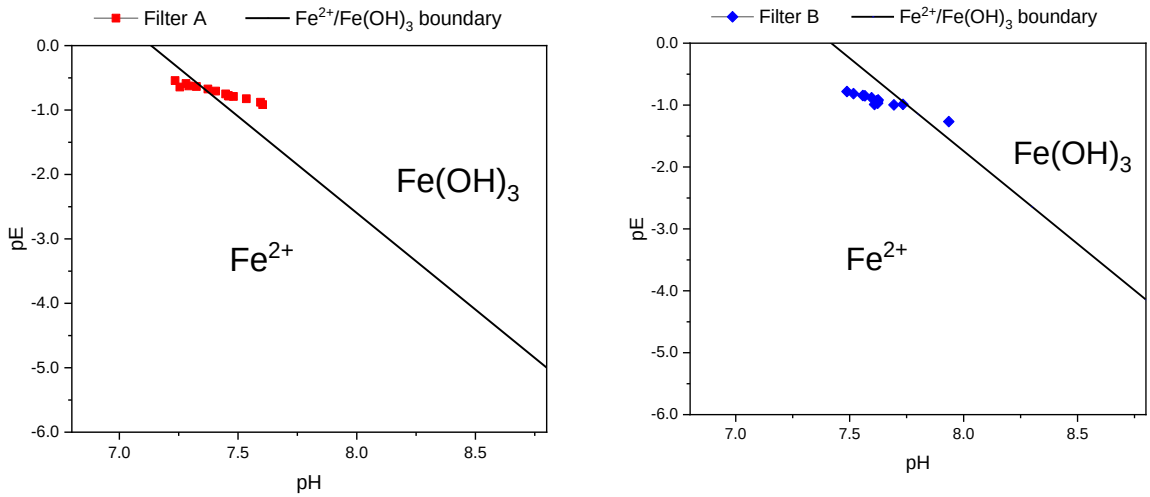


Figure 6.13: Implementation of experimental data in a pE-pH iron diagram.

6.3.3.3 Manganese

The manganese inlet and outlet concentrations were monitored throughout the time (Figure 6.14). High values of outlet concentrations were observed in all assays in the first hours of the experiment. Similar results were observed in the adsorption column operated in Portugal (6.3.2). The $FeCl_3$ solution has been identified as a source of manganese contamination in filters for water treatment using ferric salts (Gabelich, Knocke et al. 2005, Gabelich, Gerringer et al. 2006). To confirm that, the manganese content was measured in the ICG samples (after acid digestion) before and after the experiments. As expected, a manganese content was found in the fresh ICG, in the concentration of 0.33 ± 0.01 mg Mn g^{-1} ICG. After each experiment, the manganese content was 0.055 ± 0.008 mg Mn g^{-1}ICG, 0.096 ± 0.008 mg Mn g^{-1}ICG 0.197 ± 0.009 mg Mn g^{-1} ICG 0.127 ± 0.008 mg Mn g^{-1}ICG, for filter A, B, C1 and C2, respectively. This indicates a release of manganese from the adsorbent to the treated solution. The iron content, on the other hand, remained constant before and after the experiments, with an average concentration of 32 ± 2 mg Fe g^{-1} ICG.

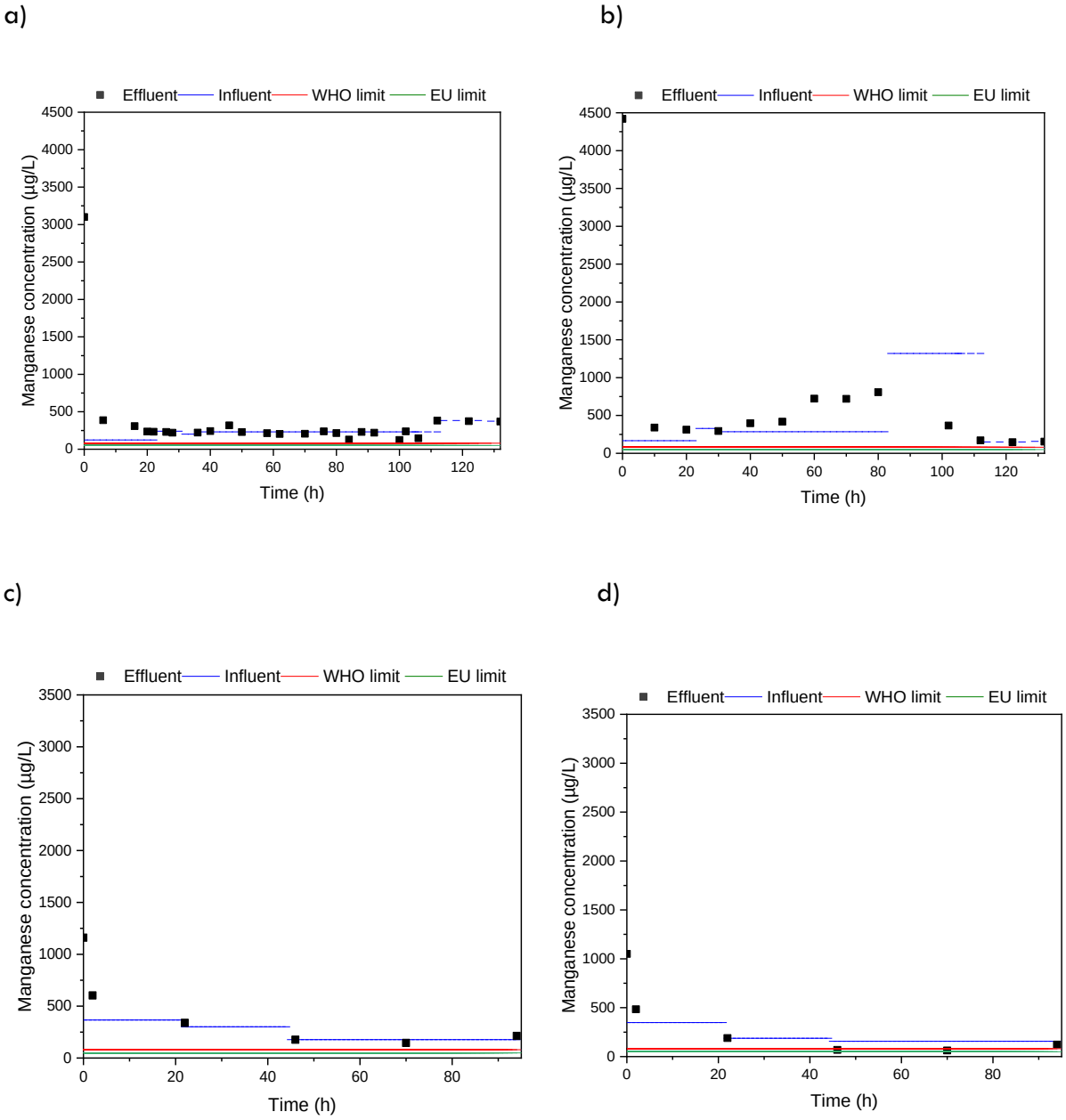


Figure 6.14: Inlet and outlet manganese concentration versus time for a) Filter A, b) Filter B, c) Filter C1, and d) Filter C2.

6.3.3.4 Arsenic

The iron-coated cork granulates performance to remove arsenic from the Dutch groundwater matrices was investigated. Filter A effluent reached 10 µg L^{-1} at 38 h after treating a volume of 10.8 L and 207 bed volumes of 0.18 ± 0.04 mg L^{-1} arsenic-spiked untreated groundwater. No breakthrough curve was possible to build in this experiment, as the arsenic concentration varied significantly through time (Figure 6.15).

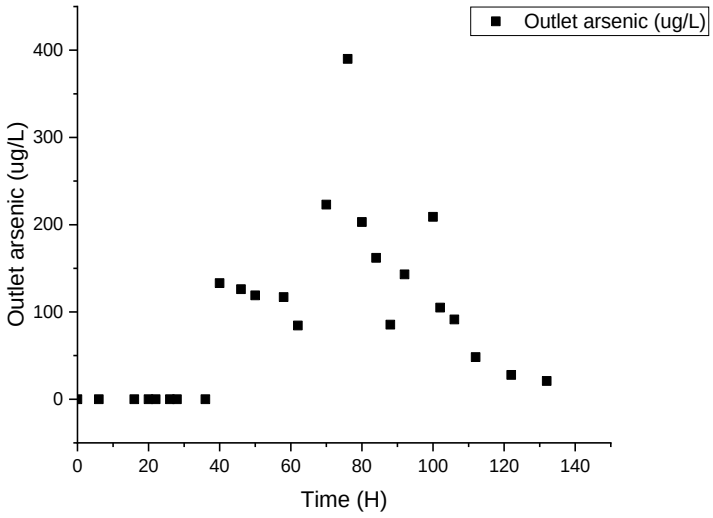


Figure 6.15: Arsenic concentration versus time on Filter A effluent.

The iron-coated cork granulates had a better performance for arsenic removal in the pretreated groundwater (Figure 6.16). Aeration followed by sand filtration system is considered a cost-effective chemical free alternative for arsenic removal in field relevant conditions (Annaduzzaman, Rietveld et al. 2021). The higher efficiency of arsenic removal in the pretreated groundwater can be due to the conversion of As(III) to As(V) in the system with higher DO levels. On neutral pH, As(V) is more easily removed by ICG than As(III) (Chapter 3).

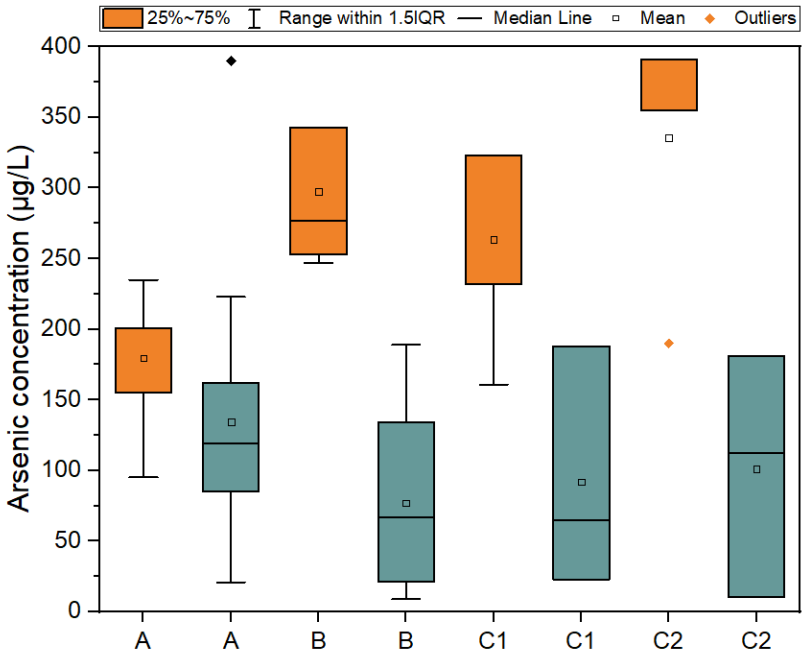


Figure 6.16: Boxplot of influent (orange/left) and effluent (green/right) arsenic concentration from the experiments with different groundwater and operation mode (A-Untreated GW under semi-continuous operation, B-Pretreated GW under semi-continuous operation, C1 and C2 – Pretreated GW under continuous operation).

The breakthrough curves of arsenic adsorption in Filters B, C1 and C2 and the experimental parameters are shown in Figure 6.17 and Table 6.9, respectively. The similarity between the breakthrough curves suggests that the different conditions (Table 6.4) did not influence the performance of the iron-coated cork granulates.

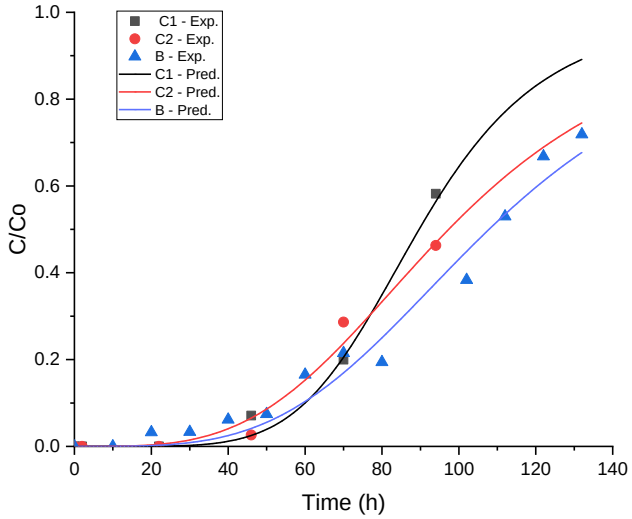


Figure 6.17: Experimental – dots - and predicted (Yan model) – lines - breakthrough curves of arsenic adsorption onto ICG in the pretreated Dutch groundwater matrix (FR = 5 mL.min^{-1}, adsorbent mass = 6 g, EBCT = 12 min, BV = 59 mL).

Table 6.9: Experimental and predicted parameters (Yan model) of arsenic continuous adsorption from arsenic-spiked groundwater onto ICG (flow rate 5 mL.min^{-1} and 6 g of ICG, bed height 25.5 cm).

Parameter	Filter B	Filter C1	Filter C2	Average
pH	7.6 ± 0.1	7.61 ± 0.06	7.52 ± 0.07	7.6 ± 0.2
$Co_{average}$ (mg L^{-1})	0.30 ± 0.04	0.26 ± 0.07	0.34 ± 0.08	0.3 ± 0.1
t_b (h)	39 ± 1	32 ± 1	45 ± 1	39 ± 5
BV_b	201 ± 6	168 ± 6	235 ± 6	202 ± 27
V_b (L)	11.7 ± 0.4	9.7 ± 0.3	13.6 ± 0.4	12 ± 2
q_b (mg g^{-1})	0.56 ± 0.09	0.4 ± 0.1	0.8 ± 0.3	0.6 ± 0.3
y_b (%)	97.5 ± 0.5	99.77 ± 0.08	99.3 ± 0.2	99 ± 1
q_{ya} (mg g^{-1})	1.6 ± 0.1	1.2 ± 0.3	1.5 ± 0.4	
a_{ya}	3.6 ± 0.5	5.4 ± 0.5	3.5 ± 0.5	
SE (mg g^{-1})	0.05	0.02	0.03	
r^2	0.968	0.992	0.981	

6.3.3.5 Pearson correlation

A Pearson correlation matrix was created to identify the interaction between the parameters (Table 6.10). A strong correlation between pH x EC ($r \geq |0.965|$) in all the column assays carried out using the Dutch groundwater matrix. The negative value indicates that the increase in the pH is correlated with the decrease in EC. That can be explained by the formation of iron hydroxide salts which decreases the EC value and increases the pH by the formation of more hydroxyl groups. Also, a good correlation was observed between iron and arsenic concentration ($|0.783| < r < |0.564|$). In Filter A the correlation was positive, meaning that an increasing iron concentration in the effluent can be correlated with an increase in the arsenic concentration in the effluent. Oppositely, in Filters B, C1, and C2, using pretreated groundwater, the correlation was negative, with an opposite effect from the observed in Filter A, using natural groundwater. A strong positive correlation was observed between EC and Mn only in Filters B ($r = 0.746$) and C1 ($r = 0.996$). A strong positive correlation between EC and Mn ($r = 0.501$) was also found in groundwater from Bangladesh (Khan and Paul 2023). Mn and pH were also correlated to pH in Filter A ($r = -0.627$), Filter B ($r = -0.562$), and Filter C1 ($r = -0.997$). Manganese and arsenic inverse correlation with pH were reported in groundwater matrix from Amazonia (de Meyer, Wahnfried et al. 2023).

Table 6.10: Pearson correlation between filter effluent parameters a) Filter A (raw groundwater), b) Filter B - treated groundwater with overnight interruption, c) Filter C1 – treated groundwater with manual sampling, d) Filter C2 – treated groundwater with automatic sampling. Legend for the colors: green = $r > 0.900$, red = $0.900 > r > 0.500$, black = $r < 0.500$.

a) Filter A

	pH	EC	As	Fe	Mn
pH	1.000				
EC	**-0.982**	1.000			
As	0.397	-0.193	1.000		
Fe	-0.063	0.485	**0.696**	1.000	
Mn	**-0.627**	0.266	-0.247	-0.149	1.000

b) Filter B

	pH	EC	As	Fe	Mn
pH	1.000				
EC	**-0.965**	1.000			
As	0.523	**-0.992**	1.000		
Fe	**-0.675**	-	**-0.607**	1.000	
Mn	**-0.562**	**0.746**	-0.363	0.224	1.000

c) Filter C1

	pH	EC	As	Fe	Mn
pH	1.000				
EC	**-0.999**	1.000			
As	**0.737**	**0.735**	1.000		
Fe	**-0.987**	**0.986**	**-0.564**	1.000	
Mn	**-0.997**	**0.996**	**-0.608**	-0.035	1.000

d) Filter C2

	pH	EC	As	Fe	Mn
pH	1.000				
EC	**-0.998**	1.000			
As	0.282	-0.353	1.000		
Fe	-0.264	-0.209	**-0.783**	1.000	
Mn	0.335	-0.388	-0.434	**0.671**	1.000

6.3.3.6 Dissolved oxygen and flow rate campaign

Flow rate changes were observed during the column studies and the parameter had to be daily adjusted to the initial value of 5 $mL.min^{-1}$. To better understand the flow rate variation through the time, it was continuously monitored for two days. An oscillation of the flow rate was observed when the groundwater was pumped in the aeration/sand filter system every four minutes, from -16% to 16% (**Error! Reference source not found.**a). After approximately 20h, a reduction of 1 3% was observed in the average flow rate, with minimum values reducing to 28% of the initial flow rate.

The instability in the flow rate of the groundwater system is related to the pressure variation in the piping in the activation of the pretreatment system, but also to the groundwater well pressure change. Variations in arsenic concentration may occur in wells resulting from the activation/deactivation of the pumps (Steinberg and Hering 2001) which must be included when modelling a real-world system.

The dissolved oxygen and the temperature were monitored along with the flow rate. The average DO value was 6 ± 3 ppm after the pretreatment (**Error! Reference source not found.**), w hich is higher than the DO measured in untreated groundwater, from 0.0 to 0.6 ppm (Au - Klymenko, Au - Nanninga et al. 2023). The DO values are in agreement with those observed by a groundwater iron removal system comparing the oxic and anoxic conditions, which revealed DO levels of 0.07 ±0.06 $mg.L^{-1}$ and 6.2 ± 0.2 $mg.L^{-1}$ values, respectively (Annaduzzaman, Rietveld et al. 2021).

Temperature and DO variation trends are very similar (**Error! Reference source not found.**b), s howing a direct correlation.

6.3.4 Comparison of arsenic removal efficiency from the groundwater sources

The performance of ICG on the Dutch and Portuguese groundwater matrices are summarized in Table 6.11. In the Dutch matrix, the adsorption column reached breakthrough times of 31±1 and 36±1 h, whereas 26±2 and 321±3 h were achieved in the Portuguese matrix. Given that increasing the arsenic concentration in solution reduces adsorbent´s performance in terms of breakthrough time and treated volume, the ICG worked better in the Dutch matrix than the Portuguese for arsenic removal. This can be attributed to a higher competitiveness for the ferric sites in the ICG of the anions in the Portuguese matrix, such as nitrate (30 mg L^{-1}), compared to the anions in the Dutch matrix, such as chloride (1,096.7 mg L^{-1}),

Table 6.11: Experimental parameters of arsenic continuous adsorption from different groundwater matrices onto ICG (flow rate 5 $mL.min^{-1}$ and 6 g of ICG, EBCT of 12 min, breakthrough point of 10 µg L^{-1}).

Feed	**Treated As-spiked groundwater**	**Untreated As-spiked groundwater**	**Untreated As-spiked groundwater**	**Untreated groundwater**
Groundwater	The Netherlands	The Netherlands	Portugal	Portugal
pH	7.6 ± 0.2	7.4 ± 0.1	7.09 ± 0.01	6.95
$Co_{average}$ (mg L^{-1})	0.3 ± 0.1	0.18 ± 0.04	0.1	0.011 ± 0.002
t_b (h)	31 ± 1	36 ± 1	26 ± 2	321
BV_b	202 ± 27	189 ± 6	140 ± 13	1706 ± 78
V_b (L)	9.3 ± 0.3	10.9 ± 0.4	7.9 ± 0.5	96.3 ± 0.1
q_b (mg g^{-1})	0.45 ± 0.07	0.33 ± 0.08	0.12 ± 0.01	0.09 ± 0.04
y_b (%)	96.9 ± 0.6	100.0	99.2 ± 0.6	53 ± 14
Ref.	This Chapter	This Chapter	Chapter 4	This Chapter

The performance of emerging adsorbents in real water is not frequently discussed in the literature. The overall performance of iron-coated cork granulates removal of arsenic from groundwater in continuous mode is higher than other modified biosorbents such as iron-iron chitosan spacer granulates (ICS) (Gupta and Sankararamakrishnan 2010), xanthated chitosan flakes (Gupta, Yunus et al. 2012) and iron-chitosan granules (ICB) (Gupta, Chauhan et al. 2009) which removed arsenic under 10 µ.g L^{-1} for about 64 (C_0 = 179 µ.L^{-1}), 99 (C_0 = 200 µ.L^{-1}) and 147 (C_0 = 500 µ.L^{-1}) BVs, respectively. The adsorption capacity was also higher than reported by biochars and nanobiochars (Kumari Sharma, Kumar Singh et al. 2023).

6.4 Conclusions

This work investigated the performance of iron-coated cork granulates (ICG) to remove arsenic from different groundwater matrices. The ICG demonstrated the capacity to treat real groundwater across a wide range of arsenic concentrations (11 - 300 µg L^{-1}) under the WHO guidelines and the European Commission's legal limit of 10 µg L^{-1}. The ICG performed better in the groundwater matrix from The Netherlands than that from Portugal. This could be attributed to the elevated concentrations of nitrate in the Portuguese matrix, which might have a stronger competitiveness with the arsenic oxyanions for the ferric sites in the adsorbent, compared to the more abundant chloride in the Dutch matrix. The pretreatment using the aeration/sand filter reactor improved the arsenic removal in the Dutch matrix, and it reached values of breakthrough time, treated volume at breakthrough and bed volumes at breakthrough of 39 ± 5 h, 12 ± 2 L, 202 ± 27 and, respectively, for an initial concentration of 300 ± 10 µg L^{-1} compared to 26 ± 2 h, 7.9 ± 0.5 L and 140 ± 13 obtained with the Portuguese matrix (As = 0.1 mg L^{-1}).

Further research should be conducted to improve the efficiency of ICG filters for manganese removal and unpleasant release, either by improving the $FeCl_3$ coating process or by combining the treatment with a pos treatment step to remove manganese and other possible contaminants not removed by the filter (e.g., nitrates). These results helped to improve the iron-coated cork granulates technology readiness level (TRL) from 4 to 5.

6.5 References

(MOH), M. o. H. o. t. P. s. R. o. C. (2006). Chinese National Standards GB 3838-2002: Sanitary Standards for Drinking Water Quality;. S. A. o. C. (SAC). Hongkong, China., China Water Risk:.

Annaduzzaman, M., L. C. Rietveld, B. A. Hoque, M. N. Bari and D. van Halem (2021). "Arsenic removal from iron-containing groundwater by delayed aeration in dual-media sand filters." Journal of Hazardous Materials **411**: 124823.

Au - Klymenko, R., H. Au - Nanninga, E. Au - de Kroon, L. L. F. Au - Agostinho, E. C. Au - Fuchs, J. Au - Woisetschläger and W. F. L. M. Au - Hoeben (2023). "Preparation of Free-Surface Hyperbolic Water Vortices." JoVE(197): e64516.

Bhattacharya, S., A. Talukdar, S. Sengupta, T. Das, A. Dey, K. Gupta and N. Dutta (2023). "Arsenic contaminated water remediation: A state-of-the-art review in synchrony with sustainable development goals." Groundwater for Sustainable Development **23**: 101000.

BIS (2012). Indian standard drinking water — Specification (Second Revision): IS 10500: 2012. B. o. I. S. (BIS). New Delhi, India.

Bondu, R., V. Cloutier, E. Rosa and M. Benzaazoua (2017). "Mobility and speciation of geogenic arsenic in bedrock groundwater from the Canadian Shield in western Quebec, Canada." Science of The Total Environment **574**: 509-519.

Bretzler, A., F. Lalanne, J. Nikiema, J. Podgorski, N. Pfenninger, M. Berg and M. Schirmer (2017). "Groundwater arsenic contamination in Burkina Faso, West Africa: Predicting and verifying regions at risk." Science of The Total Environment **584-585**: 958-970.

Canada, H. (2006). Guidelines for Canadian Drinking Water Quality: Guideline Technical Document - Arsenic. W. Q. a. H. Bureau. Ottawa, Ontario.

Cao, H., X. Xie, Y. Wang and Y. Deng (2021). "The interactive natural drivers of global geogenic arsenic contamination of groundwater." Journal of Hydrology **597**: 126214.

Carneiro, M. A., J. F. R. Coelho, A. M. A. Pintor, R. A. R. Boaventura and C. M. S. Botelho (2022). "Multi-cycle regeneration of arsenic-loaded iron-coated cork granulates for water treatment." Journal of Water Process Engineering **50**: 103291.

Carneiro, M. A., A. M. A. Pintor, R. A. R. Boaventura and C. M. S. Botelho (2021). "Current Trends of Arsenic Adsorption in Continuous Mode: Literature Review and Future Perspectives." Sustainability **13**(3): 1186.

Carneiro, M. A., A. M. A. Pintor, R. A. R. Boaventura and C. M. S. Botelho (2022). "Efficient removal of arsenic from aqueous solution by continuous adsorption onto iron-coated cork granulates." Journal of Hazardous Materials: 128657.

Chaturvedi, S. and P. N. Dave (2012). "Removal of iron for safe drinking water." Desalination **303**: 1-11.

Christodoulidou, M., C. Charalambous, M. Aletrari, P. Nicolaidou Kanari, A. Petronda and N. I. Ward (2012). "Arsenic concentrations in groundwaters of Cyprus." Journal of Hydrology **468-469**: 94-100.

Covatti, G., T. N. A. Hoang and T. Grischek (2023). "Release of arsenic during riverbank filtration under anoxic conditions linked to grain size of riverbed sediments." Science of The Total Environment **900**: 165858.

de Meyer, C. M. C., I. Wahnfried, J. M. Rodriguez Rodriguez, R. Kipfer, P. A. García Avelino, E. A. Carpio Deza and M. Berg (2023). "Hotspots of geogenic arsenic and manganese contamination in groundwater of the floodplains in lowland Amazonia (South America)." Science of The Total Environment **860**: 160407.

Dotto, G. L. and G. McKay (2020). "Current scenario and challenges in adsorption for water treatment." Journal of Environmental Chemical Engineering **8**(4): 103988.

European Union, C. (2020). Council Directive 2020/2184 of 16 December 2020, Off. J. Eur. Commun. L: 62.

Feng, W. and D. Nansheng (2000). "Photochemistry of hydrolytic iron (III) species and photoinduced degradation of organic compounds. A minireview." Chemosphere **41**(8): 1137-1147.

Gabelich, C., W. R. Knocke, B. Coffey, R. Johnston, H. Do and A. Mofidi (2005). "Manganese desorption from filter media: Experiences with biological filtration." AWWA 124th Annual Conference and Exposition: The World's Water Event, ACE 2005.

Gabelich, C. J., F. W. Gerringer, C. C. Lee and W. R. Knocke (2006). "Sequential Manganese Desorption and Sequestration in Anthracite Coal and Silica Sand Filter Media." Journal AWWA **98**(5): 116-127.

Genç-Fuhrman, H., H. Bregnhøj and D. McConchie (2005). "Arsenate removal from water using sand–red mud columns." Water Research **39**(13): 2944-2954.

Guo, H., D. Wen, Z. Liu, Y. Jia and Q. Guo (2014). "A review of high arsenic groundwater in Mainland and Taiwan, China: Distribution, characteristics and geochemical processes." Applied Geochemistry **41**: 196-217.

Gupta, A., V. S. Chauhan and N. Sankararamakrishnan (2009). "Preparation and evaluation of iron–chitosan composites for removal of As(III) and As(V) from arsenic contaminated real life groundwater." Water Research **43**(15): 3862-3870.

Gupta, A. and N. Sankararamakrishnan (2010). "Column studies on the evaluation of novel spacer granules for the removal of arsenite and arsenate from contaminated water." Bioresource Technology **101**(7): 2173-2179.

Gupta, A., M. Yunus and N. Sankararamakrishnan (2012). "Equilibrium and dynamic studies of the removal of As(III) and As(V) from contaminated aqueous systems using a functionalized biopolymer." Journal of Chemical Technology & Biotechnology **87**(4): 546-552.

Hossain, S., T. Hosono, K. Ide, M. Matsunaga and J. Shimada (2016). "Redox processes and occurrence of arsenic in a volcanic aquifer system of Kumamoto Area, Japan." Environmental Earth Sciences **75**(9): 740.

Jesus, J., R. Nunes da Silva and A. Pintor (2023). "Advances in Cork Use in Adsorption Applications: An Overview of the Last Decade of Research." Separations **10**(7): 390.

Jha, P. K. and P. Tripathi (2021). "Arsenic and fluoride contamination in groundwater: A review of global scenarios with special reference to India." Groundwater for Sustainable Development **13**: 100576.

Khan, M. S. and S. K. Paul (2023). "Groundwater quality assessment and health issues in coastal zone of Bangladesh." Journal of Hazardous Materials Advances **10**: 100278.

Kumari Sharma, P., R. Kumar Singh, R. Kumar, N. Kumar, A. Ghosh, P. Sharma and A. Kumar (2023). "Synthesis and exploration of physical properties of nanobiochar synthesized from rice

straw for its applications in arsenic remediation from contaminated water environments." Materials Today: Proceedings.

Laglera, L. M. and C. M. G. van den Berg (2007). "Wavelength Dependence of the Photochemical Reduction of Iron in Arctic Seawater." Environmental Science & Technology **41**(7): 2296-2302.

Li, Y., L. Ji, W. Mi, S. Xie and Y. Bi (2021). "Health risks from groundwater arsenic on residents in northern China coal-rich region." Science of The Total Environment **773**: 145003.

Lueder, U., B. B. Jørgensen, A. Kappler and C. Schmidt (2020). "Photochemistry of iron in aquatic environments." Environmental Science: Processes & Impacts **22**(1): 12-24.

Manahan, S. E. (2017). Environmental chemistry, CRC press.

Netherlands, O. (2023). Drinkwaterbesluit.

Panthi, S., S. Sharma and A. Mishra (2006). "Recent status of arsenic contamination in groundwater of Nepal - a review." Kathmandu University J Sci Eng Technol **2**.

Parrone, D., S. Ghergo, E. Frollini, D. Rossi and E. Preziosi (2020). "Arsenic-fluoride co-contamination in groundwater: Background and anomalies in a volcanic-sedimentary aquifer in central Italy." Journal of Geochemical Exploration **217**: 106590.

Pintor, A. M. A., C. C. Brandão, R. A. R. Boaventura and C. M. S. Botelho (2021). "Multicomponent adsorption of pentavalent As, Sb and P onto iron-coated cork granulates." Journal of Hazardous Materials **406**: 124339.

Pintor, A. M. A., B. R. C. Vieira, R. A. R. Boaventura and C. M. S. Botelho (2020). "Removal of antimony from water by iron-coated cork granulates." Separation and Purification Technology **233**: 116020.

Pintor, A. M. A., B. R. C. Vieira, C. C. Brandão, R. A. R. Boaventura and C. M. S. Botelho (2020). "Complexation mechanisms in arsenic and phosphorus adsorption onto iron-coated cork granulates." Journal of Environmental Chemical Engineering **8**(5): 104184.

Pintor, A. M. A., B. R. C. Vieira, S. C. R. Santos, R. A. R. Boaventura and C. M. S. Botelho (2018). "Arsenate and arsenite adsorption onto iron-coated cork granulates." Science of The Total Environment **642**: 1075-1089.

Pokhrel, D., B. S. Bhandari and T. Viraraghavan (2009). "Arsenic contamination of groundwater in the Terai region of Nepal: An overview of health concerns and treatment options." Environment International **35**(1): 157-161.

Prieto García, F., O. A. Acevedo Sandoval, F. Pérez Moreno, J. Prieto Méndez and R. A. Canales Flores (2016). "Arsenic contamination in groundwater in Zimapan, Hidalgo, Mexico." Desalination and Water Treatment **57**(28): 13038-13047.

Rahman, M. A. and M. A. Hashem (2019). "Arsenic, iron and chloride in drinking water at primary school, Satkhira, Bangladesh." Physics and Chemistry of the Earth, Parts A/B/C **109**: 49-58.

Rahnamarad, J., R. Derakhshani and A. Abbasnejad (2020). "Data on arsenic contamination in groundwater of Rafsanjan plain, Iran." Data in Brief **31**: 105772.

Rehman, F., T. Azeem, R. A. Hashmi, J. Siddique, A. Shahab, S. Mustafa and F. Rehman (2023). "Drinking and irrigation quality of groundwater and health risk assessment due to arsenic exposure in Sheikhupura district, Punjab, Pakistan." Kuwait Journal of Science **50**(3): 368-375.

Romić, Ž., M. Habuda-Stanić, B. Kalajdžić and M. Kuleš (2011). "Arsenic distribution, concentration and speciation in groundwater of the Osijek area, eastern Croatia." Applied Geochemistry **26**(1): 37-44.

Shaji, E., M. Santosh, K. V. Sarath, P. Prakash, V. Deepchand and B. V. Divya (2021). "Arsenic contamination of groundwater: A global synopsis with focus on the Indian Peninsula." Geoscience Frontiers **12**(3): 101079.

Sharma, P. K., R. K. Singh, R. Kumar, N. Kumar, A. Ghosh, P. Sharma, A. Kumar, P. Bhattacharya and M. Kar (2023). "Adsorptive behavior of Fe/Zn-modified nanobiochar for arsenic removal from naturally contaminated groundwater." Groundwater for Sustainable Development **23**: 101011.

Sharma, S. K., B. Petrusevski, D. Owore and J. Schippers (2003). "Optimisation of floc formation in iron removal from groundwater." Proceedings of the Asian Waterqual.

Steinberg, L. J. and J. Hering (2001). Variations in arsenic concentrations within a groundwater distribution system. Bridging the Gap: Meeting the World's Water and Environmental Resources Challenges.

Tan, W., J. Zhang, J. Wu, Y. Sheng, X. Liu, M. Lei, Z. Zhang, H. Lin, G. Sun and P. Guo (2022). Correlation Analysis of Water Temperature and Dissolved Oxygen Based on Water Quality Monitoring Data. Advances in Artificial Intelligence and Security, Cham, Springer International Publishing.

van de Griend, M. V., F. Warrener, M. van den Akker, Y. Song, E. C. Fuchs, W. Loiskandl and L. L. F. Agostinho (2022). "Vortex Impeller-Based Aeration of Groundwater." Water **14**(5): 795.

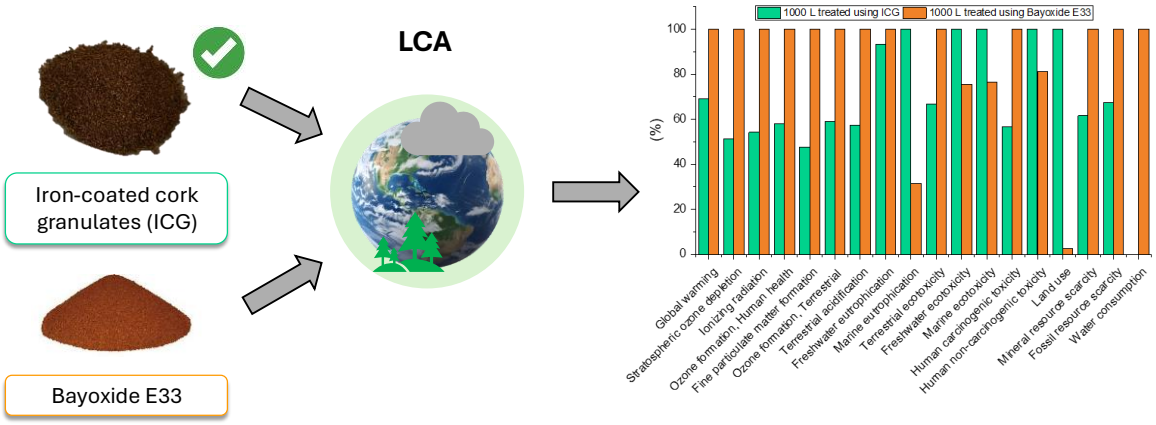
WHO (2022). Guidelines for drinking-water quality: incorporating the first and second addenda. Geneva, World Health Organization.

World Health, O. (1993). Guidelines for drinking-water quality: volume 1: recommendations. Geneva, World Health Organization.

Zoroufchi Benis, K., A. Motalebi Damuchali, K. N. McPhedran and J. Soltan (2020). "Treatment of aqueous arsenic – A review of biosorbent preparation methods." Journal of Environmental Management **273**: 111126.

7 ENVIRONMENTAL IMPACTS OF ARSENIC REMOVAL FROM WATER USING IRON-COATED CORK GRANULATES

This chapter is based on: M. A. Carneiro, Tomasi, I. T., R. A. R. Boaventura, C. M. S. Botelho and A. M. A. Pintor. *Environmental impact and cost analysis of arsenic removal from water using iron-based adsorbents: comparison between natural and commercial materials*. Journal of Environmental Chemical Engineering (under review)



The present study evaluates the environmental impacts associated with the production of 1 kg of iron-coated cork granulates (ICG) on lab-scale using life-cycle analysis (LCA). Also, a comparison of the environmental performance between the treatment of arsenic-contaminated water using either ICG or the commercial iron oxide adsorbent Bayoxide E33 was carried out. Finally, the environmental impact of the adsorption using regenerated ICG was investigated. SimaPro 9.5 software and the ReCiPe 2016 Midpoint (H) method were used to assess the environmental impacts. The treatment of arsenic-contaminated water using ICG (Global warming 3.70 kg CO_2 eq.) had a lower impact on 13 out of 18 categories compared to the use of the commercial adsorbent Bayoxide E33 (Global warming 5.36 kg CO_2 eq.). The results showed that the electricity required for ICG production was the input that contributed the most to the environmental impacts. Expanding the lifespan of the adsorbent by carrying out adsorption-desorption cycles (using NaOH 0.1 M) had a higher environmental impact than using the adsorbent only once, because of the need to add a hazardous waste treatment for the desorbed solution containing high concentrations of arsenic. The cost comparison evaluation of arsenic-contaminated water treatment using ICG and Bayoxide E33 indicated that the more ecological option is also the most economically feasible. The results were calculated considering a lab-scale, however, it is expected that production on an industrial scale will further reduce the environmental impacts of ICG due to economies of scale in electricity consumption.

7.1 Introduction

In the previous chapter, iron-coated cork granulates has been shown to be successful at removing arsenic from aqueous solutions and groundwater matrices at different concentrations and compositions. The desorption of saturated ICG was also pointed as a good solution to extend the life span of the material. The adsorption mechanism of ICG has been identified as similar to that of pure iron oxides (Pintor, Vieira et al. 2020), but its environmental performance has yet to be investigated. Life cycle assessment (LCA) is recommended for assessing the environmental impacts of the modification of the emerging low-cost adsorbents (Eniola, Sizirici et al. 2023).

The LCA method evaluates the inputs, outputs and possible environmental impacts of a product system across its entire life cycle (da Costa, Maranduba et al. 2022). It is important to quantify these parameters and provide tools for decision-making through comparative analysis. However, it is important to remember that LCA does not precisely predict the future environmental performance of water and wastewater systems and cannot be used in place of mandatory methodologies such as Environmental Impact Assessment (EIA) (Corominas, Byrne et al. 2020).

In this chapter, the environmental impacts of producing iron-coated cork granulates (ICG) on lab-scale was calculated. Considering that most of the environmental impact assessments reported in the literature focus only on the production phase of an adsorbent, this study also evaluated the environmental performance of the treatment of arsenic-contaminated water using ICG and compared the results to those of a commercial iron oxide adsorbent, Bayoxide E33. Finally, LCA of the ICG arsenic adsorption after desorption cycles was carried out.

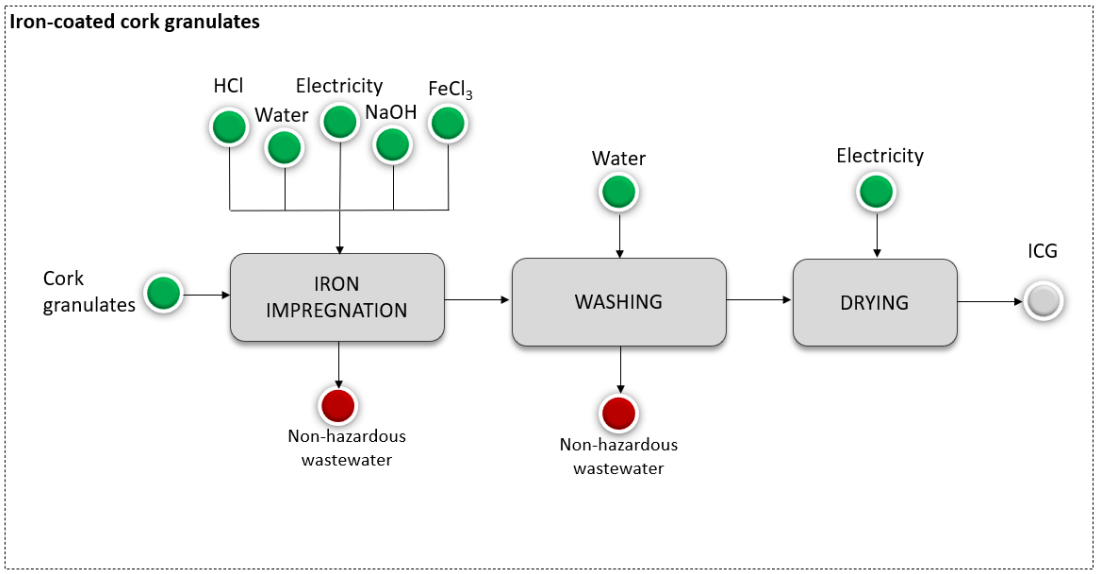
7.2 Materials and methods

7.2.1 Goal and scope definition

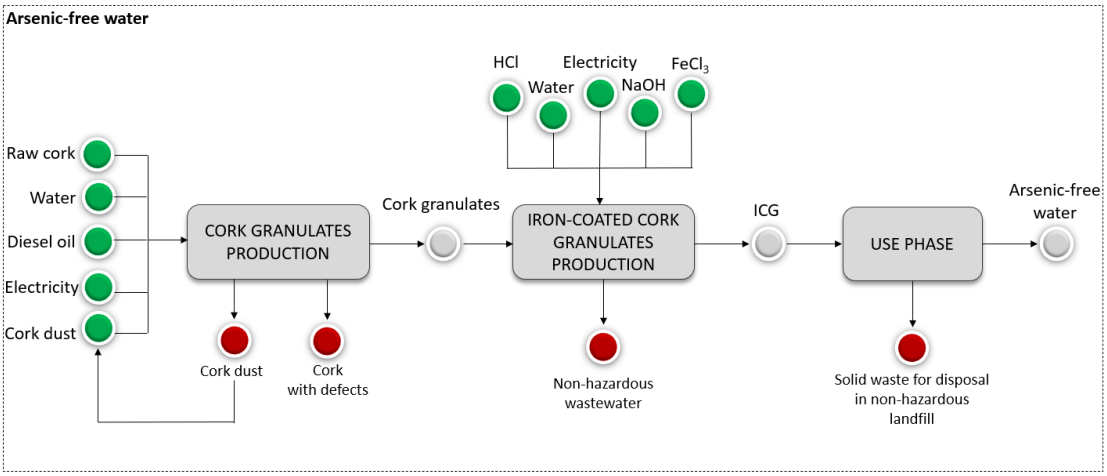
The proposed LCA aimed to: i) evaluate the environmental impacts of each step of the production (iron impregnation, washing and drying) of iron-coated cork granulates (ICG) on lab-scale to produce 1 kg of adsorbent; ii) compare the environmental impacts of ICG with those of a commercial adsorbent, Bayoxide E33 (modified granular ferric hydroxide (GFH)), and iii) compare the use of fresh ICG and regenerated ICG (after adsorption-desorption cycles). The functional units (FUs) for goals ii) and iii) were selected as the amount (mass) of adsorbent needed to treat 1000 L of water, at pH 7, under 10 µg L^{-1} containing 1 mg As(V) L^{-1} and 100 µg L^{-1} of total arsenic, respectively. The amount of adsorbent needed to satisfy the FUs varied according to the adsorption performance in continuous mode, using a lab-scale fixed-bed column, as will

be discussed in the following sections. Since the water treatment process uses very little energy and material, its emissions are not included in the impact analyses (Goyal, Tyagi et al. 2023). The system boundaries for the ICG production, and the production of arsenic-free water using ICG and Bayoxide E33 are shown in Figure 7.1.

a)



b)



c)

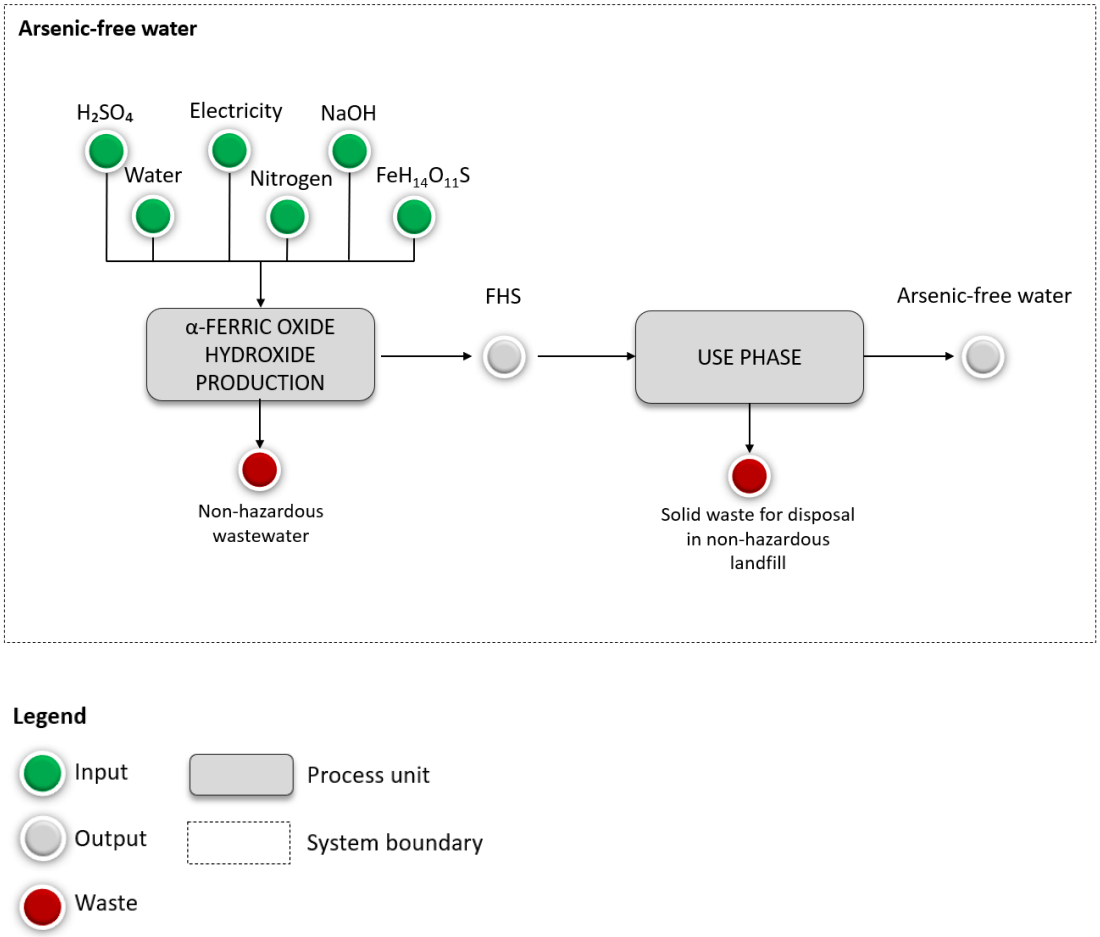


Figure 7.1: System boundaries for the production of a) iron-coated cork granulates, and 1000 L of arsenic-free water using b) iron-coated cork granulates and c) crystalline α-ferric oxide hydroxide (Bayoxide E33).

7.2.2 Life cycle inventory

7.2.2.1 Adsorbents

The LCA of cork granulates can be conducted by two approaches: i) by allocating the impacts of cork granulates as a byproduct from the LCA of cork stoppers manufacturing (Demertzi, Silva et al. 2016, Amorim 2019, Flor-Montalvo, Martínez-Cámara et al. 2022); and ii) through direct LCA using the inventory for cork granulates calculated by Rives, Fernandez-Rodriguez et al. (2012). Because it was a more straightforward, the last approach was used in this study.

Iron-coated cork granulates are novel adsorbents consisting of cork granulates impregnated with iron. They have been successfully tested on lab-scale for the adsorption of arsenic and antimony

in both batch (Pintor, Vieira et al. 2018, Pintor, Vieira et al. 2020, Pintor, Brandão et al. 2021) and continuous modes in Chapter 3 and 4. The iron modification of the cork granulates was performed on small and medium lab scales. The small-scale methodology was determined by Pintor, Vieira et al. (2018). The medium lab-scale methodology is a scale-up adaptation of the previous method, which is described in Chapter 6. Briefly, cork granulates were put in contact with a 0.05 M $FeCl_3$ solution where iron (oxy)hydroxides were precipitated through the addition of NaOH until pH 7.0, at 20 g L^{-1}, in a rotating shaker at 20 rpm, for 16 h, at room temperature. Following the coating time, the granulates were washed with distilled water until the iron excess was removed, after which they were put to dry for 24 hours. The ICG particle size ranges from 0.5 to 1 mm.

For Bayoxide E33, the data were obtained from a study that examined the commercial adsorbent's impact as equivalent to a ferrous hydroxide-based sorbent composed of > 99% α-Ferrous oxide hydroxide (Hu, Rana et al. 2020). Particle size of the Bayoxide E33 ranges from 0.4 to 1.7 mm (Water 2024).

7.2.2.2 Adsorption in continuous mode in lab-scale

Adsorption assays were carried out in continuous mode for each adsorbent to calculate the amount of adsorbent needed to treat 1000 L of arsenic-contaminated water. The amount of adsorbent was used as the functional unit for the calculation of the environmental impact of removing arsenic by either natural-based adsorbent, iron-coated cork granulates or commercial adsorbent, Bayoxide E33.

The Bayoxide® E33 sample was supplied by a water treatment plant in Portugal. Arsenic inlet solutions were prepared by diluting, in distilled water, an arsenic commercial standard of 1,000 mg L^{-1} (Chem-Lab). The pH was regulated at the influent reservoir using 0.1 M, 1 M and 10 M NaOH or HNO_3 solutions. Total arsenic concentrations were measured by inductively coupled plasma-optical emission spectroscopy (ICP-OES) in the range of 0.005–10 mg L^{-1}. The ICP-OES apparatus was an ICP-OES Thermo X Series.

The lab-scale system employed for the adsorption of total arsenic onto Bayoxide E33 in continuous mode was the same as the one shown in Figure 3.1 and described in section 3.2.4. The same operational conditions were applied in the assays performed with each adsorbent: Flow rate = 5 mL min^{-1}, Bed height = 12 cm, Bed volume = 59 mL and pH = 7. As previously published, 6 g of ICG was able to treat 7.4 L of 1 mg As(V) L^{-1} aqueous solution before the breakthrough point where the outlet concentration reached 10 µg L^{-1}, following the WHO

guideline for arsenic in drinking water (Chapter 3). In the same conditions, a fixed-bed column was filled with 35 g of Bayoxide E33, and the filter was able to treat 114 L of aqueous solution before it reached the breakthrough point.

To compare the environmental impact of using fresh or regenerated ICG, the data were obtained from Chapter 4. The fresh ICG treated 7.9 L of 100 µg As L^{-1} groundwater under 10 µg L^{-1}, whilst regeneration using NaOH 0.1 M allowed for up to 12.8 L. Table 7.1 summarizes the operational conditions for the assay carried out with each adsorbent.

Table 7.1: Operating conditions of lab-scale fixed-bed column treatment with ICG and Bayoxide E33.

Parameter	Goal ii)		Goal iii)	
	ICG	**Bayoxide E33**	**ICG**	**Regenerated ICG**
Flow rate (mL min^{-1})	5	5	5	5
Bed height (cm)	12	12	12	12
Arsenic initial concentration (mg L^{-1})	1	1	0.1	0.1
pH	7	7	7	7
Bed height (cm)	12	12	12	12
Bed volume (mL)	59	59	59	59
Adsorbent density (g cm^{-3})	0.10	0.59	0.10	0.10
Adsorbent mass (g)	6	35	6	6
Treated volume before breakthrough (L)	7.4	114	7.9	12.8
Ratio of treated volume per adsorbent mass (L g^{-1})	1.233	3.257	1.32	2.13
Reference	Chapter 4	This work	Chapter 4	

7.2.2.3 Toxicity Characteristic Leaching Procedure (TCLP)

For assessing leaching from arsenic-loaded adsorbents, TCLP is frequently used (Yadav, Saidulu et al. 2022). It defines whether a waste is hazardous or non-hazardous, and the disposal method is chosen accordingly. Hence, the TCLP method was used to verify if the saturated adsorbents from the column experiments were hazardous, as arsenic can be leached out from the adsorbent.

In brief, 1.5 g of adsorbent was put in contact with 30 mL of extraction fluid (5.7 mL of glacial CH3COOH added to 500 mL of distilled water, plus 64.3 mL of 1 M NaOH and diluted to 1 L, pH 4.93±0.05) for 18 ±1 h in a rotating shaker (Stuart, SB3), at 30 rpm and a controlled temperature of 23.0 ± 0.5 °C. The liquid phase was then separated from the solid phase by filtration through a 0.45 µm cellulose acetate filter and analyzed for As (EPA 1999). The total arsenic concentration was measured by inductively coupled plasma-optical emission spectroscopy (ICP-OES) in the range of 0.005–10 mg L^{-1}.

7.2.2.4 Assumptions in inventory preparation

a) The iron-coated cork granulates were prepared in a medium lab scale as described in the Chapter 6.

b) The effluent of the $FeCl_3$ 0.05 M coating solution was assumed to be non-hazardous wastewater.

c) The Bayoxide E33 and ICG production data were assumed to be equivalent, that is, corresponding to a similar laboratory scale.

d) After the column was clogged three times, the arsenic adsorption experiments in the fixed-bed column using Bayoxide E33 were considered to be completed.

e) The transport impacts for each adsorbent were excluded from this analysis.

7.2.3 Software and LCA methodology

The environmental impacts of the iron-based adsorbents necessary to treat 1000 L of arsenic-contaminated water were compared using SimaPro 9.5 software. The ReCiPe 2016 Midpoint (H) method was selected. The impact categories considered were: Global warming; Stratospheric ozone depletion; Ionizing radiation; Ozone formation, human health; Fine particular matter formation; Ozone formation, terrestrial ecosystem; Terrestrial acidification; Freshwater eutrophication, Marine eutrophication, Terrestrial ecotoxicity; Freshwater ecotoxicity;

Marine ecotoxicity; Human carcinogenic toxicity; Human non-carcinogenic toxicity; Land use; Mineral resource scarcity; Fossil resource scarcity; and Water consumption.

7.2.4 Cost analysis

A preliminary study was conducted to compare the cost of arsenic removal from water using iron-coated cork granulates and Bayoxide E33. The cost of producing ICG was calculated based on the life-cycle inventory (section 7.2.2), considering industrial market costs for materials and energy. The price of Bayoxide E33 was obtained from the market. Municipal solid waste disposal costs less than 1% of the total, therefore, it was removed from the calculations. The prices were estimated based on the Portuguese market in 2024.

7.3 Results and discussion

7.3.1 Life cycle inventory (LCI)

The inventory data for treating 1000 L of arsenic-contaminated water by adsorption onto iron-coated cork granulates or Bayoxide E33 are presented in

Table 7.2, Table 7.3, Table 7.4 and Table 7.5.

The arsenic-saturated adsorbents were considered non-hazardous solid waste, as the TCLP results found an arsenic concentration < 5 mg L^{-1} in the leachate from the saturated iron-coated cork granulates (0.113 ± 0.002 mg L^{-1}) and from the Bayoxide E33 (0.056 ± 0.009 mg L^{-1}). The disposal method chosen for both adsorbents was a sanitary landfill, also proven to be the disposal method with a lower environmental burden for arsenic-saturated iron-based media for water treatment (van Genuchten, Etmannski et al. 2022). Alternative disposal methods, such as incineration with energy recovery, performed better than landfilling for end-of-life management of cork stoppers (Demertzi, Dias et al. 2015). Because ICG is composed of more than 90% cork granulates, it could also be an environmentally friendly option for saturated ICG disposal.

Table 7.2: Inventory of 1kg iron-coated cork granulates as an adsorbent for treating arsenic-contaminated water.

Parameter	**Value for 1kg (without desorption)**	**Value for 1kg (with desorption)**	**Source**	**Ecoinvent Unit Process**
		Material		
Cork granulates (kg)	1.00	1.00	Calculated	Table 7.3
Distilled water (coating solution) (L)	50.0	50.0	Calculated	
Distilled water (washing) (L)	217	217	Calculated	Water, deionised {Europe without Switzerland}| market for water, deionised | Cut-off, S
Distilled water (desorption solution) (L)	-	483	Chapter 4	
$FeCl_3$ (kg)	0.406	0.406	Calculated	Iron(III) chloride, without water, in 14% iron solution state {GLO}| market for iron(III) chloride, without water, in 14% iron solution state | Cut-off, S
HCl (30%) (L)	0.575	0.575	Calculated	Hydrochloric acid, without water, in 30% solution state {RER}| market for hydrochloric acid, without water, in 30% solution state | Cut-off, S
NaOH (kg) (neutralizing agent)	0.58	0.58	Calculated	Neutralising agent, sodium hydroxide-equivalent {GLO}| market for neutralising agent, sodium hydroxide-equivalent | Cut-off, S
NaOH (kg) (desorbing agent)	-	1.93	Chapter 4	
		Energy		
Mixing (kWh)	2.222	2.222	Calculated	Electricity, low voltage {PT}| market for electricity, low voltage | Cut-off, S
Drying (kWh)	3.601	3.601	Calculated	
		Waste		
Wastewater (L)	267	267	Calculated Chapter 4	Wastewater, average {Europe without Switzerland}| market for wastewater, average | Cut-off, S
Non-hazardous solid waste (kg)	1.00	1.00	Calculated	Municipal solid waste (Ahmed, Mavukkandy et al.)| treatment of

Parameter	Value for 1kg (without desorption)	Value for 1kg (with desorption)	Source	Ecoinvent Unit Process
				municipal solid waste, sanitary landfill | Cut-off, S
Hazardous waste (kg)	-	483	Calculated	Hazardous waste, for incineration {Europe without Switzerland}| market for hazardous waste, for incineration | Cut-off, S

Table 7.3: Inventory for producing 1 ton of cork granulates (0.25 – 8 mm).

Category	Parameter	Value	Source	Ecoinvent Unit Process
Material	Raw cork (kg)	1546.8	(Rives, Fernandez-Rodriguez et al. 2012)	Cork, raw {PT}| market for cork, raw | Cut-off, S
	Water (L)	193.9	(Rives, Fernandez-Rodriguez et al. 2012)	Tap water {Europe without Switzerland}| market for tap water | Cut-off, S
Energy	Diesel oil (kg)	2.2	(Rives, Fernandez-Rodriguez et al. 2012)	Diesel {Europe without Switzerland}| market for diesel | Cut-off, S
	Cork dust (kg) [a]	8.6	(Rives, Fernandez-Rodriguez et al. 2012)	-
	Electricity (MJ)	1327	(Rives, Fernandez-Rodriguez et al. 2012)	Electricity, medium voltage {PT}| market for electricity, medium voltage | Cut-off, S
Wastes	Cork dust (particle <0.25 mm) (kg)	530.4	(Rives, Fernandez-Rodriguez et al. 2012)	Waste wood, untreated {PT}| market for waste wood, untreated | Cut-off, S
	Cork with unpleasant defects	15.4	(Rives, Fernandez-Rodriguez et al. 2012)	

[a]Considered carbon neutral.

Table 7.4: Energy necessary to produce 1 kg of iron-coated cork granulates in medium lab scale.

Energy Process	Equipment type	Time (h)	Power (W)	Energy(kWh)/ 0.288 kg	Converted value for 1kg
Electricity used to mix the iron chloride solution with the cork granulates	Mixer/rotator operating at 20 rpm	16	40[a]	0.64	2.222
Electricity used for drying the final produced ICG	Drying oven operating at 60ºC[b]	24	432[c]	1.037	3.601
Total				**1.677**	**5.823**

[a]Equipment specification: 80 W for 40 rpm. [b]Drying oven estimated capacity to dry approximately 2.88 kg of ICG. [c]Equipment specification: 1800 W for 250ºC.

Table 7.5: Inventory for using 1 kg of Bayoxide E33 (crystalline α-ferric oxide hydroxide) as adsorbent for treating arsenic-contaminated water. The inventory data were obtained from Hu, Rana et al. (2020), who extracted data from Bonton, Bouchard et al. (2012), Encina, Distaso et al. (2015), Gurung, Tang et al. (2018) and Villacís-García, Ugalde-Arzate et al. (2015).

Parameter (unit)	**Value for 1 kg**	**Ecoinvent Unit Process**
Ferrous sulfate heptahydrate (kg)	3.88	Iron sulfate {RER}| market for iron sulfate | Cut-off, S
Sulfuric acid (kg)	1.10	Sulfuric acid {RER}| market for sulfuric acid | Cut-off, S
Sodium hydroxide (kg)	11.42	Neutralising agent, sodium hydroxide-equivalent {GLO}| market for neutralising agent, sodium hydroxide-equivalent | Cut-off, S
Deionized water (kg)	82.50	Water, deionised {Europe without Switzerland}| water production, deionised | Cut-off, S
Nitrogen (m^3)	2.5 [a]	Nitrogen, liquid {RER}| market for nitrogen, liquid | Cut-off, S
Heating (kWh)	2.81	Electricity, low voltage {PT}| market for electricity, low voltage | Cut-off, S
Mixing (kWh)	0.05	
Nitrogen purging (kWh)	0.30	
Drying (kWh)	0.03	
Wastewater (L)	80.00	Wastewater, average {Europe without Switzerland}| market for wastewater, average | Cut-off, S
Non-hazardous solid waste (kg)	1	Municipal solid waste (Ahmed, Mavukkandy et al.)| treatment of municipal solid waste, sanitary landfill | Cut-off, S

[a]Converted from 2.5 m^3 to 2.975 kg, using a density of 1.19 kg/m^3.

7.3.2 Impact assessment of iron-coated cork granulates production

The production of iron-coated cork granulates on lab-scale consisted of three steps: i) iron impregnation with $FeCl_3$ solution in batch, ii) washing off the adsorbent to remove the iron excess, and iii) drying of the material before storage for further use Figure 7.1a. Figure 7.2 Table 7.6 present the comparisons of the environmental impacts of each production phase on lab scale, including the production of cork granulate, for 1 kg of ICG.

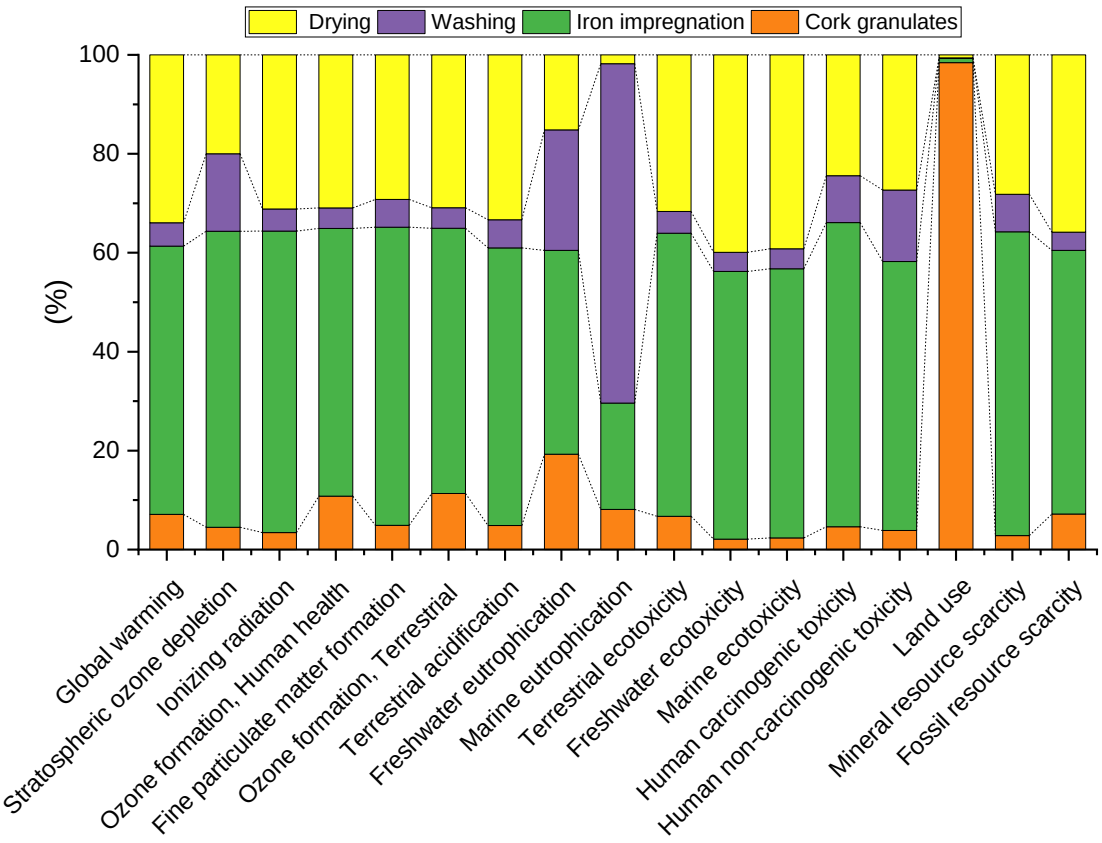


Figure 7.2: Process contribution to environmental impacts associated with the production of 1 kg iron-coated cork granulates on lab-scale production.

Table 7.6 : Environmental impacts of each lab scale production phase for 1 kg of iron-coated cork granulates, including cork granulates impacts.

Impact category	Unit	Cork granulates	Iron impregnation	Washing	Drying	Total
Global warming	kg CO_2 eq.	0.27	2.08	0.181	1.30	3.83
Stratospheric ozone depletion	kg CFC-11 eq.	1.26×10^{-7}	1.67×10^{-6}	4.38×10^{-7}	5.59×10^{-7}	2.79×10^{-6}
Ionizing radiation	kBq Co-60 eq. to air	0.0156	0.277	0.0203	0.142	0.454
Ozone formation, Human health	kg NOx eq.	1.04×10^{-3}	5.23×10^{-3}	4.02×10^{-4}	2.99×10^{-3}	9.68×10^{-3}
Fine particular matter formation	kg PM2.5 eq.	3.23×10^{-4}	4.00×10^{-3}	3.71×10^{-4}	1.94×10^{-3}	6.63×10^{-3}
Ozone formation, Terrestrial ecosystem	kg NOx eq.	1.15×10^{-3}	5.41×10^{-3}	4.16×10^{-4}	3.12×10^{-3}	0.0101
Terrestrial acidification	kg SO_2 eq.	8.45×10^{-4}	9.76×10^{-3}	9.85×10^{-4}	5.80×10^{-3}	0.0174
Freshwater eutrophication	kg P eq.	4.76×10^{-4}	1.02×10^{-3}	6.02×10^{-4}	3.75×10^{-4}	2.47×10^{-3}
Marine eutrophication	kg N eq.	1.19×10^{-4}	3.15×10^{-4}	1.01×10^{-3}	2.61×10^{-5}	1.47×10^{-3}
Terrestrial ecotoxicity	kg 1,4-DCB eq.	1.61	13.7	1.06	7.61	24.0
Freshwater ecotoxicity	kg 1,4 DB eq.	7.47×10^{-3}	0.190	0.0136	0.141	0.352
Marine ecotoxicity	kg 1,4-DB eq.	0.0106	0.245	0.0182	0.176	0.450
Human carcinogenic toxicity	kg 1,4-DB eq.	0.0114	0.152	0.0235	0.0605	0.248
Human non-carcinogenic toxicity	kg 1,4-DB eq.	0.226	3.19	0.849	1.60	5.87
Land use	Annual crop eq.·y	7.32	0.0680	4.16×10^{-3}	0.0453	7.43
Mineral resource scarcity	kg Cu eq.	4.86×10^{-4}	0.0105	1.30×10^{-3}	4.83×10^{-3}	0.0172
Fossil resource scarcity	kg oil eq.	0.0752	0.559	0.0387	0.376	1.05

Iron impregnation is the step that contributes the most to environmental impacts, primarily due to the high impact of sodium hydroxide added to $FeCl_3$ solution until iron precipitation at neutral pH. Additionally, the electricity consumed in the mixing equipment for 16 hours contributes to the overall burden. In agreement with these findings, the impregnation process was also the largest contributor to the environmental impacts of the production of modified activated carbon from olive waste cake (Hjaila, Baccar et al. 2013).

The second most impacting step is the drying phase, which was expected since it requires heat energy for 24 hours. Finally, the washing step performed better environmentally, except for freshwater and marine eutrophication. That can be justified by the generation of 267 L of wastewater for each 1 kg of ICG produced. However, the wastewater produced in the washing step is only composed of water (distilled water) and the ferric oxide excess from the iron impregnation. Hence, it is unlikely that the wastewater from ICG production will cause aquatic eutrophication because it does not contain nitrogen or phosphorus. In comparison to the production steps, the cork granulates, ICG's main component, are the smallest contributor to environmental impacts, except for land use. Even though cork is a renewable resource, its production requires large forest areas and has a significant impact on land use compared to other inputs.

The LCA results do not necessarily represent the environmental burdens caused after scaling up to a typical mass production (Shibasaki, Fischer et al. 2007). Activities undertaken at different scales will have non-linear effects on life cycle impacts because of economies of scale, industrial synergies, efficiency improvements and system design (Pizzol, Sacchi et al. 2021). The scale-up to the industrial scale might give different results, where optimization will result in less environmental impact. For instance, the reuse of chemicals, water and wastewater can be shown as a negative output (to be deducted from input values) and give different LCA results on an industrial scale (Norberto, Zoroufchi Benis et al. 2023).

Other authors have reported the environmental impact associated with the production of adsorbents (Table 7.7). The production of nanocomposite from aluminum waste, activated carbon and granular activated carbon had a higher impact on global warming than ICG production. On the other hand, alginate extraction waste and thermal-treated laterite soil synthesis were more environmentally friendly than the synthesis of ICG.

Table 7.7: Comparison between the environmental impact of producing 1 kg of each adsorbent.

	Global warming (kg CO_2 eq.)	Stratospheric ozone depletion (kg CFC-11 eq.)	Terrestrial acidification (kg SO_2 eq.)	Ref.
Mercapto-functionalized silica aerogels	118	1.90×10^{-5}	0.466	(Zhang, Yuan et al. 2023)
Nanocomposite γ-Al_2O_3 derived from Al-waste[1]	19	-	0.115	(Halawy, Osman et al. 2022)
AC from olive-waste cakes	11.096	5.46×10^{-7}	0.108	(Hjaila, Baccar et al. 2013)
GAC from coconut shell	7.54	-	0.00859	(Vilén, Laurell et al. 2022)
GAC from wood	9.21	-	0.0150	(Vilén, Laurell et al. 2022)
$ZnCl_2$ activated biochar	1.479	3.80×10^{-8}	0.00429	(Maiti, Siddiqi et al. 2023)
Alginate extraction waste	0.263	-	0.00105	(Nishikawa, da Silva et al. 2018)
Thermally treated laterite soil	0.264	4.9×10^{-12}	0.00180	(Rathore and Mondal 2018)
Alginate-HNTs beads	14.19	-	0.027	(Chiew, Gourich et al. 2022)
Iron-coated cork granulates	3.83	2.79×10^{-6}	0.0174	This work

[1]Environmental impact calculated for 1 kg of base material which yields less than 1 kg of adsorbent.

7.3.3 Environmental impact of arsenic removal from water

The environmental impacts of treating 1000 L of arsenic-contaminated water (C_0 = 1 As(V) mg L^{-1}), under the WHO guideline for arsenic in drinking water (10 µg L^{-1}), by adsorption onto iron-coated cork granulates or Bayoxide E33 were evaluated. The amount of adsorbent required was 0.81 kg for iron-coated cork granulates and 0.31 kg for Bayoxide E33, based on adsorption experiments performed in a fixed-bed column (section 7.2.2.2). The life cycle analysis trees for ICG and Bayoxide E33 are presented in Figure 7.3 and Figure 7.4, respectively. In 13 of 18 categories, the water treatment using iron-coated cork granulates performed better than that with Bayoxide E33 (Figure 7.5). The commercial iron oxide adsorbent had less impact on marine eutrophication, land use, freshwater and marine ecotoxicities, and human non-carcinogenic toxicity. For land use, the main burden of ICG is associated with cork tree cultivation, as discussed in section 3.2. The wastewater was the main contributor to the higher impact of ICG on marine eutrophication (Figure 7.6) as a result of the large amount of water needed to wash the excess iron from the adsorbent, which generates high amounts of wastewater during ICG production. Hence, further studies should improve ICG production to better retain iron in cork granulates and improve the washing process. The municipal solid waste treatment was the largest contributor to the impacts related to toxicity (freshwater, marine and human non-carcinogenic) (Figure 7.7) and the second most contributor to marine eutrophication (Figure 7.6). This is justified by the fact that more ICG is required to treat 1000 L of water than Bayoxide E33, resulting in a larger amount of spent adsorbent for disposal after use. That can be mitigated by finding an alternative destination for the spent adsorbent, such as incorporation into composites used for construction (Matos, Nunes et al. 2015, Verbinnen, Block et al. 2015, Dairi, Bellili et al. 2022, Cobo-Ceacero, Moreno-Maroto et al. 2023, Menor, Caballero et al. 2024).

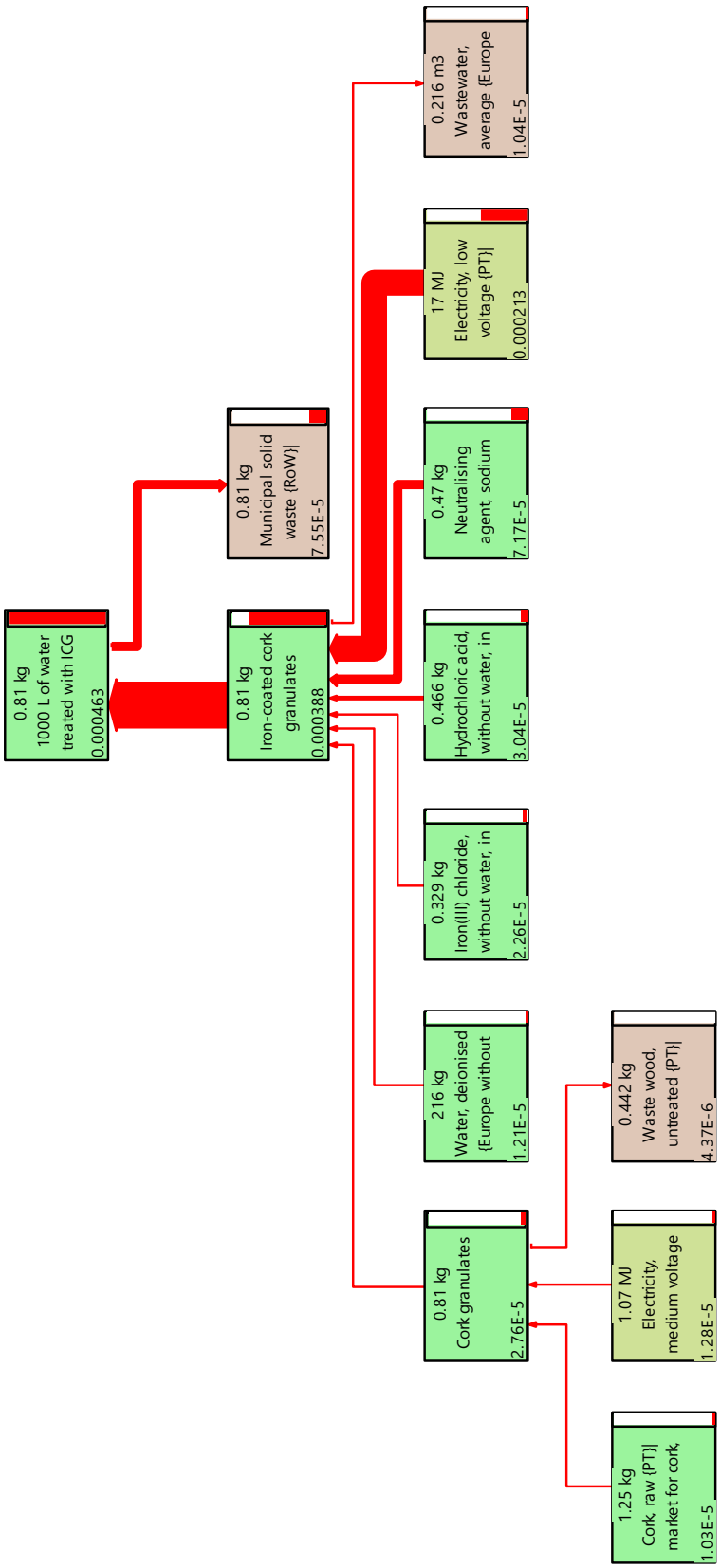


Figure 7.3: Life cycle analysis tree for iron-coated cork granulates (ICG) production: material, energy and waste treatment and their corresponding impact on global warming for the treatment of 1000L of arsenic-contaminated water (C_0 = 1 mg L^{-1}).

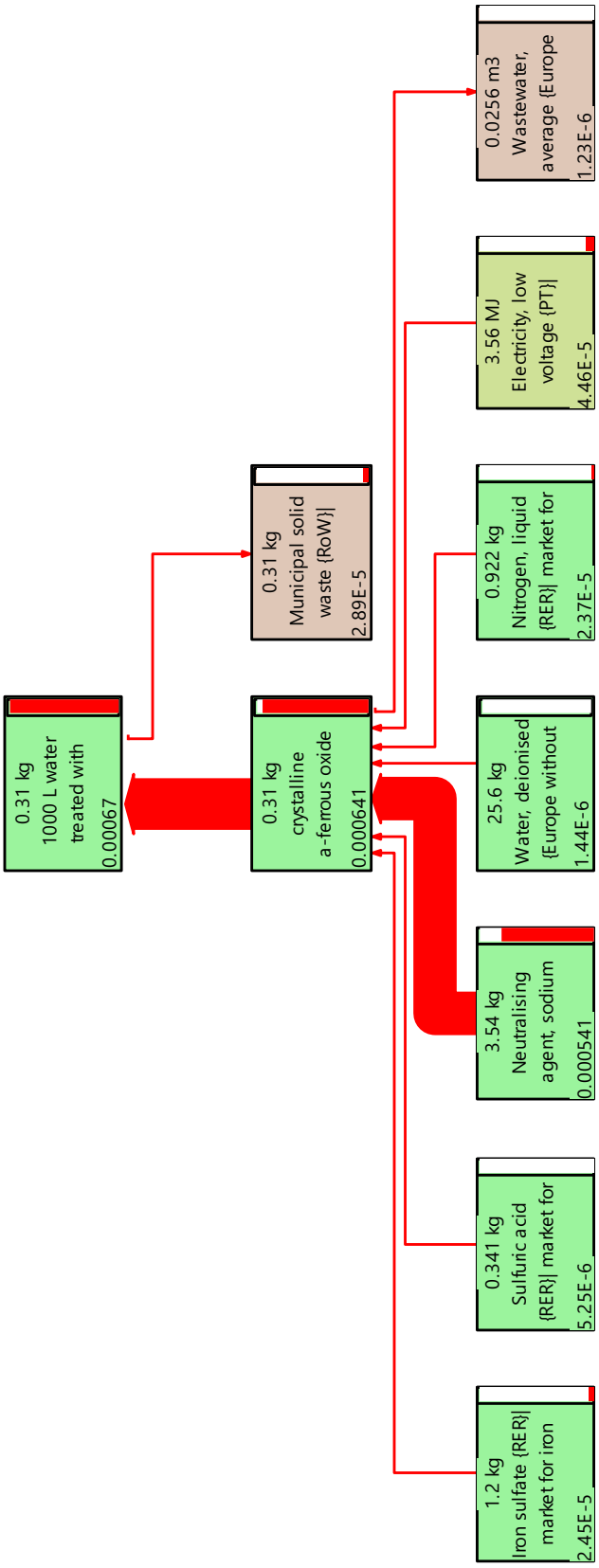


Figure 7.4: Life cycle analysis tree for Bayoxide E33 production: material, energy and waste treatment and their corresponding impact on global warming for the treatment of 1000L of arsenic-contaminated water (C_0 = 1 mg L^{-1}).

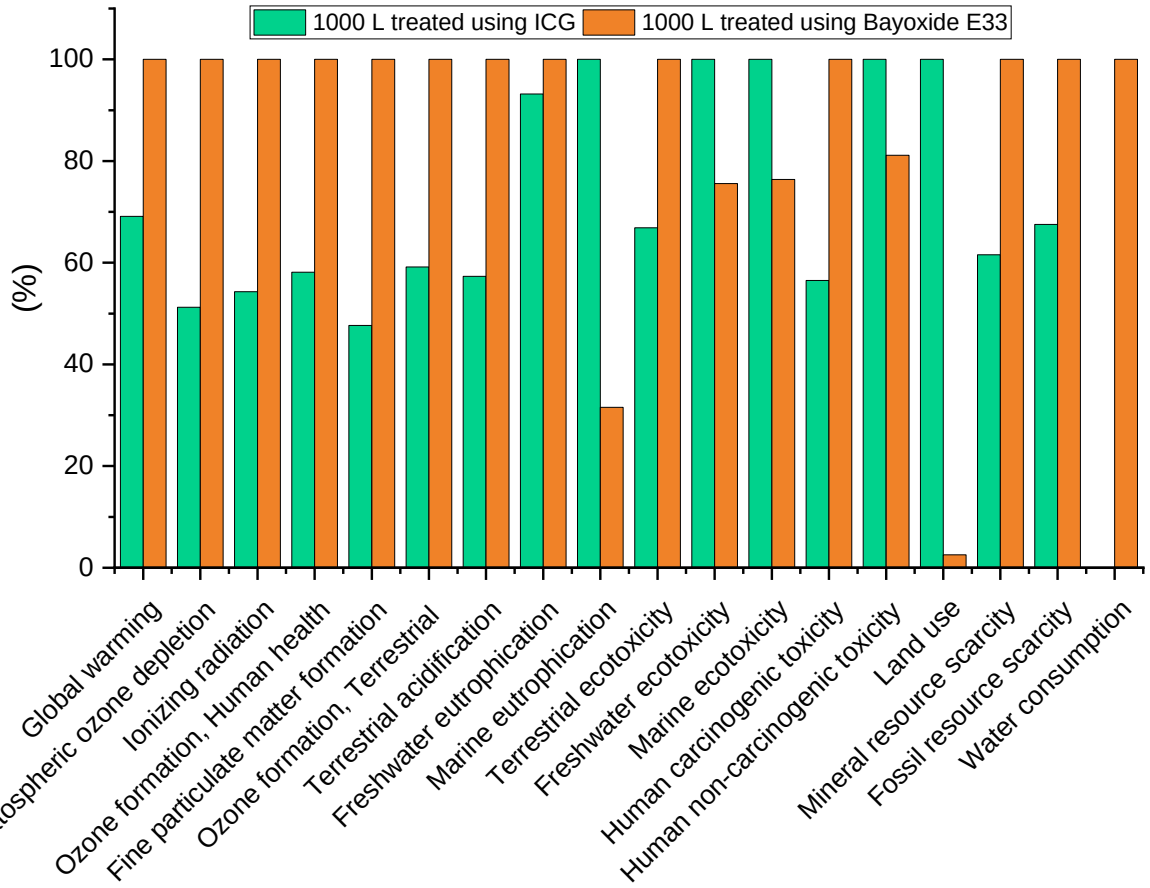


Figure 7.5: Relative comparison between the environmental impacts of the treatment of arsenic-contaminated water (C_0 = 1 As(V) mg L^{-1}) by adsorption onto iron-cork granulates and Bayoxide E33, using the ReCiPe 2016 Midpoint (H) method.

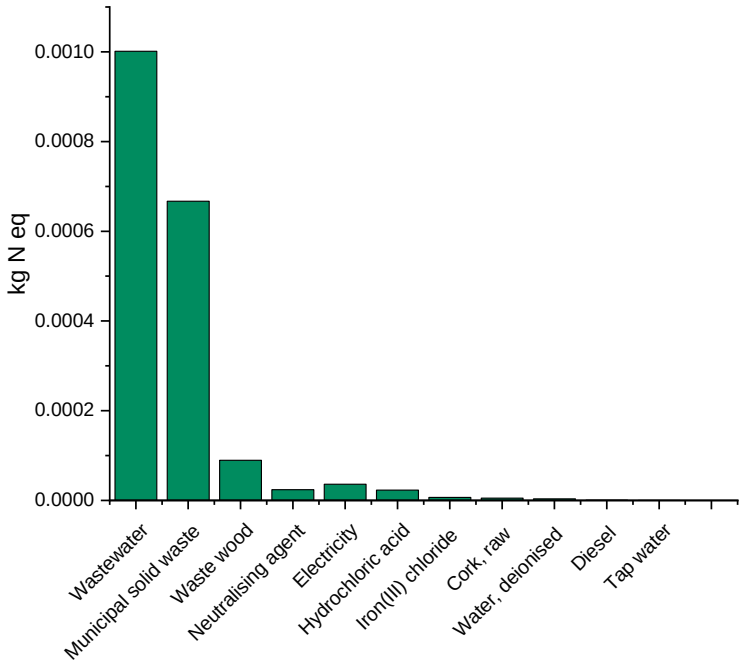


Figure 7.6: Material contribution for marine eutrophication in the treatment of 1000 L of arsenic-contaminated (C_0 = 1 mg L^{-1}) water using iron-coated cork granulates.

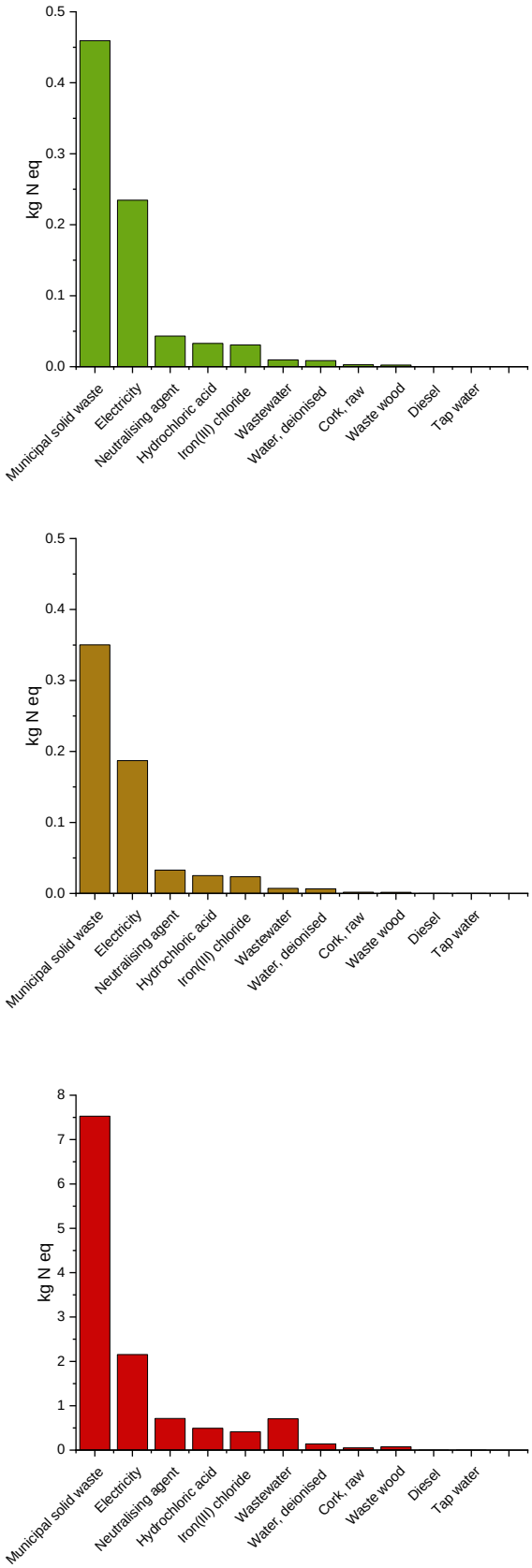


Figure 7.7: Material contribution for a) marine toxicity, b) freshwater toxicity and c) non-carcinogenic toxicity in the treatment of 1000 L of arsenic-contaminated (C_0 = 1 mg L^{-1}) water using iron-coated cork granulates.

Figure 7.8 and Figure 7.9 present the contributions of each component from the inventory of iron-coated-cork-granulates and Bayoxide E33, respectively. The most impacting input for ICG is electricity, followed by the neutralizing agent (NaOH) and hydrochloric acid. For land use, however, the cork granulates presented the higher impact contribution, as previously discussed. Initiatives to improve energy production and to achieve energy saving in industrial processes are important for reducing the environmental burden associated with electricity consumption (Carneiro, Da Fonseca-Soares et al. 2022, Li, Zhang et al. 2022, Reaney, Walsh et al. 2023).

The primary contributor to the environmental impacts of Bayoxide E33 is the neutralizing agent (NaOH). This was expected, considering that neutralizing agents are used to precipitate the iron. Bayoxide E33 is composed mainly of iron hydroxide, whereas ICG contains approximately only 2-3% iron in the form of oxides and hydroxides (Pintor, Vieira et al. 2018).

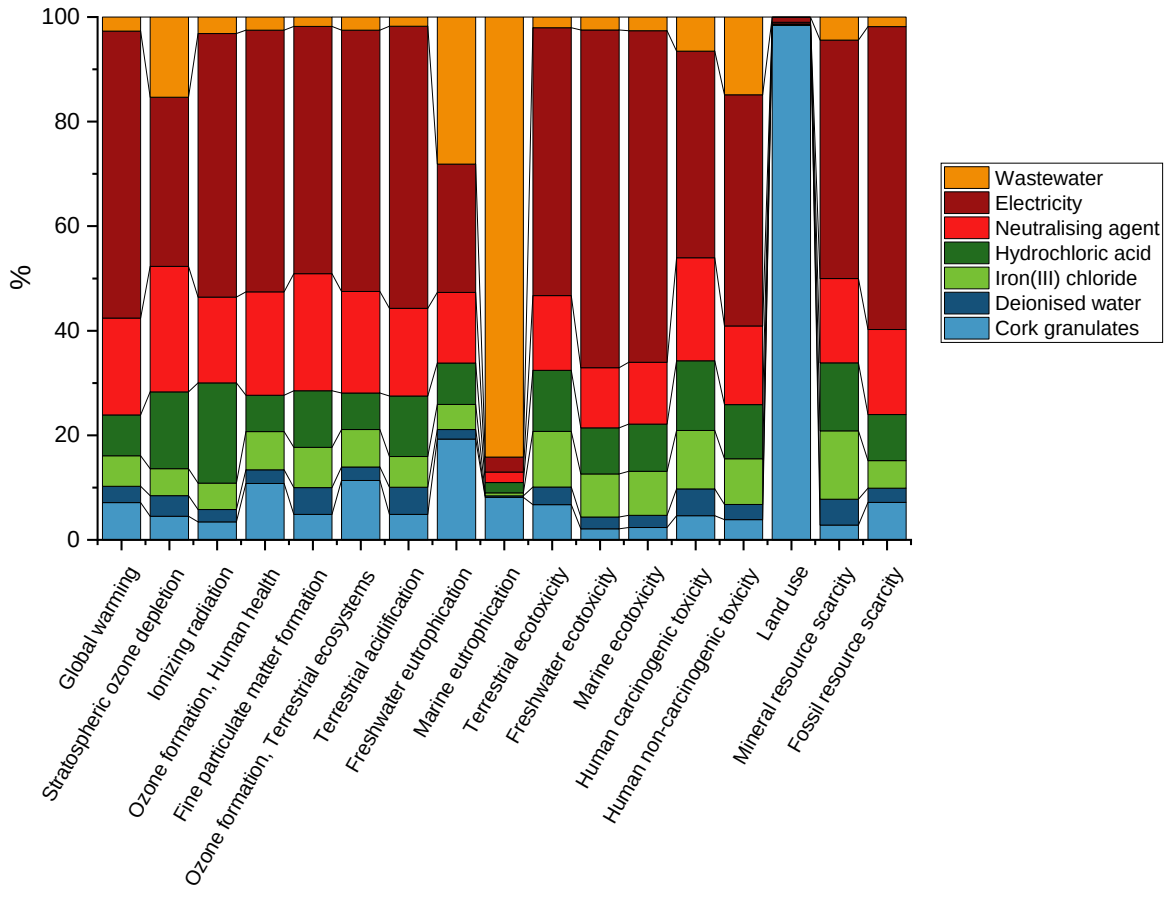


Figure 7.8: Contributions of materials/energy emission for the environmental impacts of iron-coated cork granulates (%).

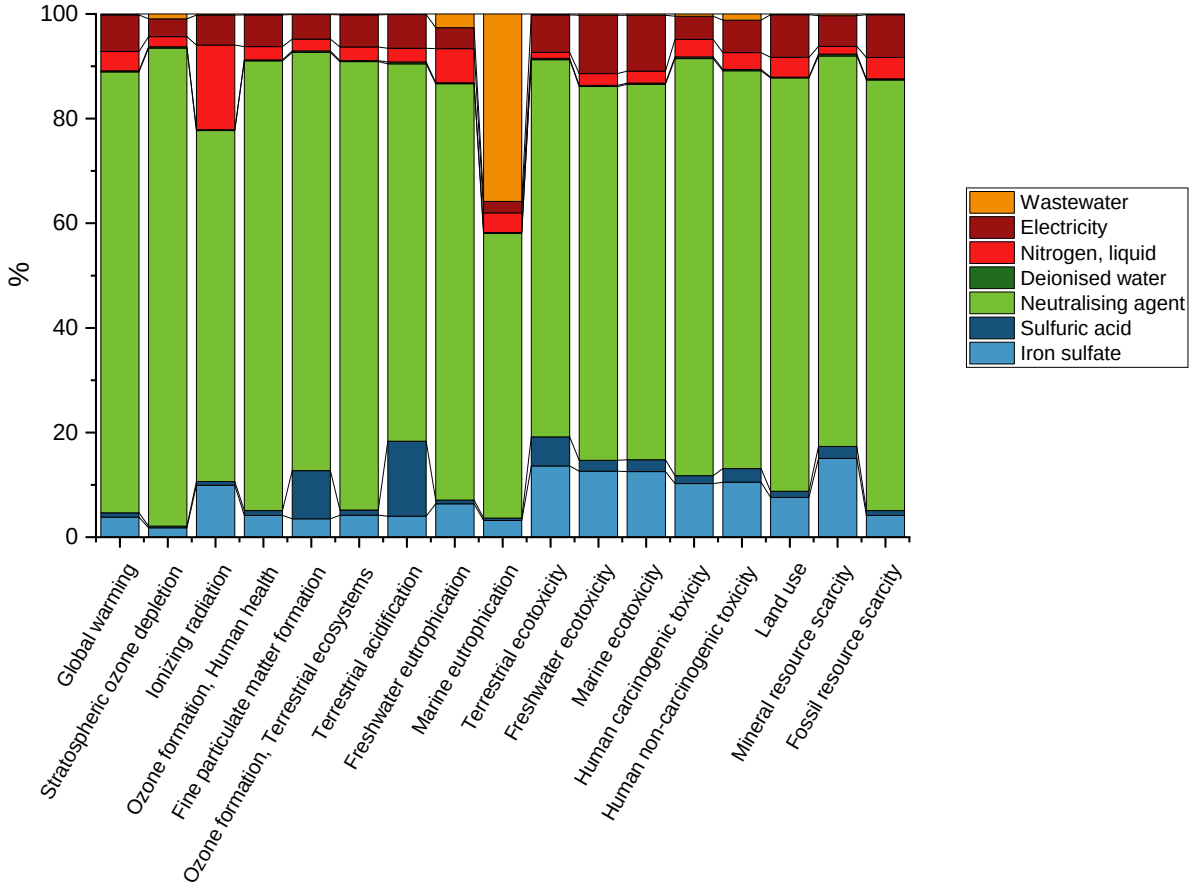


Figure 7.9: Contributions of materials/energy emission for the environmental impacts of Bayoxide E33 (%).

Table 7.8 presents the comparison of the environmental impacts of ICG and Bayoxide E33 with granulated activated carbon (GAC) and iron-impregnated granular activated carbon (GAC-Fe). The comparison between the environmental impacts of different adsorbents is challenging since different inventory assumptions were used for each LCA. The ICG and Bayoxide E33 environmental impacts might be overestimated in comparison to the ones from GAC and GAC-Fe since the last were calculated for the treatment of 0.2 mg As L^{-1} using the adsorption capacity in batch mode of 1.013 mg g^{-1}, as reported by Kalaruban, Loganathan et al. (2019). However, the referenced authors found lower adsorption capacities of 0.306 and 0.133 mg g^{-1} for GAC-Fe and GAC, respectively, in column experiments. These results imply that substantially more GAC and GAC-Fe would be required to treat 1000 L of arsenic-contaminated water, increasing the environmental impact.

Moreover, the methodology employed to assess the environmental impact of ICG might have led to an overestimation. First, this study assumed that 100% of the raw cork material originated from forests. Studies employing various ratios of forest to industrial sources of cork granulates

have indicated a lower environmental impact of industrial rather than forest sources (Rives, Fernandez-Rodriguez et al. 2012). Second, calculating the environmental impact of cork granulates through commercial value allocation reveals an even lower impact, given the respective prices of 1.45 EUR per kg for cork granulates and 53.80 EUR per kg for cork stoppers (Flor-Montalvo, Martínez-Cámara et al. 2022). Therefore, the extent of the differences in the environmental impacts between ICG and GAC/GAC-Fe remains uncertain. Nevertheless, it can be observed that, among the four alternatives examined (as detailed in Table 7.8), Bayoxide E33 had the highest environmental impact.

Table 7.8: Estimates of the life cycle impacts of the amount of each adsorbent needed for the treatment of 1000 L of arsenic-contaminated water by ReCIPe 2016 method.

	Unit	**ICG[a]**	**Bayoxide E33[a]**	**GAC[b]**	**GAC-Fe[b]**
Global warming	Kg CO_2 eq.	3.10	5.13	2.75	1.91
Stratospheric ozone depletion	kg CFC-11 eq.	2.26×10^{-6}	4.48×10^{-6}	1.28×10^{-6}	8.86×10^{-7}
Ionizing radiation	kBq Co-60 eq. to air	0.368	0.679	0.0453	0.0311
Ozone formation, Human health	kg NOx eq.	7.84×10^{-3}	1.36×10^{-2}	3.76×10^{-3}	2.63×10^{-3}
Fine particular matter formation	kg PM2.5 eq.	5.37×10^{-3}	1.13×10^{-2}	9.09×10^{-4}	6.34×10^{-4}
Ozone formation, Terrestrial ecosystem	kg NOx eq.	8.17×10^{-3}	1.39×10^{-2}	3.78×10^{-3}	2.64×10^{-3}
Terrestrial acidification	kg SO_2 eq.	1.41×10^{-2}	2.47×10^{-2}	2.71×10^{-3}	1.89×10^{-3}
Freshwater eutrophication	kg P eq.	2.00×10^{-3}	2.55×10^{-3}	1.09×10^{-5}	7.77×10^{-6}
Marine eutrophication	kg N eq.	1.19×10^{-3}	3.31×10^{-4}	8.22×10^{-5}	5.73×10^{-5}
Terrestrial ecotoxicity	kg 1,4-DCB eq.	19.5	29.1	0.445	0.307
Freshwater ecotoxicity	kg 1,4 DB eq.	0.285	0.346	1.96×10^{-4}	1.41×10^{-4}
Marine ecotoxicity	kg 1,4-DB eq.	0.365	0.453	0.0491	3.49×10^{-4}
Human carcinogenic toxicity	kg 1,4-DB eq.	0.201	0.373	8.67×10^{-4}	6.21×10^{-4}
Human non-carcinogenic toxicity	kg 1,4-DB eq.	4.75	7.08	0.0645	0.0461
Land use	Annual crop eq.·y	6.02	0.153	0.214	0.147

	Unit	ICG[a]	Bayoxide E33[a]	GAC[b]	GAC-Fe[b]
Mineral resource scarcity	kg Cu eq.	1.39×10^{-2}	2.26×10^{-2}	5.10×10^{-3}	3.74×10^{-3}
Fossil resource scarcity	kg oil eq.	0.849	1.26	1.28	0.89
Water consumption	m^3	-2.97×10^{-3}	0.126	0.0115	0.0118
Ref.		This study	This study	(Goyal, Tyagi et al. 2023)	(Goyal, Tyagi et al. 2023)

[a]Calculated for the treatment of a solution containing an arsenic concentration of 1 mg L^{-1}.
[b]Calculated for the treatment of a solution containing an arsenic concentration of 0.1 mg L^{-1}.

7.3.4 Impact assessment of desorption cycles

The success of a novel adsorbent is usually associated with its regeneration capacity. The most common method for the regeneration of saturated media is chemical desorption, which employs a chemical substance, usually a base or an acid, to separate the adsorbate from the adsorbent. This process increases the lifespan of the adsorbent, reducing the frequency of adsorbent acquisition and, consequently, the operational costs of a water treatment facility. Two scenarios were proposed to assess the environmental sustainability of operating an ICG adsorption column employing adsorption-desorption cycles:

- Scenario 1: Treatment of 1000 L of arsenic-spiked groundwater (C_0 = 100 µg L^{-1}) using new ICG. For that, 0.76 kg of ICG was necessary, according to the performance of iron-coated cork granulates reported in Chapter 4. After the saturation of the adsorbent, the lifespan of the material was reached, and it was sent to disposal as municipal solid waste. No desorption cycle was carried out.
- Scenario 2: Treatment of 1000 L of arsenic-spiked groundwater (C_0 = 100 µg L^{-1}) using regenerated ICG. For that, 0.47 kg of ICG was necessary, according to the performance of iron-coated cork granulates reported in Chapter 4. The adsorbent was reused twice, following desorption cycles using 0.1 M NaOH. After the third adsorption cycle, the saturated adsorbent was sent to disposal as municipal solid waste. The alkaline desorption solution containing high concentrations of arsenic was disposed of as hazardous waste.

The inventories of scenarios 1 and 2 were calculated based on

Table 7.2, adjusted to 0.76 kg of ICG without desorption and 0.47 kg of ICG with desorption, respectively. The life cycle analysis trees for ICG without desorption and with desorption are presented in Figure 7.10 and Figure 7.11, respectively.

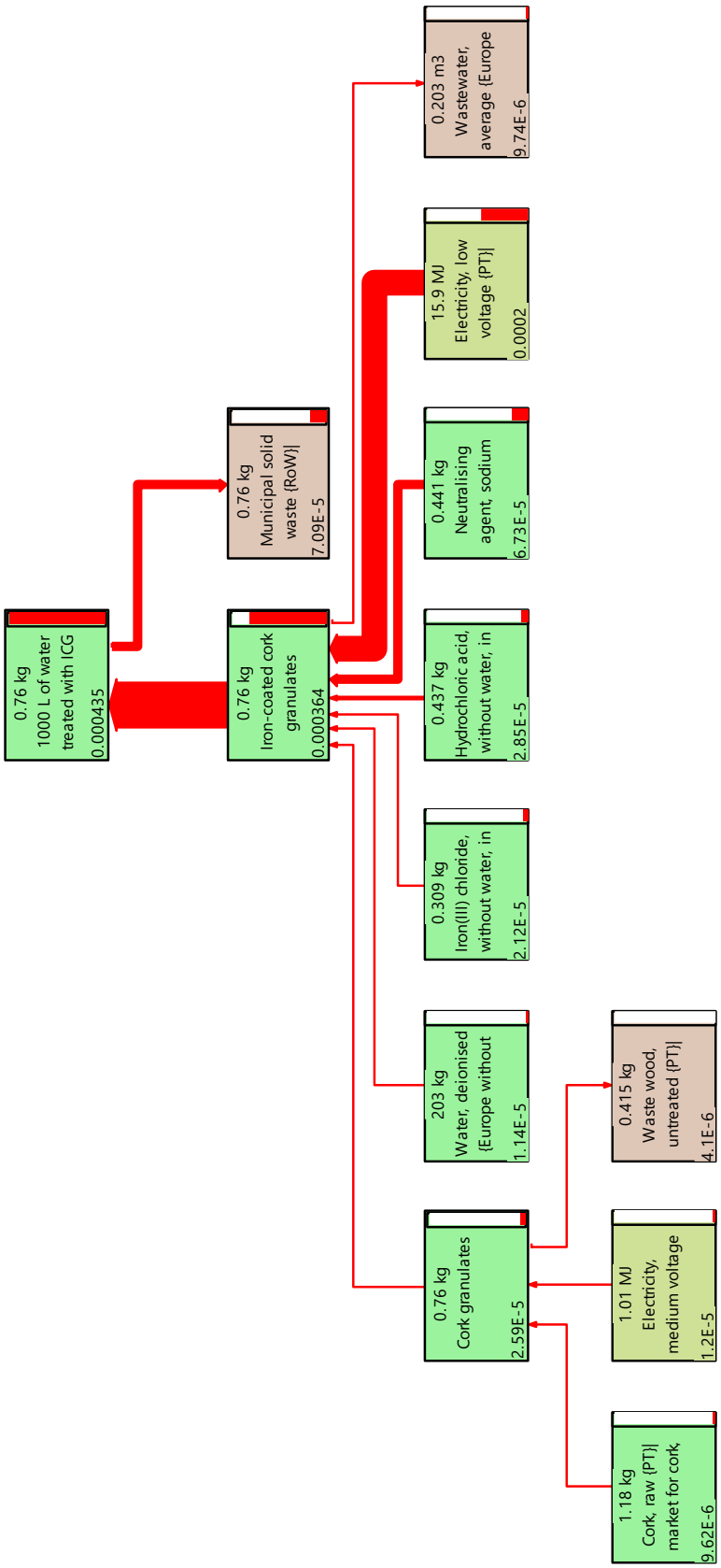


Figure 7.10: Life cycle analysis tree for the treatment of 1000 L of arsenic-spiked groundwater (C_0 = 100 μL^{-1}) using ICG without desorption cycles: material, energy and waste treatment and their corresponding impact on global warming.

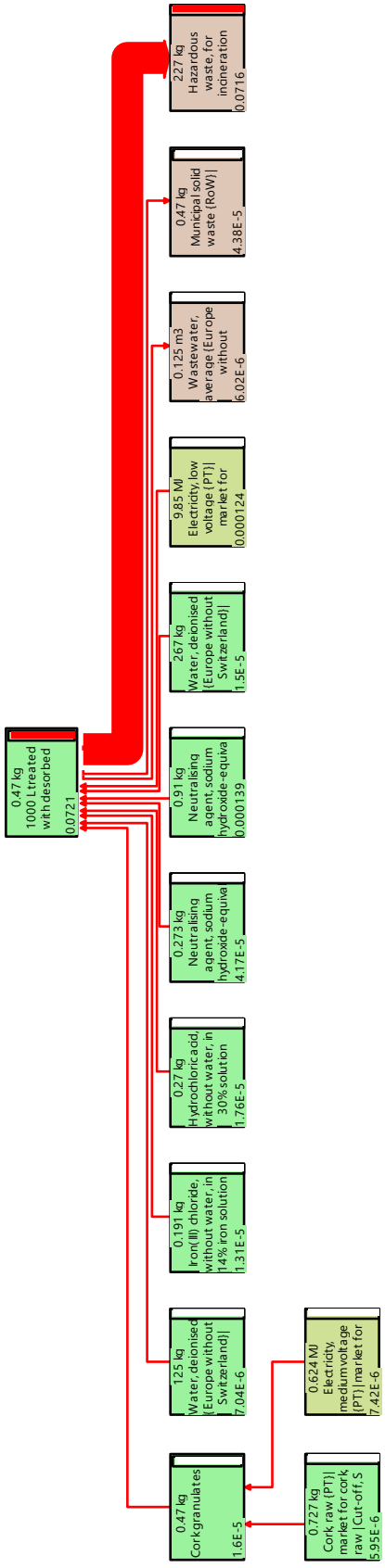


Figure 7.11: Life cycle analysis tree for the treatment of 1000 L of arsenic-spiked groundwater (C_0 = 100 µg L-1) using regenerated ICG with desorption cycles: material, energy and waste treatment and their corresponding impact on global warming.

The operation in adsorption-desorption cycles was not environmentally feasible for iron-coated cork granulates since all the impacts were much higher in Scenario 2 in comparison to Scenario 1 (Figure 7.12). This is attributed to the large amount of hazardous waste generated (Figure 7.11), which is the desorbing solution containing high concentrations of arsenic. Recently, arsenic was added to the European Commission's list of Critical Raw Materials (Commission, Directorate-General for Internal Market et al. 2023). This classification will increase the value of As-rich groundwater treatment waste (Wang, Holm et al. 2023). If the recovered arsenic from the desorbing solutions can be reused as an input for another industrial process, the environmental impact of the desorption process will decrease significantly, and its economic relevance will increase.

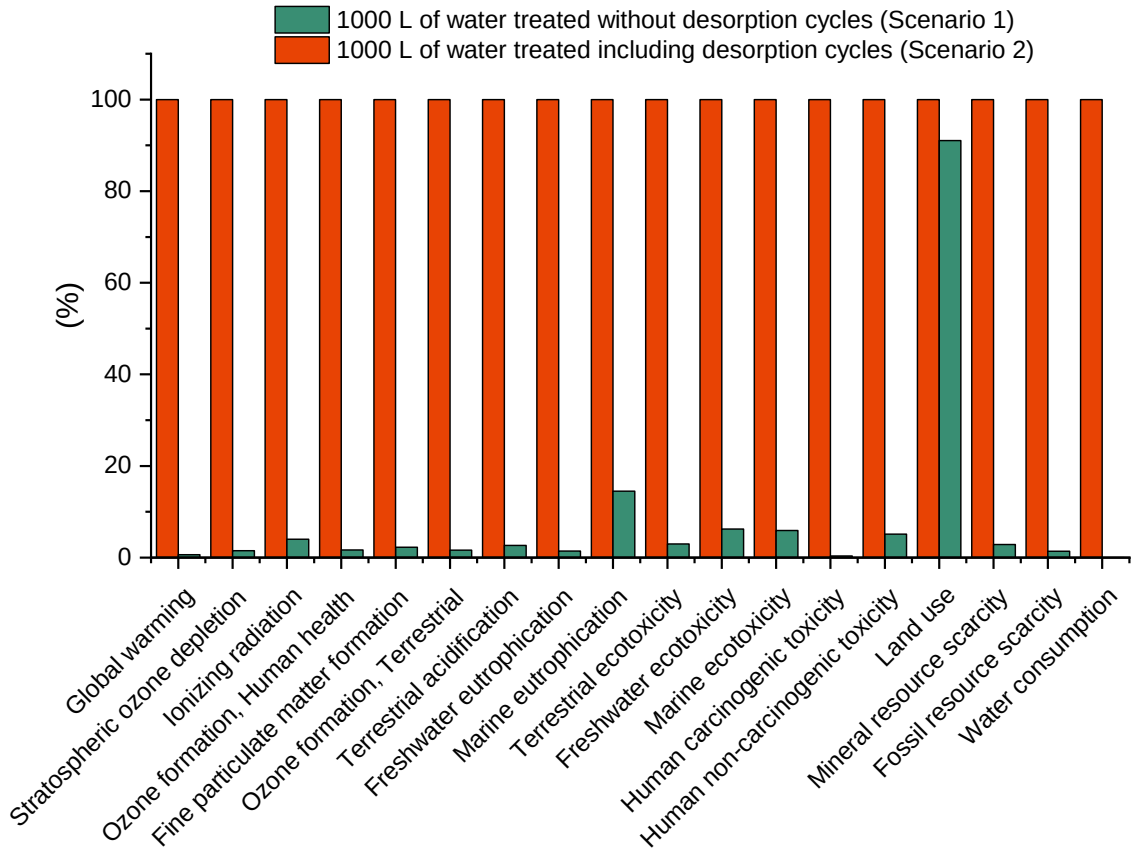


Figure 7.12: Environmental impacts of scenarios 1 and 2 for arsenic removal from water using iron-coated cork granulates.

7.3.5 Cost analysis

The adsorbent cost for treating 1000 L of arsenic-contaminated water (C_0 = 1 mg As(V) L^{-1}) with 0.81 kg of iron-coated cork granulates was 2.58 €, whereas the cost of 0.31 kg of Bayoxide E33 was 10.85 € (Table 7.9). Although the ICG costs may not represent the ultimate market price, in contrast to the commercial adsorbent, the combined material and energy cost of 3.18

€/kg offers a substantial margin when compared to the final market price of Bayoxide E33, which is 35 €/kg. Water (37%) and cork granulates (16%) had the most influence on the overall ICG cost, whereas sodium hydroxide and electricity contributed the most to ICG environmental impacts (Figure 7.3).

It is important to note that the material and energy quantities for ICG production were calculated based on the lab scale, potentially resulting in an overestimation compared to the industrial scale production. The increase in scale could lead to an overall reduction in the cost of ICG.

Table 7.9: Cost analysis for arsenic removal from water (C_0 = 1 mg As(V) L^{-1}) by adsorption onto iron-coated cork granulates or Bayoxide E33 (1 m^3).

ICG						
Parameter	**Value**	**Unit**	**Unitary price (€)**	**Unit**	**Ref.**	**Total Price (€)**
Cork granulates	1	kg	1.183	kg	(CORTICA24.PT 2024)	1.18
Water	267	kg	1.8524	m^3	(Porto 2024)	0.49
$FeCl_3$	0.406	kg	0.79	kg	(CAMACHEM 2024)	0.32
HCl (33%)	0.575	kg	0.25	kg	(CAMACHEM 2024)	0.14
NaOH	0.58	kg	0.62	kg	(CAMACHEM 2024)	0.36
Electricity, low voltage PT	5.823	kWh	0.04	kWh	(HUB 2021)	0.24
Wastewater	267	L	1.6594	m^3	(Porto 2024)	0.44
Total /kg						3.18
Total / m^3						**2.58**
Bayoxide E33						
Parameter	**Value**	**Unit**	**Unitary price (€)**	**Unit**	**Ref.**	**Total Price (€)**
Bayoxide E33	1	kg	35	kg	(Treatment. 2024, Water 2024)	35
Total / kg					Calculated	35.00
Total / m^3						**10.85**

7.4 Conclusions

In this work, an LCA was carried out to assess the environmental impact of iron-coated cork granulates (ICG), novel adsorbents, for arsenic removal from water. The electricity consumed in the laboratory-scale production of ICG was identified as the input with the highest contribution to environmental impacts. Compared to the commercial adsorbent Bayoxide E33, ICG had a

lower impact on 13 out of the 18 categories. The cost comparison evaluation of arsenic-contaminated water treatment using ICG and Bayoxide E33 indicated that the more ecological option is also the most economically feasible. The results were calculated considering lab-scale study, and it must be noted that the industrial-scale production of adsorbents and water treatment may result in different life cycle impacts and an overall reduction in the cost of ICG.

Extending the lifespan of the adsorbent by carrying out adsorption-desorption cycles had a higher environmental impact than using the adsorbent only once, mainly due to the additional process of hazardous waste treatment for desorbed solutions containing high concentrations of arsenic. Therefore, adsorbents claiming suitability for arsenic removal due to longer lifespans associated with multiple adsorption-desorption cycles should require to evaluate the environmental impacts associated with their reuse.

Even if considered more environmentally friendly, landfill disposal of saturated media could be essentially converting direct As emissions to an imminent As toxicity risk for future generations. Hence, options to reduce the amount of waste sent for disposal by recycling or reincorporating it to other materials and processes should be investigated.

In the future, updating the LCA to include the transportation inputs from the raw material sources to the adsorbent production site and from the production site to the end user is recommended. This comprehensive approach may be necessary due to the significant environmental burdens associated with transportation, which could lead to variations in the environmental performance of low-density ICG across different countries.

7.5 References

Ahmed, M., M. O. Mavukkandy, A. Giwa, M. Elektorowicz, E. Katsou, O. Khelifi, V. Naddeo and S. W. Hasan (2022). "Recent developments in hazardous pollutants removal from wastewater and water reuse within a circular economy." npj Clean Water 5(1): 12.

Amorim, G. d. A. M. S. (2019). Avaliação Comparativa do Ciclo de Vida da Rolha de Cortiça Natural e de uma Técnica produzidas na empresa Cork Supply Portugal. Master Master thesis, University of Porto.

Bonton, A., C. Bouchard, B. Barbeau and S. Jedrzejak (2012). "Comparative life cycle assessment of water treatment plants." Desalination 284: 42-54.

CAMACHEM. (2024). "Caustic Soda Pearls 99% (Sodium Hydroxide Pearls 99%)." Retrieved 27 Feb 2024, from https://camachem.com/vn/industrial-chemicals/caustic-soda-pearls/caustic-soda-pearls-99-sodium-hydroxide-pearls99.html.

CAMACHEM. (2024). "Ferric Chloride 96%." Retrieved 29 Feb 2024, from https://camachem.com/vn/water-chemicals/ferric-chloride/ferric-chloride-96.html.

CAMACHEM. (2024). "Hydrochloric Acid (HCL) 33%." Retrieved 29 Feb 2024, from https://camachem.com/vn/hydrochloric-acid-hcl-33.html.

Carneiro, M. A., D. Da Fonseca-Soares, L. H. M. Pereira and A. F. Ramos-Ridao (2022). "An Approach for Water and Energy Savings in Public Buildings: A Case Study of Brazilian Rail Company." Sustainability 14(23): 15921.

Chiew, C. S. C., W. Gourich, P. Pasbakhsh, P. E. Poh, B. T. Tey, C. P. Song and E.-S. Chan (2022). "Life cycle assessment on alginate-based nanocomposite beads for the removal of lead(II) from aqueous solutions." Journal of Water Process Engineering 45: 102531.

Cobo-Ceacero, C. J., J. M. Moreno-Maroto, M. Guerrero-Martínez, M. Uceda-Rodríguez, A. B. López, C. Martínez García and T. Cotes-Palomino (2023). "Effect of the addition of organic wastes (cork powder, nut shell, coffee grounds and paper sludge) in clays to obtain expanded lightweight aggregates." Boletín de la Sociedad Española de Cerámica y Vidrio 62(1): 88-105.

Commission, E., I. Directorate-General for Internal Market, Entrepreneurship, SMEs, M. Grohol and C. Veeh (2023). Study on the critical raw materials for the EU 2023 – Final report, Publications Office of the European Union.

Corominas, L., D. M. Byrne, J. S. Guest, A. Hospido, P. Roux, A. Shaw and M. D. Short (2020). "The application of life cycle assessment (LCA) to wastewater treatment: A best practice guide and critical review." Water Research 184: 116058.

CORTICA24.PT. (2024). "Granulado de cortiça 0,5 - 1mm - 10kg - BESTSELLER!" Retrieved 29 Feb 2024, from https://cortica24.pt/loja/122-05---10-mm/913-granulado-de-corticcedila-05---1mm---10kg---bestseller/.

da Costa, J. S., H. L. Maranduba, S. de Sousa Castro, J. A. de Almeida Neto and L. B. Rodrigues (2022). "Environmental performance of orange citrus waste as raw material for pectin and essential oil production." Food and Bioproducts Processing 135: 165-177.

Dairi, B., N. Bellili, N. Hamour, A. Boulassel, H. Djidjelli, A. Boukerrou and R. Bendib (2022). "Cork waste valorization as reinforcement in high-density polyethylene matrix." Materials Today: Proceedings 53: 117-122.

Demertzi, M., A. C. Dias, A. Matos and L. M. Arroja (2015). "Evaluation of different end-of-life management alternatives for used natural cork stoppers through life cycle assessment." Waste Management 46: 668-680.

Demertzi, M., R. P. Silva, B. Neto, A. C. Dias and L. Arroja (2016). "Cork stoppers supply chain: potential scenarios for environmental impact reduction." Journal of Cleaner Production 112: 1985-1994.

Encina, E. R., M. Distaso, R. N. Klupp Taylor and W. Peukert (2015). "Synthesis of Goethite α-FeOOH Particles by Air Oxidation of Ferrous Hydroxide Fe(OH)2 Suspensions: Insight on the Formation Mechanism." Crystal Growth & Design 15(1): 194-203.

EPA, U. (1999). Toxicity Characteristics Leaching Procedure. U. E. P. Agency: 11798.

Flor-Montalvo, F. J., E. Martínez-Cámara, J. L. García-Alcaraz, E. Jiménez-Macías, J.-I. Latorre-Biel and J. Blanco-Fernández (2022). "Environmental Impact Analysis of Natural Cork Stopper Manufacturing." Agriculture 12(5): 636.

Goyal, H., T. Tyagi and P. Mondal (2023). "Life cycle analysis and economic evaluation of adsorptive removal of arsenic from groundwater using GAC and GAC-Fe adsorbents." Journal of Cleaner Production 429: 139557.

Gurung, K., W. Z. Tang and M. Sillanpää (2018). "Unit Energy Consumption as Benchmark to Select Energy Positive Retrofitting Strategies for Finnish Wastewater Treatment Plants (WWTPs): a Case Study of Mikkeli WWTP." Environmental Processes 5(3): 667-681.

Halawy, S. A., A. I. Osman, N. Mehta, A. Abdelkader, D.-V. N. Vo and D. W. Rooney (2022). "Adsorptive removal of some Cl-VOC's as dangerous environmental pollutants using feather-like γ-Al2O3 derived from aluminium waste with life cycle analysis." Chemosphere 295: 133795.

Hjaila, K., R. Baccar, M. Sarrà, C. M. Gasol and P. Blánquez (2013). "Environmental impact associated with activated carbon preparation from olive-waste cake via life cycle assessment." Journal of Environmental Management 130: 242-247.

Hu, G., A. Rana, H. R. Mian, S. Saleem, M. Mohseni, S. Jasim, K. Hewage and R. Sadiq (2020). "Human health risk-based life cycle assessment of drinking water treatment for heavy metal(loids) removal." Journal of Cleaner Production 267: 121980.

HUB, R. D. (2021). "Mercado de Eletricidade em 28 fev 2024." Retrieved 28 Feb 2024, from https://datahub.ren.pt/pt/eletricidade/mercado/.

Kalaruban, M., P. Loganathan, T. V. Nguyen, T. Nur, M. A. Hasan Johir, T. H. Nguyen, M. V. Trinh and S. Vigneswaran (2019). "Iron-impregnated granular activated carbon for arsenic removal: Application to practical column filters." Journal of Environmental Management 239: 235-243.

Li, F., D. Zhang, J. Zhang and G. Kou (2022). "Measuring the energy production and utilization efficiency of Chinese thermal power industry with the fixed-sum carbon emission constraint." International Journal of Production Economics 252: 108571.

Maiti, P., H. Siddiqi, U. Kumari, A. Chatterjee and B. C. Meikap (2023). "Adsorptive remediation of azo dye contaminated wastewater by ZnCl2 modified bio-adsorbent: Batch study and life cycle assessment." Powder Technology 415: 118153.

Matos, A. M., S. Nunes and J. Sousa-Coutinho (2015). "Cork waste in cement based materials." Materials & Design 85: 230-239.

Menor, M. C. P., M. J. A. Caballero, A. M. García and P. S. Ros (2024). "Multiproperty characterization of non-structural concrete for block made with granulated cork with bark." Construction and Building Materials 418: 135404.

Nishikawa, E., M. G. C. da Silva and M. G. A. Vieira (2018). "Cadmium biosorption by alginate extraction waste and process overview in Life Cycle Assessment context." Journal of Cleaner Production 178: 166-175.

Norberto, J., K. Zoroufchi Benis, K. N. McPhedran and J. Soltan (2023). "Microwave activated and iron engineered biochar for arsenic adsorption: Life cycle assessment and cost analysis." Journal of Environmental Chemical Engineering 11(3): 109904.

Pintor, A. M. A., C. C. Brandão, R. A. R. Boaventura and C. M. S. Botelho (2021). "Multicomponent adsorption of pentavalent As, Sb and P onto iron-coated cork granulates." Journal of Hazardous Materials 406: 124339.

Pintor, A. M. A., B. R. C. Vieira, R. A. R. Boaventura and C. M. S. Botelho (2020). "Removal of antimony from water by iron-coated cork granulates." Separation and Purification Technology 233: 116020.

Pintor, A. M. A., B. R. C. Vieira, C. C. Brandão, R. A. R. Boaventura and C. M. S. Botelho (2020). "Complexation mechanisms in arsenic and phosphorus adsorption onto iron-coated cork granulates." Journal of Environmental Chemical Engineering 8(5): 104184.

Pintor, A. M. A., B. R. C. Vieira, S. C. R. Santos, R. A. R. Boaventura and C. M. S. Botelho (2018). "Arsenate and arsenite adsorption onto iron-coated cork granulates." Science of The Total Environment 642: 1075-1089.

Pizzol, M., R. Sacchi, S. Köhler and A. Anderson Erjavec (2021). "Non-linearity in the Life Cycle Assessment of Scalable and Emerging Technologies." Frontiers in Sustainability 1.

Porto, C. E. d. Á. e. E. d. M. d. (2024). "Tarifário." Retrieved 28 Feb 2024, from https://www.aguasdoporto.pt/files/uploads/cms/Tarif%C3%A1rio%20Geral%202024.pdf.

Rathore, V. K. and P. Mondal (2018). "Life cycle assessment of defluoridation of water using laterite soil based adsorbents." Journal of Cleaner Production 180: 716-727.

Reaney, I. M., B. Walsh and P. M. Vilarinho (2023). "Resource efficiency and energy efficiency (REEE) in the Portuguese ceramic industry: Towards net zero carbon production." Open Ceramics 15: 100390.

Rives, J., I. Fernandez-Rodriguez, X. Gabarrell and J. Rieradevall (2012). "Environmental analysis of cork granulate production in Catalonia – Northern Spain." Resources, Conservation and Recycling 58: 132-142.

Shibasaki, M., M. Fischer and L. Barthel (2007). Effects on Life Cycle Assessment — Scale Up of Processes. Advances in Life Cycle Engineering for Sustainable Manufacturing Businesses, London, Springer London.

Treatment., G. W. (2024). "BAYOXIDE® E 33 (ARSENIC REMOVAL) 20 KG/40 LITRES." Retrieved 28 Feb 2024, from https://www.gapswater.co.uk/acatalog/Bayoxide--Arsenic-Removal--15-Kg-30-Litres-0900011353.html.

van Genuchten, C. M., T. R. Etmannski, S. Jessen and H. M. Breunig (2022). "LCA of Disposal Practices for Arsenic-Bearing Iron Oxides Reveals the Need for Advanced Arsenic Recovery." Environmental Science & Technology 56(19): 14109-14119.

Verbinnen, B., C. Block, J. Van Caneghem and C. Vandecasteele (2015). "Recycling of spent adsorbents for oxyanions and heavy metal ions in the production of ceramics." Waste Management 45: 407-411.

Vilén, A., P. Laurell and R. Vahala (2022). "Comparative life cycle assessment of activated carbon production from various raw materials." Journal of Environmental Management 324: 116356.

Villacís-García, M., M. Ugalde-Arzate, K. Vaca-Escobar, M. Villalobos, R. Zanella and N. Martínez-Villegas (2015). "Laboratory synthesis of goethite and ferrihydrite of controlled particle sizes." Boletín de la Sociedad Geológica Mexicana 67(3): 433-446.

Wang, K., P. E. Holm, U. B. Trettenes, S. R. S. Bandaru, D. van Halem and C. M. van Genuchten (2023). "Molecular-scale characterization of groundwater treatment sludge from around the world: Implications for potential arsenic recovery." Water Research 245: 120561.

Water, A. F. (2024). "AdEdge Bayoxide E33 Arsenic Media - 2.0 cu. ft." Retrieved 28 Feb 2024, from https://store.afwfilters.com/arsenic-filters/adedge-bayoxide-e33/.

Yadav, M. K., D. Saidulu, P. S. Ghosal, A. Mukherjee and A. K. Gupta (2022). "A review on the management of arsenic-laden spent adsorbent: Insights of global practices, process criticality, and sustainable solutions." Environmental Technology & Innovation 27: 102500.

Zhang, Y., K. Yuan, L. Magagnin, X. Wu, Z. Jiang and W. Wang (2023). "Selective adsorption of Pb (II) and Cu (II) on mercapto-functionalized aerogels: Experiments, DFT studies and LCA analysis." Journal of Cleaner Production 393: 136126.

8 CONCLUSIONS AND FUTURE WORK

8.1 General Conclusions

This thesis presented a novel ecological adsorption system, consisting of a fixed-bed column with iron-coated cork granulates for arsenic or antimony removal from water. Current technologies for arsenic and antimony removals can be of high cost, have more impact on the environment, limited to a low range of adsorbate initial concentration, and can be challenging for handling and dispose after use. Iron-coated cork granulates can be considered as an alternative, due to its potential to be cheaper, efficient at a wide range of influent concentrations and more eco-friendly. The adsorption column filled with ICG was able to remove arsenic or antimony from water, under the WHO guidelines, through continuous adsorption. Additionally, desorption and recovery of arsenic and antimony were feasible using different eluents. Moreover, arsenic adsorption from different groundwater matrices were also accomplished using ICG, which was

shown to be environmentally friendly than a commercial adsorbent based on granular ferric hydroxides.

The strengths and weakness of this work are summarized below:

i. The adsorption column using iron-coated cork granulates proposed in this work were of simple operation and removed arsenic and antimony from water under legal limits;
ii. Maximum adsorption capacities of 4.2 mg As(V) g^{-1}, 1.8 mg As(III) g^{-1}, 10 mg Sb(V) g^{-1} and 13 mg Sb(III) g^{-1} were achieved in continuous mode.
iii. The system successfully removed arsenic below legal limits from groundwater matrices in Portugal and The Netherlands;
iv. The technology readiness level (TRL) for arsenic removal increased from 3 to 5;
v. Arsenic and antimony, two elements of economic importance that are also in critical risk of supply in EU, were efficiently recovered in high concentrated desorbing solutions.
vi. Technically, the regeneration of saturated media after arsenic desorption proved feasible for up to five cycles in aqueous solution and up to three cycles in groundwater. Nevertheless, the process was found to be environmental challenging due to the high impact of the hazardous waste generated. The incorporation of the recovered arsenic in other industrial process can mitigated the overall environmental burden of the process.
vii. The regeneration of the saturated media after antimony desorption was limited due to elution of the adsorbent's iron coating.
viii. Manganese leaching from the adsorbent was identified in levels above the EU limit in drinking water, possibly due to contamination of the coating iron salt $FeCl_3$.
ix. ICG environmentally friendliness and lower cost makes it an attractive adsorbent for arsenic removal.

8.2 Future Work

Some suggestions for future work are presented below:

1. This study showed that iron-coated cork granulates successfully removed antimony from aqueous solution in continuous mode. Further studies should investigate the adsorption behaviour of antimony removal from real samples (e.g., mine drainage water).
2. Iron-coated cork granulates effectively remove oxyanions As(III), As(V), Sb(III) and Sb(V) from water. The removal of other toxic oxyanions such as selenium species Se(IV) and

Se(VI), and chromium species Cr(III) and Cr(VI) by ICG should be as well investigated. Furthermore, the removal of other pollutants such as contaminants of emerging concern (CECs), might open up new lines of study for ICG or other cork granulate-based adsorbents.

3. Even though arsenic is a major concern to drinking water in the world, the populations with most risks of its consumption live in areas with a lack of infrastructure and few alternative water sources. Hence, field testing of iron-coated cork granulates arsenic filters, a simple and low-cost technology, is recommended in the Bengal-Delta region, which is the world´s most affected area with arsenic pollution from groundwater. This could be achieved by collaborating with non-governmental organizations (NGO´s), public institutions and universities to bring the treatment to those who need the most.
4. Exploring the fate of the saturated iron-coated cork granulates is essential. This work found, after TCLP tests, that these granulates can be safely disposed of in sanitary landfill. Nevertheless, alternative destinations of the spent media should be investigated. Considering the high desorption efficiency of arsenic and antimony achieved from the saturated media, it is recommended to study the spent adsorbent as a potential safe source for recycling in other cork granulates products, or to develop innovative applications.
5. This work increased the TRL of the arsenic adsorption using iron-coated cork granulates from 3 to 5. Since the feasibility of this methodology has been confirmed and optimised at lab scale, as well as validated in relevant environment (groundwaters), future work should address the challenges faced by scaling up of the process, with a focus on pilot and industrial scale units for commercial applications. For that, the installation of a pilot system in partnership with water treatment companies and utilities is then necessary to increase the TRL to 6 and 7, and so on.
6. Cork granulates has proven to be a stable base material for fixed-bed column adsorption. The iron coating was successful to increase the removal capacity of the cork granulates for arsenic and antimony, however the regeneration of the ICG for antimony was limited due to the iron removal during the acid desorption. The overall improvement of the adsorbent might be investigated and some suggestions are pointed out: by: i) to use different coating techniques, such as ultrasound coating which can better retain the iron active site and reduce both $FeCl_3$ waste and coating time (potential reduction of environmental impacts), ii) test different iron-based composites which can reduce the manganese contamination.

7. The outcomes from this work might contribute to and encourage the development of novel cork-based materials for water treatment and other environmentally relevant applications. This research group has already made progress in developing biochar from cork granulates for the adsorption of phosphate. Moreover, promising results were observed in the production of adsorbents using cork powder, an even more abundant coproduct from the cork sector. Future work can focus on improving the cork powder for possible adsorption of arsenic in fixed-bed columns by increasing its particle size or through gelification, for example.
8. Finally, this study confirms that iron impregnating cork granulates produces an adsorbent with great affinity for oxyanions, with only a 3% iron content material, and has lower environmental impacts than commercial adsorbents such as Bayoxide E33, which contain around 99% iron. This opens up opportunities to testing the iron impregnation in other organic materials. Then, the possibility for developing innovative, ecological, cost-effective adsorbents by iron-coating locally accessible organic materials (for example, wood and bark from other tree species) should be explored. Promising results were already achieved by arsenic adsorption of iron-coated wood from locally available trees in Nepal, a country close to the Bengal-Dental region and highly affected by the consumption of arsenic contaminated groundwater.